DE GRUYTER

Kaushik Kumar, J. Paulo Davim (Eds.)

BIODEGRADABLE COMPOSITES

ADVANCED COMPOSITES

Kaushik Kumar, J. Paulo Davim (Eds.)

Biodegradable Composites

Advanced Composites

Also of interest

Series: Advanced Composites
J. Paulo Davim (Ed.)
ISSN 2192-8983
Published titles in this series:
Vol. 9: Wear of Composite Materials (2018) Ed. by J. P. Davim
Vol. 8: Hierarchical Composite Materials (2018) Ed. by K. Kumar, J. P. Davim
Vol. 7: Green Composites (2017) Ed. by J. P. Davim
Vol. 6: Wood Composites (2017) Ed. by A. Alfredo, J. P.Davim
Vol. 5: Ceramic Matrix Composites (2016) Ed. by J. P. Davim
Vol. 4: Machinability of Fibre-Reinforced Plastics (2015) Ed. by J. P. Davim
Vol. 3: Metal Matrix Composites (2014) Ed. by J. P. Davim
Vol. 2: Biomedical Composites (2013) Ed. by J. P. Davim
Vol. 1: Nanocomposites (2013) Ed. by J. P. Davim, C. A. Charitidis

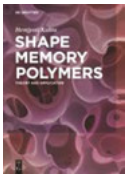

Shape Memory Polymers
Kalita, Hemjyoti, 2018
ISBN 978-3-11-056932-2, e-ISBN 978-3-11-057017-5

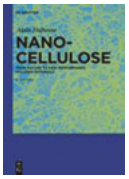

Nanocellulose
From Nature to High Performance Tailored Materials
Dufresne, 2017
ISBN 978-3-11-047848-8, e-ISBN 978-3-11-048041-2

Biomaterials
Biological Production of Fuels and Chemicals
Luque, Xu, 2016
ISBN 978-3-11-034230-7, e-ISBN 978-3-11-034242-0

Biodegradable Composites

Materials, Manufacturing and Engineering

Edited by
Kaushik Kumar and J. Paulo Davim

DE GRUYTER

Editors
Dr. Kaushik Kumar
Associate Professor Birla Institute of Technology
Department of Mechanical Engineering
Mesra, Ranchi
Jharkhand 835215
India
kkumar@bitmesra.ac.in, kaushik.bit@gmail.com

Prof. Dr. J. Paulo Davim
Professor University of Aveiro
Department of Mechanical Engineering
Campus Santiago
3810-193 Aveiro
Portugal
pdavim@ua.pt

ISBN 978-3-11-060203-6
e-ISBN (PDF) 978-3-11-060369-9
e-ISBN (EPUB) 978-3-11-060284-5
ISSN 2192-8983

Library of Congress Control Number: 2018967114

Bibliographic information published by the Deutsche Nationalbibliothek
The Deutsche Nationalbibliothek lists this publication in the Deutsche Nationalbibliografie; detailed bibliographic data are available on the Internet at http://dnb.dnb.de.

Typesetting: Integra Software Services Pvt. Ltd.
Printing and binding: CPI books GmbH, Leck
Cover image: gettyimages/thinkstockphotos, Abalone Shell

www.degruyter.com

Preface

The editors are pleased to present the book *Biodegradable Composites: Materials, Manufacturing and Engineering* under the book series Advanced Composites. The book title was chosen as it depicts upcoming trends in composite materials for the next decade. This book is a compilation of different biodegradable and natural composites being used as well as achievements, progress, and recent developments that are being made with them.

In the material science and engineering world, most researchers often refer to pivotal eras in human history by the materials that dominated them – most notably, starting from the Stone Age, then Bronze Age, and the Iron Age. All these periods lasted for a long period of time. Since two centuries ago, the development and discovery of cement (1824), carbon fiber (1879), fiber glass (1938), polyester (1941), and nanostructural materials like the fullerence molecule (1985) and carbon nanotubes (1991) has revolutionized new research focuses on designing new structural materials with better properties and qualities, for different kinds of engineering applications.

Over the past 50 years composite materials have grown rapidly. Due to its versatility, the volume and number of areas of use of composite materials have increased constantly, developing new solutions in order to improve product quality and attractiveness for new markets. They are no longer the privilege of the aerospace or defense industry or even high-value goods. They have made way to become medium for achieving high structural applications at a low cost and are evidently present all around us. Initially usage of the same was to achieve increased strength and stiffness properties in comparison to classical materials wherein these properties could not be improved further. From this point of view it is understood that the maximum efficiency of the reinforcement of a certain material is obtained by introducing some reinforcement elements in its structure. Representing the most well-known category and marking the beginning of the industrial application of the new materials, the polymeric composites were mainly considered in the form of polymer matrices reinforced with fibers or fillers. As a result of using high-performance fibers, polymeric composites are continuously replacing traditional materials in all domains. The unique properties of the polymeric materials as well as the possibility of their adaptation to the applicative needs have dominating factor for their usage in all the domains of human activity and industrial applications. However, due to the shortage of natural resources, such as fossil fuels, many countries have been striving for better alternatives to use renewable resources for new material development and energy harvesting.

Thus, the return to nature, both through the processes of obtaining polymers from renewable raw materials and by inducing their end-of-life biodegradability, is the strategy to build the sustainability of nowadays society. The only solution to meet material needs is to obtain synthetic materials to replace natural materials

https://doi.org/10.1515/9783110603699-201

and whose production can be adjusted as needed. A variation of synthetic materials that has conquered all current fields of activity, through the extraordinary ability to adapt their properties to the applicative requirements, is the composite polymeric materials.

Mankind has realized that unless environment is protected and steps are taken to protect it, he himself will be threatened by the pollution by various sources. In tune to this, recently, there has been a rapid growth in research and innovation in the biodegradable and natural composite area. Over the past decade, several studies have been done to look at the possibilities of using natural materials such as plant- or animal-based fibers to mix with different types of soft materials to form a new class of biocomposites. The term "biocomposite" refers to a material which is formed by a matrix and a reinforcement of natural fiber. The matrix can be a polymeric or cementitious material depending on applications. The fiber normally plays a role in taking load while the matrix protects the fiber by holding them together, avoiding environmental degradation, and maintaining the shape of resultant structures. The major purpose of biocomposites is to ensure that the new materials are either recyclable or biodegradable after disposal. The resin is also made of renewable resources, to allow a new composite to be degraded naturally, without the need for extra chemicals or energy to decompose it.

Common types of plant-based fibers are crop fibers which are extracted from cotton, flax, hemp, sisal, or regenerated cellulose materials. Biocomposites made from plant-based fiber are commonly seen in automobile, construction, and some interior components inside aircraft or railway coaches. In fact, plant-based fiber has been commonly used since ancient times; for example, straw was added into mud to make a wall for a house. Animal-based fibers, commonly extracted from spiders, silkworm cocoons, chicken feathers, and even human hair, have also demonstrated their effectiveness of reinforcing biocompatible and bioresorbable polymers for implant applications. As the major content of these fibers is protein, it is suitable to be mixed with bioresorbable polymers for temporary reinforcing elements used inside the human body.

In present time, biodegradable composite is the key for major discipline and many researchers and scholars are working in these areas. This book provides an insight for all researchers, academicians, post graduate or senior undergraduate students working in the area.

The chapters in the book have been provided by researchers and academicians working in the field and have gained considerable success in the field.

The book is divided into three parts, namely, Part I: Introduction and Material (Chapters 1 and 2); Part II: Manufacturing and Properties (Chapters 3–7); and Part III: Machining and Application (Chapters 8 and 9).

Chapter 1 provides the readers an insight into plant-based biodegradable composites. The chapter reviews the research trends, production techniques, challenges, and future prospects for the biodegradable composites derived from plant

proteins and biopolymers. It starts with increasing concern over the depleting petroleum resources with added concerns for environment. It then moves to one alternative solution, that is, biodegradable materials, a key replacement to the petroleum-based products, which has motivated the research community to use them to meet the needs of mankind to the extent possible.

Chapter 2 discusses the fibers, polymers, composites, and applications of corn or maize. Corn, a tropical cereal plant, domesticated about 8,000 years ago mainly as a food. In recent times the demand for corn has flourished dramatically, for use in production of various food and edible oils as well as manufacturing biocomposites, and biopolymers. Furthermore, corn plant is the second largest source of renewable energy in the form of bioethanol via fermentation process for the sugar glucose of the corn starch and cellulose of corn fibers. The main aim of this review chapter is to present a comprehensive study about corn plant as an essential source of biodegradable polymers and fiber-based biocomposites, along with its current and potential applications. The chapter also provides information on most recent developments of corn biocomposites and presents a detailed report on surface treatments, extraction methods, and mechanical properties of corn starch and corn fibers as well.

Chapter 3 reviews production of biodegradable composites from agricultural waste. The chapter discusses some of the literature available on biodegradable composites developed mainly from common agricultural products, their properties, production method, challenges, and sustainability. Although recent researchers have led to the development of biodegradable composites with reasonable tensile and flexural characteristics, there are short falls with regard to some of the biodegradable composites when they come in contact with moisture, which affects their performance under certain conditions like in aqueous medium or under high humidity. The chapter has considered and reported works on rice husk, soybean, sugarcane bagasse, and cassava peel.

Chapter 4 illustrates effect of orientation on mechanical properties of natural fiber-based biocomposites. It indicates that the mechanical properties of the final product depend largely on the adjustment of the fiber orientation field during processing. The chapter deals with the study of the fiber orientation prediction using Jeffrey and Folgar-Tucker descriptions and their effect on composite mechanical properties by evoking several models, namely, Voigt, Reuss, Halpin-Tsai, Hashin and Shtrikman, and Hirsch and Tsai Pagano.

Chapter 5 discusses mechanical properties of bamboo yarn, a biodegradable composite material for structural works. Bamboo yarn as reinforcement of polymer composite is nonabrasive, ecofriendly, and biodegradable, and it can serve as a raw material for industrial engineering application. In this chapter investigation to study mechanical properties of bamboo yarn, both woven or bidirectional and unwoven or 45° orientation, as reinforcement in polymer composite have been extensively done and influence of bamboo yarn orientation, yarn content, size, and

treatment agents on the mechanical properties of the composite were investigated. The impact, flexural, tensile, and scanning electron microscope (SEM) have been performed to evaluate the properties and surface morphology. The chapter further discusses the thermal stability and thermal degradation of the composite utilizing thermogravimetric analysis (TGA) and differential thermogravimetry analysis (DTA) under a nitrogen atmosphere.

Chapter 6 deals with aggrandized flexural properties of assorted natural biological materials. The chapter starts with the fact that natural biocomposites such as molluscan shell, teeth, and bone exhibit mutually exclusive mechanical properties due to their hierarchical stratified microarchitectures comprise of mineral tablets and interweaved with organic biomaterials – hence, all engineering applications like construction, defense, energy, and aerospace. Therefore, biomimicking of these high flexural natural materials (e.g., the flexural strength of the nacreous structure is 220 MPa) can help the engineering community in developing high flexural materials. The chapter discusses the biomimicking of various animal- and plant-based biologically inspired materials for the developing composites materials that have high flexural strength and concludes with the discussion on the future scope of the natural composites.

Chapter 7 highlights mechanisms and formalism of hygrothermoelastic behavior of natural fiber-based composites. It underlines the hygrothermoelastic behavior of composites reinforced with natural fibers with various behaviors including hygroscopic, thermal, hygrothermal, hygroelastic, thermoelastic, and hygrothermoelastic behaviors. The chapter concludes with application of the equations governing the hygrothermoelastic effect on the case of the laminated composite structure.

Chapter 8 relates the influence of drilling parameters on the thrust force and mechanical properties of biodegradable particleboard composite panels. The present chapter provides an overview review on the same. It commences the discussion with the fact that among the numerous conventional machining, drilling is the most commonly used procedure for machining of particleboard, whereas milling and turning are less frequently used. The different machining parameters like feed rate, spindle speed, and drill bit diameter/point angle are found to have major influence on the thrust force during drilling operation. The chapter provides a detailed review considering the effect of machining parameters in the drilling of particleboard. Summarized outlines are presented on surface characteristics of the hole produced in drilling operation. The chapter also provides optimized delamination factor of particle board using optimization techniques like Taguchi and Response Surface Methodology. Fuzzy approach in assessment of frequency response function (FRF) analysis of functionally graded plates (FGP) was also undertaken. The fuzziness has been considered due to variability in material properties corresponding to the various α-cuts. The Power law was implied for characterizing the material modeling, and a parametric study was carried out to observe the effect of

location of drive point and cross points on uncertain bounds of frequency response function with respect to crisp values.

Chapter 9, the last chapter of the book, does a numerical study of rotating functionally graded annular fin made of biodegradable composite. The governing differential equation for such fins of rectangular and triangular profiles has been derived to evaluate the temperature distribution and efficiency of the fins with insulated tip boundary condition. Nonlinearity in the governing equation material heterogeneity and rotation at various speeds is imposed and analyzed to compare the performance for both rectangular and triangular cross section. The formulation has been validated with benchmark results, and good agreement was observed.

First and foremost the editors would like to thank God. In the process of putting this book together, it was realized how true this gift of writing is for anyone. You have given the power to believe in passion, do hard work, and pursue dreams. This could never have been done without the faith in You, the Almighty. The editors would also like to thank all the chapter contributors, the reviewers, the editorial board members, project development editor, and the complete team of publisher Verlag Walter de Gruyter GmbH for their availability for work on this editorial project.

Kaushik Kumar
J. Paulo Davim

Contents

List of contributors

Kamardeen O. Abdulrahman
Department of Mechanical Engineering Science
University of Johannesburg
Auckland Park Kingsway Campus
Johannesburg 2006
South Africa

Esther T. Akinlabi
Department of Mechanical Engineering Science
University of Johannesburg
Auckland Park Kingsway Campus
Johannesburg 2006
South Africa

Damenortey R. Akwada
Department of Mechanical Engineering Science
University of Johannesburg
P. O. Box 524
Auckland Park 2006
South Africa
rich.akwada@gmail.com

Mohammed Ouadi Bensalah
Mechanics of Materials Laboratory
Faculty of Science
Mohammed V University
Rabat
Marocco

Shubhankar Bhowmick
Department of Mechanical Engineering
National Institute of Technology
Raipur
India
sbhowmick.mech@nitrr.ac.in

Sumit Bhowmik
Department of Mechanical Engineering
National institute of Technology
Silchar – 788010
India

Rachid Bouhfid
Moroccan Foundation for Advanced Science,
Innovation and Research (MAScIR)
Institute of Nanomaterials and
Nanotechnology (NANOTECH)
Laboratory of Polymer Processing
Rabat
Morocco

Opeoluwa R. Dada
Department of Mechanical Engineering Science
University of Johannesburg
Auckland Park Kingsway Campus
Johannesburg 2006
South Africa

J. Paulo Davim
Department of Mechanical Engineering
University of Aveiro
Aveiro
Portugal

Ahmed Edhirej
Department of Mechanical and Manufacturing
Engineering
Universiti Putra Malaysia
43400 UPM Serdang
Selangor
Malaysia

Vivek Kumar Gaba
Department of Mechanical Engineering
National Institute of Technology
Raipur
India

Swaroop Gharde
Rapid Prototyping Laboratory
Department of Metallurgical and Materials
Engineering
Defence Institute of Advanced Technology (DU)
Ministry of Defence, Girinagar
Pune – 411025
India

https://doi.org/10.1515/9783110603699-202

Rajendra Goud
Rapid Prototyping Laboratory
Department of Metallurgical and Materials Engineering
Defence Institute of Advanced Technology (DU)
Ministry of Defence, Girinagar
Pune – 411025
India

Fatima-Zahra Semlali Aouragh Hassani
Moroccan Foundation for Advanced Science, Innovation and Research (MAScIR)
Institute of Nanomaterials and Nanotechnology (NANOTECH)
Laboratory of Polymer Processing
Rabat
Morocco

M.I.J Ibrahim
Department of Mechanical and Manufacturing Engineering
Universiti Putra Malaysia
43400 UPM Serdang
Selangor
Malaysia

Rahul Jayasval
Department of Mechanical Engineering
National institute of Technology
Silchar – 788010
India
bhowmiksumit04@yahoo.co.in

Balasubramanian Kandasubramanian
Rapid Prototyping Laboratory
Department of Metallurgical & Materials Engineering
Defence Institute of Advanced Technology (DU)
Ministry of Defence, Girinagar
Pune – 411025
India
meetkbs@gmail.com

Kaushik Kumar
Department of Mechanical Engineering
Birla Institute of Technology Mesra
Ranchi
India

Rahul Kumar
School of Engineering
Department of Mechanical Engineering
Dayanand Sagar University
Bangalore – 560068
India

Sunil Nimje
Department of Mechanical Engineering
DIAT (DU)
Ministry of Defence, Girinagar
Pune – 411025
India

Wafa Ouarhim
Moroccan Foundation for Advanced Science, Innovation and Research (MAScIR)
Institute of Nanomaterials and Nanotechnology (NANOTECH)
Laboratory of Polymer Processing
Rabat
Morocco

Abou el kacem Qaiss
Moroccan Foundation for Advanced Science, Innovation and Research (MAScIR)
Institute of Nanomaterials and Nanotechnology (NANOTECH)
Laboratory of Polymer Processing
Rabat
Morocco
a.qaiss@mascir.com

S. M. Sapuan
Department of Mechanical and Manufacturing Engineering
Universiti Putra Malaysia
43400 UPM Serdang
Selangor
Malaysia
sapuan@upm.edu.my

Anil Kumar Tiwari
Department of Mechanical Engineering
National Institute of Technology
Raipur
India

E. S. Zainudin
Department of Mechanical and Manufacturing Engineering
Universiti Putra Malaysia
43400 UPM Serdang
Selangor
Malaysia

Nadia Zari
Moroccan Foundation for Advanced Science, Innovation and Research (MAScIR)
Institute of Nanomaterials and Nanotechnology (NANOTECH)
Laboratory of Polymer Processing
Rabat
Morocco

Divya Zindani
Research Scholar, Department of Mechanical Engineering
National Institute of Technology Silchar
Silchar – 788010
India

M.Y.M. Zuhri
Department of Mechanical and Manufacturing Engineering
Universiti Putra Malaysia
43400 UPM Serdang
Selangor
Malaysia

Editors' biographies

Kaushik Kumar, B.Tech (Mechanical Engineering, REC (Now NIT), Warangal), MBA (Marketing, IGNOU) and Ph.D. (Engineering, Jadavpur University), is presently an Associate Professor in the Department of Mechanical Engineering at Birla Institute of Technology, Ranchi, India. He has 17 years of teaching and research and more than 11 years of industrial experience in a manufacturing unit of global repute. His areas of teaching and research interest are quality management systems, optimization, nonconventional machining, CAD/CAM, rapid prototyping, and composites. He has 9 patents, 23 book, 12 edited books, 38 book chapters, 131 international journal publications, and 18 international and 8 national conference publications to his credit. He is on the editorial board and review panel of 7 international and 1 national journals of repute. He has been felicitated with many awards and honors.

J. Paulo Davim received his Ph.D. in Mechanical Engineering, M.Sc. in Mechanical Engineering (materials and manufacturing processes), and Mechanical Engineering degree (5 years) from the University of Porto (FEUP); the Aggregate title (Full Habilitation) from the University of Coimbra; and the D.Sc. from London Metropolitan University. He is EurIng by FEANI-Brussels and Senior Chartered Engineer by the Portuguese Institution of Engineers with an MBA and Specialist title in Engineering and Industrial Management. Currently, he is Professor at the Department of Mechanical Engineering at the University of Aveiro, Portugal. He has more than 30 years of teaching and research experience in Manufacturing, Materials, Mechanical, and Industrial Engineering, with special emphasis in Machining and Tribology. He has also interest in Management, Engineering Education, and Higher Education for Sustainability. He has guided large numbers of postdoc, Ph.D., and master's students, as well as has coordinated and participated in several financed research projects. He has received several scientific awards. He has worked as evaluator of projects for international research agencies as well as examiner of Ph.D. thesis for many universities in different countries. He is the editor in chief of several international journals, guest editor of several journals, editor of books, editor of book series, and scientific advisor for many international journals and conferences. Presently, he is an editorial board member of 30 international journals and acts as reviewer for more than 100 prestigious SCI-Web of Science journals. In addition, he has also published more than 100 books as editor (and coeditor) and more than 10 books, 80 book chapters, and 400 articles in journals and conferences (more than 200 articles in journals indexed in SCI-Web of Science core collection/h-index 47+/6500+ citations and SCOPUS/h-index 54+/9000+ citations) as author (and co-author).

https://doi.org/10.1515/9783110603699-203

Part I: **Introduction and Material**

Divya Zindani, Kaushik Kumar, J. Paulo Davim

1 An insight into plant-based biodegradable composites

Abstract: There has been increasing concern over the depleting petroleum resources. The added concern for environment has also motivated the research community to search for alternative material solutions to meet many of the mankind needs. Biodegradable materials are surely one of the key alternative solution and have been at the center stage of the scientific research. Biodegradable composite materials derived from plant fibers and biopolymers are the materials that have been of great interest recently in the domain of biodegradable materials as they have the potential in meeting the market needs and a key replacement to the petroleum-based products, ultimately promoting environmental sustainability. Furthermore, biodegradable composites are relatively cheap. This chapter therefore reviews the research trends, production techniques, challenges, and future prospects for the biodegradable composites derived from plant proteins and biopolymers.

Keywords: Green composites, biodegradable composites, sustainability, natural fiber/filler, green polymers

1.1 Introduction

Green composites are material classes that are renewable and biodegradable. Being renewable these composites take care of the environmental and sustainability concerns. Green composites have received special attention in the era where community is concerned mainly with climatic change and the regulations pertaining to the clean environment. Thus, their attractiveness from environmental perspective is one of the major reason behind wide acceptability in engineering domain. Polymers and other synthetic materials, which poses serious concerns such as in medical, agriculture, and so on, are being replaced with the green composite materials. Nonrenewable nature of petroleum-based products further demands for alternate materials that are biodegradable and have low toxicity. Therefore, there has been intense interest from the scientific community to explore new biodegradable materials and their

Divya Zindani, Department of Mechanical Engineering, National Institute of Technology Silchar, Silchar, India
Kaushik Kumar, Department of Mechanical Engineering, Birla Institute of Technology Mesra, Ranchi, India
J. Paulo Davim, Department of Mechanical Engineering, University of Aveiro, Aveiro, Portugal

https://doi.org/10.1515/9783110603699-001

applicability [1]. With the advent of green composites, opportunities have been presented to enhance the living standard of societies around the globe [2].

Green composites have aroused interest of mankind in applications where products possesses short life, disposable characteristics, and so on. Therefore, they have been used for applications such as consumer products, packaging, and so on. These materials have now become integral part of mankind evolution in era of environmental concerns.

Composites have undergone series of improvements considering the disadvantages associated with the performance of traditional materials. The series of advancements are often referred to as five generations [2]. Efforts have also been made in the development of green polymers that are environmentally favorable as well as possesses degradability characteristics. Therefore, the use of green polymers with natural plant fibers as reinforcement has led to the newer class of material known as green composite. The term biodegradability signifies a complete dissolution of the product after use into the natural environment. After degradation they may become food source for the microorganisms in the soil [3–5], resulting in effective carbon balance within the ecosystem.

Existence of natural polymers as well as the resulting biodegradable composites dates back to historical years as for instance paper, silk, and so on. Great Wall of China made from willow branches, stone, reeds, and clay and bows made from animal horns, silk, or wood are among the few existing biodegradable composite materials [2]. Since their inception, the wheels of advancements have been running intermittently.

Given the importance of green composites, this chapter reviews on the advancements and development made. Discussion is made on the fabrication techniques as well as on the related properties. Applications of green composites have been discussed toward the end of the chapter. The chapter finally ends with the concluding remarks.

1.2 Techniques for processing

Comprehending processing steps is quintessential for the fabrication of a new product that may be green composite. The development of a green composite incepts with the suitable selection of biopolymer matrix and the reinforcement. Application area dominates the selection process. Next stage is that of suitable surface treatment technique, if demanded, to be opted for the treatment of reinforcing material. Mixing of the treated or untreated reinforcing material with the selected biopolymer is the next step in the development phase. Next the fabrication process is selected that should be economical and should have high rates of production. The fabrication process to be employed depends on the properties of the constituting ingredients, that is, matrix

and reinforcement. In case of nanocomposites, recent developments in fabrication involves that of nanomanufacturing. In that case of nanobiocomposite materials, various processing methods include melt intercalation, solution intercalation, solution casting, intercalative polymerization, and so on [6, 7].

Few important concerns that should considered through the processing stage includes the availability of reinforcements in the desired form (powders, fibers, and whiskers), low shrinkage of the mold, less abrasiveness, appearance, and so on. Some of the recent materials for matrix that have been investigated include L-polylactide acid, polylactic acid, poly-3 hydroxyl butyrate, polyhydroxyalkanoates, and starch, while that of reinforcements are plant based. Matrices based on plant oil, for instance, soya oil and puree of mango, have also been used in the fabrication of biocomposites on nanoscale [8, 9]. However, such matrices have poor mechanical and thermal properties [10].The shortcomings have been taken care by the addition of suitable nano- or microfillers. The addition of suitable fillers not only enhances the properties but also objectifies to reduce the total cost of final specimen [11]. Nanosized reinforcements have been able to provide better properties owing to their high specific area [12, 13]. This work reviews microcomposites and nanobiocomposites.

1.3 Properties and morphological study

Processing conditions, properties of the constituting ingredients, processing method, applied pressure, temperature, amount of reinforcements, and so on dictate the microstructure and properties of the resulting composite material. The type of plasticizers and the compatibilizers used also dictate the properties of the resulting composite material. There have been array of research articles that have been published over the years related to the biodegradable polymers such as corn, starch, potato, wheat, rice, cassava, poly-lactic acid, polyhydroxy butyrate, polyhyrodoxyalkanoates, and so on. Many aspects, such as synthesis, properties as well as the degradation mechanism, have been reported in various research articles [14, 3, 4, 15, 16, 17]. Some of the prominently investigated starch-based systems have been tabulated in Table 1.1, whereas Table 1.2 lists it for the poly families.

One of the most easily and abundantly available natural polymer is starch, which is also inexpensive. The starch-based polymers have cellulosic origin and possess linear structure with strong hydrogen bonding. These characteristics impart these polymers high strength [2, 34]. The final properties of composites depend on the source from which the starch-based polymer has been extracted, the type, amount, and aspect ratio of reinforcements used, the processing method and conditions employed. Increasing tensile strength has generally been reported for green composites with increased amount of reinforcements.

Table 1.1: Few literature on starch-based green composites.

Reinforcement	Matrix	Processing
Fibers in castor bean oil cake [18]	Castor bean oil cake and glycerol	Thermomolding
Nanofibers from wheat straw [19]	Plasticized Maize starch	High shear mixer
Banana/sugarcane bagasse [20]	Cassava Starch and glycerol (commercial and recovered)	Single screw extruder
Oat or sugarcane fibers [10]	Cassava starch and glycerol	Single screw extruder
Bamboo cellulosic crystals [21]	Starch and glycerol	Film casting
Nanocellulose of raftwood [18]	Castor bean oil cake and glycerol	Thermomolding
Coir fibers [22, 23]	Cassava starch and glycerol	Thermomolding
Wheat bran [24]	Cassava starch, glycerol, and potassium sorbate	Casting
Cellulose fibers [25]	Starch acetates	Twin screw extruder

Table 1.2: Few literature on poly-based green composites.

Reinforcement	Matrix	Processing
Cellulose nanofibers [26]	Mango puree-based edible films	Film casting
Bamboo fiber [27]	Poly(lactic Acid) and poly(butylene succinate)	Compression molding
Flax fiber and mats from balsa [28, 29]	L-polylactide acid	Vacuum bag molding
Cellulose fibrils of bleached wood pulp [30]	Poly(lactic acid) and polyethylene glycol	Solvent casting
Hemp, kenaf, cotton, and man-made cellulose fibers (lyocell) [31]	Poly(lactic acid)	Compression molding
Flax fibers [32]	Poly 3-hydroxylbutyrate, polylactic acid, L-polylactide acid, poly-caprolactone and starch, polybutyleneadipate-*co*-terephtalate, and polybutylene succinate	Film stacking
Recycled disposable chopsticks fibers [33]	Polylactic acid	Melt mixing

Castor oil has qualified itself as a potential agro waste to be used in the fabrication of green composites. The reason may be attributed to the fact that castor oil possesses fibrous material in addition to the starch content [35]. The other natural polymeric materials include soybean oil, mango puree-based edible films, and polyurethane based on plant oil [3, 4, 2].

It has been revealed that composites based on cassava starch have better mechanical and structural properties. Fractographs obtained after mechanical testing of the composite specimen explains the basis of better mechanical characteristics for starch-based composites. Fractographs reveal the bonding between matrix and the reinforcing particles and also intramolecular bonding. The fracture surface of starch as reported is smoother in comparison to that obtained by the incorporation of the fiber material. Better interfaces between the reinforcements and the matrix material have been reported with the coated fiber material. Good mechanical properties are obtained with the better interfacial bonding.

Green polymers range from feed stocks that are renewable such as the varied lignocellulosic materials to the once that degrade over their lifetime. One of the most versatile green polymer is polylactic acid belonging to polyfamily. The mechanical properties such as strength and Young's modulus and high biocompatibility of polylactic acid are comparable to that of polystyrene and polyethylene and hence the most attractive option to be used as a matrix for development of green composites. The presence of asymmetric carbon atoms is one of the main reason behind their comparable characteristics [4].

The properties of these polymeric matrices have been improved by the addition of fibers as reinforcements. For instance, the addition of cassava root fiber to polybutylene succinate increased its Young's modulus and flexural modulus. Therefore, with fiber addition the resulting composite was more rigid and stiffer in comparison to standalone PBS [36]. Tensile and flexural strengths were, however, found to decrease with increased fiber amount, while insignificant changes in impact strength were reported for impact strength. To enhance the interfacial bonding between the hydrophobic polymers and hydrophilic fibers, surface treatment of fibers [33] have been attempted or the addition of compatabilizer has been investigated [30]. Improved mechanical properties have been reported in comparison to standalone matrix and matrix with fibers without any treatment. Array of work have been reported on polylactic acid-based green composites consisting of different natural fibers, for instance, hemp, cotton, coir, and so on [28, 31]. Comparison of mechanical properties has been made between green composites obtained from different processing techniques [23], while different processing techniques used for polylactic-based green composites have also been investigated [28]. Applications of obtained green composites depending on their technical capabilities have also been reported in the aforementioned literatures.

Morphological studies for polylactic-based green composites have revealed a smoother fragile fracture in case of polylactic matrix, while uneven fracture surfaces have been reported for its nanocomposites without a compatabilizer. The

composites with compatabilizers have reported to have more uneven surfaces, with relatively more tread-like structures and holes.

Optimal properties for any given application can be achieved with proper selection of matrix-reinforcement systems in tandem with the suitable processing technique. The importance of green composites from environmental perspective has led to great revolution and advancements in the domain of material science. Applications based on green composites have increased since their inception, discussed in the next section.

Sandwich composites based on biofillers and polymers have also been investigated for their structural properties with due consideration to weight of such materials. Such composites have been employed in weight critical domains such as aerospace, ships, and other logistics [28, 37, 38, 29, 39, 40, 41, 42]. Bio-based sandwich composites have been obtained with high stiffness-to-weight and strength-to-weight ratios. Such composites are obtained by generally attaching two skins that are thin but stick to a lightweight and thicker material, which can be a synthetic or a natural fiber. Bio-based cores such as wood or cork have also been used for the fabrication of sandwich composite structures. Such sandwich composites have gained wide range acceptability because of being recyclable and ease of being composted. The interfacial properties for the sandwich structures have been known to be affected by the processing temperature used for their processing [28, 29].

Failure modes have been investigated for PLLA-flax-balsa-based green composites. Different temperatures, that is, 180, 190, and 200 °C were taken into account. It was revealed that for panels manufactured at 180 and 190 °C, the failure modes were similar. In both the cases, failures were reported with delamination occurring in lower face and shear crack taking place at core. Debonding between core and skins was, on the other hand, reported for the panel manufactured at 200 °C. The causes of such failure as well as the degradation have been discussed in the chapter [28].

There are umpteen reports besides the one mentioned in earlier discussion on green polymer-based composite materials. The readers can refer to these references for a deeper insight into the domain of green composite [14, 43, 3, 8, 24, 4, 44, 2, 17, 45].

1.4 Applications

Green composites have been employed in different sectors owing to their environmental attributes, continued research, and advancements in domain of green composite materials [2]. Some of the effective and prominent application areas include that of hurricane-resistant housing, automotive sector, entertainment and sports accessories, textile, and infrastructure. Low dielectric materials from green composites have been developed to be used in electronic applications. These composites

are based on keratin fibers and soybean oil [46]. Green composites based on kenaf fibers and polylactic matrix have been proposed for transport sector [47].

Nanogreen composite materials have recently overtaken the microcomposites in terms of production and usability. These have been widely used for the development of automotive parts such as housings for mirror, liners in truck, engine covers and upholstery, vacuum cleaner blades and impeller, mobile phone casings and covers, housings for power tools, and covers for electronic equipment [27, 48, 49]. Some of the other application possibilities include capacitors, paper-based displays, communication devices, paper batteries [50], packaging material for food and pharmaceutical industries, cellulosic natural fibers-based paperboards for dairy products and fruit juice, ID tags for computers, and so on. Potential application in biomedical arena includes that of tissue engineering [30]. Strategic sectors such as defense are also the future benefit explorers of green composite materials.

1.5 Conclusion

Green composites have been in existence for long time. Since their inception, they have been employed in vast engineering domain such as Great Wall of China to the present-day consumer products such as automobile bumpers, tennis rackets, displays for computer monitor, digital cameras, mobile phones, golf balls, and so on. Decreasing nonrenewable sources of materials as well as their increasing cost and strict environmental regulations and encompassing laws have corroborated the employability of green composites in vast engineering domains. Biodegradability and biocompatibility are some of the unique characteristics that have boosted the scientists and engineers to promote the usage of green composites in academia apart from industrial perspectives. A number of resources with bio and natural characteristics have been identified for both the reinforcements and matrix that have promoted the usage of sustainable green composite materials. Various manufacturing techniques have been developed to fabricate green composites both at nano- and microlevels. Many investigations have been carried out on such materials and revelations on structural properties have been encouraging. However, a few disadvantages include poor ductility, dimensional stability, and so on. The underlying limitations should be overcome to remove the barrier of restricted applicability.

Some of the future work that can be done in the domain of green composites include modeling and simulation of green composite material and employability of artificial neural network to establish the relationship between processing parameters and the mechanical properties obtained; biomimetic processing approaches could be adopted wherein biological structures for fibers and fillers are considered.

References

[1] Shaver, M. P. (2013). The development of Green Materials.
[2] Satyanarayana, K. G., Arizaga, G. G., & Wypych, F. Biodegradable composites based on lignocellulosic fibers—An overview. Progr. Polym. Sci., 2009, 34(9), 982–1021.
[3] Adeosun, S. O., Lawal, G. I., Balogun, S. A., & Akpan, E. I. Review of green polymer nanocomposites. J. Miner. Mater. Charact. Eng, 2012.11(04), 385.
[4] Luckachan, G. E., & Pillai, C. K. S. Biodegradable polymers-a review on recent trends and emerging perspectives. J. Polym. Environ., 2011, 19(3),637–676.
[5] Narayan, R., Balakrishnan, S., & Shin, B. Y. (2009). U.S. Patent No. 7,553,919. Washington, DC: U.S. Patent and Trademark Office.
[6] Sorrentino, A., Gorrasi, G., &Vittoria, V. Potential perspectives of bio-nanocomposites for food packaging applications. Trends in Food Sci. Technol., 2007, 18(2), 84–95.
[7] Oksman, K., Mathew, A. P., Bondeson, D., &Kvien, I. Manufacturing process of cellulose whiskers/polylactic acid nanocomposites. Compos. Sci. Technol., 2006, 66(15), 2776–2784.
[8] Xie, Y., Hill, C. A., Xiao, Z., Militz, H., & Mai, C. Silane coupling agents used for natural fiber/polymer composites: A review. Composites Part A: Appl. Sci. Manuf., 2010, 41(7), 806–819.
[9] Athijayamani, A., Thiruchitrambalam, M., Natarajan, U., & Pazhanivel, B. Effect of moisture absorption on the mechanical properties of randomly oriented natural fibers/polyester hybrid composite. Mater. Sci. Eng.: A, 2009, 517(1–2), 344–353.
[10] Debiagi, F., Mali, S., Grossmann, M. V. E., & Yamashita, F. Effects of vegetal fibers on properties of cassava starch biodegradable composites produced by extrusion. Ciência e Agrotecnologia, 2010, 34(6), 1522–1529.
[11] Azizi Samir, M. A. S., Alloin, F., & Dufresne, A. Review of recent research into cellulosic whiskers, their properties and their application in nanocomposite field. Biomacromolecules, 2005, 6(2), 612–626.
[12] Dalmas, F., Cavaillé, J. Y., Gauthier, C., Chazeau, L., & Dendievel, R. Viscoelastic behavior and electrical properties of flexible nanofiber filled polymer nanocomposites. Influence of processing conditions. Compos. Sci. Technol., 2007, 67(5), 829–839.
[13] Woehl, M. A. (2009). Bionanocompósitos de amidoplastificado com glicerolreforçados com nanofibras de celulosebacteriana.
[14] Bajpai, P. K., Singh, I., &Madaan, J. Development and characterization of PLA-based green composites: A review. J. Thermoplastic Compos. Mater., 2014, 27(1), 52–81.
[15] La Mantia, F. P., &Morreale, M. Green composites: A brief review. Composites Part A: Appl. Sci. Manuf., 2011, 42(6), 579–588.
[16] Tate, J. S., Akinola, A. T., & Kabakov, D. Bio-Based Nanocomposites: An Alternative to Traditional Composites. J. Technol. Stud., 2009, 35(1), 25–32.
[17] Mano, J. F., Silva, G. A., Azevedo, H. S., Malafaya, P. B., Sousa, R. A., Silva, S. S., … & Neves, N. M. Natural origin biodegradable systems in tissue engineering and regenerative medicine: present status and some moving trends. J. Royal Soc. Interface, 2007, 4(17), 999–1030.
[18] Caillol, S., Desroches, M., Carlotti, S., Auvergne, R., &Boutevin, B. Synthesis of new polyurethanes from vegetable oil by thiol-ene coupling. Green Mater., 2013, 1(1), 16–26.
[19] Kaushik, A., Singh, M., & Verma, G. Green nanocomposites based on thermoplastic starch and steam exploded cellulose nanofibrils from wheat straw. Carbohydr. Polym., 2010, 82(2), 337–345.
[20] Guimarães, J. L., Wypych, F., Saul, C. K., Ramos, L. P., &Satyanarayana, K. G. Studies of the processing and characterization of corn starch and its composites with banana and sugarcane fibers from Brazil. Carbohydr. Polym., 2010, 80(1), 130–138.

[21] Liu, D., Zhong, T., Chang, P. R., Li, K., & Wu, Q. Starch composites reinforced by bamboo cellulosic crystals. Bioresour. Technol., 2010, 101(7), 2529–2536.
[22] Baishya, P., &Maji, T. K. Studies on effects of different cross-linkers on the properties of starch-based wood composites. ACS Sustainable Chem. Eng., 2014, 2(7), 1760–1768.
[23] Ramírez, M. G. L., Satyanarayana, K. G., Iwakiri, S., de Muniz, G. B., Tanobe, V., & Flores-Sahagun, T. S. Study of the properties of biocomposites. Part I. Cassava starch-green coir fibers from Brazil. Carbohydr. Polym., 2011, 86(4), 1712–1722.
[24] Famá, L., Gerschenson, L., & Goyanes, S. Starch-vegetable fibre composites to protect food products. Carbohydr. polym., 2009, 75(2), 230–235.
[25] Guan, J., & Hanna, M. A. Selected morphological and functional properties of extruded acetylated starch–cellulose foams. Bioresour. Technol., 2006, 97(14), 1716–1726.
[26] Azeredo, H. M., Mattoso, L. H. C., Wood, D., Williams, T. G., Avena-Bustillos, R. J., & McHugh, T. H. Nanocomposite edible films from mango puree reinforced with cellulose nanofibers. J. food sci., 2009, 74(5), N31–N35.
[27] Lee, S. H., & Wang, S. Biodegradable polymers/bamboo fiber biocomposite with bio-based coupling agent. Composites Part A: Appl. Sci. Manuf., 2006, 37(1), 80–91.
[28] Le Duigou, A., Deux, J. M., Davies, P., & Baley, C.. PLLA/flax mat/balsa bio-sandwich—environmental impact and simplified life cycle analysis. Appl. Compos. mater., 2012, 19(3–4), 363–378.
[29] Le Duigou, A., Deux, J. M., Davies, P., &Baley, C. PLLA/flax mat/balsa bio-sandwich manufacture and mechanical properties. Appl. Compos. Mater., 2011, 18(5), 421–438.
[30] Qu, P., Gao, Y., Wu, G., & Zhang, L. Nanocomposites of poly (lactic acid) reinforced with cellulose nanofibrils. BioResources, 2010, 5(3), 1811–1823.
[31] Graupner, N., Herrmann, A. S., & Müssig, J. Natural and man-made cellulose fibre-reinforced poly (lactic acid)(PLA) composites: An overview about mechanical characteristics and application areas. Composites Part A: Appl. Sci. Manuf., 2009, 40(6–7), 810–821.
[32] Bodros, E., Pillin, I., Montrelay, N., & Baley, C. Could biopolymers reinforced by randomly scattered flax fibre be used in structural applications?. Compos. Sci. Technol., 2007, 67(3–4), 462–470.
[33] Shih, Y. F., Huang, C. C., & Chen, P. W. Biodegradable green composites reinforced by the fiber recycling from disposable chopsticks. Mater. Sci. Eng.: A, 2010, 527(6), 1516–1521.
[34] Vazquez, A. & Alvarez, V.A. (2009). Starch/cellulose fibers. Biodegradable Polymer Blends and Composites from Renewable Resources. Editor Long Yu. John Wiley & Sons Inc., Canada, 241–286.
[35] Scudamore, R. J., & Cantwell, W. J. The effect of moisture and loading rate on the interfacial fracture properties of sandwich structures. Polym. Compos., 2002, 23(3), 406–417.
[36] Tantatherdtam, R., Tran, T., Chotineeranat, S., Lee, B. H., Lee, S. N., Sriroth, K., & Kim, H. J. Preparation and Characterization of Cassava Fiber-Based Polypropylene and Polybutylene Succinate Composites. Kasetsart J. (Nat. Sci.), 2009, 43, 245–251.
[37] Torres, J. P., Hoto, R., Andrés, J., & García-Manrique, J. A. Manufacture of green-composite sandwich structures with basalt fiber and bioepoxy resin. Adv. Mater. Sci. Eng., 2013, 214506.
[38] Haldar, S., Imo, J.K., Bruck, H.A. (2011) Mechanical behavior of bio-inspired sandwich composites. Experimental and Applied Mechani. Proulx T (editor),Vol.6, Conference Proceedings of the Society for Experimental and Mechanics Series.
[39] Zhu, X., Kim, B.J., Wang, Q., Wu, Q. Recent advances in the sandwich insulation properties of biobased materials. Biores, 2014, 9, 1764–1768.
[40] Dweib, M. A., Hu, B., O'donnell, A., Shenton, H. W., & Wool, R. P. All natural composite sandwich beams for structural applications. Compos. Struct., 2004, 63(2), 147–157.

[41] Hong, C. K., & Wool, R. P. Low dielectric constant material from hollow fibers and plant oil. J. Nat. Fibers, 2004, 1(2), 83–92.
[42] Ning, H., Janowski, G. M., Vaidya, U. K., & Husman, G. Thermoplastic sandwich structure design and manufacturing for the body panel of mass transit vehicle. Compos. Struct., 2007, 80(1), 82–91.
[43] Way, C., Dean, K., Wu, D. Y., &Palombo, E. A. Polylactic acid composites utilising sequential surface treatments of lignocellulose: chemistry, morphology and properties. J. Polym. Environ., 2011, 19(4), 849–862.
[44] Fabunmi, O. O., Tabil, L. G., Panigrahi, S., & Chang, P. R. Effects of incorporating polycaprolactone and flax fiber into glycerol-plasticized pea starch (p. 1). Am. Soc. Agric. Biol. Eng., 2009, 841–848. https://doi.org/10.1007/s10924-011-0374-5.
[45] Ashori, A. Wood–plastic composites as promising green-composites for automotive industries!. Bioresour. Technol., 2008, 99(11), 4661–4667.
[46] Nakamura, R., Goda, K., Noda, J., & Ohgi, J. High temperature tensile properties and deep drawing of fully green composites. eXPRESS Polym. Lett., 2009, 3, 1.
[47] Bax, B., & Müssig, J. Impact and tensile properties of PLA/Cordenka and PLA/flax composites. Compos. Sci. Technol., 2008, 68(7–8), 1601–1607.
[48] Agarwal, M., Xing, Q., Shim, B. S., Kotov, N., Varahramyan, K., & Lvov, Y. Conductive paper from lignocellulose wood microfibers coated with a nanocomposite of carbon nanotubes and conductive polymers. Nanotechnology, 2009, 20(21), 215602.
[49] Pandey, J. K., Chu, W. S., Lee, C. S., & Ahn, S. H. (2007, October). Preparation characterization and performance evaluation of nanocomposites from natural fiber reinforced biodegradable polymer matrix for automotive applications. In International Symposium on Polymers and the Environment: Emerging Technology and Science, BioEnvironmental Polymer Society (BEPS).
[50] Zweig, S. E. From smart tags to brilliant tags: Advances in drug stability monitoring. Biopharm. Int., 2005, 18(11), 36–44.

M.I.J. Ibrahim, S.M. Sapuan, E.S. Zainudin,
M.Y.M. Zuhri, Ahmed Edhirej

2 Corn (maize) – its fibers, polymers, composites, and applications

A review

Abstract: Corn or maize is a tropical cereal plant. It was domesticated for the first time about 8,000 years ago. In recent times, the demand for corn has flourished dramatically for use in production of various food and edible oils as well as in manufacturing biocomposites and biopolymers. Furthermore, corn plant is the second largest source of renewable energy in the form of bioethanol via fermentation process for the sugar glucose of the corn starch and cellulose of corn fibers. The main aim of this chapter is to present a comprehensive study about corn plant as an essential source of biodegradable polymers, and fiber-based biocomposites along with its current and potential applications. Moreover, this chapter demonstrates the most recent developments of corn biocomposites and gives a detailed report about surface treatments, extraction methods, and mechanical properties of corn starch and corn fibers as well.

Keywords: Corn biopolymers, biocomposites, physiochemical properties, surface treatment

2.1 Introduction

The contemporary environmental concerns such as global warming, nondegradable disposal materials, air and water contamination, and deforestation forced the researchers and scientists to move toward manufacturing and developing ecofriendly engineering materials from renewable sources to replace conventional nonbiodegradable materials in several applications that could preserve the green environment [1]. Synthetic fibers from organic or nonorganic materials along with petroleum-based materials are extensively used as matrix and reinforcements in modern composites. Therefore, the sector of natural composite materials has

M.I.J. Ibrahim, E.S. Zainudin, M.Y.M. Zuhri, Ahmed Edhirej, Department of Mechanical and Manufacturing Engineering, Universiti Putra Malaysia, Serdang, Selangor, Malaysia
S.M. Sapuan, Department of Mechanical and Manufacturing Engineering, Universiti Putra Malaysia, Serdang, Selangor, Malaysia; Institute of Advanced Technology (ITMA), Universiti Putra Malaysia, Serdang, Selangor, Malaysia; Institute of Tropical Forestry and Forest Products (INTROP), Universiti Putra Malaysia, Serdang, Selangor, Malaysia

https://doi.org/10.1515/9783110603699-002

recorded a rapid development in manufacturing renewable and sustainable reinforced composites from natural sources to replace man-made counterpart materials [2]. Natural fibers are characterized by low density and porous cell structure, which made them increasingly common and are available in abundance. They are also nonabrasive, and have lower health hazards through handling and processing [3, 4]. Composite materials are material systems manufactured by combining two or more compatible elements having different physical and chemical properties. The structural properties and performance of the new generated materials are entirely different from the individual component. The newly produced material is generally offering a low cost, biodegradable characteristics, higher strength, lighter, and recyclability [5]. In order to improve and increase the mechanical characteristics and moisture resistance of the composite materials, it is desirable to hybridize the natural fiber-like synthetic fiber and kenaf [6].

In recent decades, the green technology has focused on producing natural fibers and biopolymers (biodegradable materials) from agricultural crops such as corn, banana, cassava, pineapple, rubber wood, palm oil and rice. These renewable resources could substitute nongreen materials in many applications [7, 8]. The characteristics of natural plant fibers and polymers are based on origin, location, quality of the plant, weather, and processing; furthermore, they are highly affected by their physicochemical properties such as degree of polymerization, and cellulose content [9]. The agricultural residues from different plants could be an essential source for obtaining natural fibers. This source is costless and is considered as recyclability process [10]. The extracted starches from agricultural crops offer several advantages making them an excellent alternative to synthetic polymers in plastics industries due to their very low cost, nontoxicity, biodegradability, availability, and nonabrasiveness [11].

Corn (maize) is one of the most abundant agricultural cereals and grains on the world. According to the FAO organization, the total world production of corn reached 602,026,822 Mt in 2002. Globally, the demand for corn is growing up until becoming the third important food grain after rice and wheat [12]. In addition, corn is considered as the main source of starch that is commercially available, besides other minor sources such as rice, wheat, potato, and cassava. Starch is a water-soluble polymer, which is characterized by acceptable mechanical properties and biodegradability. Moreover, it is a relatively cost-effective choice by the combination of two main polymers amylopectin and amylose with different quantities of each component [13]. Furthermore, in recent years, corn plant has become an important source of biofuel production; hence, many fuel industries and organizations are moved toward extracting bioethanol from corn fiber, where thousands of hectares of agricultural land were allocated for maize cultivation. Ethanol from biosources is extensively recognized as an ecologically friendly, potentially inexpensive, and acceptable as alternative for gasoline or as an additive to petroleum fuels [14]. However, few researches have been performed to date on the significance of corn polymers, fibers and its composites. Hence, this chapter presents the latest developments in researches about corn

polymers and fibers from corn plant and their composites. It also demonstrates the recent product development along with the challenges and efforts that have made to improve the characteristics of corn fiber composites. This chapter also attempts to discover other possible applications of corn and its fiber composites to additionally develop corn plant as an innovative crop in the near future.

2.2 Corn plant

2.2.1 History of corn plant

Corn or maize, a tropical cereal plant, was domesticated for the first time in Central America nearly 8,000 years ago. The world demand for corn has increased dramatically in the recent times, where in 2014, the total world production of corn estimated by 1.04 billion tons, which is equivalent to 31% of the world's cereal production [15]. There are six types of corn plant, namely, dent, flint, pop, flour, pod, and sweet corn, which vary significantly in physical and chemical characteristics. Dent corn is rightly called dent due to the dimple that forms at the center of the corn's grain. Approximately 99% of the world dent corn production is in the USA. It is characterized by mealy texture and bland flavor; moreover, much of the granule is starch which made it as an efficient raw material. Dent corn is used for producing natural corn syrup, beverages, and sanitizers, as well as in ethanol production. Flint corn is also called Indian corn. It is mostly grown in South and Central America and is distinguished by a glassy tough outer shell characterized by a varied range of colors, which is used as food source and in decoration. Popcorn has a tough exterior shell with a little amount of soft starch content at the center. It is commonly used for human consumption. Flour corn characterized by soft starchy center and soft outer shell makes it easier to grind to be used in baked foods. Pod corn characterized by unique kernel with a multicolor pattern is used for ornamental purposes rather than commercial purposes. Sweet corn is the most common sort of corn and is typically available in groceries. Essentially, its kernel contains more sugar than starch. These differences in corn types have been attributed to environmental factors [12]. In general, an individual corn plant consists of one or more stalks (stems) grown up from a set of short roots. The stalk branches at each node ended in inflorescences [16]. A fully grown corn plant has about 15–20 nodes and a jointed, bamboo-like culm or stem. Both the male and female flowers are borne in particular structures known as the ear shoot and tassel, respectively [17]. Figure 2.1 shows the main parts of a typical corn plant.

The growing of environmental issues has encouraged the production of biodegradable materials from ecofriendly resources to substitute nonbiodegradable materials in several applications. Among them, corn plant composites offer a considerable amount of advantages for the replacement of artificial plastics due to

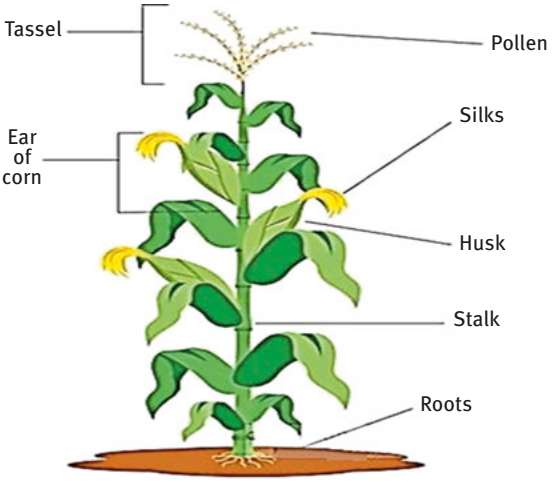

Figure 2.1: Corn plant parts [18].

their availability and biodegradability [11]. Furthermore, maize is used extensively in the production of bioethanol, which is currently the main source of starch and is the second largest biofuel source after soybean. The starch of corn plant is a valuable component to food factories. It is being usually used as a bulking agent, gelling agent, water retention agent, and thickener [19]. Each corn kernel (granule) contains more than 70% starch in its composition and the rest is hemicellulose/cellulose, protein, oil, sugar, and ash. Corn starch is a polymer type alpha-linked glucose that can be fermented to bioethanol and decomposed to glucose monomers. Grain processing industry modified starch via chemical, physical, or genetic methods to be used in the food and nonfood applications [20]. Table 2.1 shows the composition of corn kernel.

Additionally, corn plant is a source of natural fibers. Many fibers are extracted from its stalk, straw, and husk. Among all agricultural bioproducts, corn fiber offers

Table 2.1: Corn grain composition [20].

Composition	Amount (%)
Starch	72
Hemicellulose/cellulose	10.5
Protein	9.5
Oil	4.5
Sugar	2
Ash	1.5
Total	100%

some favorable features such as low cost (which is saving about 90% of cost in comparison with other agricultural fibers) and is more available than other natural fibers [21].

2.2.2 Bioethanol from corn

The growth of human population along with the progressive economic development, the world demand for energy, is increasing dramatically. Nevertheless, the contemporary energy source is the fossil fuel, which is a noncontinuous source and is not ecofriendly to the environment. This highlights the need to renewable energy sources, such as agricultural crops and biofuels. Hence, the biological ethanol is produced by fermenting the sugar components of starches and Stover (leaves and stalks) fiber extracted from various plant resources. Among them, maize plant is the second largest source of biofuel after soybean and is increasingly being used as an alternative for petroleum fuel [22]. Maize Stover contains a substantial amount of cellulose-type beta-linked glucose polymer, which is more difficult to decompose to sugar glucose than the alpha-linked polymer in starch [20]. The potential production of ethanol from corn is influenced by climatic and weather conditions and crop management operations as well. In 2000, in the United States about 1.48 billion gallons of bioethanol was merged with gasoline to be used in automobiles. Likewise, the generated bioethanol in the United States between 1996 and 2007 has recorded steep jump in production from 4.16 billion liters to 24.6 billion liters (Association of Renewable Fuels, 2008). Furthermore, the anticipated use of biofuel by 2022 was estimated in 2007 by about 136 billion liters, of which half of this amount could be produced from corn starch (United States Department of Energy, 2007) [23].

Corn granule contains more than 70% starch-type alpha-linked glucose polymer which is decomposed to sugar glucose and then fermented to ethanol, and most of the bioethanol fuels in the world are extracted by either wet milling or dry milling processes [20]. The first step of bioethanol production converts lignocellulose in starch to sugar by adding enzymes and in the second step, fermentation of sugars by using different yeasts [24]. In the wet milling process, corn is converted to corn oil, and starch-based products such as ethanol, corn syrups, or corn starch; meanwhile, the outcomes from dry milling process are ethanol and animal food products. Due to modern technology in energy generation and fuel extraction, the quantity of bioethanol produced from one bushel of maize increased steadily from around 2 gallons to 2.8 gallons [20].

Eventually, bioethanol from maize plants could be generated just from two parts: the granule, which is primarily made of starch, and Stover, which is mainly made of cellulosic and lignin components. To produce ethanol from them efficiently, a series of approaches via genetic engineering have been discovered. One

approach is adapting the physiochemical characteristics of starch or lignocellulose with the aim of converting them easily to the required products. The other approach is to provide biomass conversion enzymes [22].

2.3 Corn starch

Corn plant is the main source of commercial starch available, and the maize granule contains almost more than 70% of starch beside protein, oil, sugar, and ash [20]. Corn starch is a semicrystalline polymer consisted of a combination of a linear polysaccharide amylose and an extremely branched polysaccharide amylopectin [25, 26]. Roughly more than 80% of world starch production is from corn, and other important botanical sources of starch are cassava, rice, wheat, and potato. Table 2.2 displays the approximate 2015 production of starch from different sources along with the estimated production of raw materials [27].

Table 2.2: World 2015 starch and raw material production [27].

Production and uses	Corn starch	Cassava starch	Wheat starch	Potato starch	Rice starch
2015 global production (million tons/year).	64.6	10.2	6	3.4	0.05
2011 global production of raw material (million tons/year).	880	250	704	374	723

The granule of corn starch composed of linear amylose ranged between 20% and 28%, and the rest is amylopectin [28]. Corn starch is used extensively in cereal processing industries. It is a valuable ingredient used in applications of food and nonfood industries. The modified maize starch by genetic and physiochemical methods is widely used as a reinforcement matrix to composites. Besides the amylopectin and the linear amylose, the chemical composition of maize starch granule contains minor ingredients of proteins, lipids, and minerals, and the amount of these ingredients varies based on the botanical source [5]. Table 2.3 shows the approximate percentages of minor chemical composition of maize starch from different references. Likewise, the attractive characteristics of corn starch such as biodegradability, natural availability, low cost, and ease of exposing to chemical modifying lead to many other applications including medical instruments, packaging, furniture, and alternative to plastic parts of automobiles [29].

Table 2.3: Minor ingredient of maize starch from different references.

Reference	Lipids (%)	Protein (%)	Ash (%)	Phosphorus (%)
[27]	0.6–0.8	0.4	0.1	0.01–0.02
[30]	0.7	0.35	0.1	0.02

2.3.1 Corn starch isolation

The extraction methods of starch have great influence on its physical properties and chemical composition. These influence both physiochemical properties and kernel structure of starch, attributed to nonrigid composition structure of starch granules [31]. All processes of starch isolation almost pass through the same steps and procedures. The first step is to pick up and clean well the corn kernels to remove broken kernels and foreign materials, and then the cleaned corn kernels steep into the steeping solution with certain concentration for interval of time, in order to obtain soft kernels and optimal separation of corn components. During steeping process, the kernels absorb the steeping solution [32]. Different steeping solutions such as sodium metabisulfite, sodium hydrogen sulfite, potassium metabisulfite, and sulfur dioxide are used. In the second step, the pericarp and germs are removed manually followed by adding distilled water to the slurry and grind it whether by lab blinder or mortar. In the next step, the ground slurry is screened through a proper sieve, and the residue is washed with distilled water until becoming free of starch. Then the filtrated starch–protein mixture is separated by sedimentation or centrifugation; lastly, the separated starch is collected and dried in an oven at certain temperature and time. Table 2.4 lists different methods of starch extraction.

2.3.2 Corn starch film preparation

The methods for preparing starch-based films follow almost the same procedures using casting technique, where a certain amount of corn starch is sprinkled in distilled water by adding the required plasticizer in order to achieve polysaccharide suspensions [37]. To obtain a full dispersion, the mixture is stirred constantly at a certain interval of time with a magnetic stirrer. Afterward the desired plasticizer is loaded into a polysaccharide mixture with the known weight/weight percentage. The suspension is then transferred to a water bath at a required temperature and time by stirring with a magnetic stirrer. Thereafter, the homogenous suspension is cooled in a Teflon casting plate. Following that the plate is dried on an air circulation oven, and then the dried film is cut to rectangular pieces and stored at ambient condition before the characterization process [13, 38, 39].

Table 2.4: Different methods of starch isolation.

Reference	Maize quantity	Steeping solution type	Steeping solution quantity and concentration	Steeping time and temperature	Filtration method	Separation method
[31]	10 kernels	Sodium metabisulfite	5 mL, 0.67%	48–72 h at 45 °C	30 µm nylon filter	Centrifugal
[33, 34]	500 g	Sodium hydrogen sulfite	1.25 L, 0.1%	20–24 h at 50 ± 2 °C	Nylon cloth with 100 mesh	Centrifugal
[12]	300 g	Sodium hydrogen sulfite	0.16%	12 h at 50 °C	Nylon cloth with 100 mesh	Sedimentation
[35]	1 kg	Distilled water	4 L	12 h at 4 °C	75 µm mesh sieve	Centrifugal
[19]	500 g	Sodium hydrogen sulfite	1.25 L, 0.1%	12–20 h at 50 °C	Nylon cloth with 0.15 mm	Centrifugal
[36]	–	Potassium metabisulfite	–	30 min	Mesh sieve 149 µm	Decantation
[27]	–	Sulfur dioxide	–	20–24 h at 48–52 °C	–	Centrifugal

2.3.3 Corn starch properties

Physicochemical properties

Amylose and amylopectin content (%)

A technique developed by Williams, Kuzina, and Hlynka (1970) is usually used to determine the amount of amylose and amylopectin on extracted starch [12, 40, 41]. In general, the amylose content on starches range between 14% and 29%, and the rest is amylopectin [42, 43]. Starch with only amylopectin and zero amylose is called "waxy" and is present in corn, cassava, wheat, potato, and rice starches [27]. A part of Table 2.5 shows the amylose and amylopectin content in corn starch with definite number of molecules and degree of polymerization per gram of corn starch.

Swelling power (g/g) and solubility (%)

Swelling and solubility of starch is an index used to identify interactions between the starch chains and water molecules in both crystalline and amorphous zones [35]. Zakpaa et al. [44] employed a method to obtain swelling power and solubility of corn starch, where a gram of corn starch mixed with distilled water is placed in a weighed graduated centrifuge tube. Then the mixture is heated up to 70 °C for 15 min with continuous stirring. Afterward the mixture is removed and cooled at room temperature, followed by centrifugation at 2,200 rpm for 15 min [19]. The swelling power represents the ratio between the weight of wet sedimented slurry to its dry weight, and the solubility expressed by the ratio between evaporating the supernatant to the weight of residue [45]. First part of Table 2.5 shows the swelling power and solubility properties of corn starch.

Light transmittance (%) and turbidity

A technique developed by Craig et al. is commonly utilized to measure the light transmittance of corn starches paste [46]. About 100 g of maize starch was heated in water bath at 90 °C for 1 h with constant stirring. The starch paste was cooled and then stored for 5 days in a refrigerator; thereafter, the transmittance was measured by a spectrophotometer-type Shimadzu UV-1601 (Shimadzu Corporation, Kyoto, Japan). The percentage of transmittance was calculated when water blank reaches 640 nm by a colorimeter [47]. The findings that show low light transmittance by corn starch is due to granule morphology. The degree of light transmittance could be increased by acetylation treatment which induced swelling power [36].

Turbidity of starch suspensions increased gradually during storage time, which is attributed to the good interaction between amylopectin chains and leached out amylose. Figure 2.2 shows the effect of storage time in corn starch turbidity. This interaction generated junction region, which scatters and reflects light [48]. During storage of

Table 2.5: Properties of corn starch.

Swelling power (g/g) and solubility (%)		**Reference [52]**	**Reference [53]**
	1. Starch concentration	1.0	2.0
	2. Temperature (°C)	95	95
	3. Swelling power (g/g)	23	11
	4. Solubility (%)	17	18
Retrogradation Properties		Reference [54]	Reference [55]
	1. Starch:water ratio	1:3	3:7
	2. Storage surroundings [days/temperature (°C)]	7/4	7/−22
	3. Enthalpy change of starch *DH* (J/g)	5.8	3
Pasting properties		Reference [56]	Reference [54]
	1. Starch concentration (%)	8	8
	2. Pasting temperature (°C)	82	82
	3. Max. viscosity (mPa s)	2,100	1,800
	4. Cold paste viscosity (mPa s)	2,000	2,000
Morphological properties [27]	1. Shape		Round, polygonal
	2. Diameter, range (mm)		5–20
	3. Volume mean diameter (mm)		15
	4. Number mean diameter (mm)		13
	5. Number of granules per g starch $\times 10^8$		6
	6. Specific surface area (m^2/kg)		270
Amylose and amylopectin content [30]	1. Amylose content (%)		28
	2. Amylopectin content (%)		72
	3. Amylose, degree of polymerization (DP)		800
	4. Amylopectin, degree of polymerization $\times 10^6$		2
	5. Number of amylose molecules per g starch $\times 10^{20}$		130
	6. Number of amylopectin molecules per g starch $\times 10^{17}$		130
	7. Ratio of number of molecules of amylose:amylopectin		1,000
	8. Average degree of polymerization of starch molecules		3,000

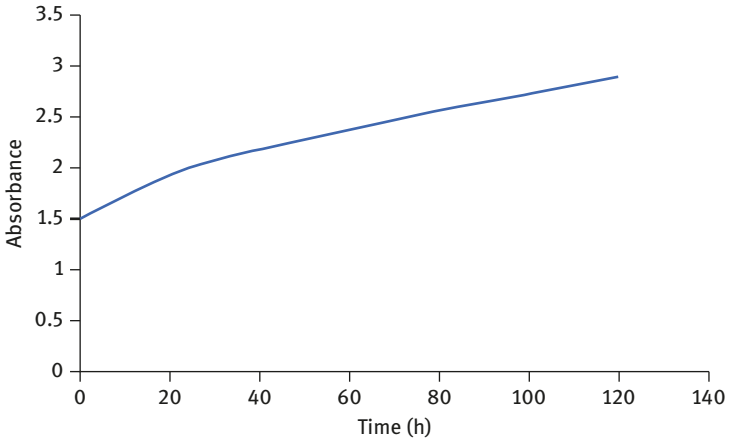

Figure 2.2: Effect of storage on turbidity of corn starch [36].

starch paste, the development of turbidity values influenced by many factors included kernel swelling, and filtered amylose and amylopectin, as well as amylose and amylopectin chain length [49].

Pasting properties

Pasting is a process of measuring the swelling index of the starch kernel, polysaccharides leaching, and change in viscosity and basic formation of amylose after gelatinization [50]. Both of a viscoamylograph or a rapid viscoanalyzer could be used to measure the viscosity of starch; meanwhile the pasting temperature could be observed through increasing of onset viscosity at the end of the cooling and heating cycle [27]. Figure 2.3 shows the pasting properties of corn starch compared with other famous sources of starch, and Table 2.5 shows the pasting properties of corn starch measured by a rapid viscoanalyzer.

Morphological properties

The shape and size of corn starch granule relay on the origin of maize. A scanning electron microscopic device type Jeol JSM-6100 introduced by Jeol Ltd. (Tokyo, Japan) is used to measure the dimensions and shape of starch granule [12]. Figure 2.4 shows the shape of corn starch granule. The mean diameters of granules could be measured based on either the weight of granules or the number of granules. The following formulas are used to calculate the number mean diameter and volume mean diameter:

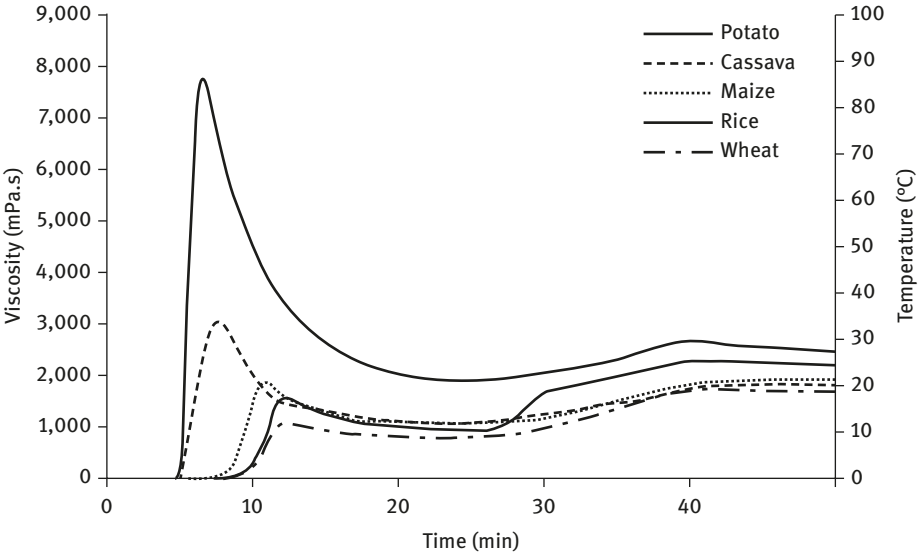

Figure 2.3: Pasting properties of different starch sources [27].

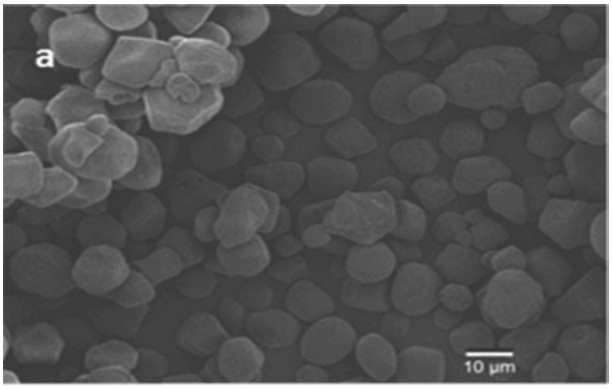

Figure 2.4: Shape of corn starch granule [27].

$$Dn = \frac{\sum_1^n dl_i}{n} \tag{2.1}$$

$$Dv = \frac{\sum_1^n dl_i^4}{\sum_1^n dl_i^3} \tag{2.2}$$

where Dn is the number mean diameter, Dv is the number mean volume, dl_i is the particle (i) diameter, and n is the total particle number [27].

Retrogradation properties

The term retrogradation is used to illustrate the effect of cooling and storage on starch properties. To eliminate retrogradation, either modify starch by recrystallization or use amylopectin starch and increase the storage stability [51]. Corn starch was heated at 85 °C for 30 min, and then cooled rapidly in frozen water to ambient temperature. Then the sample of starch was kept at 4 °C for 120 h; finally, the starch was centrifugalized at 3,200 rpm for 15 min. The percentage of released water after centrifugation represents the retrogradation [12]. Table 2.5 exhibits properties of corn starch, including swelling power and solubility, retrogradation, pasting, morphological property, and amylose and amylopectin content.

Rheological properties

The volume and shape of swollen granule along with deformability, concentration, and composition of the continuous phase are parameters used to determine the rheological behavior of starch paste [57, 58]. The rheological properties such as loss modulus (G''), storage modulus (G'), storage modulus temperature (TG'), and loss factor (tan ϱ) are determined by the branded dynamic rheometer device (Carri-Med CSL2-100, TA Instruments Ltd., Surrey, England), where the corn starch samples are placed into rheometer and subjected to certain temperature for certain time at a constant rate [6]. Table 2.6 shows the rheological properties of different types of corn starch.

Table 2.6: Rheological properties of different corn starch types [12].

Corn type	TG' (°C)	Peak G' (Pa)	Peak G'' (Pa)	Breakdown in G' (Pa)	Peak tan ϱ
Dent corn	73.7	2,919	427	1,177	0.146
Pop corn	73.4	3,620	438	2,020	0.122
Baby corn	73.7	4,884	813	2,944	0.166

Thermal properties (gelatinization)

Differential scanning calorimetry (DSC) is used to evaluate the thermal properties of starch. Thermal parameters such as peak gelatinization temperature (T_p), gelatinization onset temperature (T_o), gelatinization conclusion temperature (T_c), and enthalpy of gelatinization (ΔH) are measured by DSC [45, 59]. A

Table 2.7: Thermal properties of corn starch.

References	Starch-to-water ratio	T_o (°C)	T_P (°C)	T_c (°C)	T_c_T_o (°C)	ΔH (J/g)
[36]	–	69.6 ± 0.6	73.3 ± 0.9	75.2 ± 0.8	–	7.3 ± 0.3
[55, 60, 61]	1:3	64–67	68–71	72–75	8–11	11–12
[56]	3:7	63	67	72	9	9
[62]	1:4	67	71	–	–	12
[63]	1:9	66	71	–	–	12

sample of corn starch is steeped on distilling water to achieve a starch–water suspension, and then the sample is sealed tightly and lifted to stand for 1 h at ambient temperature; later on the sample is placed into DSC to find out the galvanization and thermal characteristics of corn starch. The obtained results are used to identify the functionality of starch [12, 34, 41]. Table 2.7 demonstrates the thermal properties of corn starch.

2.4 Corn fibers

2.4.1 Corn husk fiber

Corn husks fiber is extracted chemically from the husks of corn ears via an alkalization process, where the majority of noncellulose materials (lignin, pectin, waxes, proteins, and ash) are removed. The remainder are lignocellulosic fiber including fine cellulose fibers and hemicellulose [64, 65]. The approximate chemical composition of corn husk fibers is estimated to be cellulose 43%, hemicellulose 31%, lignin 22%, and ash 1.9% [8]. Reddy and Yang stated that corn husk fiber is a fiber bundle held together by hemicelluloses, lignin, and pectin, where they extracted fiber bundles from corn husks through alkalization technique followed by an enzymatic treatment. The resulting corn husk fiber provided higher toughness and higher elongation with moderate strength and low modulus as reported in Table 2.8, and Figure 2.5 shows the typical stress–strain curve for corn husk fiber.

Table 2.8: Tensile properties of corn husk fibers [67].

Tenacity/g den–1	Elongation (%)	Modulus/g den–1	Work of rupture/g den–1	Moisture regain (%)
2.7 ± 0.11	15.3 ± 2.15	70 ± 01.65	0.23 ± 0.05	9.5

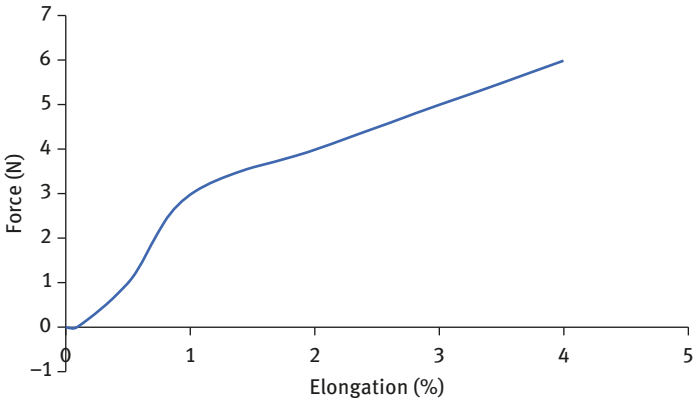

Figure 2.5: A typical stress–strain curve of corn husk fibers [66].

2.4.2 Corn stalk fiber

Corn Stover (leaves and stalks) is also called corn straw, which is the remains generated in the corn manufacturing process such as the maize wet-milling process, and it could be used for several purposes. Corn fiber is like other lignocellulosic materials containing about 70% carbohydrates (cellulose, hemicellulose, and residual starch) [24]. Maize stalk fibers are obtained from maize stem manually. First, maize stalks are cut into desired sizes and shapes. Then the stalks are dried either on oven or in direct sunlight for 2 or 3 days. Later, after collecting the dried stems, the outer skin of the maize stems is removed. Lastly, the required maize stalk fibers are obtained[14]. Table 2.9 shows the chemical composition of corn stalk fiber obtained from different sources, whereas corn straw fiber is obtained by steeping maize straw in distilled water for 24 h and dried in direct sunlight and cut into desired length. Then the straw fiber is extracted from the dried corn straw and soaked into ethanol for 6 h. Later on, the fiber is dehydrated in an oven at 60 °C temperature for 16 h [68].

Table 2.9: Chemical composition of corn stalk fibers.

Cellulose (%)	Hemicellulose (%)	Lignin (%)	References
28–36	23–28	12–16	[68]
38–42	21–23	10–13	[69]
38–40	28	7–21	[70, 71]
40.28	–	19.35	[72]

2.4.3 Corn hull fiber

In addition, there is another type of fiber extracted from the corn granule pericarp (hull). During the process of corn starch isolation, the remains after starch filtration are washed by amylolytic enzymes (at 120 °C for 1 h followed by 90 °C for 1 h) to remove all starch components, after that the detached fiber is washed several times by hot distilled water followed by centrifugalizing the slurry to separate liquid from solid fractions. These solid fractions consist mostly of cellulose and a small amount of lignin [24, 73].

2.4.4 Treatment of corn fiber composites

The most remarkable drawback of natural fibers is their weak bonding with the matrix materials, that is due to tendency of their surfaces to dissolve and mix with water. Therefore, surface treatment is an important step in manufacturing natural fiber polymer composites [74]. To date, many methods of treatment are used in order to enhance mechanical performance for natural fiber composites, these methods include alkali treatment, silane treatment, enzyme treatment, benzoylation treatment, and maleated coupling [21]. Table 2.10 states the different methods of fiber treatment with clarification from the obtained results of each method.

2.4.5 Applications of corn fiber composites

Fibers from lignocellulosic sources like corn plant are used in several applications such as particle boards, construction materials, insulation, human food and animal feed, as well as medical instruments [76]. Chemical substances such as carbon, ammonia, ethanol, methanol, charcoal, acetone, acetic acid, and hydrocarbon oils are extracted from maize lignocellulosic via fermentation and hydrolysis process [77]. Fibers produced from corn Stover and straw could be utilized to manufacture all kinds of paper and paper boards. Lignin is characterized by high energy content and fuel value; thus, it is frequently used as a fuel for burning. Moreover, lignin is used to produce adhesives and binders, but these applications provide limited additional value [78]. Nevertheless, numerous chemical substances such as phenols, acetic acid, ethylene, and charcoal could be obtained from lignin [79]. Corn husks hydrolyze cellulose into single fibers or individual cells to be used for textile products and other industrial applications. For the first time, natural cellulosic fibers are obtained from corn husk with structure and performance properties that would make it appropriate for various high-quality fibrous applications [67]. Maize husk fibers show high performance when used as an acoustic material, where it is tested as a sound absorption material under low-frequency range between 1.6 and

Table 2.10: Methods of fiber treatment [75].

	Treatment method	Treatment substance	Obtained results
1	Alkaline treatment	Sodium hydroxide (NaOH)	1. Modifies cellulose molecular structure 2. Changes crystalline cellulose orientation 3. Forms amorphous region
2	Silane treatment	Coupling agent	1. Forms chemical link between fiber and matrix 2. Provides hydrocarbon chain restrains fiber swelling
3	Acetylation treatment	Acetyl group (CH_3CO)	1. Takes out the existed moisture 2. Improves dimensional stability of fiber 3. Provides rough surface topography
4	Benzoylation treatment	Benzoyl chloride (C_6H_5COCl)	1. Enhances thermal stability of fiber 2. Enhances interfacial adhesion
5	Peroxide treatment	Benzoyl peroxide ($C_{14}H_{10}O_4$)	1. Induces grafting of polyethylene onto fiber surface 2. Initiates radical to react with the hydroxyl group of fiber and matrix 3. Improves thermal stability 4. Reduces moisture absorbing tendency
6	Maleated coupling agents	Maleic anhydride polypropylene (MAPP)	1. Provides efficient interaction between fiber surface and matrix 2. Provides better wettability and interfacial adhesion
7	Sodium chlorite treatment	Sodium chlorite ($NaClO_2$) and chloric acid ($HClO_2$)	1. Removes moisture from fiber surface 2. Enhances hydrophobic nature of fiber
8	Acrylation and acrylonitrile grafting	Acrylic acid (CH_2=CHCOOH)	1. Enhances interfacial bonding between fiber and matrix 2. Improves moisture resistance properties
9	Isocyanate treatment	Isocyanate group (–N=C=O)	1. Provides strong covalent bonds between the fiber and matrix 2. Provides higher moisture resistance properties of fiber
10	Stearic acid treatment	Stearic acid ($CH_3(CH_2)_{16}COOH$) and ethyl alcohol solution (C_2H_5OH)	1. Improves water resistance properties 2. Removes noncrystalline constituents from the fiber structure

(continued)

Table 2.10 (continued)

	Treatment method	Treatment substance	Obtained results
11	Permanganate treatment	Potassium permanganate ($KMnO_4$) and acetone solution $(CH_3)_2CO$	1. Enhances chemical interlocking for better adhesion with matrix 2. Provides higher thermal stability for fiber
12	Triazine treatment	Triazine ($C_3H_3N_3$)	1. Provides linkage between cellulose and coupling agent 2. Provides better moisture resistance properties 3. Provides cross-linking between cellulose and matrix
13	Fatty acid derivate treatment	Oleoyl chloride acid ($C_{18}H_{33}ClO$)	Improves wettability and interfacial adhesion characteristics
14	Fungal treatment	Oxidase enzymes	1. Removes noncellulose components from fiber surface 2. Increases hemicellulose solubility 3. Provides better interlocking between fiber surface and matrix

Table 2.11: Some products from corn fibers.

Products and chemicals	Biomass source	Biomass component	References
Fibers for textiles and composites Lactic acid Ethanol and other alcohols	Corn Stover	Cellulose/hemicellulose	[77, 82–85]
Fiber-reinforced starch foams	Corn stalks	Cellulose	[86]
Adhesives and binders	Corn straw	Lignin	[85, 87–89]
Textile and other industrial applications	Corn husk	Cellulose	[67]
Acoustic material	Corn husk		[80]

3.250 kHz [80]. Table 2.11 shows some of the common chemicals and products from agricultural corn bioproducts.

Consequently, making use of maize fiber composites is a better approach. Nonetheless, when compared to other natural fiber resources, the development of maize fibers' ecofriendly composites recorded less progress. This is attributed to poor mechanical characteristics of corn fiber composites [67, 81].

2.5 Conclusion

Corn plant is abundant and is relatively inexpensive; furthermore, corn is the largest origin of commercial starch available and is the second main source of biofuels. Therefore, corn composites are being used widely in variety of applications. The extracted starch from corn grains offers some structural and functional properties such as exhibiting great variety in gelatinization, rheological, and swelling power properties. Specific alteration in starch structure could be led to enhance chemical, physical, and enzymatic properties. Similarly, additional modifications for corn fibers are still required in order to improve the advantages of such fiber type. Despite of developing and modifying several successful maize composite products, still less progress has been recorded on the development of maize biocomposites as compared to other natural composites. Hence, more researches need to be conducted to reveal the importance of corn biocomposites as well as to promote its utility for the benefits of the society.

References

[1] Ibrahim, M., & Yusoff, M.Z.M. Akademia Baru. J. Adv. Res. Appl. Sci. Eng. Technol., 2018, 10(1),p. 1–17.
[2] Lee, B.-H., Kim, H.-J., & Yu, W.-R.. Fabrication of long and discontinuous natural fiber reinforced polypropylene biocomposites and their mechanical properties. Fibers and Polym., 2009, 10(1), p. 83–90.
[3] Arenas, J.P., & Crocker, M.J. Recent trends in porous sound-absorbing materials. Sound & vibration, 2010, 44(7),p. 12–18.
[4] Fatima, S., & Mohanty, A. Acoustical and fire-retardant properties of jute composite materials. Appl. Acoustics, 2011, 72(2–3), p. 108–114.
[5] Zakaria, N.H., Ngali, Z., & Selamat, M.Z. Preliminary Investigation to Determine the Suitable Mixture Composition for Corn Starch Matrix. in IOP Conference Series: Materials Science and Engineering. 2017. IOP Publishing.
[6] Edhirej, A., et al. Cassava: Its polymer, fiber, composite, and application. Polym. Compos., 2017, 38(3), p. 555–570.
[7] Saheb, D.N., & Jog, J.P. Natural fiber polymer composites: a review. Adv. Polym. Technol, 1999, 18(4), p. 351–363.
[8] Youssef, A.M., El-Gendy, A., & Kamel, S. Evaluation of corn husk fibers reinforced recycled low density polyethylene composites. Mater. Chem. Phys., 2015, 152,p. 26–33.
[9] Nam, S., & Netravali, A.N. Green composites. I. Physical properties of ramie fibers for environment-friendly green composites. Fibers Polym., 2006, 7(4),p. 372–379.
[10] Edhirej, A., et al. Preparation and characterization of cassava bagasse reinforced thermoplastic cassava starch. Fibers Polym., 2017, 18(1), p. 162–171.
[11] Mendes, J., et al. Biodegradable polymer blends based on corn starch and thermoplastic chitosan processed by extrusion. Carbohydr. Polym., 2016, 137, p. 452–458.
[12] Sandhu, K.S., Singh, N., & Kaur, M. Characteristics of the different corn types and their grain fractions: physicochemical, thermal, morphological, and rheological properties of starches. J. Food Eng., 2004, 64(1), p. 119–127.

[13] Aminzare, M., et al. Evaluation of in vitro antioxidant characteristics of corn starch bioactive films impregnated with Bunium persicum and Zataria multiflora essential oils. Annu. Res. Rev. Biol., 2017, 15(5), p. 1–9.
[14] Schell, D.J., et al. A bioethanol process development unit: initial operating experiences and results with a corn fiber feedstock. Bioresour. Technol., 2004, 91(2), p. 179–188.
[15] Singh, R., Ram, L., & Srivastava, R. A journey of hybrids in maize: an overview. Indian Res. J. Extension Educ., 2016, 12(2), p. 340–344.
[16] Weatherwax, P. The history of corn. Scientific Monthly, 1950, 71(1), p. 50–60.
[17] Johri, M., & Coe, E. Clonal analysis of corn plant development. Genetica, 1996, 97(3), p. 291–303.
[18] Hanway, J.J. How a corn plant develops. 1966.
[19] Rayan, A.M., et al. Physicochemical properties of starch isolated from genetically modified corn (Ajeeb YG).
[20] McAloon, A., et al. Determining the cost of producing ethanol from corn starch and lignocellulosic feedstocks. 2000, National Renewable Energy Lab., Golden, CO (US).
[21] Luo, H., et al. Mechanical and thermo-mechanical behaviors of sizing-treated corn fiber/ polylactide composites. Polym. Test., 2014, 39, p. 45–52.
[22] Torney, F., et al. Genetic engineering approaches to improve bioethanol production from maize. Curr. Opin. Biotechnol, 2007, 18(3), p. 193–199.
[23] Persson, T., et al. Maize ethanol feedstock production and net energy value as affected by climate variability and crop management practices. Agric. Syst., 2009, 100(1–3), p. 11–21.
[24] Meszaros, E., et al. Thermal behavior of corn fibers and corn fiber gums prepared in fiber processing to ethanol. J. Anal. Appl. Pyrolysis, 2009, 85(1–2), p. 11–18.
[25] Maiti, M., et al. Synthesis and characterization of corn starch based green composites reinforced with Saccharum spontaneum L graft copolymers prepared under micro-wave and their effect on thermal, physio-chemical and mechanical properties. Polym. Degrad. Stab., 2010, 95(9), p. 1694–1703.
[26] Lu, D., Xiao, C., & Xu, S. Starch-based completely biodegradable polymer materials. Express Polym. Lett., 2009, 3(6), p. 366–375.
[27] Waterschoot, J., et al. Production, structure, physicochemical and functional properties of maize, cassava, wheat, potato and rice starches. Starch Stärke, 2015, 67(1-2), p. 14–29.
[28] Bertoft, E. Understanding starch structure: Recent progress. Agronomy, 2017, 7(3), p. 56.
[29] Guimarães, J., et al. Studies of the processing and characterization of corn starch and its composites with banana and sugarcane fibers from Brazil. Carbohydr. Polym., 2010, 80(1), p. 130–138.
[30] Swinkels, J. Composition and properties of commercial native starches. Starch Stärke, 1985, 37(1), p. 1–5.
[31] Ji, Y., Seetharaman, K., & White, P. Optimizing a small-scale corn-starch extraction method for use in the laboratory. Cereal Chem., 2004. 81(1): p. 55–58.
[32] BeMiller, J.N., & Whistler, R.L. Starch: chemistry and technology. Elsevier: Academic Press. 2009, p. 392–405.
[33] Singh Sandhu, K., & Singh, N. Relationships between selected properties of starches from different corn lines. Int. J. Food Properties, 2005, 8(3), p. 481–491.
[34] Sandhu, K.S., Singh, N., & Malhi, N.S. Physicochemical and thermal properties of starches separated from corn produced from crosses of two germ pools. Food Chem., 2005. 89(4): p. 541–548.
[35] Ali, A., et al. Comparative study of the physico-chemical properties of rice and corn starches grown in Indian temperate climate. J. Saudi Soc. Agric. Sci., 2016, 15(1), p. 75–82.
[36] Singh, G.D., et al. Physicochemical, pasting, thermal and morphological characteristics of Indian water chestnut (Trapa natans) starch. Starch Stärke, 2009, 61(1), p. 35–42.

[37] Ghasemlou, M., et al. Physical, mechanical and barrier properties of corn starch films incorporated with plant essential oils. Carbohydr. Polym., 2013, 98(1), p. 1117–1126.
[38] Ghanbarzadeh, B., Almasi, H., & Entezami, A.A. Improving the barrier and mechanical properties of corn starch-based edible films: Effect of citric acid and carboxymethyl cellulose. Indus. Crops Prod., 2011, 33(1), p. 229–235.
[39] Garcia, M.A., Martino, M.N., & Zaritzky, N.E. Microstructural characterization of plasticized starch based films. Starch Stärke, 2000, 52(4): p. 118–124.
[40] Williams, P., Kuzina, F., & Hlynka, I. Rapid colorimetric procedure for estimating the amylose content of starches and flours. Cereal chemistry, 1970.
[41] Sandhu, K.S., & Singh, N. Some properties of corn starches II: Physicochemical, gelatinization, retrogradation, pasting and gel textural properties. Food Chem., 2007, 101(4), p. 1499–1507.
[42] Manaois, R.V. Modification of rice starch properties by addition of amino acids at various pH levels. 2009.
[43] Juliano, B., et al. Varietal differences in properties among high amylose rice starches. Starch Stärke, 1987, 39(11), p. 390–393.
[44] Zakpaa, H., Al-Hassan, A., & Adubofour, J. An investigation into the feasibility of production and characterization of starch from Apantu plantain (giant horn) grown in Ghana. Afr. J. Food Sci., 2010, 4(9), p. 571–577.
[45] Sui, Z., et al. Effects of heat–moisture treatment reaction conditions on the physicochemical and structural properties of maize starch: Moisture and length of heating. Food Chem., 2015, 173, p. 1125–1132.
[46] Craig, S.A., Maningat, C.C., Seib, P.A., & Hoseney, R.C. Starch paste clarity. Cereal Chem, 1989, 66, p. 173–182.
[47] Sandhu, K.S., et al. A comparison of native and oxidized normal and waxy corn starches: Physicochemical, thermal, morphological and pasting properties. LWT-Food Sci. Technol., 2008, 41(6), p. 1000–1010.
[48] Perera, C., & Hoover, R. Influence of hydroxypropylation on retrogradation properties of native, defatted and heat-moisture treated potato starches. Food Chem., 1999. 64(3): p. 361–375.
[49] Jacobson, M.R., Obanni, M., & Bemiller, J.N. Retrogradation of starches from different botanical sources. Cereal Chem., 1997, 74(5), p. 511–518.
[50] Atwell, W., The terminology and methodology associated with basic starch phenomena. Cereal foods world, 1988. 33: p. 306–311.
[51] Hermansson, A.-M., & Svegmark, K. Developments in the understanding of starch functionality. Trends Food Sci. Technol., 1996. 7(11): p. 345–353.
[52] Ring, S. Some studies on starch gelation. Starch-Stärke, 1985, 37(3), p. 80–83.
[53] Takahashi, S., & Seib, P. Paste and gel properties of prime corn and wheat starches with and without native lipids. Cereal Chem., 1988, 65(6), p. 474–483.
[54] Jane, J., et al. Effects of amylopectin branch chain length and amylose content on the gelatinization and pasting properties of starch. Cereal Chem., 1999, 76(5), p. 629–637.
[55] Teng, L., Chin, N., & Yusof, Y. Rheological and textural studies of fresh and freeze- thawed native sago starch–sugar gels. II. Comparisons with other starch sources and reheating effects. Food Hydrocolloids, 2013. 31(2): p. 156–165.
[56] Setiawan, S., et al. Effects of drying conditions of corn kernels and storage at an elevated humidity on starch structures and properties. J. Agric. Food Chem., 2010, 58(23), p. 12260–12267.
[57] Waterschoot, J., et al.. Starch blends and their physicochemical properties. Starch-Stärke, 2015, 67(1–2), p. 1–13.

[58] Doublier, J., Llamas, G., & Le Meur, M. A rheological investigation of cereal starch pastes and gels. Effect of pasting procedures. Carbohydr. Polym., 1987, 7(4), p. 251–275.
[59] Krieger, K., et al. Thermal properties of corn starch extracted with different blending methods: Microblender and homogenizer. Cereal Chem., 1997, 74(5), p. 553–555.
[60] Schirmer, M., et al. Physicochemical and morphological characterization of different starches with variable amylose/amylopectin ratio. Food Hydrocolloids, 2013, 32(1), p. 52–63.
[61] Hoover, R., Sailaja, Y., & Sosulski, F. Characterization of starches from wild and long grain brown rice. Food Res. Int, 1996. 29(2): p. 99–107.
[62] Anggraini, V., et al. Characterization of cassava starch attributes of different genotypes. Starch-Stärke, 2009, 61(8), p. 472–481.
[63] Li, J.-Y., & Yeh, A.-I. Relationships between thermal, rheological characteristics and swelling power for various starches. J. Food Eng., 2001, 50(3). p. 141–148.
[64] Chen H. Chemical Composition and Structure of Natural Lignocellulose. In: Biotechnology of Lignocellulose. Springer, Dordrecht, 2014. p. 25–71.
[65] Musil, S.S., Keane, P., & Kriven, W. Green Composite: Sodium-Based Geopolymer Reinforced with Chemically Extracted Corn Husk Fibers. Developments in Strategic Materials and Computational Design IV, 2013, p. 123–133.
[66] Yılmaz, N.D. Effects of enzymatic treatments on the mechanical properties of corn husk fibers. J. Text. Inst., 2013, 104(4), p. 396–406.
[67] Reddy, N., & Yang, Y. Properties and potential applications of natural cellulose fibers from cornhusks. Green Chem., 2005, 7(4), p. 190–195.
[68] Li, D., et al. Preparation and characterization of cellulose fibers from corn straw as natural oil sorbents. Ind. Eng. Chem. Res., 2012, 52(1), p. 516–524.
[69] Bavan, D.S., & Kumar, G.M. Morphological and thermal properties of maize fiber composites. Fibers Polym., 2012, 13(7), p. 887–893.
[70] Gomes, A., et al. Development and effect of alkali treatment on tensile properties of Curaua fiber green composites. Compos. Part A: Appl. Sci. Manuf., 2007,. 38(8), p. 1811–1820.
[71] Reddy, N., & Yang, Y. Structure and properties of high quality natural cellulose fibers from cornstalks. Polymer, 2005, 46(15), p. 5494–5500.
[72] Valchev, I., et al. Use of enzymes in hydrolysis of maize stalks. Bioresources, 2009, 4(1), p. 285–291.
[73] Doner, L.W., et al. An improved process for isolation of corn fiber gum. Cereal Chem., 1998, 75(4), p. 408–411.
[74] Koo, G.-H., & Jang, J. Surface modification of poly (lactic acid) by UV/Ozone irradiation. Fibers Polym., 2008, 9(6), p. 674–678.
[75] Kabir, M., et al. Chemical treatments on plant-based natural fibre reinforced polymer composites: An overview. Compos. Part B: Eng., 2012, 43(7), p. 2883–2892.
[76] Reddy, N., & Yang, Y. Biofibers from agricultural byproducts for industrial applications. Trends Biotechnol., 2005, 23(1), p. 22–27.
[77] Majumdar, P., et al. Chemical profile of some lignocellulosic crop residues. Indian J. Agr. Bioch., 2001, 14, p. 29–33.
[78] Bungay, H.R. Confessions of a bioenergy advocate. Trends Biotechnol., 2004, 22(2), p. 67–71.
[79] Burger, H., et al. GK 95/07/475-Transl. serial no. 12907-Use or natural fibres and environmental aspects. Int. Polym. Sci. Technol., 1995, 22(8), p. 25–34.
[80] Sari, N.H., et al. Physical and acoustical properties of corn husk fiber panels. Adv. Acous. Vibr., 2016, p. 8.
[81] Kaparaju, P., & Felby, C. Characterization of lignin during oxidative and hydrothermal pre-treatment processes of wheat straw and corn Stover. Bioresour. Technol., 2010, 101(9), p. 3175–3181.

[82] Van Wyk, J.P. Biotechnology and the utilization of biowaste as a resource for bioproduct development. Trends Biotechnol., 2001, 19(5), p. 172–177.
[83] Mohanty, A., Misra, M., & Hinrichsen, G. Biofibers, biodegradable polymers and biocomposites: an overview. Macromol. Mater. Eng., 2000, 276(1), p. 1–24.
[84] Reddy, N., & Yang, Y. Structure of novel cellulosic fibers from cornhusks. in Papers presented at the meeting-American Chemical Society. Division of Polymer Chemistry. 2004. 45(2): pp. 411–411.
[85] Prabhakar, G., & Raju, D. Value-added chemicals from the byproducts of sugar agro industry. Bioenergy: vision for the new millennium. Eco-Friendly Technologies for Biomass Conversion to Energy and Industrial Chemicals, Tirupati, India, September 1996, 2000: p. 85–89.
[86] Ganjyal, G., et al. Biodegradable packaging foams of starch acetate blended with corn stalk fibers. J. Appl. Polym. Sci., 2004, 93(6), p. 2627–2633.
[87] Paster, M., Pellegrino, J.L., & Carole, T.M. Industrial bioproducts; today and tomorrow, in Industrial bioproducts; today and tomorrow. 2003, DOE-EERE.
[88] Sundstrom, D.W., & Klei, H.E. Uses of by-product lignins from alcohol fuel processes. in Biotechnol. Bioeng. Symp. (United States). 1982: Univ. of Connecticut, Storrs.
[89] Datta, R., & Tsai, S.-P. Lactic acid production and potential uses: a technology and economics assessment. American Chemical Society, Washington, 1997, p. 13.

Part II: **Manufacturing and Properties**

Opeoluwa R. Dada, Kamardeen O. Abdulrahman,
Esther T. Akinlabi

3 Production of biodegradable composites from agricultural waste

A review

Abstract: The development of biodegradable composite as an alternative to nondegradable composite continues to wax stronger. Composite materials are materials popularly formed from the combination of matrix and reinforcements, where one of these is commonly from renewable sources. However, biodegradable composites are produced from the combination of matrix (resin) and reinforcement solely from natural fibers unlike ordinary composites that do contain synthetic polymers which are not biodegradable. Thus, studies are continued to produce biodegradable composites using different biodegradable materials and techniques. Recent activities have led to the development of biodegradable composites with reasonable tensile and flexural characteristics. However, there are shortfalls with regard to some of the biodegradable composites when they come in contact with moisture, which affects their performance under certain conditions as in aqueous medium or under high humidity. Notable works have come up with biodegradable composite materials from common agricultural wastes. Among the common materials that have been studied in the development of biodegradable composites are rice husk, soybean, sugarcane bagasse, and cassava peel. This chapter discusses some of the literature available on biodegradable composites developed mainly from common agricultural products, their properties, production method, challenges, and sustainability.

Keywords: Agricultural waste, biodegradable, composites, matrix, reinforcement

3.1 Introduction

Agricultural wastes or residue is a term used to describe all organic materials that are produced as by-product from harvesting and processing of agricultural crops. Agricultural crops provide food for both humans and animals for their energy. Recently, the waste generated during the harvesting and processing of these crops has

Opeoluwa R. Dada, Esther T. Akinlabi, Department of Mechanical Engineering Science, University of Johannesburg, Johannesburg, South Africa
Kamardeen O. Abdulrahman, Department of Mechanical Engineering Science, University of Johannesburg, Johannesburg, South Africa; Department of Mechanical Engineering, University of Ilorin, Nigeria

https://doi.org/10.1515/9783110603699-003

been deemed to be very beneficial to other industries or sectors. For instance, agricultural waste material has been exploited for heavy metal remediation based on the fact that research has found it to be highly efficient, it is of low cost, and it is a renewable source of biomass [1]. Another example is the use of rice husk, which is one of the most common agricultural wastes to generate clean energy. Precisely, rice husk can be used to provide electricity due to its high calorific value. Furthermore, rise husk ash, which is a by-product of rice husk power plants, can be used in the production of cement for construction purposes [2]. Agricultural wastes can be broadly classified into two major categories based on the time of generation such as primary and secondary wastes or residues.

Primary residues are wastes generated during the time of harvesting agricultural crops such as sugarcane top, maize stalks, coconut empty bunches and frond, paddy straw, and palm oil bunches and fronds. On the other hand, secondary residues are wastes generated during the time of processing and they include, but not limited to, maize cob, coconut shell, paddy husk, coir dust, sawdust, bagasse, palm oil shell, wastewater, fiber, and empty bunches. In general, secondary residues are produced in large amounts; hence, they cannot be exhausted by reusing or recycling for a particular application, which is the motivating factor for investigating its usage in the production of composites in the manufacturing industry rather than just dumping on the landfill sites. Some of the most common agricultural waste materials are shown in Figure 3.1.

Figure 3.1: Images of rice straw, rice husk, corn cobs, and wheat husk.

It is important to note that agricultural wastes are part of crop residues originating from different sources. For example, cereals are from rice, maize or corn, sorghum,

barley, and wheat; millet is from straw, leaves, stalk, husk, peel, and stubbles. Other agricultural wastes originate from cotton, legumes, coffee, tea, groundnut, fruits, and palm oil.

Research has found that various agricultural wastes can be used as raw materials in various sectors such as energy, construction, and manufacturing. More recently, investigations are ongoing in channeling these wastes to produce more biocomposite materials.

3.2 Classification of composites

Composites can be broadly classified into three major categories, namely, particle reinforced, fiber reinforced, and structural. These three categories can also be subdivided into various categories as shown in Figure 3.2.

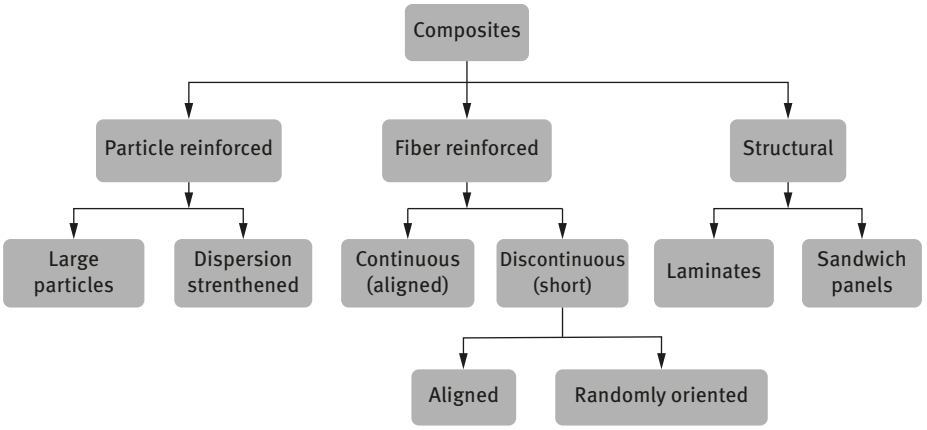

Figure 3.2: Composite classification [3].

3.3 Structural and nonstructural composites

Composite materials can further be classified into structural and nonstructural composites. Structural composites are load-bearing composites and as the name implies they are manufactured in order for them to carry loads. Also, their performance ranges from high to low depending on the purpose they are to serve. Structural composites performance can be improved by chemical modification techniques to modify the fiber properties. On the other hand, nonstructural composites are not designed to carry loads; as a result, they could be made from materials such as

thermoplastics, textiles, and wood particles. The manufacturing process also varies but most common processes include and not limited to thermopressing, sheet and injection molding.

3.4 Biodegradable composites from common agricultural products

Composites are combination of at least two distinct, different materials that are combined together to provide an engineering performance that far exceeds that of any individual component [4]. Also, composites are artificially produced multiphase materials having a desirable combination of the best properties of the constituent phases [3]. In other words, a composite is made up of a primary constituent element and embedded in it is the another constituent element which serves as a reinforcement as shown in Figure 3.3. Composites have been found to be the most advanced and adaptable engineering materials. Despite the fact that composites are capable of meeting diverse design requirement with significant weight savings and high strength to weight loss, the composite industry is still faced with some challenges such as health and safety, emission of volatile organic compounds, energy consumption, and toxicity from manufacturing. The use of composites cuts across many sectors across the world; hence, its importance cannot be overemphasized. In 2011, the world's composite market was estimated to be worth $19.6 billion, and in

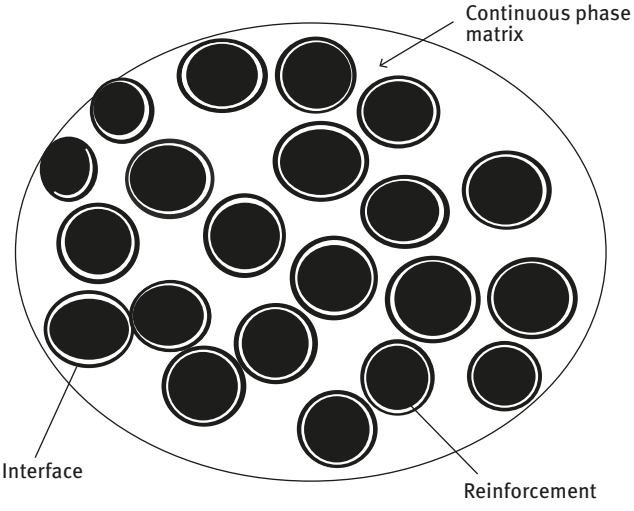

Figure 3.3: Constituent materials of a composite.

2017, the composite industry was estimated to be worth $29.9 billion [5]. It is important to stress that the usage of composite is fast growing and the end products made with composite materials are also growing sporadically.

The production of composites has dated over many centuries especially in the automobile industry. In 1940, Henry Ford began the experimentation of composites using compressed soybeans to produce plastic-like components for cars [6]. At that time, petroleum-based chemicals were very cheap and soy-based plastics were not economical for production [7]. Over a very long decade, manufacturing of components using the conventional methods has contributed immensely to the development of societies and the world at large started receiving global attention due to the depletion of petroleum resources, global awareness, and campaign to make the world more environmentally friendly and sustainable. These led researchers to investigate on more innovative ways of manufacturing composites from biodegradable materials. Biodegradable composite known as "biocomposites" are a new distinct composites, which are generally defined as biocompatible and ecofriendly composites [8, 9]. Several researchers have defined biocomposites based on their research interests such as combination of biodegradable polymer and biodegradable fillers usually biofibers [10]. Composite materials comprise one or more phase(s) derived from biological origin [11]. Biocomposites have also been defined as a resin-based composite [12]. In general, the aim of producing biocomposites is basically to improve basic mechanical properties and functionality of materials while ensuing they are ecofriendly.

3.5 Properties of biodegradable composite from common agricultural products

Generally, agricultural products or wastes have gained more usage in the production of biocomposites because they have a good biodegradability especially when subjected to various atmospheric conditions. Also, agrobased composite resources such as fiber, labor, water, energy, and processing equipment are well managed. Nevertheless, more emphasis is placed on the production of biocomposites from nonfood crops. This is done in order not to create a negative impact on food supply. As a result, agro-based composites are products of sustainable agriculture, which creates a balance between conservation and utilization of agricultural lands to serve both social and economic needs from local, national, and global vintage points [13]. Basically, properties of biocomposites are a function of the intrinsic properties of the constituent materials that can broadly be classified into thermal and mechanical properties. Although fiber-reinforced plastic composite has played a major dominant role for a long time in the manufacturing sector because of their utilization in various application as a result of their specific strength and Young's

modulus [14], agro-based composites or biocomposites now have more advantages over it. Among such advantages include the following:

1. Acceptable specific strength properties
2. Reduction in weight and cost
3. Good thermal properties
4. Enhanced energy recovery
5. Ecofriendliness as a result of biodegradability

Several research works have been carried out and published on biocomposites, and their various properties among such works are biocomposite properties based on lignocellulosic fillers [15], mechanical properties of poly(butylene succinate) biocomposites reinforced with surface-modified jute fiber [16], the effect of fiber content on mechanical and thermal expansion properties of biocomposites based on microfibrillated cellulose [17], thermal and mechanical properties of biocomposites using additive manufacturing [18]. Nevertheless, very few findings have been reported on the properties of biocomposites from agricultural by-products.

3.6 Classification and production methods for biodegradable composites

Various factors that can influence the classification of composites are densities, uses, manufacturing methods or other systems [13], and these factors help easily classify composites into three major categories as stated earlier. Also, biocomposites can be broadly classified into two major categories, namely, matrix and natural fibers as shown in Figure 3.4. Matrix types of biocomposites are made up of biodegradable homogenous and monolithic materials, where the fiber system of a composite is embedded while natural fibers are derived either directly from agricultural sources or as processing or production residues when crops are processed for their primary uses such as nutrition [19].

There is no generic way of producing biocomposites due to the fact that various biocomposites are produced to meet several demands or purposes. However, there are several types of biocomposites just like we have many types of composites such as wood–plastic composite, glass fiber epoxy composites, cement composites, filament–wound composites square tubes, carbon nitride/titania nanotube composites, and ZnS–ZnO composites.

Many biocomposites have been produced using various techniques such as biodegradable composites produced from polylactic acid and polyhydroxybutyrate, which contains 40 wt% of paper pulp and mixing them with short and long fiber pulps using torque rheometer [21]. Biocomposites are produced from biodegradable starch and jute strands fabricated using injection molding process [22].

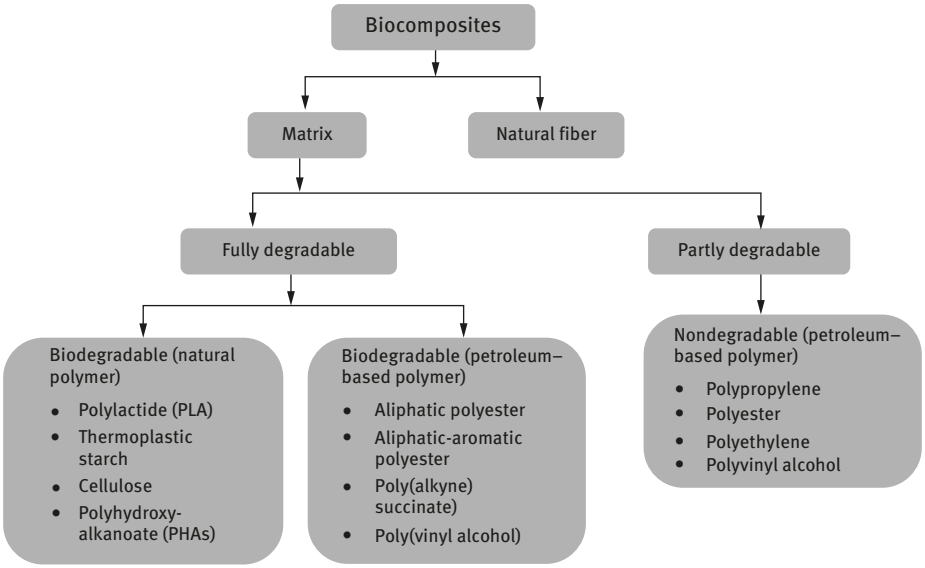

Figure 3.4: Biocomposite classification [20].

3.7 Applications of biodegradable composites

Biodegradable composites have found a drastic increase in its usage due to the fact that they offset significantly the use of fossil fuels and reduce greenhouse gas emissions when compared to the conventional petroleum-based composites. There are various applications where the use of biocomposites is gaining momentum such as in the aeronautical space, automotive industry, packaging, marine, construction, and furniture. Biocomposites have also been used majorly in the medical field as in the case where it was used as a bone-regenerative implant [23]. The reason behind the general acceptability of biocomposites globally is not far-fetched, especially when performance is the key criteria for utilization as illustrated in Figure 3.5.

Ong et al. [25] evaluated the effectiveness of treated and untreated palm kernel shell as filler in a polypropylene matrix at various filler loadings to create biocomposite materials. The analysis was carried out to assess the water absorbability, surface morphology, and tensile and flexural properties. The findings revealed that the treated palm kernel shell possesses more desirable mechanical properties with reduced water absorption as compared to nontreated palm kernel shell. The morphology of the treated palm kernel shell composites also revealed a better filler–matrix interaction because of surface modification. In conclusion, the inclusion of amino silane–palm kernel shell as a filler into the matrix provided an improved biocomposite with better flexural, tensile, and water absorbability properties. In a similar work

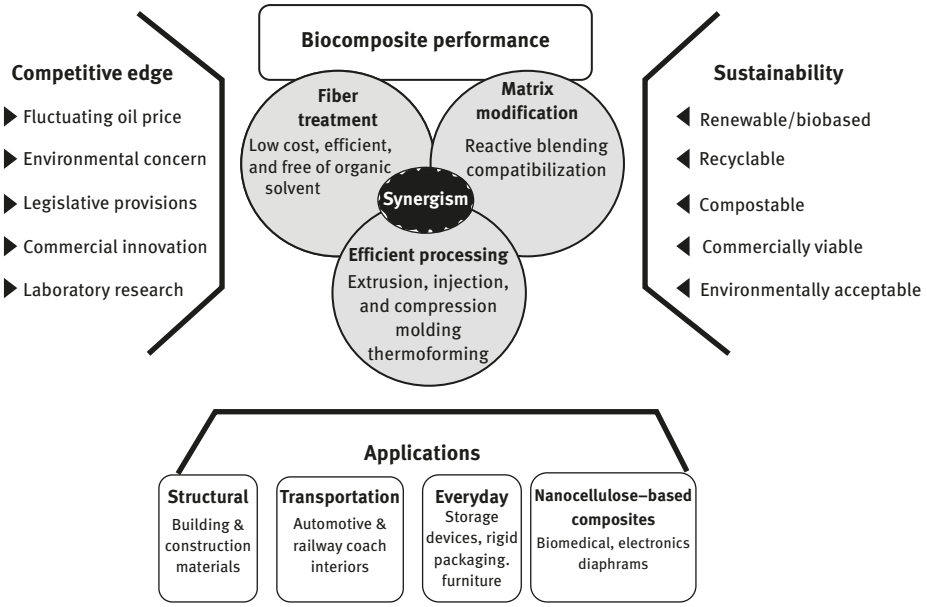

Figure 3.5: Biocomposite performance, competitiveness, sustainability balance, and applications [24].

carried out by Safwan et al. [26], the Brabender internal mixer was used to produce biocomposites of palm kernel shell/nanosilica-filled and palm kernel shell-filled maleated polypropylene biocomposites. The thermal analysis revealed an improved mechanical property of the biocomposites. The research on the produced composites also recorded minimal water absorption percentages as compared to palm kernel shell/polypropylene composite.

3.8 Sustainability and future work in biodegradable composites

The use of agro-based composite has been proven to be sustainable considering the fact that biocomposites are renewable, recyclable, compostable, commercially viable, and environmentally acceptable [24]. The rate at which technologies are disrupting the business world, especially in the manufacturing sector globally is paramount to produce biocomposites that find application in all sectors of life and eradicating the shortcomings of conventional or ordinary composites. Research is ongoing to improve the properties of existing biocomposites and increase its utilization. Also, campaign for more effective and environmentally friendly way of manufacturing will continue to be encouraged.

3.9 Summary

Considering the fact that the world is revolutionizing and transiting into the Fourth Industrial Revolution (Industry 4.0), it is important to start replacing conventional materials (composites) that contribute greatly to environmental waste with biodegradable composites or natural composites that have been tested and proven to have displayed low environmental impact and a low cost across a wide range of applications. However, researches are ongoing to improve on the properties of biocomposite materials and make them more suitable for engineering applications. The use of agricultural by-products provides an alternative raw material to some food crops currently being used in the development of biocomposites, thereby easing the effect of food shortage supply.

References

[1] Sud, D., Mahajan, G., & Kaur, M. P.. Agricultural waste material as potential adsorbent for sequestering heavy metal ions from aqueous solutions – a review. Bioresour. Technol., 2008, 99, 6017–6027.
[2] Zafar, S.. Biomass Resources from Rice Industry. 2018. Retrieved September 10, 2018, from https://www.bioenergyconsult.com/tag/agricultural-wastes/
[3] Allemang, R., Clerck, J, De, Niezrecki, C, & Wicks, A. Composite. In Materials Science and Engineering Introduction, 2014. 45, 577–617.
[4] Getu, A., & Sahu, O. Green Composite Material from Agricultural Waste. Int. J. Agri. Res. Rev., 2014, 2(5), 56–62.
[5] Chuck, K. Growth Opportunities in global Composites Market 2012-2017. 2011, Retrieved October 10, 2018, from https://www.lucintel.com/lucintel-globalcompositemarketanalysis-acma2012-educationalsession.pdf
[6] Ford, H. Soybean Car. Retrieved September 9, 2018, from https://www.thehenryford.org/collections-and-research/digital-resources/popular-topics/soy-bean-car/
[7] Drzal, L. T., Mohanty, A. K., & Misra, M. Bio-Composite Materials As Alternatives To Petroleum-Based Composites for Automotive Applications. 2014, Retrieved from https://www.researchgate.net/profile/Lawrence_Drzal/publication/228474911_Bio-composite_Materials_as_Alternatives_to_Petroleum-based_Composites_for_Automotive_Applications/links/00b7d51b62c2e6a18a000000/Bio-composite-Materials-as-Alternatives-to-Petroleum-based-Composites-for-Automotive-Applications.pdf
[8] John, M. J., & Thomas, S. Biofibres and biocomposites. Carbohydr. Polym., 2008, 71(3), 343–364.
[9] Omar, F., Bledzki, A. K., Hans-Peter, F., & Mohini, S. Biocomposites reinforced with natural fibers: 2000-2010. Prog. Polym. Sci., 2012, 37(11), 1552–1596.
[10] Anne, B. Environmental-friendly biodegradable polymers and composites. In M. S. Kumar (Ed.), Integrated Waste Management. 2011, 1st ed., I, 341–364. Rijeka, Croatia: InTech Open Science.
[11] Fowler, Paul A, Hughes, J. M., & Elias, R. M. Review Biocomposites: technology, environmental credentials and market forces. J. Sci. Food Agri., 2006, 86, 1781–1789.

[12] Lewandowska-Szumiel, M., & Ruminski, S. Cellular response to biocomposites. In L. Ambrosio (Ed.), Biomedical Composites. Elsevier 2017, 2nd ed., pp. 335–356. Woodhead Publishing.
[13] Rowell, R. M. 'Composite Materials from Agricultural Resources', in O. Olesen, F. Rexen, & J. Larsen (eds) Research in industrial application of non food crops, I. 1995, Copenhagen: Denmark Academy of Technical Science. 27-41.
[14] Cao, Y., Shibata, S., & Fukumoto, I. Mechanical properties of biodegradable composites reinforced with bagasse fibre before and after alkali treatments. Compos. Part A: Appl. Sci. Manuf., 2006. 37(3), 423–429.
[15] Avérous, L., & Le Digabel, F. Properties of biocomposites based on lignocellulosic fillers. Carbohydr. Polym., (2006), 66(4), 480–493.
[16] Liu, L., Yu, J., Cheng, Longdi, & Qu, W. Mechanical properties of poly(butylene succinate) (PBS) biocomposites reinforced with surface modified jute fibre. Compos. Part A: Appl. Sci. Manuf., 2009, 40(5), 669–674.
[17] Nakagaito, A. N., & Yano, H. The effect of fiber content on the mechanical and thermal expansion properties of biocomposites based on microfibrillated cellulose. Cellulose, 2008, 15(4), 555–559.
[18] Navarrete, J. I. M., Hidalgo-Salazar, M. A., Nunez, E. E., & Arciniegas, A. J. R. Thermal and mechanical behavior of biocomposites using additive manufacturing. Int. J. Interact. Des. Manuf. (IJIDeM), 2017, 12(2), 449–458.
[19] Väisänen, T., Das, O., & Tomppo, L. (2017). A review on new bio-based constituents for natural fiber-polymer composites. J. Cleaner Prod., 149, 582–596.
[20] Mohanty, A. K., Misra, M., & Drzal, L. T. Natural Fibers, Biopolymers, and Biocomposites. 2005, Ed. L. T. D. Amar K. Mohanty & Manjusri Misra, 1st ed. Boca Raton: CRC Press.
[21] Ren, H., Zhang, Y., Zhai, H., & Chen, J. Production and Evaluation of Biodegradable Composites Based on Polyhydroxybutyrate and Polylactic Acid Reinforced With Short and Long Pulp Fibers. Cellulose Chem. Technol., 2015, 49, 7–8.
[22] Vilaseca, F., Mendez, J. A., Pelach, A., Llop, M., Canigueral, N., Girones, J., & Mutje, P. Composite materials derived from biodegradable starch polymer and jute strands. Process Biochem., (2007), 42(3), 329–334.
[23] Ahmed, I., Parsons, A. J., Jones, I. A., Walker, G. S., & Rudd, C. D. Biodegradable Composite Materials as Bone Regenerative Implants. 2009, Retrieved October 23, 2018, from https://pdfs.semanticscholar.org/32d7/9b750a00ca3f4cfb6599a32543c9396864ea.pdf
[24] Pandey, J. K., Nagarajan, V., Mohanty, A. K., & Misra, M. Commercial potential and competitiveness of natural fiber composites. Biocomposites: Design and Mechanical Performance. 2015, 14th ed. Elsevier Ltd, USA.
[25] Ong, H. L., Yee, T. G., Nik Nur Azza, N. A., Muhammad Safwan, M., Villagracia, A. R., Mern, C. K., & Al Bakri Abdullah, M. M. Utilization of Modified Palm Kernel Shell for Biocomposites Production. Key Eng. Mater., (2016), 700 (July),60–69.
[26] Safwan, M. M., Lin, O. H., & Akil, H. M. Preparation and characterization of palm kernel shell/polypropylene biocomposites and their hybrid composites with nanosilica. BioResources, 2013, 8(2), 1539–1550.

Fatima-Zahra Semlali Aouragh Hassani, Wafa Ouarhim,
Nadia Zari, Rachid Bouhfid, Abou el kacem Qaiss

4 Natural fiber-based biocomposites

Effect of orientation on mechanical properties

Abstract: Recently, natural fibers are attracting considerable interest because of their various advantages (low cost, low density, biodegradability, availability, etc.). In addition, their coupling with the thermoplastic matrix significantly improves the performance of the materials in terms of weight, stability, strength, and durability. However, the mechanical properties of the final product depend largely on the adjustment of the fiber-orientation field during processing. In this context, this chapter deals with the study of the fiber-orientation prediction using Jeffrey and Folgar–Tucker descriptions and their effect on composite mechanical properties by evoking several models (Voigt, Reuss, Halpin–Tsai, Hashin and Shtrikman, Hirsch and Tsai Pagano).

Keywords: Natural fibers, thermoplastic materials, fiber orientation;orientation mechanisms, mechanical properties, Jeffrey, Folgar–tucker, Voigt, Reuss, Halpin–Tsai, Hashin and Shtrikman, Hirsch and Tsai Pagano models, closure approximation

4.1 Introduction

The need for more versatile polymer-based materials and environmental issues have aroused a growing interest, particularly for natural fiber-based thermoplastic composites [1–3]. Indeed, addition of natural fibers in thermoplastic matrix was shown to dramatically improve their mechanical performance without compromising their process ability because of their weight-resistance ratios and high specific properties [4, 5]. It has been shown in several studies that the composite mechanical properties are mainly related to the nature of the matrix, fiber morphology, aspect ratio, fiber–matrix adhesion, concentration, and orientation distribution [4].

The most extensive investigation has focused on the study of the fiber-orientation state and its impact on the composite performances, depending on the mold thickness.

Fatima-Zahra Semlali Aouragh Hassani, Wafa Ouarhim, Moroccan Foundation for Advanced Science, Innovation and Research (MAScIR), Institute of Nanomaterials and Nanotechnology (NANOTECH), Laboratory of Polymer Processing, Rabat, Morocco; Mohammed V-Rabat, University, Faculty of Science, Mechanics of Materials Laboratory, Rabat, Morocco
Nadia Zari, Rachid Bouhfid, Abou el kacem Qaiss, Moroccan Foundation for Advanced Science, Innovation and Research (MAScIR), Institute of Nanomaterials and Nanotechnology (NANOTECH), Laboratory of Polymer Processing, Rabat, Morocco

https://doi.org/10.1515/9783110603699-004

Undoubtedly, during filling the molding of a thick cavity, the fountain flow effect has a non-negligible role in terms of fiber orientation. First, it moves the material from the central zone of the mold to the wall, thus forming two distinct layers: (1) the core layer (central zone) with a transverse orientation because of the stretching flow, and (2) the skin layer (near the wall) without specific orientation. Indeed, a solid layer is formed immediately when the composite touches the cold walls not allowing time for the fibers to orient in a given direction. Furthermore, between these two cited layers, the shearing flow tends to orient a large quantity of the material toward the direction of the flow, thus forming the shell layer [6–8]. The obtained structure is termed as the core–shell–skin structure, which disappears by decreasing the mold cavity. Thereby, in thin cavity, the convergent–divergent flow is greater, which leads to the production of a layer with a similar, specific, and planar orientation throughout the thickness. When the plastic comes into contact with the walls, the shear flow tends to align the majority of the fibers in the direction of flow because of rapid cooling of the polymer. Conversely, at the central line, the stretching flow tends to align the fibers in the transverse direction, thus forming a form of parabolic orientation [9].

Regardless of this, it is important to note that the final orientation state may be much influenced by the molding parameters, such as the effect of gate position, main injection parameters, matrix, reinforcement, and the mold geometry.

An accurate determination of the composite mechanical properties requires the prediction or measurement of the fiber-orientation field setup in an injection molding. Several mathematical representations exist, such as orientation functions, orientation distribution functions,orientation tensors, or Hemans orientation. Jeffrey [10] was the first to propose a description of a single ellipsoidal particle immersed in a diluted solution in terms of the second- and fourth-order orientation tensors. Since this model does not take into account the fiber–fiber interaction and does not consider the effect of fiber orientation on the velocity field, Folgar and Tucker [11] modified the Jeffrey equation by adding a Brownian diffusion coefficient, D_r, in order to take into consideration the interaction between fibers. It should be emphasized that the description using the orientation tensor is easier to use than the orientation distribution function; however, it cannot be solved from its evolution equation in which the fourth- or sixth-order tensor intervene, and so on. Therefore, the closure approximation has been called to give an approximation of a higher order tensor in terms of the lower order (tensor $\overline{\overline{a_4}}$ as a function of the tensor $\overline{\overline{a_2}}$) [12]. Various theoretical models have been developed to predict the mechanical properties of composites based on the relationship between parameters affecting their performances such as fiber orientation [12]. Three types of orientation state can be distinguished: (1) parallel, (2) transversal, and (3) random. Models such as Voigt, Reuss, modified rule of mixtures (ROM), Halpin–Tsai, modified Halpin–Tsai, Hui–Shia, Hashin and Shtrikman, have used the simplest way to predict the material performances assuming that fibers are completely oriented in parallel or in series. Contrariwise, others represent the relative

contributions of both longitudinal and transversal approaches for their prediction, among them are the Tsai–Pagano model, Hirsch model, and the self-consistent approach based on the modified Hirsch model.

This chapter will shed more light on the injection–orientation mechanisms of natural fiber-based thermoplastic composites, in addition to evoking the parameters that influence it. Then, the fiber orientation is mathematically detailed to facilitate the subsequent understanding of the described theoretical models. The modeling of the fiber orientation in flow for a single fiber (Jeffrey) and a population of fibers (Folgar–Tucker) is more detailed. Finally, the effect of the natural fiber orientation on mechanical properties of the biocomposite materials is investigated by citing several models that allow it.

4.2 Fiber classification on the basis of dimensional properties

Before integrating natural fibers into a matrix, it is first necessary to know the target of their use and then to study the mechanical properties of the composite in order to improve it. Natural fibers can not only be classified according to their type and origin but also on their dimensional properties (length, waviness, kink, coarseness, and width) [13]. The waviness represents the non-straight fiber with a certain degree of curvature, while kinks refer to the multiple sharp bends caused by mechanical damage. The ratio of fiber length-to-fiber breath (diameter) is referred to as shape factor or aspect ratio (β). It is a dimensionless number that allows to admit that natural fibers are short or long. If the shape factor is less than 15, the natural fibers are considered as short, and they are long if the aspect ratio is greater than 15 [14]. Thus, knowledge of the dimensional properties of the reinforcement and their distribution in the matrix can allow the determination of certain properties of the given material. For example, natural fibers generally have a cylindrical shape; it is therefore possible to control the anisotropy of the composite material according to the orientation of the fiber in the matrix. Additionally, the fibrous structure in the polymer matrix affects the behavior of the viscous flow [15].

On the other hand, the distribution of fiber orientation in the matrix affects some properties of the composite; thus, their experimental determination requires some tools and techniques of measurement. Generally, the way to use is to take images from polished cross-sections cut from the molded plates along and across the flow directions [16, 17]. Then, analyzing images electrically either by using reflected light or scanning electron microscopy or manually by digitalizing the desired points from photographs, which is a bit slower or it should be noted that the two different ways of measuring, manual digitization, and image analysis present source of errors that must be taken into account.

4.3 Fiber orientation

It is possible to determine the properties of composites by knowing the orientation of the fibers in the polymer that directly affects these properties. In this section, both mechanisms governing fiber orientation and the parameters influencing their orientation will be discussed.

4.3.1 The injection orientation mechanisms

This section is devoted to studying the fiber orientation in the suspension during the shaping process. During the filling process, the fibers will be oriented in preferred directions depending on the applied stress. In order to understand the phenomena that govern the orientation of the fibers, we will describe their movement once subjected respectively to a shear and elongation flow.

A single fiber orientation in a shear flow

Several studies have cited that an isolated fiber, in shear flow with a Newtonian fluid, is animated by a periodic movement. This period T is inversely proportional to the shear rate γ and approximately proportional to the aspect ratio β of the fiber, defined as being the ratio between the length and the diameter of the fiber according to eq. (4.1) [18]:

$$T = \frac{2\pi}{\gamma}.\beta.\ (1+\beta) \tag{4.1}$$

Thus, the fiber never tends toward an equilibrium position. Indeed, its rotation speed is not constant, it rotates rapidly when the fiber is perpendicular to the direction of the flow and slowly when it is aligned with the flow. In the case of a non-Newtonian flow, the fiber also undergoes a rotational movement [11]. For example, this type of flow is found mainly in the mold feeding channels, especially between parallel plates as shown in Figure 4.1 and in a thin cavity.

A single fiber orientation in a elongational flow

An elongational flow allows a fiber to be oriented parallel to or perpendicular to the direction of the flow during filling; this is dependent on the rate of elongation, whether it is positive or negative. If the elongation rate is positive, the flow is convergent and it is divergent if the elongation rate is negative. In this type of flow, the particles evolve to a stationary state by moving in the stretching direction of

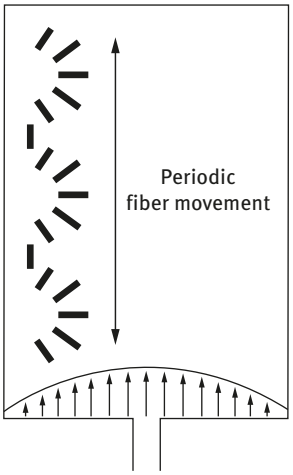

Figure 4.1: Movement of a single fiber suspended in a Newtonian fluid.

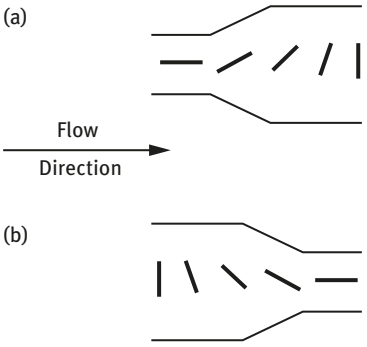

Figure 4.2: Movement of a single fiber suspended in the elongation flow: (a) negative elongational flow and (b) positive elongational flow.

the fluid; thus there is a stable equilibrium position [11]. For instance, this type of flow is found in the axis of a convergent or divergent geometry as illustrated in Figure 4.2.

Injection orientation mechanisms

In general, the plastic injection molding leads to the realization of a cavity of different thickness, and the obtained piece is classified as thin or thick.Thus, the fiber orientation varies in the thickness of the piece [19] and it is observed that in the thick part, this orientation has a rather special structure, commonly called core–skin structure. Figure 4.3 illustrates the core–shell–skin structure and the orientation distribution of the fibers throughout the thickness of a disk injected by the

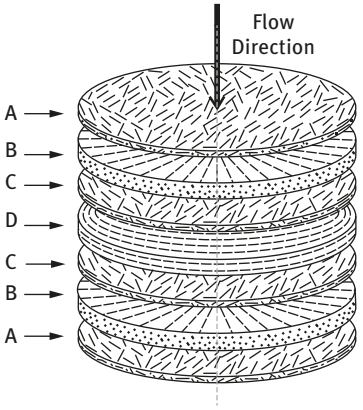

Figure 4.3: Fiber orientation distribution in a disk injected by the center.

center. Several distinct layers are observed and there is symmetry relative to the median plane of the disc (the D layer). Indeed, in the thin skin layer (A), the fiber tends to orient in an isotropic way. In the two layers (B), the fibers are oriented in the flow direction because of the interested stress shear. The core layer (D) is characterized by the dominance of elongational stress, which means that the fibers tend to orient perpendicular to the flow direction. Finally, the layer (C) is a transition layer of the orientation state (D) and (B) which is characterized by its random fiber orientation [20].

During injection molding process and near the walls, a solidified polymer layer is formed, which allows the fibers not to have a determined orientation. The fountain flow effect has a non-negligible role in terms of fiber orientation close to the flow front. In order to further clarify this phenomenon, it is useful to think of the fountain region as a "machine" that absorbs fibers near the midplane, changes their orientation, and ejects them near the mold wall.

Thus, the fountain flow moves the material of the core layer to the skin layer where it is frozen prior to alignment of the fibers in the flow direction by shearing in space. So, the fountain flow effect is the main actor in the formation of the skin layer allowing perpendicular fiber orientation and to the flow direction in the free surface [6–8]. Additionally, it creates a divergent flow (stretching flow) near the free surface as shown in Figure 4.4. Between the core and the skin layer, a shell layer is formed accounting for the majority of material because of the high shearing; this shear leads to a high orientation in the flow direction. It is worth noting that cooling speed of the polymer allows more or less accentuation of the fountain flow effect. Indeed, if the mold is filled slowly the skin layer appears and the surface orientation freezes contrary to the fast filling, which causes the disappearance of the skin layer and the effacement of the fountain flow by the shear flow [6–8].

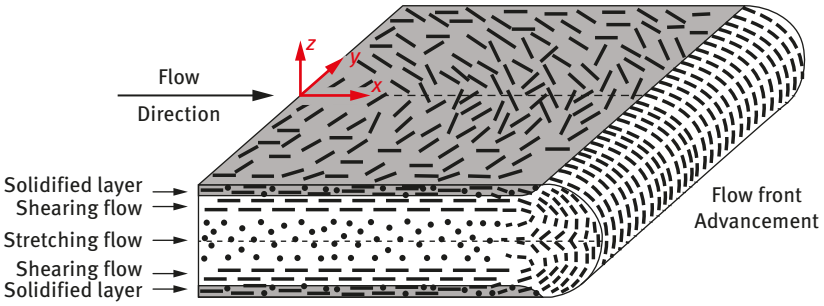

Figure 4.4: Fountain flow effect.

4.3.2 Analysis of the parameters influencing the fiber orientation

For a given geometry, fiber orientation is governed by many factors related to the injection process. Among these factors, we can find the influence of the gate position, the injection parameters, the reinforcement, the matrix, and the mold geometry.

Influence of gate position

The presence of gates leads, when they are the seat of elongation, to the formation of a core layer with transverse fiber orientation. The gate geometries that do not create such a flow (case gate film or carrots injections) facilitate, for their part, the formation of a core region with fiber orientation in the flow direction [19].

P.Shokri et al. [21] tested several asymmetrical gate locations to show their effect on fiber orientation. To infer that, the asymmetric gate position causes an asymmetric viscosity state in the transverse flow direction (width of the mold) leading to asymmetric fiber patterns in the flow plane.

Influence of the main injection parameters

a. **Influence of mold and melt temperature**
Generally, a decrease in the mold temperature (or the material temperature) increases the solidified polymer layer, which induces maximum shear values shifted toward the center of the part. This temperature diminution leads to an increase in the thickness of the shell–skin layer. The phenomena observed are mainly related to the fountain effect, which is accentuated by the cooling rate of the polymer [14].

However, R. Bay et al. [6] when evaluating the effect of a slight variation of mold and melt temperature on fiber orientation for a center-gated disk, they

luckily obtained interesting reports. First, fiber orientation was predicted for three mold temperature values: T_w = 337, 347, and 357 K, respectively. The results show that in this small temperature variation, T_w does not have much influence on fiber orientation, while it can greatly affect the molecular orientation or crystallinity in some polymers. On the other hand, the same procedure was done for three melt inlet temperature values: T_{in} = 540, 550, and 560 K, respectively and it was observed that fiber orientations are not much sensitive to T_{in}, apart from the fact of adjusting the transition layer between the core and shell layers.

b. **Influence of filling time and injection speed**

In most cases, a high injection speed causes an increase in the core layer and diminution of the skin layer. Indeed, the fountain flow greatly affects the skin area without giving the fibers time to orient themselves, thus shifting the zone of strong shear toward the walls of the mold [14].

To investigate the effect of the filling time on fiber orientation, R. Bay et al. [6] showed the prediction for four filling time values; T_{fill} = 0.5, 2, 2.5, and 3 s, respectively and concluded that fiber orientation and thickness of different layers are controlled by the filling speed. Indeed, for a very fast filling rate, there is virtually no skin layer [6].

For their parts, S.T.Chung et al. [22] evaluated the core fiber orientation at different filling time; T = 0.081, 0.255, 0.557, and 0.81 s, respectively for a tensile testing specimen. First, fibers are aligned transversely to the direction of flow because of the strong divergent flow, but as the filling time increases, the fibers tend to align in the flow direction [22].

Influence of the matrix

The nature of the speed profile in the mold results from the rheofluidifying nature of the used polymers. The pseudoplastic nature of polymers gives rise to a flow characterized by a much flatter velocity profile than that of Newtonian fluids. It appears that the thickness of the core zone is an increasing function of the pseudo plasticity index of the polymer. At the same time, the addition of fibers increases the pseudo plasticity of the matrix. It must always be remembered that many of these effects acts identically. However, it should also be noted that, in the vast majority of cases, these studies remain qualitative.The matrix viscoelastic nature also affects the periodicity of fiber movement in shear flow. It has been shown that for a non-Newtonian fluid, the period of a particle increases strongly. In addition, it has been observed that this increase in the periodicity of the movement is exacerbated by the shear rate [14].

To explore how the thermal and rheological properties of the polymer matrix could affect fiber orientation, R. Bay et al. [6] simulated the filling of the disk using

three polymers with different properties (nylon, polypropylene [PP], and polycarbonate [PC]). The nylon has a smaller heat of fusion and a wider range of freezing, unlike PP has a large heat of fusion and a narrow range of freezing temperatures, while PC has no heat of fusion. The viscosity of nylon is sensitive to shear rate and temperature in the range of the experiments, while the PC is relatively insensitive and the PP has strong shear thinning and very sensitive to temperature. It was observed that the differences between the velocity profiles of these three matrices lead to different orientation distribution. The flatter velocity profile of PP produces a much thicker core layer and shearing near the wall. On the other hand, the large heat of fusion erases the fountain flow effects, so no skin layer is formed. Nevertheless, the PC has the same skin layer as nylon, but the core region is smaller than even the nylon and PP moldings. To conclude, small changes in the speed profile can affect the fiber orientation. An imprecision speed profile prediction inevitably leads to inaccuracy in the fiber orientation. The importance of fountain flow is also evoked in terms of the skin layer prediction because the speed profiles can provide only little information [6].

Influence of the reinforcement

Several studies have shown that shape factor of fibers plays a major role on fiber orientation. Indeed, increasing the aspect ratio leads to necessary increase in the core thickness, defined by a transversal fiber orientation. It will be concluded that the core thickness is very sensitive to the increase in the initial fiber length. It is also important to note that more fibers are long more they tend to adopt a planar orientation [23] because their length prevents them from turning freely (Figure 4.5).

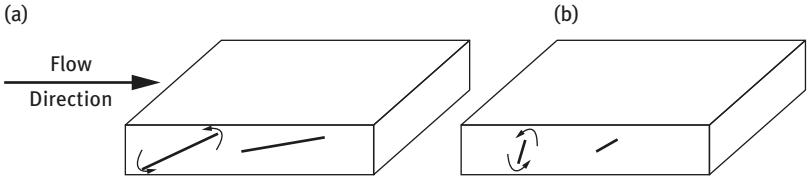

Figure 4.5: (a) Long fiber orientation. (b) Short fiber orientation.

Otherwise, it seems that the fiber concentration also influences the orientation because its decrease causes the disappearance of the core–skin structure, whereas its increase causes the increase in the size of the core zone. Fiber concentration is associated with the aspect ratio of the fibers (L/D), and its volume fraction (V_f) [17].

For a cylindrical particle, the volume fraction is calculated according to the following relation (eq. (4.2)) [17].

$$V_f = n.\pi.\frac{D^2}{4}.L \tag{4.2}$$

Where n is the number of particles per unit volume.

There are three regimes of concentration:

1. **Dilute solution**: It is the regime where there is no interaction between the fibers. It means that, the distance between adjacent fibers is approximately equal to the fiber length and they can turn freely without touching each other. Then the maximum permissible volume fraction V_f verifying the following relation (eq. 4.3) [17].

$$V_f \leq \left(\frac{D}{L}\right)^2 \tag{4.3}$$

2. **Semi-concentrated solution**: This characterizes the suspension where the distance of the fibers is between the length and diameter of the fibers. In this case, the volume fraction V_f must be verifying the following inequality (eq. (4.4)) [17].

$$\left(\frac{D}{L}\right)^2 \leq V_f \leq \left(\frac{D}{L}\right) \tag{4.4}$$

3. **Concentrated solution**: It is defined according to following relation (eq. 4.5), when the average distance between fibers is lower than the fibers' diameter [17].

$$V_f \geq \left(\frac{D}{L}\right) \tag{4.5}$$

When talking about concentrated or semi-concentrated types, it is important to experimentally determine the interaction coefficient (C_i), which depends on the fiber aspect ratio, L/D, and the volume fraction. An empirical expression (eq. 4.6) was proposed by Tucker and Advani to predict approximately the interaction coefficient when the latter is not available experimentally [6, 17, 24].

$$C_i = 0.0184.\exp\left(-0.7148\ .V_f.\frac{L}{D}\right) \tag{4.6}$$

This expression is valid only for concentrated regimes [17].

To demonstrate how the interaction coefficient affects the orientation, R. Bay et al. [6]. made predictions of C_i = 0.005, 0.01, and 0.05 for the center-gated disk. It is clear that the fiber orientation state approaches the randomized orientation state as the magnitude of C_i increases [6, 17]. Increasing the interaction coefficient necessarily leads to random orientation states, whereas low values tend the shell layer to a high orientation in the flow direction and the core layer to a highly transverse orientation. C_i also affects the layered structure, indeed increasing the interaction coefficient decreases the core and increases the shell thicknesses [6].

Influence of the geometry of the mold

Some authors have shown that the reduction on the cavity thickness for rectangular molds with uniform thickness via qualitative microscopic observations greatly affects the fiber orientation in the core zone. Indeed, more the mold thickness decrease more the core zone will disappear, thus resulting in nearly the same planar orientation throughout all the thickness [14, 19].

Generally, two types of molds can be distinguished (Figure 4.6): (1) thin-walled cavity (less than 1 mm) and (2) thick-walled cavity (more than 1 mm). M. Vincent et al. [25] evaluated the orientation of fibers at different mold thicknesses (1.1, 1.7, 3, and 5 mm). The results revealed the appearance of a skin–core structure above 3 mm as well as the increase and accentuation of the core layer with increasing thickness to 5 mm. On the other hand, it was observed that decreasing the cavity thickness necessarily leads to the decrease in the structure of the core–skin until obtaining one layer where the fibers adopted a specific planar orientation throughout all the thickness. Usually, this converging–diverging flow is more significant in thin parts.

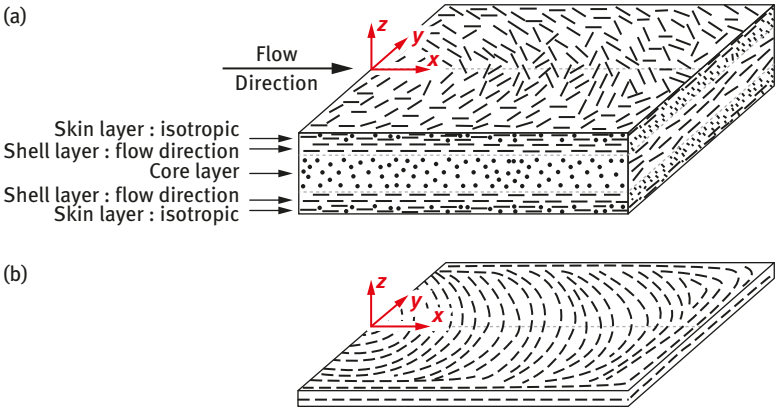

Figure 4.6: (a) Fiber orientation in thick mold and (b) fiber orientation in thin mold.

When the plastic contacts the mold surfaces, a frozen layer is immediately formed along the mold walls, where the converging flow tends to flow-align the fibers. Near the center line and because of the decrease in the solid layer, the diverging flow tends to align the fibers perpendicular to the flow, thus forming a parabolic shape of fiber orientation [9].

Changing the mold width also plays a major role in the distribution of fiber orientation. M. Vincent et al. [5] compared the fiber orientation in a thin rectangular plate for 20 and 40 mm width. It was observed that reducing the mold width leads fibers to orient in the flow direction in the whole thickness, whatever the position taken along the plate (Figure 4.7).

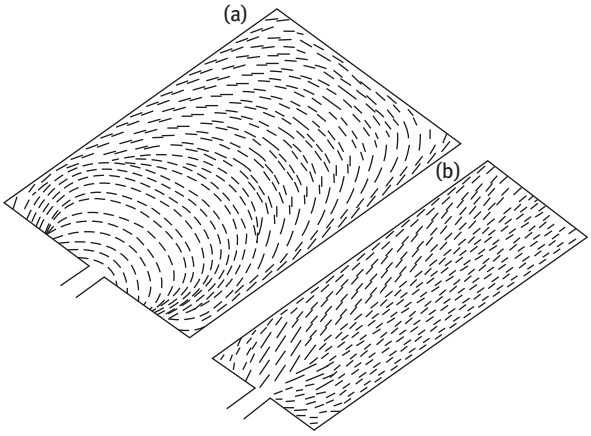

Figure 4.7: (a) Fiber orientation in large mold width and (b) fiber orientation in small mold width.

For their part, R. Bay et al. [6] reported the fiber orientation measurements for the two injection molding parts: (1) center-gated disk and a (2) film-gated strip with the same thickness (3.18 mm). It was concluded that both parts have the same layered structure, with outer shell layers of flow-aligned fibers surrounding a central core of either random-in-plane (strip) or transversely aligned fibers (disk), but they also represent significant differences. The center-gated disk core has a transverse orientation much more pronounced than the film-gated strip, since the core is formed by the circumferential stretching, which dominates at the midplane. In addition, a thick frozen layer is formed on the disk walls during filling, hence forming the skin layer in the contrary of the strip where the frozen layer is very small.

4.4 Fiber orientation description

4.4.1 Vector representation of a single fiber orientation

A single fiber orientation can be described conventionally according to the Cartesian coordinates of a unit vector representing the main fiber direction or using two angles (θ, φ). As illustrated in Figure 4.8, each single fiber could be represented by a vector P directed along the main axis of the fiber, thereby defining the fiber orientation by its projection in a fixed landmark. It is worth noting that the sense of P is arbitrary because of the two undifferentiated ends. As a result, the orientation description must be unchanged if the transformation $(\theta \rightarrow \pi - \theta)$ and $(\varphi \rightarrow \varphi + \pi)$ is carried out. To conclude, the components of this vector P related to angles (θ, φ) are expressed by eq. (4.7) [26–28]:

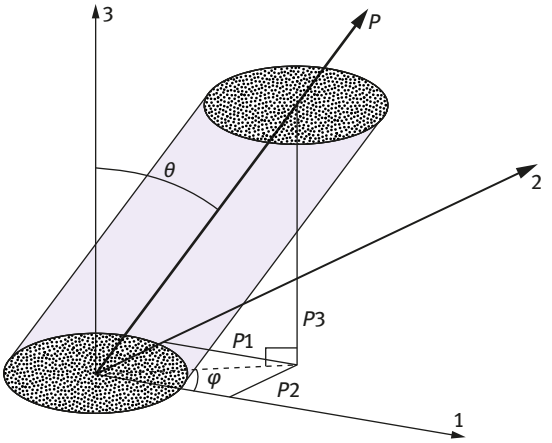

Figure 4.8: Fiber orientation.

$$\begin{cases} P_1 = \sin\theta\cos\varphi \\ P_2 = \sin\theta\sin\varphi \\ P_3 = \cos\theta \end{cases} \tag{4.7}$$

where θ is the tilt angles denoted as the angle formed by the Z axis at the direction of the fiber, and φrefer to the azimuthal angles and it is defined in the plane (X, Y) with respect to the X axis. Since a fiber has no orientation sense, the values of θ and φ are respectively between (0°; 180°) and (–90°; 90°) [26–28].

Short fiber composite materials generally consists of very large number of fibers. In order to more concisely describe the orientation distribution of a fiber population, several mathematical representations exist, such as orientation functions, orientation distribution functions, orientation tensors, or Hemans orientation coefficient, which will be revealed in the next paragraphs.

4.4.2 Orientation distribution function

A complete description of long- or short fiber-orientation state requires the calling of an orientation distribution function $\Psi(P, t)$ or equivalent $\Psi(\theta, \varphi)$, which expresses the probability of obtaining a fiber having a certain orientation "P" at time "t."

So, the probability P of finding a fiber between the angles $(\theta, \theta + d\theta)$ and $(\varphi, \varphi + d\varphi)$ is expressed by eq. (4.8) [28]:

$$\mathrm{P} = \int_{\theta}^{\theta+\mathrm{d}\theta} \int_{\varphi}^{\varphi+\mathrm{d}\varphi} \psi(\theta, \varphi) \sin\theta \, \mathrm{d}\varphi \mathrm{d}\theta \tag{4.8}$$

This function must satisfy the following conditions [29, 30]:

– It must be unchanged by the P → –P transformation, which translates into eq. (4.9):

$$\Psi(\theta, \varphi) = \Psi(\pi - \theta, \varphi + \pi) \text{ or } \Psi(\mathrm{P}) = \Psi(-\mathrm{P}) \tag{4.9}$$

– It must be normalized, that is, the integral of the distribution function on all possible orientations is equal to unity, verifying eq. (4.10):

$$\int_0^{2\pi} \int_0^{2\pi} \Psi(\theta, \varphi) \sin\theta \, \mathrm{d}\theta \, \mathrm{d}\varphi = 1 \text{ or } \int \Psi(\mathrm{P}) \, \mathrm{dP} = 1 \tag{4.10}$$

where dP is a surface element of the unit sphere.

The orientation distribution function obeys the Fokker Plank equation; in the case of semi-diluted or concentrated suspensions of fibers, hydrodynamic fiber interaction must be taken into account. Thus, a diffusion coefficient because of Brownian motion of fibers, D_r is introduced. If $dP = dt$ denote the matrix derivative of P with respect to time, the evolution equation is written according to eq. (4.11) [31, 32].

$$\frac{\partial \psi}{\partial t} + \frac{\partial}{\partial P}\left(\psi \frac{\partial P}{\partial t}\right) - D_r \frac{\partial^2 \psi}{\partial \mathrm{P}^2} = 0 \tag{4.11}$$

While in dilute suspension (no fiber interaction, $D_r = 0$), the orientation distribution function is written as given in eq. (4.12)) [31, 32]:

$$\frac{\partial \psi}{\partial t} + \frac{\partial}{\partial P}\left(\psi \frac{\partial P}{\partial t}\right) = 0 \tag{4.12}$$

4.4.3 Orientation tensor

The orientation distribution function is mostly not explicitly known and difficult to predict, which has lead Hand [33] to introduce a tensor of order 2, frequently noted $\overline{\overline{a_2}}$, and defined as the spatial mean of the double tensor product of $\bar{P}$. These tensors are expressed as a function of the vector of orientation P and the orientation distribution function by eq. (4.13) [28, 34]:

$$\overline{\overline{a_2}} = \int \bar{\mathrm{P}} \otimes \bar{\mathrm{P}} \psi(\bar{\mathrm{P}}) \mathrm{d}\bar{\mathrm{P}} \tag{4.13}$$

When defining these tensors, one should not neglect the properties of symmetry and the conditions of normalization expressed below (eq. (4.14)) [28, 34]:

$$\begin{cases} a_{ij} = a_{ji} \\ a_{ii} = 1 \text{ or } a_{11} + a_{22} + a_{33} = 1 \end{cases} \tag{4.14}$$

These properties indicate that only 5 of 9 components of a_{ij} are independent, so there are 5 scalars to describe this tensor in the case of a 3D flow [28].

In an orthonormal base (e_1, e_2, e_3), a_{11}, a_{22}, and a_{33}, respectively denote the alignment of the fibers along the directions e_1, e_2, and e_3. For instance, if the component $a_{11} = 1$, it means that all the fibers are oriented in the direction e_1, whereas if $a_{11} = 0$, it indicates that all the fibers are perpendicular to e_1 (they belong to the plane [e_2, e_3]) as explained in Figure 4.9 for a single fiber, and this is valid for other components too.

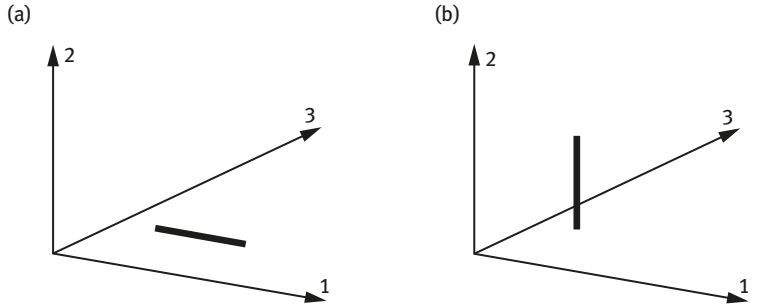

Figure 4.9: (a) Illustration of the component $a_{11} = 1$ and (b) Illustration of the component $a_{11} = 0$.

The components a_{ij} with $i \neq j$ quantify the asymmetry of the orientation distribution with respect to directions e_i or e_j. Figure 4.10 (a) and (b) illustrates the values taken by the tensor components for different orientations in the bi-dimensional and three-dimensional cases.

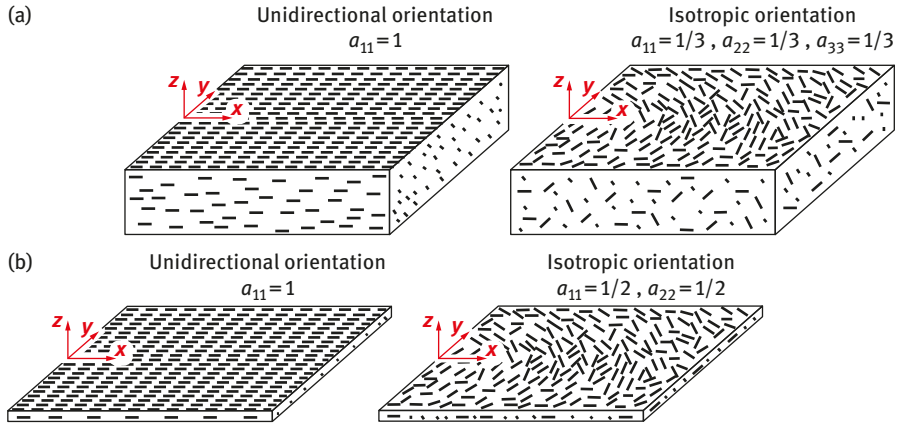

Figure 4.10: (a) Tensor component values in the bi-dimensional case and (b) tensor component values in the three-dimensional case.

Demonstration

Consider a fiber with an orientation: $\bar{P} = \begin{pmatrix} \sin\theta\cos\varphi \\ \sin\theta\sin\varphi \\ \cos\theta \end{pmatrix}$, so the orientation tensor will be written as follows:

$$\overline{\overline{a_2}} = \int_0^{\pi}\int_0^{2\pi} \begin{pmatrix} \sin^2\theta\cos^2\varphi & \sin^2\theta\cos\varphi\sin\varphi & \sin\theta\cos\theta\cos\varphi \\ \sin^2\theta\sin\varphi\cos\varphi & \sin^2\theta\sin^2\varphi & \sin\theta\sin\varphi\cos\theta \\ \sin\theta\cos\theta\cos\varphi & \sin\theta\sin\varphi\cos\theta & \cos^2\theta \end{pmatrix} \sin\theta\psi(\theta,\varphi)\mathrm{d}\theta\mathrm{d}\varphi$$

Generally, the transition from the orientation distribution function $\Psi(P)$ to the tensor $\overline{\overline{a_2}}$ generates a loss of information which has led Altan et al. [35] to use the fourth-order orientation tensor as defined by eq. (4.15) [28, 34]:

$$\overline{\overline{a_4}} = \int \bar{P}\otimes\bar{P}\otimes\bar{P}\otimes\bar{P}\psi(\bar{P})\mathrm{d}\bar{P} \tag{4.15}$$

The use of this tensor greatly increases the number of parameters describing the orientation state. However, like the second-order tensor, the fourth-order tensor is symmetric and unitary. Only 14 components are then independent on the 81 coefficients [34].

4.4.4 Orientation coefficient of Hermans

The Hermans orientation coefficient could also be used to describe the average reinforcement orientation. Thus, this technique imposes the choice of a reference axis, the orientation of the macromolecules is then defined by an angle with respect to this axis as shown in Figure 4.11.

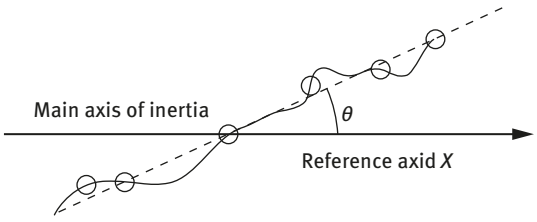

Figure 4.11: Schematization of Hermans factor.

According to the literature, it is possible to have an idea about the existence of a privileged orientation via the determination of the Hermans factor, which is expressed as follows (eq. 4.16) [36, 37]:

$$f_x = \frac{3}{2} < \cos^2\varphi_x > - \frac{1}{2} \tag{4.16}$$

where φ_x is the angle between the fiber and the reference axis x.

Theoretically, the value of f_x can range from 1, for perfectly oriented molecules, to zero for an isotropic material $<\cos^2\varphi_x \geq 1/3$, and it is equal to $-1/2$ when the fiber orientation is transverse to the reference axis [37].

This method does not allow to determine the fiber orientation state with precision, it only allows to qualitatively determine the existence of an orientation axis. The mathematical tools that provide more concrete information about the orientation state are the second- and fourth-order tensor and the orientation distribution functions.

4.5 Modeling of the fiber orientation in flow

4.5.1 Evolution model of a single fiber

Jeffrey [10] was the first to propose a theoretical work describing the orientation evolution in the case of diluted solutions of rigid spheroidal particles immersed in a Newtonian fluid.The main hypothesis is that the particle sizes are small enough that the deformation velocity field is homogeneous at a great distance.The speed of the undisturbed fluid is then a linear function of the position, and the inertial forces are neglected. Jeffrey's model is thus given by eq. (4.17) [38, 39]:

$$\frac{D\overline{P}}{Dt} = \Omega(V)\overline{P} + \lambda[\varepsilon(V)\overline{P} - (\varepsilon(V) : \overline{P}\otimes\overline{P})\overline{P}] \tag{4.17}$$

where $\frac{D\bar{P}}{Dt}$ is the matrix derivative of P defined by the eq. (4.18). It takes into account the displacement of the center of gravity of the particle and its evolution as a fluid particle [38].

$$\frac{D\bar{P}}{Dt} = \frac{\partial\bar{P}}{\partial t} + V\nabla\bar{P} \tag{4.18}$$

$\varepsilon(V)_{ij}$ and $\Omega(V)_{ij}$ are respectively the volume averaged vorticity and the strain rate tensors, which are expressed by eq. (4.19).They contribute to the particle orientation change because of the deformation and the rotation of the fluid[38].

$$\varepsilon(V)_{ij} = \frac{1}{2}\left(\frac{\partial u_i}{\partial x_j} + \frac{\partial u_j}{\partial x_i}\right) \tag{4.19a}$$

$$\Omega(V)_{ij} = \frac{1}{2}\left(\frac{\partial u_i}{\partial x_j} + \frac{\partial u_j}{\partial x_i}\right) \tag{4.19b}$$

V is the local speed field and λ is a function of the fiber form ratio β given by eq. (4.20). Concerning the symbol ":" it denotes the tonsorial product twice contracted [39].

$$\lambda = \frac{\beta^2 - 1}{\beta^2 + 1} \tag{4.20}$$

To calculate the evolution of the vector $\bar{P}$over time for a particle with an infinite form ratio ($\lambda = 1$), Hand [33] introduced a Brownian motion in the Jeffrey equation-via the insertion of a diffusion coefficient D_r. He derived eq. (4.21):

$$\frac{D\overline{P}}{Dt} = \Omega(V)\overline{P} + \lambda[\varepsilon(V)\overline{P} - (\varepsilon(V) : \overline{P}\otimes\overline{P})\overline{P}] - \frac{D_r}{\psi}\frac{\partial\psi}{\partial\overline{P}} \tag{4.21}$$

Knowing that: $\overline{P} = \begin{cases} P_x \\ P_y \\ 0 \end{cases}$

Projection on the axes (ox) and (oy) leads to the eq. (4.22):

$$\begin{cases} \frac{\partial P_x}{\partial t} + V_x\frac{\partial P_x}{\partial x} = -\frac{1}{2}P_y\left(\frac{\partial V_y}{\partial x} - \frac{\partial V_x}{\partial y}\right) + \lambda P_x\frac{\partial V_x}{\partial x}\left(1 - P_x^2 - P_y^2\right) + \frac{1}{2}\lambda P_y\left(\frac{\partial V_x}{\partial y} - \frac{\partial V_y}{\partial x}\right)\left(1 - P_x^2 - P_y^2\right) \\ \frac{\partial P_y}{\partial t} + V_y\frac{\partial P_y}{\partial y} = -\frac{1}{2}P_x\left(\frac{\partial V_y}{\partial x} - \frac{\partial V_x}{\partial y}\right) + P_y\frac{\partial V_y}{\partial y}\left(1 - P_x^2 - P_y^2\right) + \frac{1}{2}P_x\left(\frac{\partial V_x}{\partial y} - \frac{\partial V_y}{\partial x}\right)\left(1 - P_x^2 - P_y^2\right) \end{cases} \tag{4.22}$$

The direct calculation of the orientation of the movement of each fiber in reinforced thermoplastics has proved very expensive and consumes computer resources. That is why it was more legitimate to use a compact notation of the fiber orientation (orientation tensors) and to develop macroscopic models to follow the evolution of these tensors. Lipscomb et al. [40] used Jeffrey's equation to model the state of fiber orientation. This equation was homogenized in volume and combined with the Fokker–Plank equation (eq. (4.11)). So, Jeffery's analysis can also be written in terms of the second- and fourth-order orientation tensors as follows (eq. 4.23) [38, 39]:

$$\frac{D\overline{\overline{a_2}}}{Dt} = [\Omega(V)\overline{\overline{a_2}} - \overline{\overline{a_2}}\Omega(V)] + \lambda[\varepsilon(V)\overline{\overline{a_2}} + \overline{\overline{a_2}}(\varepsilon(V) - 2\varepsilon(V) : \overline{\overline{a_4}}] \tag{4.23}$$

4.5.2 Evolution models of a fiber population

In non-dilute suspensions, taking into account the interaction between the fibers is more complex. The evolution of orientation in such environments has been the subject of several studies and few macroscopic models are likely to take into account this evolution during the flow. Folgar and Tucker [11] modified the Jeffrey equation (eq. (4.24)) by adding a diffusion Brownian coefficient D_r in order to consider the interaction between fibers as shown in eq. (4.24) [38, 39]:

$$\frac{D\overline{\overline{a_2}}}{Dt} = \left[\Omega(V)\overline{\overline{a_2}} - \overline{\overline{a_2}}\Omega(V)\right] + \lambda\left[\varepsilon(V)\overline{\overline{a_2}} + \overline{\overline{a_2}}(\varepsilon(V) - 2\varepsilon(V) : \overline{\overline{a_4}}\right] + 2D_r\left(\overline{\overline{I}} - 3\overline{\overline{a_2}}\right) \tag{4.24}$$

The Brownian diffusion coefficient proposed by these authors is defined by eq. (4.25):

$$D_r = C_I\,\dot{\bar{\varepsilon}} \tag{4.25}$$

where C_I is the interaction coefficient and $\dot{\bar{\varepsilon}}$ is the magnitude of the strain-rate tensor. The main difficulty in this model lies in the interaction coefficient determination. The choice of this coefficient has a significant impact on the orientation profile. In the general case, it is suggested to take a coefficient interaction value between 10^{-3} and 10^{-2}, to have a good agreement with experience [39]. For the determination of the Brownian diffusion tensor, no complete study has been developed until today. Nevertheless, the numerical estimation allows establishing the value of this tensor.

This description is easier to use than the orientation distribution function in equation (eq. (4.23)), but cannot be solved from its evolution equation in which the tensor of order 6 intervenes and so on. This scheme is thus repeated for higher order tensors. To circumvent this difficulty and allow a complete description of the behavior, a closure approximation has been called to give an approximation of the tensor $\overline{\overline{a_4}}$ as a function of the tensor $\overline{\overline{a_2}}$ and to substitute the result in the eq. (4.24) [38].

4.5.3 Closure approximation

The closure approximation research is one of the most motivating problems concerning fiber orientation. Many methods have been employed to obtain all of these closure approximations, but none has been found to be sufficient for careful prediction of flow and orientation fields [41].

The following paragraphs detailed the different closure equations that could be integrated into a computer code to predict the fiber orientation.

These closure equations can be classified into different categories:

- Simple approximations
- Approximations obtained by simple approximation interpolation
- Approximations using adjustable coefficients

Simple approximations

The so-called "simple" closure approximations for a_{ijkl} can be formed by linear combinations of the products of a_{ij} and the unit tensor δ_{ij} [27, 42, 43].

a. **Linear closure approximation**

Hand [33] was the first to propose a so-called linear closure equation.This closure approximation is accurate for a population of randomly oriented fibers. However, for other types of flows, it can sometimes provide nonphysical results. The linear closure equation results in the following equation (eq. (4.26)) [27, 42, 43]:

$$a_{ijkl}^{\text{lin}} = \mathrm{C}_1\left(\delta_{ik}\delta_{jl} + \delta_{ij}\delta_{kl} + \delta_{il}\delta_{jk}\right) + \mathrm{C}_2\left(a_{ik}\delta_{jl} + a_{ij}\delta_{kl} + a_{il}\delta_{jk} + a_{kl}\delta_{ij} + a_{jl}\delta_{ik} + a_{jk}\delta_{il}\right) \quad (4.26)$$

In the case of two or three dimensions, C_1 and C_2, respectively are defined by eq. (4.27):

$$\begin{cases} 2d: C_1 = -\frac{1}{35} \text{ and } C_2 = \frac{1}{7} \\ 3d: C_1 = -\frac{1}{24} \text{ and } C_2 = \frac{1}{6} \end{cases} \tag{4.27}$$

b. **Quadratic closure approximation**

Hinch and Leal [44] have implemented an exact quadratic closure approximation for flows that direct fibers in a single direction. This closure approximation, which is quite simple, takes the form as in eq. (4.28)) [41–43]:

$$a_{ijkl}^{\text{quad}} = a_{ij}a_{kl} \tag{4.28}$$

The quadratic closure equation is widely used for its compact expression. Nevertheless, it does not respect all the symmetry conditions of the tensor of fourth order. Indeed, writing $a_{1122} = a_{11}a_{22}$ or $a_{1212} = a_{12}a_{12}$ gives very different results. Moreover, it is known to overestimate the alignment of the fibers in the direction of flow [41–43].

Approximations obtained by simple approximation interpolation (Hybrid approximation)

In order to set up a closure equation with a wider domain of validity,Advani and Tucker [42] proposed a hybrid closure approximation, which is the most popular model used in injection molding and compression molding simulation. The hybrid approximation is based on the combination of linear and quadratic closure approximations, summarized by eq. (4.29) [42, 43, 45].

$$a_{ijkl}^{\text{hybrid}} = (1 - \text{f})a_{ijkl}^{\text{lin}} + fa_{ijkl}^{\text{quad}} \tag{4.29}$$

$$f = 1 - n^n \det(\overline{\overline{a_2}}) \tag{4.30}$$

where f denotes a scalar independent of the coordinate system expressed according to eq. (4.30) and defined from the invariants $\overline{\overline{a_2}}$. n here indicates the spatial dimension. It is worth noting that, when $f = 1$, the fibers are aligned in the flow direction (quadratic approximation), and $f = 0$ refer to the isotropic orientation (linear approximation).

Approximations using adjustable coefficients

These particular solutions connect the fourth-order tensor to the second-order tensor by a number of parameters that are subsequently adjusted to reduce the difference between the predictions of the approximation and the significant results given by the calculation of the orientation distribution function.

a. **Natural closure approximation**

Verleye and Dupret [46] proposed the natural closure to involve the fourth-order symmetric tensor a_{ijkl} of the second symmetric a_{ij}. This approximation is valid for fibers with a high elongation ratio ($\lambda = 1$) and for a suspension without particle interaction, that is, an interaction coefficient equal to zero ($C_I = 0$) [26, 27].

For a two-dimensional orientation (2D), the natural closure approximation (NAT) is expressed eq. (4.31) [41, 46]:

$$a_{ijkl} = \frac{1}{4}(1 - II_a)S(\delta_{ij}\delta_{kl}) + S(a_{ij}a_{kl}) \tag{4.31}$$

where II_a represents the second invariant of a_2 according to eq. (4.32) and the symbol S refers to the symmetric part of a tensor, which can be written as eq. (4.33).

$$II_a = a_{pq}a_{pq} \tag{4.32}$$

$$S(T_{ijkl}) = \frac{1}{24}\left(T_{ijkl} + T_{jikl} + T_{ijlk} + \ldots\right) \tag{4.33}$$

Whereas in the three-dimensional (3D) case, the approximation can be expressed according to eq. (4.34) [41, 46]:

$$\begin{aligned} a_{ijkl} = {} & \beta_1 S(\delta_{ij}\delta_{kl}) + \beta_2 S(\delta_{ij}a_{kl}) + \beta_3 S(\delta_{ij}a_{km}a_{ml}) + \beta_4 S(a_{ij}a_{kl}) + \beta_5 S(a_{ij}a_{km}a_{ml}) \\ & + \beta_6 S(a_{im}a_{mj}a_{kn}a_{nl}) \end{aligned} \tag{4.34}$$

where β_r (with $1 \le r \le 6$) are polynomial expansions of the second and third invariants (II_a and III_a) of a_2.

b. **Orthotropic closure approximation**

The orthotropic closure equations are similar to approximation of the natural closure in terms of their philosophy and performance. This type of approximation is based on the orthotropic properties of the fourth-order orientation tensor, which have the same principal axes as the eigenvectors of the second one [41, 45]. Since the tensor a_2 is symmetric, there exist eigenvalues (α_1, α_2, and α_3) and eigenvectors (E_1, E_2, and E_3) of a_2, such that in the base of its eigenvectors a_2 is reduced to eq. (4.35).

$$\overline{\overline{a_2}} = \begin{pmatrix} \alpha_1 & 0 & 0 \\ 0 & \alpha_2 & 0 \\ 0 & 0 & \alpha_3 \end{pmatrix} \tag{4.35}$$

There are only three independent components ($\alpha_1 \ge \alpha_2 \ge \alpha_3$) among the six nonzero components because of the full symmetry and normalization conditions that apply ($\alpha_1 + \alpha_2 + \alpha_3 = 1$) [45].

Since a_2 is orthotropic, the fourth-order tensor a_4 must respect the symmetry conditions contained in a_2. A fourth-order tensor with major and minor symmetries

has 21 independent components. We can reduce this number by adopting a writing using index contraction as shown in (Table 4.1) [41].

Table 4.1: Indices contracted.

Values of *m* and *n*	Tensor notation *ij* or *kl*
1	11
2	22
3	33
4	23 or 32
5	31 or 13
6	12 or 21

The fourth-order tensor can be written on the basis of eigenvectors of a_2 as a matrix (6×6) in eq. (4.36) [41].

$$\bar{A} = \begin{pmatrix} \overline{A_{11}} & \overline{A_{12}} & \overline{A_{13}} & 0 & 0 & 0 \\ \overline{A_{21}} & \overline{A_{22}} & \overline{A_{23}} & 0 & 0 & 0 \\ \overline{A_{31}} & \overline{A_{32}} & \overline{A_{33}} & 0 & 0 & 0 \\ 0 & 0 & 0 & \overline{A_{44}} & 0 & 0 \\ 0 & 0 & 0 & 0 & \overline{A_{55}} & 0 \\ 0 & 0 & 0 & 0 & 0 & \overline{A_{66}} \end{pmatrix} \tag{4.36}$$

The later can be expressed by $\overline{A_{12}} = \overline{A_{66}}$; $\overline{A_{23}} = \overline{A_{44}}$; $\overline{A_{13}} = \overline{A_{55}}$, which reduces the number of independent components to six, thus leading to eq. (4.37) [41].

$$\begin{aligned} \overline{A_{11}} + \overline{A_{66}} + \overline{A_{55}} &= \alpha_1 \\ \overline{A_{66}} + \overline{A_{22}} + \overline{A_{44}} &= \alpha_2 \\ \overline{A_{55}} + \overline{A_{44}} + \overline{A_{33}} &= \alpha_{31} \end{aligned} \tag{4.37}$$

These properties of the fourth-order tensor permit only the determination of three values of $\overline{A_{mn}}$ in the eigenvector basis of a_2: $\overline{A_{11}}$;$\overline{A_{22}}$;$\overline{A_{33}}$.

There are different forms of orthotropic approximations in the literature [27, 41, 45]:

- ORS or "orthotropic smooth," which corresponds to a smoothed approximation
- ORF or "orthotropic fitted" valid for an interaction coefficient $C_I \approx 0.01$
- ORL valid for a relatively weak interaction coefficient $C_I \approx 0.001$
- ORT valid for a zero interaction coefficient

The purpose of these approximations is to exhibit $\overline{A_{ii}}$ values for a given flow and a given interaction coefficient.

4.6 Effect of fiber orientation on mechanical properties

Fiber orientation, fiber length, fiber dispersion, fiber geometry, and the degree of interfacial adhesion between fiber and matrix affect the materials' mechanical properties. However, it was reportedthat the "fiber orientation factor" and "fiber length factor" contribute the most to the strength of the composite [12]. Indeed in the literature, several theoretical models have been developed to predict the composite mechanical properties based on the relation between these parameters [12].

The simplest and most obvious way to predict the Young's modulus is to assume that fiber orientations are organized completely in parallel or in series as follows:

4.6.1 Voigtmodel or rule of mixture/Reuss model or inverse rule of mixture

The Voigt model assumes that all material elements are parallel to the externally applied stress, while the Reuss model assumes that the material elements are aligned perpendicular to the direction of the externally applied stress. Both models can be described respectively by eqs. (4.38) and (4.39) [47, 48]:

$$E_V = V_f E_f + \left(1 - V_f\right) E_m \tag{4.38}$$

$$E_R = \frac{E_f\, E_m}{V_f E_m + \left(1 - V_f\right) E_f} \tag{4.39}$$

where E_V and E_R are respectively the Voigt and the Reuss elastic modulus, E_f and E_m represent the fiber and the matrix elastic modulus, respectively, and V_f is the fiber volume fraction.

4.6.2 Modified rule of mixture

The ROM has been modified by introducing an efficiency factor η_e, which can be expressed as the product of the efficiency factor of orientation η_o and the efficiency factor of length η_l, being $\eta_e = \eta_o.\eta_l$. Its formulation for the Young's modulus is eq. (4.40) [49, 50]:

$$E_{m\mathrm{ROM}} = {}_e V_f E_f + \left(1 - V_f\right) E_m \tag{4.40}$$

According to Cox–Krenschel's model, the length efficiency factor η_l can be expressed by eq. (4.41) [49, 50]:

$$\eta_1 = 1 - \frac{\tanh(\beta.l/2)}{(\beta.l/2)} \text{ with } \beta = \frac{1}{r}\sqrt{\frac{E_m}{E_f.(1-\nu).\ln.\sqrt{\pi/4.V_f}}} \tag{4.41}$$

where β is the coefficient of stress concentration rate at the end of the fibers, r is the mean radius of fiber, l is the fiber's length, and ν is the Poisson's ratio.

On the other hand, Fukuda and Kawata developed a methodology for calculating the efficiency factor of orientation η_o according to the fiber distribution in the matrix by using a limit angle (α_o) (eq. (4.42)) [49, 50]:

Rectangular distribution:

$$\eta_o = \frac{\sin(\alpha_0)}{(\beta.l/2)}.\left(\frac{3.\nu.\sin(\alpha_0)}{4.\alpha_0} + \frac{(1-\nu).\sin(3.\alpha_0)}{4.3.\alpha_0}\right) \tag{4.42a}$$

Sinusoidal distribution:

$$\eta_o = \frac{\pi^2}{16}.\left(\frac{1}{\frac{\pi}{2}+\alpha_0} + \frac{1}{\frac{\pi}{2}-\alpha_0}\right) \cos(\alpha_0).\left[\frac{3-\nu}{4}.\left(\frac{1}{\frac{\pi}{2}+\alpha_0} + \frac{1}{\frac{\pi}{2}-\alpha_0}\right)\cos(\alpha_0) + \frac{1+\nu}{4}.\left(\frac{1}{\frac{\pi}{2}+3\alpha_0} + \frac{1}{\frac{\pi}{2}-3\alpha_0}\right)\cos(3\alpha_0)\right] \tag{4.42b}$$

Triangular distribution:

$$\eta_o = 4.\frac{1-\cos(\alpha_0)}{\alpha_0^2}.\left(\frac{3-\nu}{4}.\frac{1-\cos(\alpha_0)}{\alpha_0^2} + \frac{1+\nu}{4}.\frac{1-\cos(3\alpha_0)}{9.\alpha_0^2}\right) \tag{4.42c}$$

Halpin–Tsai model

It is used in the system of polymeric blends for unidirectional continuous and discontinuous phases. It also considered the fiber morphology by including an adjustable parameter noted ξ as expressed in eq. (4.43). It is worth noting that for $L \to 0$ and $\xi \to 0$, the H–T model is a reduced Reuss model. Contrariwise, for $L \to \infty$ and $\xi \to \infty$ it is reduced to Voigt model [47, 49–51].

$$E_{H-T/L} = E_m\left(\frac{1+\xi.\eta_L.V_f}{1-\eta_L.V_f}\right) with \eta_L = \frac{(E_f/E_m)-1}{(E_f/E_m)+\xi}; \xi = 2L/T \text{ or } \xi = 2L/D \tag{4.43a}$$

$$E_{H-T/T} = E_m\left(\frac{1+2.\eta_T.V_f}{1-\eta_T.V_f}\right) \text{with} \eta_T = \frac{(E_f/E_m)-1}{(E_f/E_m)+2}; \xi = 2L/T \text{ or } \xi = 2L/D \tag{4.43b}$$

where $E_{H-T/L}$ and $E_{H-T/T}$, respectively denote the Halpin–Tsai longitudinal and transversal elastic modulus. L, T, and D are the length, thickness, and diameter of

the fiber, respectively. ξ represents the measure of fiber geometry, fiber distribution, and fiber loading conditions.

Modified Halpin–Tsai model

Nielson modified the Halpin–Tsai equation by considering the particle packing fraction, which is the true (apparent) volume occupied by filler noted $\phi_{\max}$. Theoretically, it can take a maximum value of 0.785, 0.907, and 0.82 for the arrangement of square, hexagonal, and random fibers. According to eq. (4.44) [47]:

$$E_{m-H-T/L} = E_m\left(\frac{1+\xi.\eta_L.V_f}{1-\eta_L.\Psi.V_f}\right) \text{ with } \Psi = 1+1\left(-\frac{\phi_{\max}}{\phi^2{}_{\max}}\right)V_f \tag{4.44}$$

where $E_{m-\mathrm{H}-T/L}$ is the modified Halpin–Tsai longitudinal elastic modulus.

Hui–Shia model

It has been developed for longitudinal and transversal alignment fibers according to their aspect ratio α and expressed as in eq. (4.45) [47, 48]:

$$E_{H-S/L} = E_m\left(1-\frac{V_f}{\xi}\right)^{-1} \tag{4.45a}$$

$$E_{H-S/T} = E_m\left(1-\frac{V_f}{4}\left(\frac{1}{\xi}+\frac{3}{+J}\right)\right)^{-1} \tag{4.45b}$$

where

$$\xi = V_f + \frac{E_m}{E_f+E_m} + 3\left(1-V_f\right)\left[\frac{(1-g)\alpha^2-\frac{g}{2}}{\alpha^2-1}\right] \tag{4.45c}$$

$$g = 1-\frac{\ln(2\alpha)-1}{\alpha^2} \text{ with } \alpha \geq 1 \tag{4.45d}$$

$$J = \left(1-V_f\right)\left[\frac{3\left(\alpha^2+0.25\right)g-2\alpha^2}{\alpha^2-1}\right] \tag{4.45e}$$

$E_{H-S/L}$ and $E_{H-S/T}$ are respectively the Hui–Shia longitudinal and transversal elastic modulus.

Hashin and Shtrikman model

It considers the macroscopic isotropic orientation and the quasi-homogeneity of the composite, where the shape of the filler is not a limiting factor, and estimated the

longitudinal and transverse Young's modulus by adjusting the bulk moduli K and shear moduli G of the composites as expressed in eq. (4.46) [48, 52].

$$E_{\mathrm{Ha-S}} = \frac{9.K}{1+3.K/G} \tag{4.46a}$$

$$K_L = K_f + \left(1-V_f\right)\left[\frac{1}{K_m - K_f} + \frac{3.V_f}{3K_f - 4G_f}\right]^{-1}; G_L = G_f + \left(1-V_f\right)\left[\frac{1}{G_m - G_f} + \frac{6.V_f\left(K_f + 2.G_f\right)}{5.G_f(3K_f - 4G_f)}\right]^{-1} \tag{4.46b}$$

$$K_T = K_m + V_f\left[\frac{1}{K_f - K_m} + \frac{3.(1-V_f)}{3K_m - 4G_m}\right]^{-1}; G_T = G_m + V_f\left[\frac{1}{G_f - G_m} + \frac{6.\left(1-V_f\right)(K_m + 2.G_m)}{5.G_m(3K_m - 4G_m)}\right]^{-1} \tag{4.46c}$$

$E_{\mathrm{Ha-S}}$ is the Hashin and Shtrikman Young's modulus; K_L, K_T, G_L, and G_T, respectively denote the longitudinal and transversal bulk and shear modulus, and K_f, K_m, G_f, and G_m, respectively represent the fiber and the matrix bulk and shear modulus.

On the other hand, other models account for relative contributions of both longitudinal and transversal approach to predict mechanical properties among them.

Tsai–Pagano model

It assumes a random filler orientation in the matrix as well as good dispersion and perfect fiber–matrix interfacial adhesion. It also includes the reinforcing length and diameter of the fibers. According to eq. (4.47), he used values of 3/8 and 5/8 as a contribution of the longitudinal and transversal models, respectively [49, 50, 53].

$$E_{T-P} = \frac{3}{8}E_V + \frac{5}{8}E_R \tag{4.47a}$$

$$E_{T-P} = \frac{3}{8}E_{H-T/L} + \frac{5}{8}E_{H-T/T} \tag{4.47b}$$

where E_{T-P}, E_V, and E_R are the Tsai–Pagan, Voigt and Reuss elastic modulus, respectively.

Hirsch model

It takes into account the effects of fiber orientation and stress concentration (fiber ends) by introducing an empirical parameter "x" ($0 < x < 1$) into eq. (4.48), which is also the combination of parallel and serial models. A value of $x = 0.5$ has been proposed for a random fiber orientation [50, 51, 54].

$$E_H = \mathrm{x}\ E_V + (1 - x)E_R \tag{4.48}$$

where E_H is the Hirsch elastic modulus.

Self-consistent approach (modified Hirsch model)

Semlali et al. [4] developed a model based on a self-consistent approach, and in each iteration modified Hirsch model is used, to predict the composite properties while considering the effect of reinforcement content and orientation. The modification of Hirsch model consists of taking the empirical parameter (x) to be proportional to the fiber orientation factors (α), also ranging between 0 and 1 to give a best fit as given in eq. (4.49). The self-consistent approach is based on the iterative insertion of a family of fiber orientation; hence, the first category of fibers was included in the matrix to constitute an equivalent homogeneous material which, in turn, is integrated into an infinite composite.

$$E_h = \alpha\ E_V + (1 - \alpha)E_R \tag{4.49}$$

where E_h is the modified Hirsch elastic modulus.

Gupta et al. [51] assumed Young's modulus of four types of fiber arrangement in a thermoplastic material reinforced with wood fibers (L = 3.5 mm and d = 0.025 mm), using four models: (1) Voigt, (2) Reuss, (3) Hirsch, and (4) Halpin–Tsai. By neglecting the fiber length effect on the composite properties, the first arrangement assumes that the fiber orientations are completely parallel, the second considers an ideal transverse alignment,the third case assumes that the fiber are half arranged in parallel and half in series, and finally in the fourth case a random fiber orientation was considered. From the four models, results show that the parallel model gives the best prediction to the Young's modulus, while the series model predicts the lowest value, which is also under the experiment results. Regarding the Hirsch and Halpin–Tsai models, they predicted a Young's modulus lower than the parallel model but higher than the experimental results [51].

On the other hand, Sawpan et al. [54] compared the predicted tensile properties of the poly(lactic acid) reinforced with hemp fiber using the ROM, inverse rule of mixture (IROM), and Hirsch models. It was observed that the Hirsch model gives a close agreement with the experimental results when the value of x is taken as 0.6 [54].

For their parts, Facca et al. [55] investigate high-density polyethylene (HDPE) reinforced with short natural fibers (hemp–hardwood, rice hulls), the comparison between the experimental data and the results provided by various theoretical models in terms of Young's modulus such as Voigt, Reuss, Halpin–Tsai, and others are not mentioned in this work. It was observed for all the reinforcement that the Halpin–Tsai equation was the most accurate to predict tensile modulus among others [55, 56].

In addition, Krishnan et al. [47] tried the tensile prediction of thermoplastic material reinforced with long fibers using Voigt, Reuss, Hirsch's, Halpin–Tsai, modified Halpin–Tsai, Halpi–Pagano, and Hui–Shia models. The comparison shows that Hui–Shia, Series and Hirsch models best fit to the experimental results, while the parallel, Halpin–Tsai, and modified H–T models overestimate Young's modulus values [47].

Finally, Semlali et al. [4] compared the predicted elastic modulus using the self-consistent approach, Hirsch and Tsai–Pagano models of the PP/coir fibers biocomposites with the experimental one. Overall, the new model gives better predictions of the experimental data compared with the original Hirsch and Tsai–Pagano models.It seems that the absence of specific fiber morphology in the original Hirsch model had a small effect on the calculations [4].

To conclude that each of these models can be perform according to the fiber concentration, the fiber aspect ratio, the fiber adhesion to the matrix, the volume fraction, the fiber orientation, and its dispersion in the matrix [47].

4.7 Conclusion

This chapter highlights the orientation phenomena for thermoplastic composite reinforced with natural fibers. During the injection filling process, fiber orientation differs from the thick c avity to the thin cavity, so various observations are made. In a thick mold, a layered structure appears because of the fountain flow. Indeed, by moving the material from the center zone to the wall, a core layer with a transverse fiber direction is formed in the middle, a skin layer is formed on the wall of the mold with an isotropic orientation; however, between these two layers, the shear flow leads to the formation of the shell layer that flow-align fibers, producing the core–shell–skin layer. Conversely, in a thin cavity, the fibers adopt a flat and specific orientation throughout the thickness,that is nearly perpendicular at the center line because of the divergent flow and nearly parallel at the mold walls because of the convergent flow.

Additionally, the study of the parameters influencing the fibers' orientation, such as the gate position, injection parameters, matrix rheology, reinforcement nature, and the geometry mold shows that they have a direct effect on the fiber orientation distribution of the part.

Once the orientation and distribution of the fibers are determined, this will help to predict the mechanical properties of the composite. Indeed, several theoretical models have been developed, namely Voigt, Reuss, modified ROM, Halpin–Tsai, modified Halpin–Tsai, Hui–Shia, Hashin, Shtrikman, Hirsch, and Tsai–Pagano models. It should be noted that, it is important to take into account certain parameters like fiber concentration, fiber aspect ratio, the

adhesion between fiber and matrix, and the fiber orientation and its distribution in the matrix to have more accuracy between the model used and the experimental data.

Acknowledgements: This work was supported by MAScIR; Moroccan Foundation for Advanced Science, Innovation and Research, MESRSFC; and CNRST, Morocco grant no. 1970/15.

References

[1] El Mechtali, F. Z. et al. "Mechanical and thermal properties of polypropylene reinforced with almond shells particles: impact of chemical preatments." J. Bionic. Eng., 2015, 123, 483–494.
[2] Essabir, H. et al. "Bio-composites based on polypropylene reinforced with almond shells particles: mechanical and thermal properties." Mater. Des., 2013, 51, 225–230.
[3] Ouarhim, W., Bensalah, M., Rodrigue, D., Essabir, H., & Bouhfid, R. "Production and characterization of high density polyethylene reinforced by eucalyptus capsule fibers." J. Bionic. Eng., 2018, 15, 558–566.
[4] Semlali Aouragh Hassani F.Z et al. "Mechanical properties prediction of polypropylene/short coir fibers composites using a self-consistent approach." Polym. Compos.,doi.org/10.1002/pc.24967
[5] Ouarhim, W., Zari, N., Bouhfid, R., & El Kacem Qaiss, A.. "Mechanical performance of natural fibers–based thermosetting composites," Mech. Phys. Test. Biocomposites, Fibre-Reinforced Compos. Hybrid Compos., 2019, 43–60.
[6] Bay, R. S., & Tucker, C. L. "Fiber orientation in simple injection moldings. part ii: experimental results." Polym. Compos., 1992, 13,4, 317–331.
[7] Özdemir, A., Uluer, O., & Güldaş, A. "Flow front advancement of molten thermoplastic materials during filling stage of a mold cavity." Polym. Test., 2004, 23(8), 957–966.
[8] Whiteside, B. R., Coates, P. D., Hine, P. J., & Duckett, R. A. "Glass fibre orientation within injection moulded automotive pedal – Simulation and experimental studies." Plast. Rubber Compos., 2000, 291, 38–45.
[9] Gupta, M., & Wang, K. K. "Fiber orientation and mechanical properties of short-fiber-reinforced injection-molded composites: simulated and experimental results." Polym. Compos., 1993, 14(5), 367–382.
[10] Jeffery, G. B. "The motion of ellipsoidal particles immersed in a viscous fluid." Proc. R. Soc. A Math. Phys. Eng. Sci., 1922, 102715, 161–179.
[11] Folgar, Fransisco, & Tucker III, Charles L. "Orientation behavior of fibers in concentrated suspensions." J. Reinf. Plast. Compos., 1984, 32, 98–119.
[12] Kalaprasad, G., Joseph, K., Thomas, S., & Pavithran, C. "Theoretical modelling of tensile properties of short sisal fibre-reinforced low-density polyethylene composites." J. Mater. Sci., 1997, 32, 16, 4261–4267.
[13] Kurakina, T. "Characterization of fiber and verssel elements in pulp suspension images." Master's thesis, Lappeenranta University of Techonology, Lappeenranta, Finland, 2012.
[14] Redjeb, A. "Simulation numérique de l'orientation de fibres en injection de thermoplastique renforcé." Ecole Nationale supérieure des mines de Paris, 2007.
[15] Tornberg, A. K., & Shelley, M. J. "Simulating the dynamics and interactions of flexible fibers in Stokes flows." J. Comput. Phys., 2004, 1961, 8–40.

[16] Bay, R. S., & Tucker, C. L., "Stereological measurement and error estimates for three-dimensional fiber orientation." Polym. Eng. Sci., 1992, 324, 240–253.
[17] Pontes, A. J., Neves, N. M., & Pouzada, A. S. "The role of the interaction coefficient in the prediction of the fiber orientation in planar injection moldings." Polym. Compos., 2003, 243, 358–366.
[18] Givler, R. C., Crochet, M. J., & Pipes, R. B. "Numerical prediction of fiber orientation in dilute suspensions." J. Compos. Mater., 1983, 174, 330–343.
[19] Megally, A., & Etude, A. M. "Etude et modélisation de l'orientation de fibres dans des thermoplastiques renforcés." 2005.
[20] Gao, Y. et al. "Flow-induced crystallization of long chain aliphatic polyamides under a complex flow field: inverted anisotropic structure and formation mechanism." Polymer (Guildf)., 2015, 73, 91–101.
[21] Shokri, P., & Bhatnagar, N. "Effect of the post-filling stage on fiber orientation at the mid-plane in injection molding of reinforced thermoplastics." Phys. Procedia, 2012, 25, 79–85.
[22] Chung, S. T., & Kwon, T. H. "Numerical simulation of fiber orientation in injection molding of short-fiber-reinforced thermoplastics." Polym. Eng. Sci., 1995, 357, 604–618.
[23] Coulon, A. "Injection des polyamides renforcés de fibres de verre longues: Relations mise en oeuvre/comportement thermomécanique." 2008.
[24] Caton-Rose, P., Hine, P. J., & Parveen, B. "Prediction of fibre orientation in short glass fibre reinforced composite injection moulding." 19Th Int. Conf. Compos. Mater., 2013, 1706–1713.
[25] Vincent, M., Giroud, T., Clarke, A., & Eberhardt, C. "Description and modeling of fiber orientation in injection molding of fiber reinforced thermoplastics." Polymer (Guildf)., 2005, 4617, 6719–6725.
[26] Han, K., Im, Y., Han, K., & Im, Y. "Modified hybrid closure approximation for prediction of flow-induced fiber orientation." Rheology, 1999, 433, 569–589.
[27] Chung, D. H., & Kwon, T. H. "Fiber orientation in the processing of polymer composites." Korea-Australia Rheol., 2002, 144, 175–188.
[28] Bay, R. S., & Tucker, C. L. "Fiber orientation in simple injection moldings. Part I: theory and numerical methods." Polym. Compos., 1992, 134, 317–331.
[29] Advani, S. G. "The use of tensors to describe and predict fiber orientation in short fiber composites." J. Rheol. (N. Y. N. Y)., 1987, 318, p. 751.
[30] Jackson, W. C., Advani, S. G., & Tucker, C. L. "Predicting the orientation of short fibers in thin compression moldings." J. Compos. Mater., 1986, 206, 539–557.
[31] Ihsane, MODHAFFAR. "Modélisation numérique et simulation de l'orientation des fibres courtes dans une matrice thermoplastique." Faculté des sciences de Rabat, 2016.
[32] Miled, H. "Modélisation de l'orientation de fibres induite par l'écoulement et comportement élastique anisotrope à l'état solide." Ecole Nationale Supérieure des Mines de Paris, 2010.
[33] Hand, G. L. "A theory of anisotropic fluids." J. Fluid Mech., 1961, 131, 33–46.
[34] Ghering, Florian. "Etude du comportement mécanique et de l'endommagement de composites thermoplastiques renforcés de fibres courtes de chanvre: Approche expérimentale et modélisation." Université de Lorraine, 2013.
[35] Altan, M. C., Subbiah, S., Guceri, S. I., & Pipes, R. B. "Numerical prediction of three-dimensional fiber orientation in hele-shaw flows." Polym. Eng. Sci., 1990, 3014, 848–859.
[36] Crevecoeur, G. "Morphology and mechanical properties of thermoplastic composites containing a thermotropic liquid crystalline polymer." Polym. Eng. Sci., 1990, 309, 532–542.
[37] Pedicini, A., & Farris, R. J. "Mechanical behavior of electrospun polyurethane." Polymer (Guildf)., 2003, 44, 6857–6862.

[38] Aaron, P. W., Eberle, P. R., Vélez-García, Gregorio M., & Baird, Donald G. “Fiber orientation kinetics of a concentrated short glass fiber suspension in startup of simple shear flow.” J. Nonnewton. Fluid Mech., 2010, 1653–4, 110–119.
[39] Redjeb, A., Silva, L., Laure, P., Vincent, M., & Coupez, T. “Three dimensional numerical simulations of fiber orientation in injection molding.”
[40] Lipscomb, G. G., Denn, M. M., Hur, D. U., & Boger, D. V. “The flow of fiber suspensions in complex geometries.” Journal of Non-Newtonian Fluid Mechanics, 1988, 26, 297–325.
[41] Jr, J. S. C., Iii, C. L. T., Cintra, J. S., & Tucker, C. L. “Orthotropic closure approximations for flowinduced fiber orientation Orthotropic closure approximations for flow-induced fiber orientation.” Rheology, 1995, 396, 1095–1122.
[42] Advani, S. G., Iii, C. L. T., Advani, B. G., & Iii, C. L. T. “Closure approximations for three dimensional structure tensors Closure.” J. Rheol. (N. Y. N. Y)., 1990, 343, 367–386.
[43] Advani, S. G., & Tucker, C. L. “The use of tensors to describe and predict fiber orientation in short fiber composites.” J. Rheol., 1987, 318, 751–784.
[44] Hinch, B. E. J., & Leal, L. G. “Constitutive equations in suspension mechanics. Part 1. General formulation.” Fluid Mech., 1975, 71, 481–495.
[45] Chung, DU huan, & Won, Tai Hun. “Improved model of orthotropic closure approximation for flow induced fiber orientation.” Polym. Compos., 2001, 225, 636–649.
[46] Verleye, F. D. V., & Couniot, A. “Numerical prediction of fibre orientation in complex injection-moulded parts.” Trans. Eng. Sci., 1994, 4, 303–312.
[47] Krishnan, K. A., Anjana, R., & George, K. E. “Effect of Alkali-Resistant Glass Fiber on Polypropylene / Polystyrene Blends: modeling and Characterization.” Polym. Compos., 2014, 37, 1–9.
[48] Hu, H., Onyebueke, L., & Abatan, A. “Characterizing and odeling mechanical properties of nanocomposites- Review and evaluation.” J. Miner. Mater. Charact. Eng., 2010, 94, 275–319.
[49] Delgado-Aguilar, F. X. E. M., Julián, F., Tarrés, Q., Méndez, J.A., & Mutjé, P. “Bio composite from bleached pine fibers reinforced polylactic acid as a replacement of glass fiber reinforced polypropylene, macro and micro-mechanics of the Young’s modulus.” Compos. Part B Eng., 2017, 125, 203–210.
[50] Oliver-Ortega, P. M. a H., Granda, L.A., Espinach B, F.X., Delgado-Aguilar A, M., & Duranc and A, J. “Stiffness of bio-based polyamide 11 reinforced with softwood stone ground-wood fibres as an alternative to polypropylene- glass fibre composites.” Eur. Polym. J., 2016, 84, 481–489.
[51] Gupta, R., Sulaiman, N., & Gupta, A. “An improved algorithm for prediction of Young’s Modulus of wood plastic composites.” Sci. Res. Essays, 2013, 816, 649–656.
[52] Ahmed, F. R. J. S. “A review of particulate reinforcement theories for polymer composites.” J. Mater. Sci. 25, 1990, 25, 4933–4942.
[53] López, J. P., Mutjé, P., Pèlach, M. À., El Mansouri, N.-E., Boufi, S., & Vilaseca, F. “Analysis of the tensile modulus of polypropylene composites reinforced with stone groundwood fibers.” BioResources, 2012, 71, 1310–1323.
[54] Sawpan, M. A., Pickering, K. L., & Fernyhough, A. “Hemp fibre reinforced poly(Lactic Acid) composites.” Adv. Mater. Process. IV, 2007, 29–30, 337–340.
[55] Facca, A. G., Kortschot, M. T., & Yan, N. “Predicting the elastic modulus of natural fibre reinforced thermoplastics.” Compos. Part A Appl. Sci. Manuf., 2006, 3710, 1660–1671.
[56] Ku, H., Wang, H., Pattarachaiyakoop, N., & Trada, M. “A review on the tensile properties of natural fiber reinforced polymer composites.” Compos. Part B Eng., 2011, 424, 856–873.

Damenortey R. Akwada, Esther T. Akinlabi

5 Mechanical properties of bamboo yarn

A biodegradable composite material for structural works

Abstract: The hazardous effects of synthetic and petroleum-based polymers on the environment have called for environmental friendly, renewable, and sustainable materials and have become a topic of research for many scientists and other researchers across the globe, researching natural fibers as an alternative reinforcement polymer composite raw material. Natural fibers are readily available and cheap and have less weight, less energy, and superior mechanical properties such as high strength and stiffness. Bamboo yarn as reinforcement of polymer composites is nonabrasive, ecofriendly, and biodegradable and can serve as a raw material for industrial engineering applications. In this chapter, the study aims to evaluate the mechanical properties of bamboo yarn (woven or bidirectional) and (unwoven or 45° orientation) as reinforcement in polymer composite, an innovation to utilize its properties in structural designing and fabrication of laminates. The extraction and treatment processes of bamboo yarn and its application as reinforcement in polymer composite are explained in this chapter. The impact, flexural, tensile, and scanning electron microscope were performed to evaluate the mechanical properties and surface morphology of the composites. The influence of bamboo yarn orientation, yarn content, size, and treatment agents on the mechanical properties of the composite was investigated. The chapter discusses the fabrication process of the composite and examines the bamboo yarn–epoxy matrix interfacial bonding, taking into consideration the moisture effect on the composite. The thermal stability and thermal degradation of the composite were investigated using thermogravimetric analysis and differential thermogravimetric analysis in a nitrogen atmosphere.

Keywords: Bamboo yarn, bamboo extraction, epoxy matrix, mechanical properties, treatment process, thermogravimetric analysis, woven bamboo yarn

5.1 Introduction

Determining the mechanical properties of materials helps to evaluate the amount of load that can be subjected to the material and the kind of structural loads it can

Damenortey R. Akwada, Esther T. Akinlabi, Department of Mechanical Engineering Science, University of Johannesburg, Auckland Park, South Africa

https://doi.org/10.1515/9783110603699-005

bear. The study of mechanical properties when assessing natural fiber composites includes fracture toughness and impact, stiffness, and strength. The chapter also deals with the effect of thermal degradation on the mechanical properties of the composite. The impact, flexural, and tensile testing methods are the frequent tests conducted mostly on natural fiber composites, which are in accordance with the ASTM standards.

The impact strength of a material is the degree of fracture toughness of a material subjected to load, and it measures the absorbing energy before fracture of a given material [1]. The factors that influence the impact property of a given fiber-reinforced polymer composite material include the applied matrix properties, the fiber properties, the interfacial bonding strength, and the type of fabrication [2]. The available equipment used includes Charpy and Izod impact tests.

The tensile properties of a given material are determined by the tensile strength and tensile modulus of the material using ASTM D3039. To facilitate the test of the composite specimens, they are cut into a dog's bone shape for the testing process at each end of the specimen fixed in between the jaws of the machine. A universal testing machine is mostly employed to measure the tensile testing results. The cross-head speed for testing is placed into the system, and the load is applied to the specimen for generating data. The mechanical property data and graph generated from the test of the specimens are then recorded and stored in a computer system connected to the load head of the machine.

Flexural test of the composite material exhibits compression and tensile stresses as its resultant outcome. The flexural strength and modulus of the natural fiber composite can be determined using the ASTM D790 method by using the universal testing machine. The natural fiber-reinforced composite (NFRC) specimen is prepared with a rectangular cross section in either three- or four-point bending mode.

Thermal degradation is a fundamental environmental factor that has a significant influence on the mechanical properties of polymeric materials [3]. When temperatures are higher than those required for the processing, they can adversely affect the mechanical properties of the composite materials and will cause damage including fiber breakage, matrix cracking, interlaminar cracks, subsurface delamination, and intraply damage [4]. Natural fibers tend to degrade at a lower temperature compared with synthetic fibers [5]. Kabir et al. [6] stated that knowing the temperature of a composite is important for both the manufacture and users of the composite materials. The thermal degradation of certain NFRCs has been investigated [7–9]. Thermogravimetric analysis (TGA) and differential thermogravimetric analysis (DTA) are used to measure the weight loss percentage of substances monitored as a function of temperature or time in a controlled atmosphere [10, 11]. The temperature range at which a material changes its state from rigid, hard, or glassy to a more flexible, compliant, or rubbery state is known as glass transition temperature (T_g).

5.1.1 Composite material

Composites primarily consist of two or more elements that chemically bond together to produce a new material with improved properties compared with its original constituents. The fundamental components of a composite material are the matrix (bonding material) and the reinforcement material (fibers or particles) [12]. A matrix serves as a binder to the reinforcement material in the composite material, as the reinforcement material offers the shape and the internal structure of the composite [13, 14]. The reinforcing elements are stronger and stiffer than the bonding matrix as they impact their unique mechanical properties to enhance the matrix properties [15]. The matrix material is classified into three different kinds, namely, polymer matrix, metal matrix, and ceramic matrix, with each category of composite material used for specific applications [16]. When these categories of matrices are used to produce any composite, the final product is described by the name of the matrix used for the producing that composite (e.g., polymer matrix composite, metal matrix composite, and ceramic matrix composite). Currently, polymer matrix composites are the most widely used due to the numerous advantages of adhesion to other materials, with high mechanical and chemical properties, thus resulting in an increase of its application in structural works [4, 12, 16, 17]. Polymer matrix composites can be classified in two classes, namely, thermoplastics matrix and thermosets matrix materials [14, 18]. Some of the commonly used thermoplastics matrices include polypropylene, polyethene, polyvinyl chloride, polystyrene, polylactic acid, and high-density polyethene. In addition, some commonly used thermosets matrix includes epoxy, polyester, elastomer, and phenolics [7, 18–21]. Composite materials have many advantages such as lightweight, high stiffness, high tensile strength, high fracture toughness, excellent corrosion, abrasion resistance, and low cost [12, 16]. They offer designers the ability to combine functions and form and use materials to make a system more efficient [22–24]. The development of new design processes for manufacturing encourages the use of composite materials despite some technical and economic problems [23]. The utilization of synthetic polymeric products has been beneficial to industrial development, but the lifecycle disposal effects cause severe hazards to the environment, resulting in global warming as most synthetic polymers composites are derived from petroleum source and are nondegradable [16].

5.1.2 Natural fibers reinforcement

In the past few years, the serious environmental concerns across the globe have led to research sustainable materials as a substitute for synthetic and petroleum-based polymer composites, which include aramid, carbon fiber, and glass fiber [12, 13]. There has been considerable research interest in the development of NFRC [16, 17]. Research of natural fiber-reinforced polymer composites with thermoplastic and thermoset matrix

is emerging as a new area of scientific interest for modern material production for industrial applications. NFRCs are plant-based natural fibers, such as flax, hemp, jute, kenaf, sisal, and bamboo [7, 13, 18, 25]. Natural fibers used as reinforcement in polymer possess outstanding properties over synthetic fiber reinforcement, which includes low density, renewability, readily available, lightweight, biodegradability, nontoxicity, less expensive, and better mechanical properties [15, 18, 26, 27]. The properties of natural fiber composites indicate specific features that are comparable to the conventional fiber composites; in several fields of engineering applications, these materials successfully substitute inorganic fiber composites [28]. The current developments in natural fiber researches are the use of bamboo fiber in various polymeric composite products, which have been used as high-performance composite materials for structural applications [22, 25]. The characteristics and usage of bamboo fiber in different industrial applications have been widely investigated, but researches into bamboo yarn for industrial structural applications have but very scanty information [29]. The innovation to improve green construction examines the mechanical properties of bamboo yarn-reinforced epoxy composite for industrial engineering applications. Bamboo yarn is obtained from the bamboo culm in the bamboo plant, which is readily available, biodegradable, and cheap natural resource. The fabrication of bamboo fiber-reinforced composites with thermoset or thermoplastic matrix and high-volume polymers are commonly used now.

Advantages of natural fibers

Comparing natural fibers as reinforcement in a polymer matrix to the conventional-reinforcing fibers such as carbon, glass, and Kevlar, the following are the advantages of natural fibers over the traditional reinforcing ones:

i. Abundant with an unceasing supply of materials
ii. Light in weight
iii. Environmental friendly
iv. It is renewable
v. Biodegradable
vi. Low cost
vii. Low density
viii. Easy to handle
ix. Nontoxic
x. Nonabrasive during processing and use
xi. High toughness
xii. High specific strength properties
xiii. Good thermal properties
xiv. It has high insulation against heat and noise
xv. Enhanced energy recovery

xvi. Reduced tool wear
xvii. Ease of separation
xviii. Free from health hazards

Disadvantages of natural fibers

The following are the disadvantages associated with natural fibers:
i. Relatively, natural fibers are characterized by inherent high moisture absorption
ii. It has low resistance to moisture
iii. It has weak adhesion with hydrophobic polymer matrix
iv. With an extended period of storage time, the fibers degrade
v. Hygroscopicity
vi. Low thermal stability

Types of fiber reinforcement in a matrix

The two types of fiber reinforcement in polymer matrix composites are long continuous and short discontinuous fibers. The long continuous fibers include the woven fibers when embedded in an even shape arrangement in the polymer matrix; its final product has excellent mechanical characteristics in the composite when compared to short continuous fibers. On the other hand, fibers less than 3cm in length are called short continuous fibers, which can be found in the form of powder or flakes. Short continuous fibers are mostly applied as fillers in the polymer as they do not provide much reinforcement to the composites. For this reason, they are mostly described as low-performance composites.

5.1.3 Epoxy

Epoxies are the most effective choice of matrix used in fiber-reinforced composite when compared with other polymers. Epoxy matrices are characterized by high strength, fatigue resistance, simple to process, and have excellent adhesion to several surfaces [30]. Numerous researches have been conducted on the applications of epoxy composites using synthetic fibers, natural fibers, and the combination of synthetic and natural fibers (hybrid). The outcomes of some of the research work from previous studies show that epoxies are pliable to several kinds of reinforcement fibers. The outstanding properties exhibited by epoxy-based composites have paved way for its applications across several engineering fields [31, 32].

5.1.4 Bamboo

Bamboo is a type of grass with its microstructure being significantly more than timber, and a heterogeneous consisting of small dense cellulose fiber embedded in a less dense lignin matrix [15, 18, 25, 33]. Bamboo matures for harvest within 3–5 years and regenerative compared to soft and hardwood, which takes 30–70 years [25, 34–38]. Some bamboo species may grow tall in a couple of weeks, with a speed of 50 cm, while other species surge skyward as fast as 8 in in a day and reach a height of (20–40 m) in Manson climates. Bamboo is divided into upper and lower section with the upper being made of the culm, leaves and branches and the lower as roots. The culm is characterised by a hollow tube with thin walls consisting of several vascular bundles embedded in parenchyma tissue and distributed across the wall thickness [37]. The culms tissue comprises parenchyma and vascular bundles, which are made of vessels and fiber. Cellulose fibers are arranged along the length of the culm, providing maximum tensile, flexural, and rigidity strength in that direction [34]. Bamboo is a renewable and sustainable plant with about 75 genera and more than 1,500 species worldwide [25, 39]. It releases about 36% more oxygen and sequesters tons of CO_2 from the atmosphere [15, 18, 40, 41]. It is abundantly found in tropical countries and is widely distributed across the globe including Africa, Asia, and Latin and South America, where it is demand for industrial applications [25, 36]. Bamboo can be grouped into two types: herbaceous type (food and medicine) and woody type (industrial wood) [25, 34].

5.1.5 Bamboo yarn

Bamboo yarn is manufactured using a mechanical processing technique where the solid bamboo culms are crushed, after which natural enzymes are used to break the crushed bamboo culms into a soft element using a mechanical process to take out the fibers before spinning into yarn. The extracted yarn is derived from the pulp of the bamboo culm by employing the wet spinning process, hydrolysis-alkalization treatment, and multiphase bleaching process, which cause the yarn fiber to exhibit some similar characteristics as that of viscose rayon [42]. Bamboo yarn is 100% made from bamboo, which is well selected from the nonpolluted environment, and the entire distillation and production process strictly adopt green processing standards according to ISO 9000 and ISO 14000 [43, 44]. The bamboo extracted and treated cellulose fibers are processed with modern high-tech procedures to obtain the yarn with production being performed as per ISO 9000 and ISO 14000. The treatment process is carefully observed and conducted in an ecofriendly environment, with fibers being manufactured without any added chemicals. Bamboo fibers are 100% biodegradable natural cellulose fibers, which can degrade in the soil by microorganism and sunshine. The processing of bamboo yarn mechanically does not have any significant environmental effects. Bamboo fiber is described as “the natural, green, and ecofriendly construction

material of the twenty first century." A study investigated to analyze bamboo yarn properties thermal in comparison to conventional fibers to examine their chemical, mechanical, and physical properties [30].

5.2 Materials and methods

5.2.1 Materials

The experiment aspect of the study consists of 100% bamboo yarn as the reinforcement and the epoxy as the matrix used to fabricate the composite. The bamboo yarn was produced from Bambusa vulgaris, a species of Ghana. Firstly, the harvested bamboo culms were split into strips along the length of the culms. The strips of culms were steamed in a boiler to breakdown the chemical bonding of the fibers. The steamed bamboo strips are then crushed, and the bamboo cellulose is allowed in a solution of 15–20% sodium hydroxide at a temperature of between 20 and 30 °C for 24 h to allow the formation of alkali cellulose and then allow for decomposing. The bamboo alkali cellulose is then pressed to remove excess sodium hydroxide solution and is dried at a temperature 30 °C for 16 h. The partly processed bamboo alkali cellulose fiber is then sent to India for further processing through a bamboo yarn processing and to supplier Prasad Associates-Telangana (India) for the second phase and final processing using the conventional mechanical processing techniques.

The semiprocessed *Bambusa Vulgaris* alkali cellulose fibers are then further treated using hydrolysis–alkalization and multiphase bleaching to convert the material into fiber. The alkali cellulose of the bamboo fiber is threadbare, and to increase the surface area of the fiber, a grinder is used to grind the fibers to make the cellulose more accessible for continuous treatment. The ground alkali cellulose is kept an oven or is allowed to dry for a day or more so that the oxygen of the ambient air could have a strong bond with the material. The cellulose of bamboo retains high amount of alkaline during the stages of pretreatment and its resultant leads to oxidization of the material at a lower molecular weight through the degradation process. The degradation process is regulated to yield chains of short fibers that are adequate to produce yarn thicknesses in the spinning solution. During this phase of the process, an amount of carbon disulfide is introduced into cellulose to sulfurize the yarn fiber to harden it. The residual from the carbon disulfide is evaporated through the process of decompression, and the final product obtained or produced is known as bamboo cellulose sodium xanthogenate.

The further process required to produce 7–20% bamboo fiber cellulose is by adding sodium hydroxide to the cellulose sodium xanthogenate and allow it to dissolve and so to create a viscose solution of about 3%. The final process in the yarn treatment involves it being carded after which it is filtered, and the treated cellulose is spin

through nozzles of a spinning machine into a reservoir filled with a solution of sulfuric acid, which hardens the spun bamboo cellulose sodium xanthate and reconverts back to cellulose bamboo fiber that is turned into bamboo yarns. Figure 5.1 shows the processing stages of the bamboo yarn.

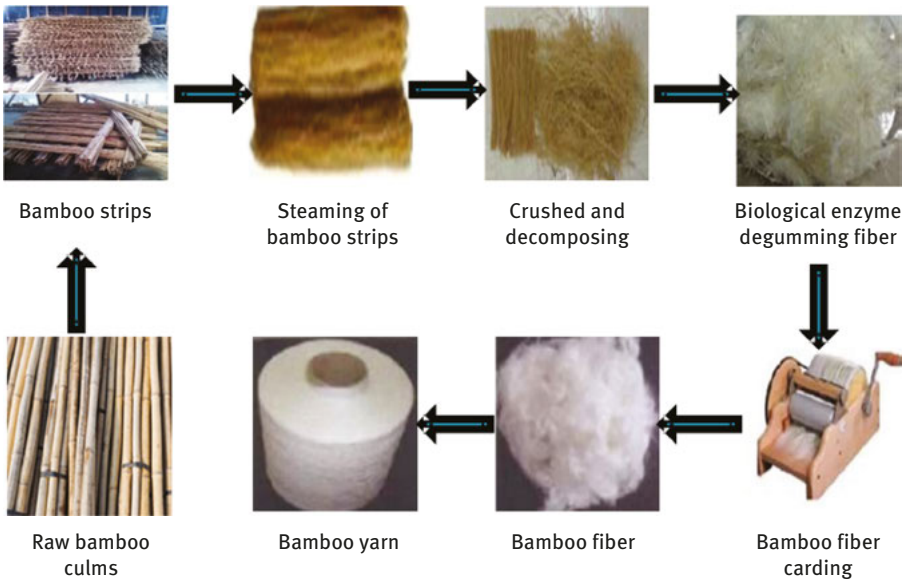

Figure 5.1: Mechanical processing of bamboo yarn.

5.2.2 Epoxy

The selected epoxy resin matrix, both resin and hardener, was supplied by AMT Composites Pty Ltd (South Africa), with the product name as Prime LV 20 Epoxy Laminating Resin and Prime 20 Slow Hardener. Besides, the epoxy resin Prime LV 20 and Prime 20 comprised of a mixed viscosity of 900–950 (mPa s), the specific gravity of 300 at 25 °C, volume at 25.2, cure time by 16 h for 65 °C, or 18 h for 40 °C. The epoxy resin portrays an excellent property of bonding with other materials as liquid epoxy is easy to formulate with another system for large and small manufacturing of parts. The epoxy resin was manufactured and formulated to work effectively under an ambient temperature state of curing when the hardener is mixed with it. Epoxy resin has numerous advantages such as being easy to determine and apply the mix ratios for resin and hardener, suitable to be mixed to uniformity, high resistance to moisture, low viscosity, and can be easily applied, and physical and adhesion performance properties are outstanding. The ratio of epoxy resin to hardener is 100:26 (g) by weight, respectively.

5.2.3 Fabrication of bamboo yarn-reinforced epoxy composite

The bamboo yarn used for the experiment consists of the following mean fiber qualities: fiber length 360 mm, fiber fineness 4.52 μg/in, uniformity ratio 93.8%, linear mass density 0.158 tex, specific density 1.51, moisture regain 11.53%, and elongation 21.56%. The bamboo yarn was woven into a mat using the Ghanaian traditional handweaving technique of Kente. The average yarn diameter was obtained by microscopic analysis, with an individual yarn measuring a value close to the four grammage mats in the order of 12 μm with mat linear mass density as 0.158 tex, and the yarn mat thickness was 5 mm.

The bamboo yarn was then innovatively hand woven into a mat using the Ghanaian Kente weaving technique (Figure 5.2). The manufactured mat (Figure 5.2c) is an innovative approach to enhance the stability and orientation of the yarn for reinforcement in the composite using the hand tool called loom (Figure 5.2b). The bamboo yarn-reinforced composite laminates were manufactured using a vacuum-assisted resin transfer mold (VARTM) method; the weight ratio of bamboo yarn to epoxy resin was given in percentage weight as 15 and 85 wt%, respectively.

Figure 5.2: Weaving bamboo yarn using the Ghanaian traditional Kente weaving technique.

A composite laminate of $270 \times 100 \times (3.5 \pm 0.1)$cm was fabricated with layers of bidirectional woven bamboo yarn (WBY) mats bonded in epoxy resin matrix with the aid of VARTM as shown in Figure 5.3a–c. The bamboo yarn possesses high

hydrophilic characteristics and as a result, it is subjected to an efficient process of drying for between 5 and 10 h in an air circulating oven at 20 °C to remove any moisture trapped in the composite and hence promote better adhesion between the bamboo yarn and epoxy resin. The epoxy resin was transferred through a tube into the mold to form a bond with the WBY using a high-vacuum pump to produce the laminate plate as shown in Figure 5.3c. The measure in-mold pressure was lower to 2,000 Pa before the epoxy resin was transferred into the mold. The mold plate was coated with a releasing agent (polyvinyl alcohol) so that the materials could be easily removed after the fabrication. The specimens were left to cure within the mold and air-tight to postcure for 16 h in an air-circulating room. Furthermore, the specimen of lathe minate plate is postcured at a temperature of 50 °C for 16 h in an oven. The relative vacuum pressure in the oven was at (–0.9bar). The laminate composite sample's thickness reduces or remains the same depending on the grammage of the yarn mats in the fabricated material. On an average the measured thickness of the composite laminate plate was 3.2 cm.

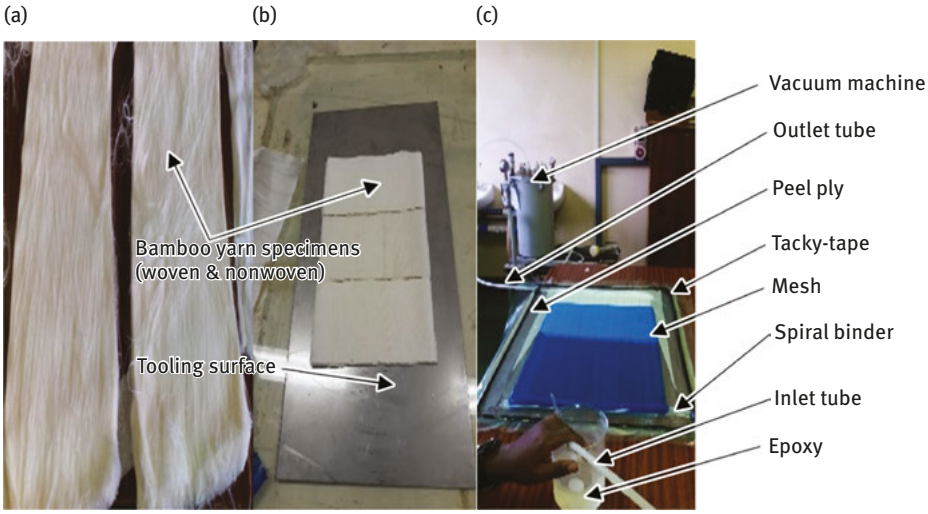

Figure 5.3: Fabricating bamboo yarn-reinforced epoxy composite using VARTM.

5.2.4 Mechanical and thermal degradation property

The tensile tests specimen of bamboo yarn was performed according to ASTM D638 to obtain both tensile strengths of the composite laminates using a Universal Testing Machine (model 3369 Instron) at a crosshead speed of 10 mm/min. The test was conducted using the load cell of 10 kN when 0.01 mm/s rate of loading was applied gradually to determine the tensile strength and was recorded in a device attached to the crosshead through a data acquisition system, which is connected to a

computer. By this, the stress–strain curves are automatically generated on a chart using the analysis software for testing. The software and record automatically calculate the tensile strength and stress values and results.

The experimental mechanical tests were performed under three-point bending to obtain flexural strengths of the bamboo yarn composite laminates according to ASTM D 790 using a Universal Testing Machine (model 3369 Instron). The specimen was subjected to the three-point bending test using a universal testing machine apparatus (model 3366, Instron) with a load applied at the center of the specimen. The bamboo yarn samples are supported on jigs fixture, with its span length of 160 cm. The test was conducted using the load cell of 10 kN at 0.01 mm/s rate of loading, which was gradually applied to determine the flexural strength and the values are recorded by a load cell device, attached to the crosshead of the machine through a data acquisition system connected to a computer. The stress–strain curves are generated automatically with the assistance of a software analysis incorporated into the machine during the testing. The software automatically calculated the flexural strength and stress values and the results were recorded. The flexural modulus values are taken from the slope of the graph generated at the initial section of the load–deflection curve.

The numerous advantages of fiber-reinforced composite materials including high specific strength and modulus, low specific density, and corrosion resistance promoted its application in structural engineering industries. Hence, it has become imperative to conduct standard tests to determine their mechanical properties. Toughness is an essential property of composite materials and shows the energy absorption capacity of the specimen. This energy is measured by impact testing. The two known methods of impact testing are Izod and Charpy using the notch in the specimen, with a load being applied at the notched section. The impact test of the bamboo yarn-reinforced composite specimen was performed using 500J Pendulum Charpy Impact Machine based on the ASTM E23. The chamber of the pendulum Charpy impact tester is calibrated to perform impact tests for a temperature from ambient to 180 °C or lower. The energy data are generated by using software incorporated into the machine, which records the energy values automatically on the display screen.

The thermal degradation curves are derived during the TGA test. An experimental investigation was performed to assess the thermal stability and thermal degradation of the neat epoxy (NEP), WBY, and woven bamboo yarn-reinforced composite (WBYRC) using TGA and DTA in a nitrogen atmosphere. The samples weighed 5–10mg and were placed in a ceramic plate to avoid any temperature differences during the thermocouple measurements. The thermal stability of the neat epoxy, bamboo yarn, and bamboo yarn-reinforced composites (woven and unwoven) was evaluated by TGA, using a Gas Controller GC 200 STAR System analyzer (Model METTLER TOLEDO). The TGA was conducted under an inert ambient nitrogen atmosphere at a flow rate of 20 mL/min. This is to help avoid oxidation at a heating rate of 10 °C/min constant as the samples were heated to temperatures of 30–800 °C. The TGA values are used to determine the mass loss about temperature, from which the DTA was obtained, to

determine the position and temperature at which sample degradation occurred. The TGA data and their derivatives DTA were analyzed using TA Instruments Universal Analysis 2000 software.

The morphology of the cross sections of the composite specimens in regions rich in longitudinal fibers was analyzed using a scanning electron microscope (SEM), JOEL JSM-6010L V. The samples were coated with a thin layer of gold since they are natural fibres and non-conducting employing an ultrasound equipment. The applied accelerating voltage was 5 kV.

5.3 Results and discussion

5.3.1 Mechanical test results

The mechanical properties of the neat epoxy resin and WBY-reinforced epoxy composite have been studied, and results are presented in tables and figures. The discussion of the results from the tables and figures is given.

Tensile strength of neat epoxy and WBY-reinforced epoxy composite

Figure 5.4a illustrates the setup of the tensile test machine used to determine the tensile strength and generate results that are displayed on the screen and are listed in (Tables 5.1 and 5.2). The result was recorded as the load is applied to the sample through a device attached to the crosshead of the machine system connected to a computer. The results recorded show variation in tensile strength between the neat epoxy resin composite and the WBY-reinforced epoxy composite (Figure 5.4b). The difference in tensile strength result between the epoxy resin and the WBY-reinforced epoxy composite shows 22.64 MPa for the unreinforced epoxy resin while that of the yarn-reinforced epoxy composite is 53.97 MPa. By reinforcing the pure epoxy with the WBY, the tensile strength is improved by 41%. The increment and improvement of the tensile strength on the epoxy resin by the woven bamboo yarn illustrate the high tensile strength property of the yarn, and subsequently, it is an application in structural designs.

The tensile modulus of neat epoxy and WBY-reinforced epoxy composite

The variation of the tensile modulus for epoxy resin from the bamboo yarn-reinforced epoxy composite is shown in Figure 5.5. The tensile modulus of the neat unreinforced epoxy is given as 0.539 GPa, and that of the WBY-reinforced epoxy composite shows 1.170 GPa. From the figure, it has been observed that the pure epoxy resin has a less

(a)

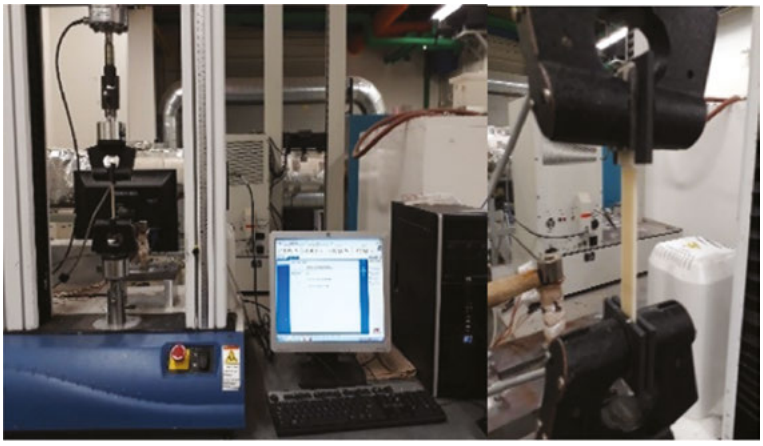

(b)

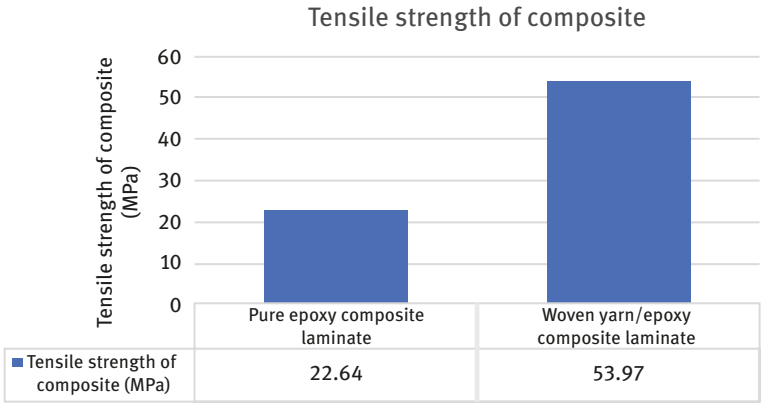

Figure 5.4: (a) Sample load for tensile strength. (b) This figure shows the tensile strength of WBY-reinforced epoxy composite laminate.

tensile modulus compared to that of WBY-reinforced epoxy composite. The woven bamboo yarn-reinforced epoxy composite shows significantly higher tensile modulus than that of the pure epoxy composite. Comparing Figures 5.4b and 5.5, it can be seen that the increase in both the tensile strength and modulus of the WBY-reinforced epoxy composite is because of the yarn stiffness and the strong ability to withstand shocks and stretch.

Flexural strength of neat epoxy and WBY-reinforced epoxy composite

Figure 5.6a illustrates the flexural test setup to determine the flexural strength with generated results (Tables 5.3 and 5.4). The result was measured as a load attached

Table 5.1: Results generated during tensile test of epoxy resin.

Epoxy samples	Tensile maximum load (N)	Tensile stress at max. load (MPa)	Load at yield (offset 0.2%) (N)	Tensile stress at yield (offset 0.2%) (MPa)	Modulus of elasticity (MPa)	Extension at yield (offset 0.2%) (mm)	Extension at max. tensile tress (offset 0.2%) (mm)
1	1,702.156	22.629	1,701.682	22.629	539.199	2.675	2.675
2	1,702.156	22.629	1,701.682	22.629	539.199	2.675	2.675
Mean	1,702.156	22.629	1,701.682	22.629	539.199	2.675	2.675
Standard deviation	0.00	0.00	0.00	0.00	0.00	0.00	0.00
Minimum	1,702.156	22.629	1,701.682	22.629	539.199	2.675	2.675
Maximum	1,702.156	22.629	1,701.682	22.629	539.199	2.675	2.675

Table 5.2: Results generated during tensile test of WBY-reinforced epoxy composite.

Epoxy samples	Maximum load (N)	Tensile stress at max. load (MPa)	Load at yield (offset 0.2%) (N)	Tensile stress at yield (offset 0.2%) (MPa)	Modulus of elasticity (MPa)	Extension at yield (offset 0.2%) (mm)	Extension at max. tensile stress (offset 0.2%) (mm)
1	2,154.307	52.550	1,705.881	39.488	1,020.293	2.444	4.042
2	2,238.591	54.550	1,703.021	39.422	1,169.447	2.443	3.558
3	2,238.591	54.550	1,703.021	39.422	1,169.447	2.443	3.558
Mean	2,210.496	53.989	1,703.974	39.444	539.199	2.443	3.719
Standard deviation	1,268.543	29.364	938.927	22.776	983.927	1.345	1.649
Minimum	2,154.307	52.868	1,703.021	39.422	1,020.293	2.443	3.558
Maximum	2,238.591	54.550	1,705.881	39.488	1,169.447	2.444	4.042

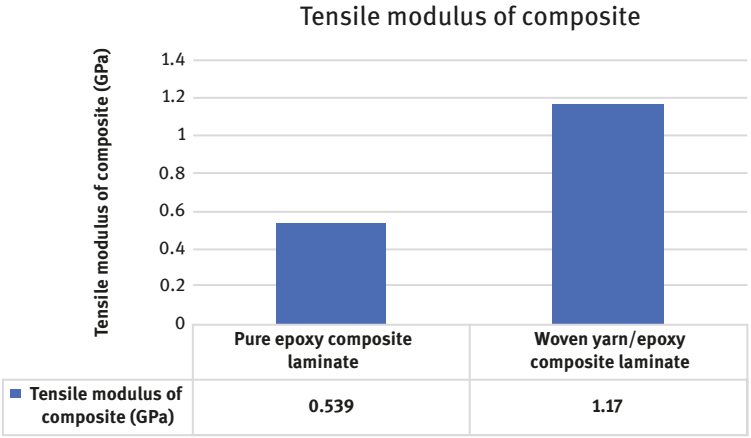

Figure 5.5: The tensile modulus of neat epoxy resin and WBY-reinforced epoxy composite laminate.

to the crosshead and applied through a data acquisition system that is connected to the computer. The variation of flexural strength in the neat epoxy composite to that of the WBYRC shows a significant improvement in flexural strength as shown in Figure 5.6b. Because of the incorporation of bamboo yarn to reinforce the epoxy resin, the strength of the composites significantly increases. The flexural strength of the unreinforced epoxy resin is found to be 61.232MPa, whereas the flexural strength of laminate bamboo yarn/epoxy-reinforced composites laminate is found to be 135.089MPa (i.e., 68.81%), which is two times higher than that of the neat epoxy resin when subjected to flexural stress with 31.19% flexural strength. The WBY has approximately 38% improved flexural strength when compared with that of the epoxy resin after bonding.

Flexural modulus of neat epoxy and WBY-reinforced epoxy composite

The variation of the flexural modulus for epoxy resin from the WBY-reinforced epoxy composite is shown in Figure 5.7. The flexural modulus of the unreinforced pure epoxy composite is 3.304 GPa, while the reinforced bamboo yarn/epoxy composite is 4.824 GPa. This observation showed a similarity between the pure epoxy composite and the reinforced yarn/epoxy composite in the case of the flexural modulus of the laminate as seen in the flexural strength of the laminated composites. The reinforced bamboo yarn/epoxy composite shows significantly higher flexural modulus than that of the neat epoxy composite. Comparing Figures 5.6b and Figure 5.7, it can be said that the increase in both the flexural strength and modulus of the reinforced yarn/

(b)

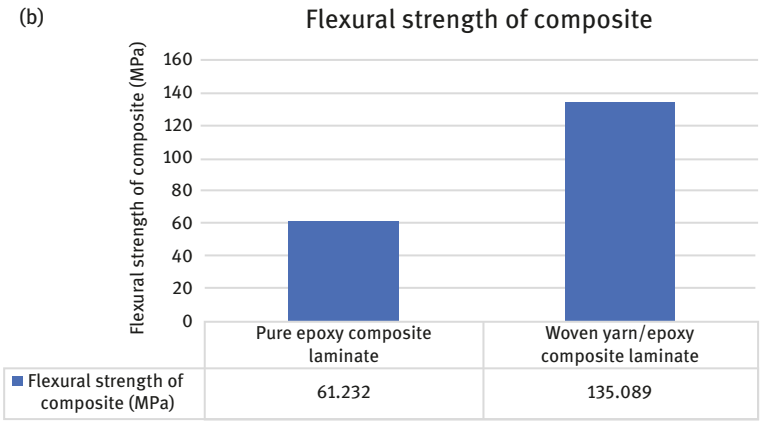

Figure 5.6: (a) Sample load for flexural. (b) The figure shows the flexural strength of WBY-reinforced epoxy composite laminate.

epoxy composite is because of the fiber stiffness and strength to withstand shocks and stretch.

Tensile stress and flexural strain at maximum load of neat epoxy and composite

The tensile stress at maximum load for WBY-reinforced epoxy composite indicates that the composite is two times higher than that of neat epoxy resin as shown in Figure 5.8a. Likewise, the flexural strain at maximum load indicates that the WBY-reinforced epoxy composite has better strain properties when compared to neat unreinforced epoxy (Figure 5.8b). Considering the percentage ratio, the WBY- reinforced epoxy composite has improved results compared to that of the neat epoxy resin by

Table 5.3: Results generated during three-point flexural (bending) test of neat epoxy resin.

Epoxy samples	Flexural load at max. flexural stress (N)	Flexural stress at max. flexural load (MPa)	Flexural extension at max. flexural stress (mm)	Flexural strain at max. flexural stress (mm/mm)	Modulus of elasticity (MPa)	Flexural stress at break (mm/mm)	Flexural load at break (N)
1	224.782	64.877	2.420	0.023	3,141.443	64.877	224.782
2	147.336	42.525	1.358	0.013	3,320.800	42.525	147.336
3	264.335	76.293	2.434	0.024	3,451.002	76.293	264.335
Mean	212.151	61.232	2.071	0.020	3,304.415	61.232	212.151
Standard deviation	59.514	17.177	0.617	0.006	155.429	17.177	59.514
Minimum	147.336	42.525	1.358	0.013	3,141.443	42.525	147.336
Maximum	264.335	76.293	2.434	0.024	3,451.002	76.293	264.335

Table 5.4: Results generated during three-point flexural test of bamboo yarn/epoxy composite.

Epoxy samples	Flexural load at max. flexural stress (N)	Flexural stress at max. flexural load (MPa)	Flexural extension at max. flexural stress (mm)	Flexural strain at max. flexural stress (mm/mm)	Modulus of elasticity (MPa)	Flexural stress at break (mm/mm)	Flexural load at break (N)
1	236.511	140.781	7,441	0.054	5,033.060	127.033	213.415
2	217.388	129.398	7,745	0.056	4,615.612	122.583	205.940
Mean	226.950	135.089	7,593	0.055	4,824.336	124.808	209.678
Standard deviation	13.522	8.049	0.215	0.002	295.180	3.146	5.286
Minimum	217.388	129.398	7,441	0.054	4,615.612	122.583	205.940
Maximum	236.511	140.781	7,745	0.056	5,033.060	127.033	213.415

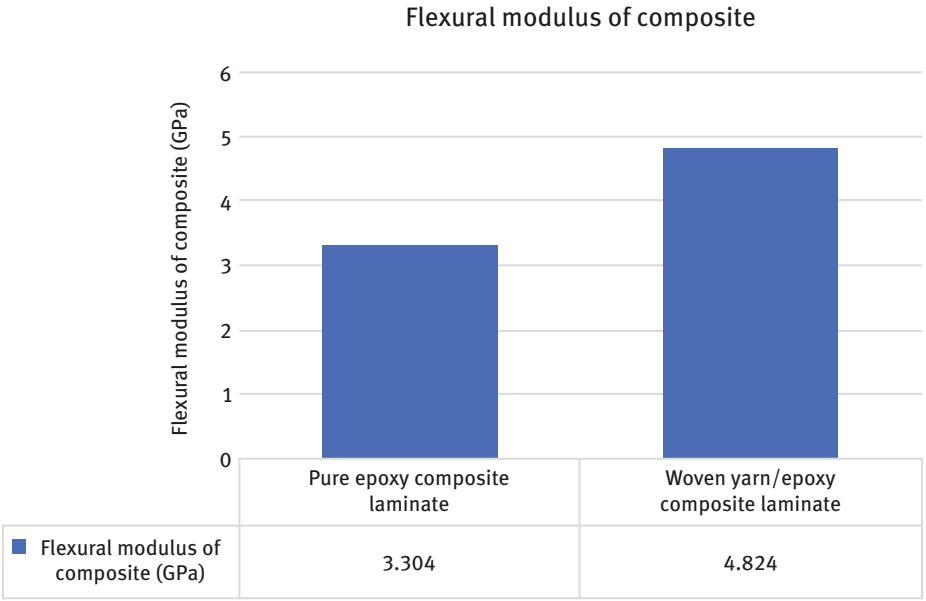

Figure 5.7: The flexural modulus of pure epoxy and WBY-reinforced epoxy composite laminate.

38 and 50% for tensile stress and flexural strain at maximum load, indicating significantly improved mechanical properties through the addition of woven yarn.

Absorbed energy on Charpy impact test of neat epoxy and woven yarn composite

The absorbed energy on Charpy impact test for neat epoxy resin and WBY-reinforced epoxy composite was calculated and is shown in Figure 5.9. The notched created at the center of the specimen on the backside and interlock in the jaws of the machine. The fracture in a specimen always occurs at the section of the notch whenever the hammer hits the specimen. The absorbed energy in Charpy impact test was calculated using the following:

$$E(J) = WgR(\cos\beta - \cos\alpha) - L \tag{5.1}$$

where E is the absorbed energy (J); W is the mass of the hammer (kg); G is gravitational acceleration (m/s^2); R is the length of the hammer arm (m); β is the angle at the end of swing (°); α is the angle of fall (°); and L is the energy loss (J).

The results recorded show variations in impact strength between the neat epoxy resin composite and the WBY-reinforced epoxy composite (Figure 5.9). The

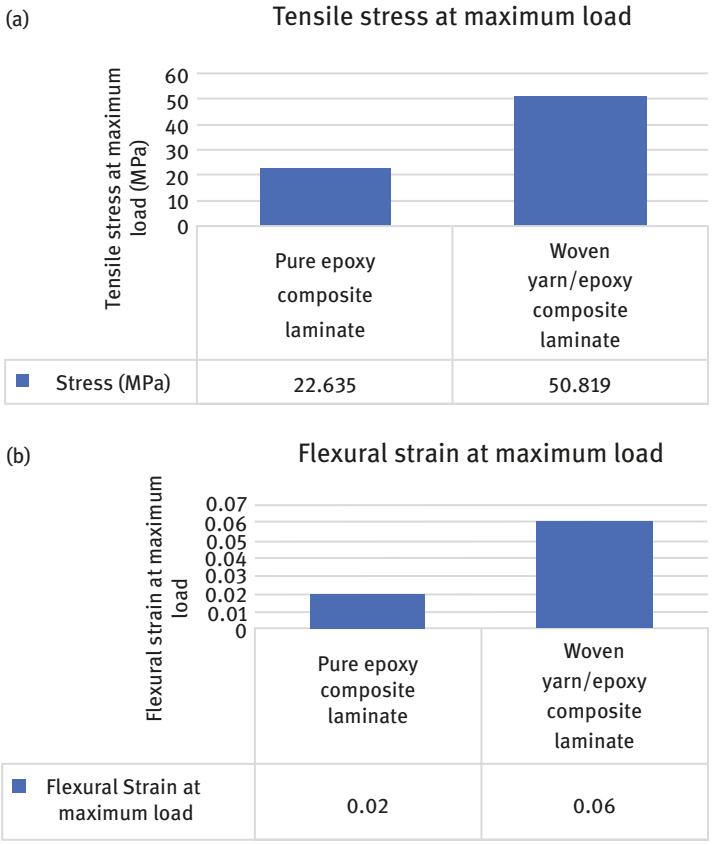

Figure 5.8: (a) Tensile stress at maximum load; (b) flexural strain at maximum load.

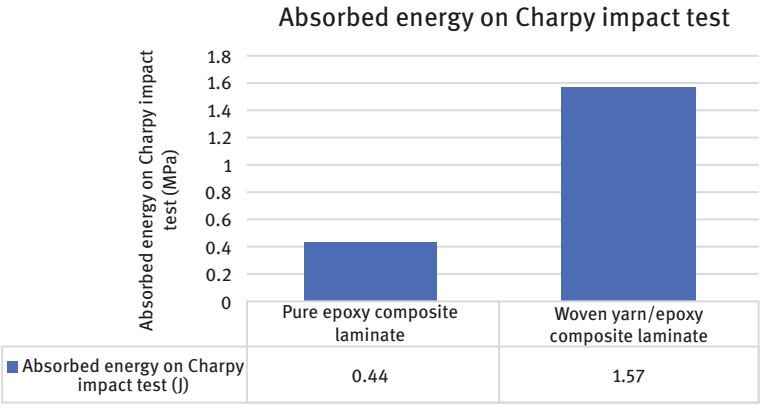

Figure 5.9: Charpy impact test on neat epoxy and WBYRC.

difference in impact strength result between the epoxy resin and the WBY-reinforced epoxy composite shows 21.89 J for the unreinforced epoxy resin, while that of the bamboo yarn-reinforced epoxy composite is 78.11 J. The outcome shows that by reinforcing the pure epoxy with the WBY, the energy absorption of the composite material has increased and improved by 78.11%, which is three times greater than that of the neat epoxy with 21.89%. The increment and improvement of the energy absorption property of the WBYRC material using impact testing indicate that bamboo yarn reinforcement improves the absorption properties of the epoxy resin. Hence, it is adopted as a reinforcement material, and subsequently, it finds applications in structural designs where shocks are essential.

Morphological structure of bamboo yarn/epoxy composite

SEM is an important technique that has been extensively employed for morphological inspection. SEM image of singles of bamboo yarn fiber, WBY, and neat epoxy were shown in Figure 5.10a–c to analyze the cross section of the base material specimens. The brittle nature of the pure epoxy composite (Figure 5.8a) was due to the sharp cut surface, and it conforms to the literature [32]. Distribution of WBY bonded in the reinforced epoxy composite is shown in Figure 5.11a and b, and Figure 5.11c shows the cross-section interlockings and bonds of the yarn fibers with the epoxy resin in the composite specimens. It was observed that (Figure 5.10c) the pure epoxy resin is dissimilar to (Figure 5.8b and c) the bamboo yarn-reinforced epoxy composite, which shows the distribution of the reinforcing yarn bonded in epoxy resin as well as the stretch yarns bonded in the composite (Figure 5.8c). The brittle nature of the pure epoxy composite (Figure 5.8a) was due to the sharp cut surface, and it conforms to the literature [10, 11, 43].

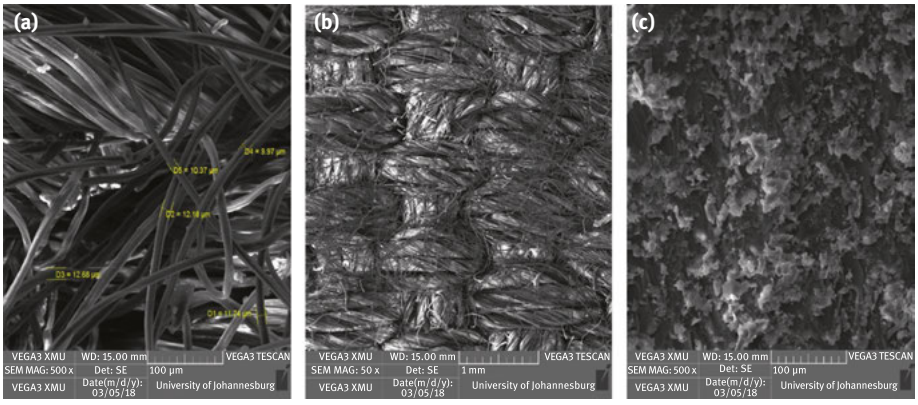

Figure 5.10: SEM images of (a) singles of bamboo yarn, (b) WBY, and (c) epoxy.

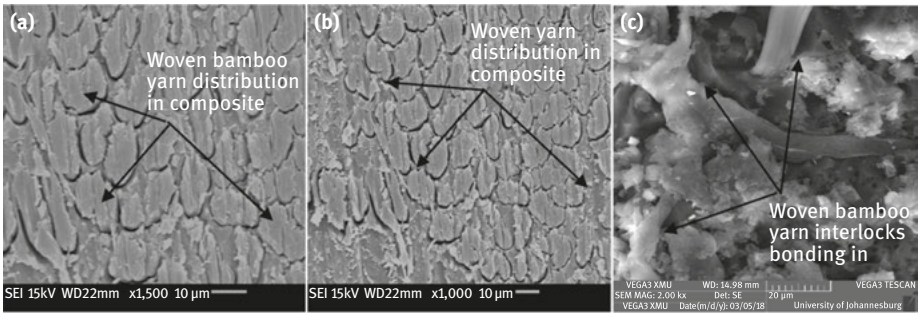

Figure 5.11: SEM images (a) and (b) of WBY distribution in composite and (c) this shows the interlocks of the yarn in the composite.

5.3.2 Thermal degradation test results

The thermal degradation properties of bamboo yarn-reinforced epoxy composite have been studied and are listed in Table 5.5. The results of the thermogravimetric decomposition behavior of the specimen showed the same trend for initial degradation temperature and final degradation temperature of the neat epoxy, WBY (bidirectional), and WBY-reinforced epoxy composite, which are shown in Figure 5.12a–c. For the TGA curve, four crucial stages were observed. A predominant signal appeared in the first stage prior to 100 °C. The second stage showed a pronounced peak between 270 and 320 °C, and the third stage occurred between 340 and 380 °C. And the fourth stage appeared between 400 and 500 °C, where the speed of mass loss is lower when compared with the two previous decomposition stages. Finally, few changes in the samples occurred as the temperature continued to increase in each of the specimens. It was observed from Figure 5.12a and b that neat epoxy resin lost weight at a lower temperature compared with WBY and WBY-reinforced epoxy composite.

Figures 5.13 and 5.14 show the overall TGA and DTA curves, which indicate small visually noticeable differences in the thermal behavior of the samples at various temperatures.

First, the TGA curves show that the WBY-reinforced epoxy composites at 250 °C behaved differently when compared to the neat epoxy and WBY. In addition, mass loss in woven bamboo-reinforced epoxy composite was less than that of the other samples between 350 and 430 °C (Figure 5.13). The DTA curves showed a strong signal at 360 °C for neat epoxy, but it appeared as a small shoulder at 340 °C (Figure 5.14).

Figure 5.14 illustrates the peak temperature of neat epoxy, WBY, WBY-reinforced epoxy composite, and non-WBY- reinforced epoxy composite. The composite profiles showed a similar trend of thermal degradation, which exhibited an exothermic peak

Table 5.5: Shows thermogravimetric degradation data (TGA) for NEP, WBY, and WBYRC.

Samples	Thermal stability (°C)	Weight loss (%) at temp. the range of (30–250 °C)	T_1 (°C) initial temp. range	Degradation temp. (50% loss) (T_{peak})	T_2 (°C) final temp. range	Weight loss (%) at temp. (420 °C)	Residual weight (%) at 800 °C
WBYRC	38.27	2.45	290–322	360	322–517	32.91	63.10
NEP	30.95	6.17	290–335	360	335–465	86.69	0.22
WBY	32.52	7.62	290–320	340	320–500	84.88	3.82

followed by an endothermic peak. The endothermic peak in the WBY-reinforced epoxy composite indicates the epoxy matrix undergoing glass transition (T_g) in those composites. Comparatively, the neat epoxy profile in Figure 5.14 exhibited an exothermic peak and endothermic peak in composites, indicating that the epoxy was fully cured.

Table 5.5 summarizes the TGA results obtained for NEP, WBY, and WBYRC. The percentage weight reduction during thermal stability indicates that WBY had the highest degradation of 7.62%. This is owing to the higher moisture absorption of the WBY [43]. Moisture can potentially exist in areas such as the multicellular structures or porous spaces of the bamboo yarn interface. For pure epoxy, WBY, and WBY-reinforced epoxy composite, moisture starts to evaporate from the initial degradation temperatures of 30.95 , 32.52, and 38.27 °C, respectively.

The percentage weight reduction of each sample reflects the quantity of residue remaining after the process. The pure epoxy, WBY, and WBY-reinforced epoxy composite reached their final degradation temperatures of 465, 500, and 517 °C, respectively. The neat epoxy has the lowest final residue percentage of 0.22% owing to the absence of char. The WBY and WBY-reinforced epoxy composite had final residue percentages of 3.82 and 63.10%.

5.4 Conclusion

The use of WBY as reinforcement in polymer composite has received limited attention in the literature, making this work an innovative one. The effect of WBY-reinforced epoxy composite was mechanically tested, SEM analysis was conducted on the composite, and TGA was performed to evaluate the mechanical properties, surface morphology, and thermal degradation behavior of the composites, respectively. On the basis of the study of the mechanical and thermal degradation properties of the specimen materials, which include neat epoxy resin, WBY, and reinforced bamboo yarn/epoxy composite, the following conclusions were drawn:

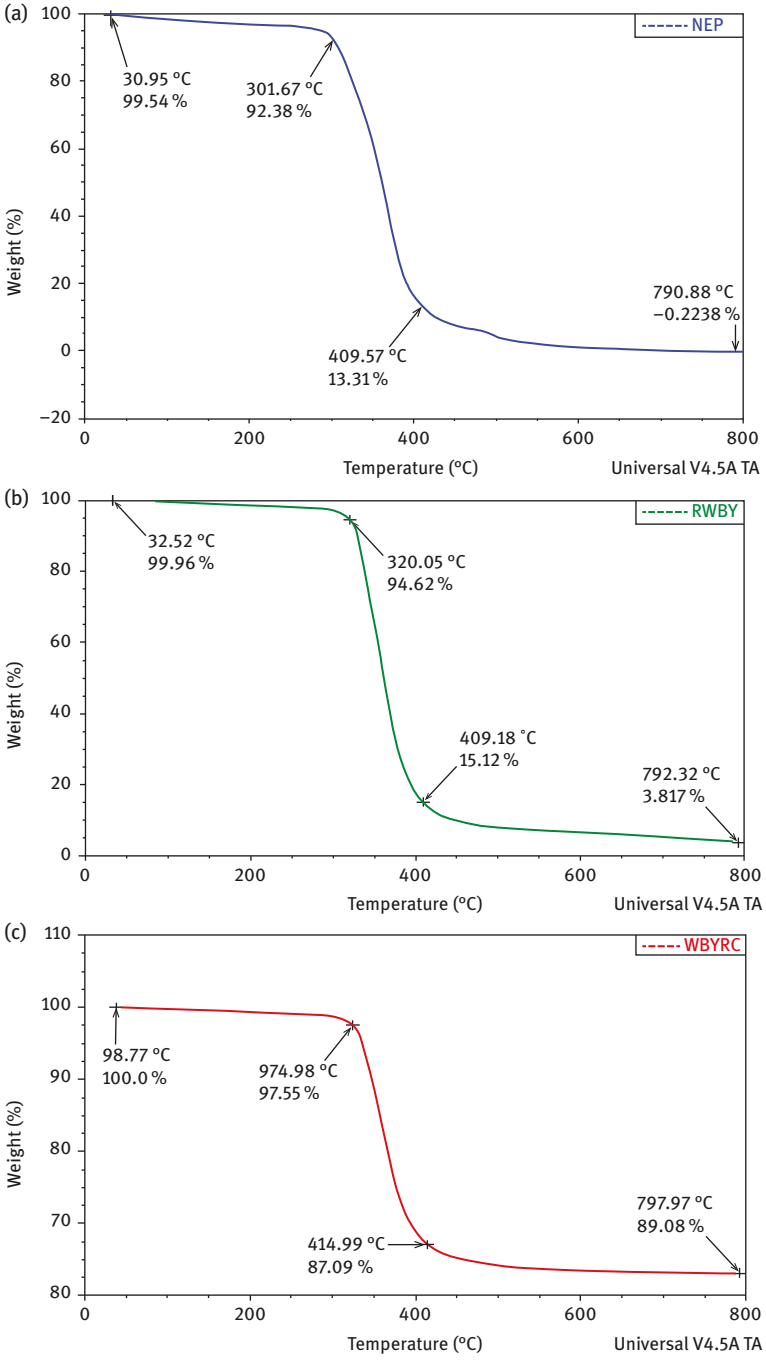

Figure 5.12: This shows TGA curves obtained for pure epoxy (a), raw WBY (b), and WBY-reinforced epoxy composite (c).

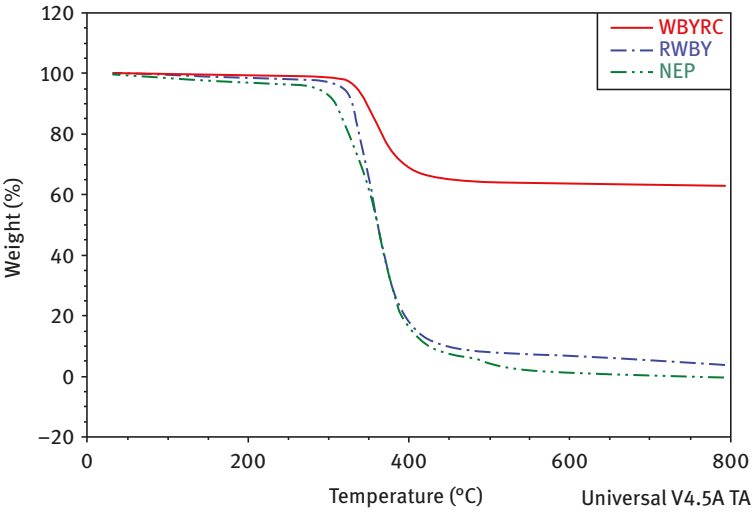

Figure 5.13: TGA curves of pure epoxy (NEP), woven bamboo yarn (RWBY), and woven bamboo yarn reinforced epoxy composite (WBYRC).

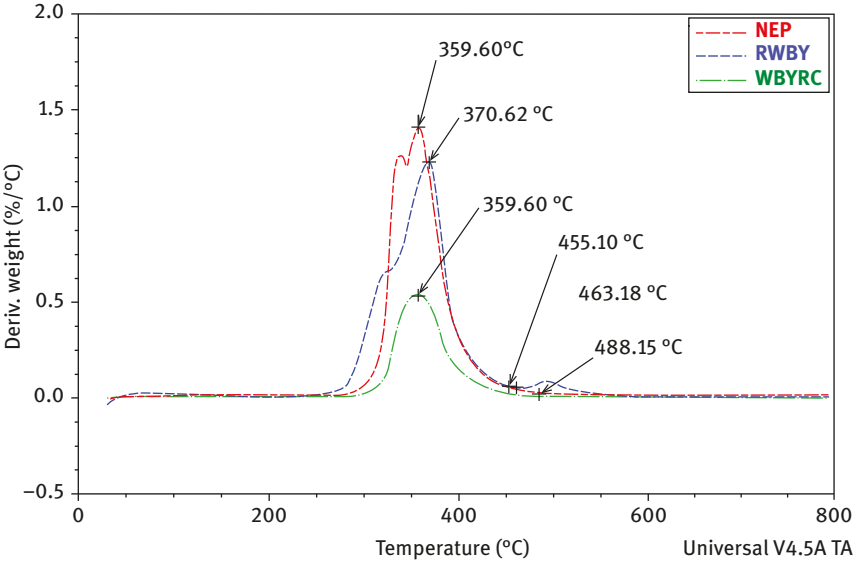

Figure 5.14: DTA curve of neat epoxy(NEP), woven bamboo yarn (RWBY), and woven bamboo yarn reinforced epoxy composite (WBYRC).

1. The single yarn fibers compared to that of the woven yarn show that the orientation of woven yarn fiber showed a stable condition for reinforcing of polymer composites.
2. The incorporation of bamboo yarn into the epoxy resin results in improvement in mechanical properties such as tension, compression, flexibility, and impact strength. This proves that its adoption and applications in manufacturing of laminates composite for structural works will be sustainable.
3. The incorporation of bamboo yarn into the epoxy resin to fabricate the composite gives an aesthetic advantage and improves the ductility property of the epoxy by reducing its brittleness.
4. The reinforced WBY/epoxy composite provides high flexural and tensile strength compared to unreinforced epoxy resin.
5. The maximum flexural strength is observed in the reinforced WBY/epoxy composite as 140.781 MPa, representing 38% flexural strength improvement over the epoxy composites after bonding.
6. The maximum tensile strength is observed in the reinforced WBY/epoxy composite as 39.488 MPa, representing 41% tensile strength improvement over the epoxy composites after bonding.
7. Furthermore, the reinforced yarn/epoxy composite provides high resistance to flexure and tensile strength to load application, unlike the neat epoxy.
8. WBY-reinforced epoxy composites showed excellent thermal stability compared to the neat epoxy and the virgin weaving yarn.
9. Woven yarn fiber-reinforced epoxy composite was more stable in the unidirectional applications.
10. SEM analysis showed the morphological changes that took place depending on the fiber orientation in epoxy composites.
11. It was observed from the TGA that WBY-reinforced epoxy composites had better thermal behavior compared to the virgin WBY fiber and the neat epoxy.
12. The WBY has a high surface area bonding and interfacial interaction with the matrix.

Finally, it can be said that the application of WBY as reinforcement in a polymer matrix or petroleum-based plastics is an innovation to help promote bamboo yarn as a sustainable reinforcement material, which is biodegradable and environmental friendly. The innovative approach that was adopted to weave the yarn fibers using the Ghanaian traditional Kente weaving techniques was to help to improve the stability strength of the yarn fiber before using for reinforcement in the polymer composite. Promoting bamboo yarn applications industrially as reinforcement material in polymer composites will assist in minimizing or eliminating the current global warming challenges. Bamboo yarn reinforcement in the epoxy exhibited significant increase in the compressive, bending, flexural, impact, and tensile strength of the resin and the composite as well. The thermal properties of the reinforced composite

also improved when compared to the epoxy resin. The excellent mechanical and thermal characteristics exhibited by the WBY in the epoxy resin in the fabrication of the laminate composite concludes that when adopted industrially, it can be used as a reinforcement material in the polymer composite manufacturing and hence finds applications in structural works.

References

[1] Boopalan, M., Niranjanaa, M., & Umapathy, M.J. Study on the mechanical properties and thermal properties of jute and banana fibre reinforced epoxy hybrid composites. Compos. B Eng., 2013, 51, 54–57.
[2] Uma Devi, L., Bhagawan, S.S., & Thomas, S. Mechanical properties of pineapple leaf fibre reinforced polyester composites. J. Appl. Polym. Sci., 1997, 64, 1739–1748.
[3] Vieille, B., Casado, V. M., & Bouvet, C. About the impact behaviour of woven-ply carbon fibre-reinforced thermoplastic- and thermosetting-composites: a comparative study. Compos. Struct., 2013, 101:9–21, 2013.
[4] Suhaily, S.S., Abdul Khalil, H.P.S., Nadirah, W.O.W., & Jawaid, M. Bamboo based biocomposite material, design and application" Mater. Sci., 2013, 549. DOI: 10.15772/56700.
[5] Araujo, J. R., Waldman, W. R., & De Paoli, M. A. Thermal properties of high-density polyethylene composites with natural fibres: coupling agent effect. Polym. Degrad. Stab., 2008, 93, 1770–1775.
[6] Kabir, M. M., Wang, H., Lau, K. T., & Cardona, F. Tensile properties of chemically treated hemp fibres as reinforcement for composites. Compos. Part B Eng., 2013, 53, 362–368.
[7] Lu, N., & Oza, S. Thermal stability and thermo-mechanical properties of hemp-high density polyethylene composites: effect of two different chemical modifications. Compos. Part B Eng., 2013, 44, 484–490.
[8] Methacanon, P., Weerawatsophon, U., Sumransin, N., Prahsarn, C., & Bergado, D. T. Properties and potential application of the selected natural fibres as limited life geotextiles. Carbohydr. Polym., 2010, 82, 1090–1096.
[9] Beg, M. D. H., & Pickering, K. L. Accelerated weathering of unbleached and bleached Kraft wood fibre reinforced polypropylene composites. Polym. Degradr. Stab., 2008, 93, 1939–1946.
[10] Yang, H., Yan, R., Chen, H., Lee, D. H., & Zheng, C. Characteristics of hemicellulose, cellulose and lignin pyrolysis. Fuel., 86(12), 1781–1788. DOI: 10.1016/j.fuel.2006.12.013.
[11] Monteiro, S.N., Calado, V., Rodriguez, J.S., & Margem, F.M. "Thermogravimetric behaviour of natural fibres reinforced polymer composites- An overview". Mater. Sci. Eng. A, 2012, 557, 17–28. DOI: 10.1016/j.fmsea.2012.05.109.
[12] John, M. J., & Anandjiwala, R. D. Recent developments in chemical modification and characterisation of natural fibre-reinforced composites. Polym. Compos., 2008, 29, 2, pp.187–207.
[13] Akinlabi, E. T., Anane-Fenin, K., & Akwada, D. R. Bamboo: The Multipurpose Plant, 2017, Springer International Publishing: Cham, Switzerland; pp. 1–147.
[14] Campbell, F.C. Structural Composite Materials, 2010, ASM International, Materials Park, OH, USA.

[15] Dittenber, D. B., & Gangarao, H. V. S. A critical review of recent publications on the use of natural composites in infrastructure. Comput. Part A Appl. Sci. Manuf., 2012, 43, 1419–1429.
[16] Eyerer, P. Polymers-Opportunities and risks I, General and environmental aspects, 2010, 11, Springer-Verlag Berlin Heidelberg, 429–435.
[17] Bottino, A., Capannelli, G., & Comite, A. Preparation and characterisation of novel porous PVDF–ZrO2 composite membranes. Desalination, 2002, 146 (2002) 35–40.
[18] Lee, B. H., Kim, H. J., & Yu, W. R. Fabrication of long and discontinuous natural fibre reinforced polypropylene biocomposites and their mechanical properties. Fibre Polym, 2009, 10, 83–90.
[19] Alamri, H., Low, I. M., & Alothman, Z. Mechanical, thermal and microstructural characteristics of cellulose fibre reinforced epoxy/organoclay nanocomposites. Compos. Part B Eng., 2012; 43:2762–2771.
[20] Huda, S., Narendra, R., & Yiqi, Y. Ultra-light-weight composites from bamboo strips and polypropylene web with exceptional flexural properties. Compos. Part B: Eng., 2012, 43(3), 1658–1664. DOI: 10.1016/j.compositesb.2012.01.017.
[21] Davies, M. "The thermoset difference: Thermoset vs. thermoplastic" (www.daviesmolding.com), 2014. Accessed on 20 August 2017.
[22] Cheremisinoff, N. P. Handbook of Engineering Polymeric Materials, 1997 (Marcel Dekker, New York).
[23] Marsh, G. Reinforced plastics prevail on the waterfront. Reinf. Plast., 2002, 46 (30–32), 34–35.
[24] Yan, L., Li, Y. S., Xiang, C. B., & Xianda, S. Effect of nano-sized Al2O3-particle addition on PVDF ultrafiltration membrane performance. J. Membr. Sci., 2006, 276(2006), 162–167.
[25] Akil, H., Zamri, M. H., & Osman, M. R. The use of kenaf fibres as reinforcements in composites. In: Biofiber reinforcements in composite materials, 2015, Woodhead Publishing and Elsevier, U.K.; 2015. p. 138–161.
[26] Klemm, D., Heublein, B., Fink, H. P., & Bohn, A. Cellulose: Fascinating biopolymer and sustainable raw material. Angew. Chem. Int. Ed., 2005, 44(22), 3358–3393.
[27] Belgacem, M N., & Gandini, A. (Eds.). Monomers, polymers and composites from renewable resources, 2008. Elsevier Science and Technology, Oxford, U.K.
[28] Mursakhanov, G. H., & Shchugorev, V. N., Analysis of temperature and impact damage of fibre reinforced composites. Theor. Appl. Fract. Mech., 1994, 20, 35–40.
[29] Liu, G., Zhang, H., & Hu, X. 'The Dyeing Behaviours of Bamboo Fibre with Reactive Dyes and the Product Development', Proceedings of the Textile Institute 83rd World Conference, 2004, Shangai, China.
[30] Xu, Y., Lu, Z., & Tang, R. Structure and thermal properties of bamboo viscose, tencel and conventional viscose fiber, J. Therm. Anal. Calorim., 2007, 891, 97–201.
[31] Erdumlu, N., & Ozipek, B. Investigation of regenerated bamboo fibre and yarn characteristics. Fibres Text. East. Eur., 2008, 164(69), 43–47.
[32] Arash, M., & Nasser, M. Viscoelastic and mechanical properties of multi-walled carbon nanotube/epoxy composites with different nanotube content, Materials and design, Elsevier Science, 2011, 2301–2307.
[33] Gratani, L., Crescente, M. F, Varone, L., Fabrini, G., & Digiulio, E. Growth pattern and photosynthetic activity of different bamboo species growing in a Botanical Garden of Rome". Flora, 2008, 203, 77–84.
[34] Mulligan, H., & Ramage, M. Tomorrow's material today: from data to design in engineered bamboo. World Archit., 2013, 12, 39–43.
[35] Waite, M. Sustainable Textiles: the role of bamboo and the comparison of bamboo textile properties. J. Text. Apparel Technol. Manage., 2009, 6(2): 1–21.

[36] Kushwaha, P K., & Kumar, R. Studies on water absorption of bamboo-epoxy composites: effect of silane treatment of mercerised bamboo. J. Appl. Polym. Sci., 2013, 115, pp. 1846–1852, 2010. doi:10.4186/ej.17.1.61,
[37] American Bamboo Society (ABS): Bamboo as a raw material. www.Bamboo.org /general info Pages/BambooAsMaterial.html, 2002.
[38] American Bamboo Society (ABS): Official Website, ABS, BAMBOO, Bamboo.org. (n.d.). http://www.bamboo.org/index.php on 12th August 2015, 2014.
[39] Akwada, D. R., & Akinlabi, E. T. Economic, Social and Environmental Assessment of Bamboo for Infrastructure Development. 5th International Conference on Infrastructure Development in Africa July in Johannesburg, South Africa, 2016.
[40] Akwada, D. R., & Akinlabi, E. T. Bamboo used in construction – how sustainable is it? International Conference on Infrastructure Development and Investment Strategies for Africa. Livingstone, Zambia. DII-2015. Livingstone, Zambia, 2015.
[41] Tara Sen, H. N., & Jagannatha, R. Application of sisal, bamboo, coir and jute natural composites in structural upgradation. Int. J. Innovation, Manage. Technol., 2011, 2, No. 3 186–191.
[42] http://www.bambrotex.com Accessed on September 13, 2018.
[43] Wang, Y., Gao X. 'Study on Structure of 6. The Nature Bamboo Fibre', Proceedings of the Textile Institute 83rd World Conference, Shangai, China, 2004.
[44] Ridzuan, M. J. M., Majid, M. S. A., Afendi, M., Azduwin, K., Amin, N. A. M., & Zahri, J. M. Moisture absorption and mechanical degradation of hybrid Pennisetum purpureum/glass–epoxy composites. Compos. Struct., 2016, 141, 110–116.

Swaroop Gharde, Rajendra Goud, Sunil Nimje,
Balasubramanian Kandasubramanian

6 Aggrandized flexural properties of assorted natural biological materials

Abstract: The changing scenario in the expeditiously developing industries requires different functionalized materials exhibiting application-oriented mechanical properties. Engineering materials have some limitations with individual materials for a broad range of mechanical properties (impact, fracture). These limitations can be overcome by composite materials, which give the ability to tailor and incorporate the specific functionality in the materials, using specific matrix and reinforcements. Synthetic materials have defied most of the materials in developing high-strength structures and adversely the presence of paradigm materials boasting an ingenious combination of mechanical properties has greatly inspired the scientific community for the advancement functional composite materials. The natural biocomposites such as molluscan shell, teeth, and bone exhibit mutually exclusive mechanical properties due to their hierarchical stratified microarchitectures comprise mineral tablets and interweaved with organic biomaterials. These biological materials have various rough interfaces such as mineral bridges, and nanoasperities on its individual tablet surfaces, which leads to further homogeneous stress distribution within the matrix of the material and augments the mechanical response (flexural strength) of bioinspired materials. Flexural strength being the substantial mechanical property helps in designing structural elements like beams, shafts, cantilevers; in predicting both resistance and durability of the objects; and in the development of constructional materials, which also has necessitated the high flexural strength value in all engineering applications like construction, defence, energy, and aerospace. Hence, biomimicking of these high flexural natural materials (e.g., the flexural strength of the nacreous structure is 220 MPa) can help the engineering community in developing high flexural materials. This chapter discusses the biomimicking of various animal- and plant-based biologically inspired materials for the developing composites materials that have high flexural strength and concludes with the discussion on the future scope of the natural composites.

Keywords: Flexural strength, biomimicking, biological materials, engineering applications

Swaroop Gharde, Rajendra Goud, Balasubramanian Kandasubramanian, Rapid Prototyping Laboratory, Department of Metallurgical and Materials Engineering, Defence Institute of Advanced Technology (DU), Ministry of Defence, Girinagar, India
Sunil Nimje, Department of Mechanical Engineering, DIAT (DU), Ministry of Defence, Girinagar, India

https://doi.org/10.1515/9783110603699-006

6.1 Introduction

Nature and humankind are interdependent and this is evident since historical times. Day by day the pollution and temperature on the earth's surface is increasing drastically owing to the expulsion of greenhouse gases like CO_2, methane, NOx, and chlorofluorocarbon (CFC) [1–3]. One of the reasons for global warming is the continuous usage of the nonbiodegradable products like metals, plastics, construction waste, and computer hardware as they are generally nonbiodegradable. The new environmental legislation [4, 5] and the unsustainable consumption of different products have directed the research toward the ecofriendly or environmentally friendly materials.

Previously, most of the engineering components were made up of metals and alloys unlike the other class of solids. The disadvantage of using metal and its alloys is the high probability of corrossion of the metallic structures that leads to the weakening of the components. This can be easily averted by using composite materials [6–10] that give the ability to tailor and incorporate specific functionality in the materials, using specific matrix and reinforcements. Synthetic materials have replaced most of the old traditional materials in the development of high-strength structures, exhibiting enhanced mechanical properties. However, the confliction between strength and toughness in synthetic materials [11] has necessitated the material scientists to develop a composite material through novel ingenious design strategies.

In the recent years, the improvement in biocomposites from different bipolymers as a matrix, resin, and reinforcement of the natural fibres have attracted researchers toward material science and engineering [12] owing to its biodegradability and environment-friendly nature [13–19]. Historically, research on biological systems started in the first phase of the twentieth century, but it was first explored by D'Arcy W. Thompson [20] in 1917, who gave a new direction to the research that biological systems used in engineering structures. Over the years, many researchers explored the biological materials and now they are extensively used in various applications including defence, biomedical [21, 22], military, automobile [23], construction industries, and maritime structures [24] due to their lightweight and high-strength structure.

Natural biomaterials are materials that reiterate important features of natural and biological counterparts [25], natural biocomposites such as molluscan shell, teeth, bones, and fibres, which exhibit mutually exclusive mechanical properties due to their hierarchically stratified microarchitectures comprising mineral tablets and interweaved with organic biomaterials [26]. These biological materials have various rough interfaces such as mineral bridges and nanoasperities on their individual tablet surfaces, which lead to further homogeneous stress distribution within the matrix of the material and thereby improve the mechanical response (flexural strength) of bioinspired materials [27, 28]. Flexural strength being the substantial

mechanical property helps in designing structural elements like beams, shafts, cantilevers in predicting both resistance and durability of the objects used in engineering applications like construction, defence, energy, and aerospace [29]. All materials of natural biocomposites are hierarchically structured and these structures are generally different in shape and size for different elements [30]. The main components of bone, teeth, and antlers are hydroxyapatite $(Ca.10(PO_4).6(OH)_2)$; calcium carbonate $(CaCO)_3$ is the primary constituent of seashells; crustaceans and sponge spicules consist of amorphous silica $(SiO(H_2O)_n)$ as the main constituent [12]. Also, all biological animal products like horns, teeth have similar layered structures such as mineralized phase that offer strength, and interleaved organic phase provides rigidity to the shell structure. Both the layers synergistically provide higher mechanical strength to the biological structures. Most of the biological materials show similarity in having porous structures, such as bird beaks, antlers, arthropod exoskeletons, and bones, resulting in lightweight structures, thereby increasing stiffness [12, 31].

The molecular-level architecture of these biomaterials can be mimicked in synthetic materials for specific engineering applications, for example, mollusc shell structures [32–36] and honeycomb structures [37] for structural applications. In this context, this chapter gives an overview of the fundamental aspects of various animal- and plant-based biological materials for engineering applications. Further, the chapter discusses the properties and applications of biomimicked materials for specific mechanical properties, that is, flexural strength, inspired from various plant- and animal-based biological materials. Finally, the chapter concludes with the discussion on the future scope of the natural composites in the scientific community.

6.2 Flexural strength

With the increasing demand for high-quality and reliable products, the flexural test has burgeoned as one of the most vital tests for both the manufacturing process and R&D activities to understand the ability of a particular material to withstand deformations under load. Flexural strength or bend strength is the resistance of a material to endure bending forces when a mechanical load is applied perpendicular to its longitudinal axis. Under uniform material distribution condition, flexural strength becomes equal to tensile strength.

Measurement of flexural strength and modulus of elements, especially composites, are rather difficult or tricky due to the concept of gross deviation. Nonuniformity and viscoelasticity of the material make the process of measurement more difficult. Flexural strength is calculated by measuring the central deflection caused due to the application of load perpendicular to the specimen's longitudinal axis.

Due to the application of load, stress and strain are developed on the specimen, on the basis of which the flexural characteristics are calculated and reported [38]. As depicted in Figure 6.1, stresses that are induced by this flexural load are due to both the tensile and compressive stresses.

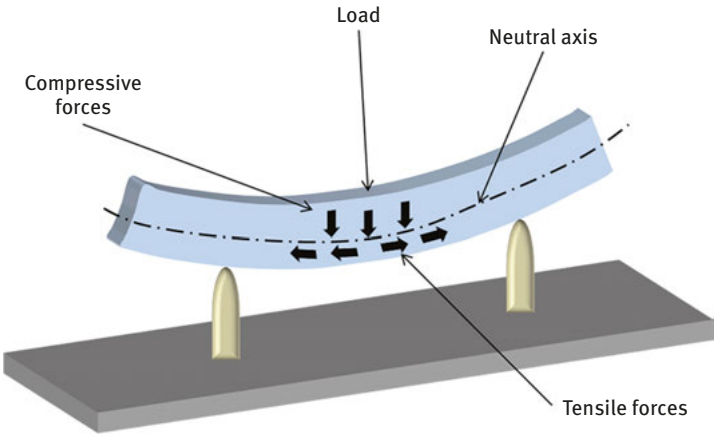

Figure 6.1: Involvement of tensile and compressive forces on a beam upon bending.

The measurement of the flexural strength of the specimens utilizes ASTM D790 that covers two methodologies for the determination of flexural properties, viz., 3-point or 4-point bending methods, which utilize beam-shaped specimens [39]. Making of beam-shaped specimens especially from porous materials, such as bone, is quite difficult compared to compression test specimens, which use either cylindrical or cube type of specimen, thus a limited number of data on flexural strength for biological elements is available for study [40].

6.3 Flexural test types

6.3.1 3-Point test method

This method utilizes center loading on a beam supported by the 2-point support. In 3-point bend test, the sample is kept on a 2-point support and loaded transversely with the help of a loading nose on its mid-span. 3-point bend test is generally preferred due to its simplicity of sample preparation and testing. The limitation of this type of test is that the testing method is a quick response to specimen loading, the geometry of the specimen, and strain rate [41].

6.3.2 4-Point test method

In a 4-point bend test, the sample is kept on two adjacent support points and loaded with two load points that are equally spaced over the span, maintaining a distance of one-third of the support span. The 4-point flexure fixture is more prone to defect and flaws owing to the extended exposure of the peak stresses along extended region of specimen. Here the test bar has been loaded at two points with the aid of loading noses, spaced equidistance from their adjacent support points as visualized in Figure 6.2b [41].

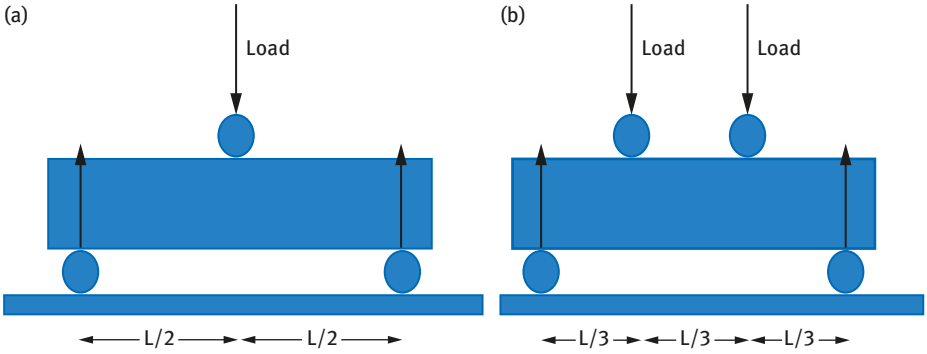

Figure 6.2: Bend test (a) 3 point (b) 4 point.

Theoretically, the breaking load for 3-point loading condition is 1.5 times lower than 4-point loading method. Practically, the value might slightly deviate from its theoretical value due to the attributes of the material such as anisotropy, imperfections, and so on. Similarly, for the same conditions, the deflection in the case of 3-point loading is 18% higher than 4-point loading.

When an object is loaded, the extreme ends of fibres experience maximum stress. If these fibres are completely free from any type of defects, then the flexural strength has to be the actual strength of the fibres. As long as the layers other than the outer layers have no defects and resist the desired applied load that is always less than maximum due to the stress gradient (Figure 6.5), the structure is safe. However, during a tensile test, all the elemental fibres develop same stress, thus if any of the fibre possesses a defect, the failure may start from that particular fibre once it reaches its critical limit. Therefore, flexural strength is always higher or at most equal to the tensile strength for similar materials under identical conditions (Figure 6.3).

When the specimen is loaded by means of loading nose, the side that is in contact with the load point is subjected to maximum compressive stress, whereasopposite side of the specimen is exposed to maximum tensile stress, resulting in a gradient of stress across the whole specimen. The stress from the maximum

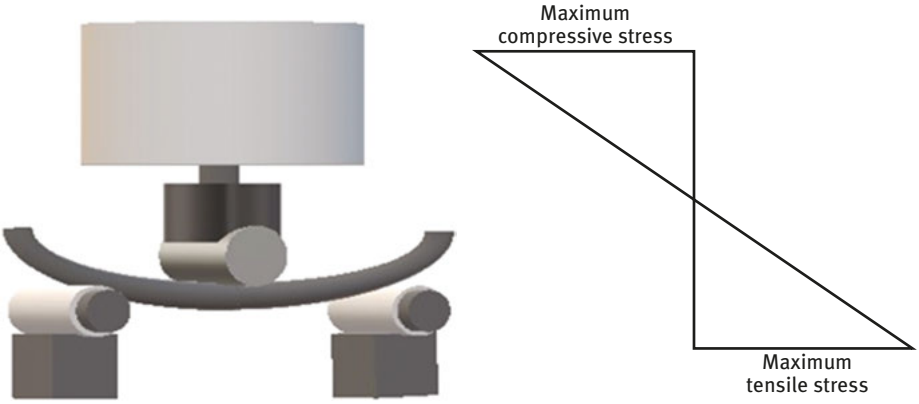

Figure 6.3: Bending of beam and stress gradient over the cross-section.

compressive stress on the upper surface gradually decreases to zero at the center of the specimen (the central fibre called as neutral fibre), which increases again and attains a maximum level at the lower surface.

Generally, the stress–strain developed in the specimen depends on the dimensions of the sample, the site of the applied load, and the cross-sectional geometry. The mathematical expressions for calculating bending strength is given by the following equations:

$$\text{For } 3-\text{point load}, \sigma = \frac{WLD}{8} \times I \tag{6.1}$$

$$\text{For } 4-\text{point load}, \sigma = \frac{WLD}{12} \times I \tag{6.2}$$

where,

W is ultimate load (lb), L is support span (inch), D is overall depth of the specimen in inch, and I is moment of inertia.

Moment of inertia being an influential parameter measures the strength and stiffness of a beam and is always defined by its size and geometry. Moment of inertia for a rectangular specimen is defined as

$$I = \frac{BD^3}{12} \tag{6.3}$$

Where,

B is the overall width of the sample in inch.

Mathematical expressions for flexural modulus can be given by

$$\text{For } 3-\text{point load}, \; E = \frac{WL^3}{48} \times YI \tag{6.4}$$

$$\text{For } 4-\text{point load}, \; E = \frac{WL^3}{56.5} \times YI \tag{6.5}$$

Where,

Y is deflection in inch.

This deflection can be calculated by

$$\text{For 3 – point load, } Y = \frac{WL^3}{48} \times EI \tag{6.6}$$

$$\text{For 4 – point load, } Y = \frac{WL^3}{56.5} \times EI \tag{6.7}$$

Bending moments (M) can be calculated from the type of geometry and type of loading.

$$\text{M} = \frac{WL}{4} \text{ for 3 – point loading condition} \tag{6.8}$$

$$\text{M} = \frac{WL}{6} \text{ for 4 – point loading condition} \tag{6.9}$$

The primary aim for the calculation of flexural strength is to determine the maximum load that the specimen can handle before failure, and similarly the foremost aim of flexural modulus calculation is to evaluate the deflection caused due to the applied load.

Both these calculations are highly responsive to the support span in comparison with the applied load, yet flexural modulus is considered to be more sensitive to parameters such as support span, humidity, temperature, and so on in comparison with flexural strength [38].

6.3.3 Factors affecting flexural strength and flexural modulus

- Flexural strength of a material reduces when there is an increase in temperature, for example, the flexural strength of HDPE-based composite materials declines to 30–60% when the ambient temperature varies from 120 to 130 F.
- Flexural strength modulus of a material enhances upon rise in the specific gravity of the material.
- Flexural modulus reduces with an increase in temperature of the material, for example, there is a decline in the flexural strength of about 1.7–2.2 times for composites based on HDPE when the ambient temperature changes from around 120 to 130 F.

6.4 Biological systems

In recent years, biological or natural materials have highly attracted the researchers in the field of material science and technology [12] due to its exceptional mechanical properties and different hierarchical biological structures [42]. Many of these natural materials exhibit enhanced toughness and significantly increased load

bearing capability [43], and exceptional mechanical and other strength enhancing properties as compared to the synthetic materials [28, 44]. Naturally occuring structures that are well designed to achieve nearly perfect geometry with variable composition of organic and inorganic complex structures can be biomimicked enhancing their flexural properties [42]. In the following section, we will discuss the fundamental aspects and biomimicking of the animal- and plant-based components (Figure 6.4).

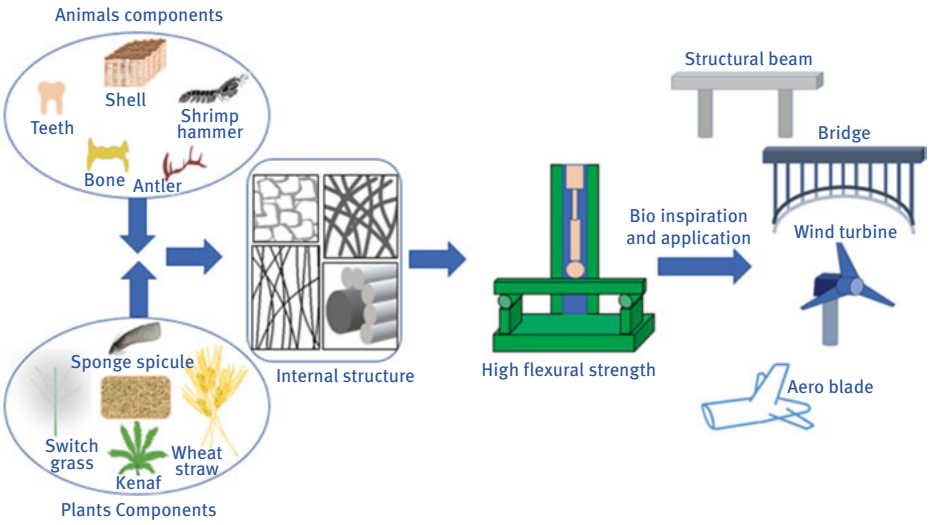

Figure 6.4: Different biomimicked structures.

6.4.1 Animal-based system

After millions of years of evolution, mother nature possesses nearly immaculate structures and functions [45]. All creatures on earth including human beings are always making efforts to achieve a better survival on the earth through evolution. They come up with various surface structures and highly innovative endurance approaches and are moulded in such a way that they adapt to the harsh environmental conditions [46]. Every animal has its unique quality such as molluscan shell, teeth, antlers, animal horns, and bone and exhibit mutually exclusive mechanical properties (i.e., strength and toughness) due to hierarchical layered microarchitectures that comprise mineral tablets and are interwoven with organic biomaterials [26]. These biological materials have various rough interfaces such as mineral bridges and nanoasperities on their individual tablet surfaces, which leads to further homogeneous stress distribution within the matrix of the material and thereby

enhances the mechanical response of bioinspired materials [27, 28]. Most of the biological materials show similarity in having porous structures such as bird beaks, antlers, arthropod exoskeletons, and bones resulting in lightweight structures, and thereby increasing stiffness [12, 31]. In the following section, we will discuss the various studies performed on biomimicking of mollusc shell structure, honeycomb structure, and miscellaneous structure.

Mollusc shell

Mollusc shell is the second largest group in the animal domain, which has hierarchical layered microarchitecture of mineral tablets and is interleaved with organic biomaterial matrices [47]. Each individual tablet has rough interfaces that contribute to the strength and toughness of mollusc shell–inspired materials, such as mineral bridges and nanoasperities. They contain 95–99.9% of $CaCO_3$ as calcite or aragonite and 0.1–5% of organic proteins, chitin fibres, acidic polysaccharides, and glycoproteins [48, 49]. The $CaCO_3$ phase provides strength and stiffness of the shell, and the organic protein layer helps in dissipating energy, which made the shell harder enough to fracture [26]. $CaCO_3$ exists in two forms, namely calcite, which has a rhombohedra type of structure, and aragonite having an orthorhombic structure [24]. The mollusc shell structures are categorized into various recognized structures, that is, nacreous (flat type), foliated (long lath-like), prismatic (columnar), cross-lamellar (plywood type), homogeneous (fine-scale type) (Figure 6.5).

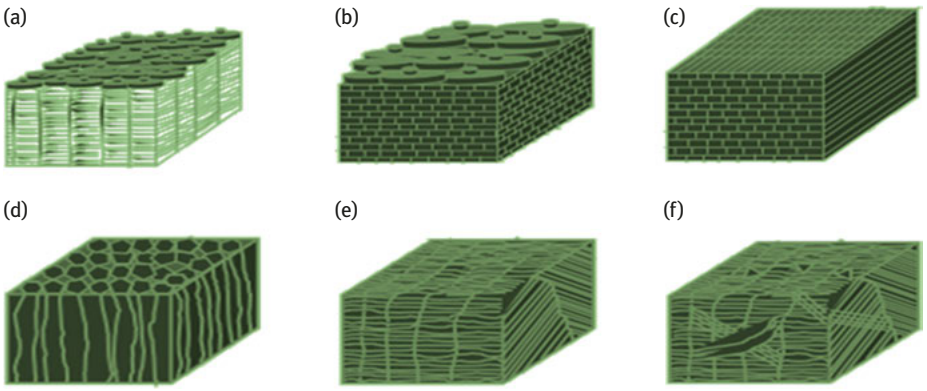

Figure 6.5: Schematic diagram of various types of mollusc shell microarchitectures (a) columnar nacre (b) sheet nacre (c) foliated (d) prismatic (e) crossed lamellar (f) complex crossed lamellar.

The nacre structure consists of tiled crystalline aragonite structure that is aligned along the c-axis with a high degree of crystallographic texture. Periodic growth

seizures develop mesolayers, which strongly helps in deflecting in crack and is tremendously significant in enhancing mechanical properties; the thicker meso layers with thickness of approximately 300 μm are separated by an inorganic layer that is about 20 μm thick [8]. In case of abalone shell, the mineral phase consists of 95 wt.% (approx.) of the total components of the composite, and there is a deposition of protein layer of 20–30 nm (approx.) for each animal without the age consideration that is consistent in dimension [9]. However, there lies a lot of differences when examining various animals having nacreous structure, generally the thickness of the abalone tiles is approximately 0.5 μm [42]. The sub membrane tiles grow in a and b directions and the mineral bridges protrude through the next organic membrane; a third tile grows above the membrane when the submembrane tiles about each other. The mineral bridges are formed by the continuous growth of minerals along the c-axis from the previous layers. The growth is arrested due to their protrusion and this in turn creates sites on the next cover of inorganic layer where mineralization continues to occur. These mineral bridges act as seeds on which the next film formation takes place [32].

Foliated structures have elongated blade-like calcite parallel crystals called laths and arrow point endings called folia, the outer layer of the mollusc shell is the prismatic layer that consists of calcite or aragonite prisms [50]. The prisms oriented vertically, that is, their long axes of the prisms lye perpendicular to the outer surface [51]. Cross-lamellar structure has a hierarchical three-tier lamellar structure, the outer, middle, and inner layers each oriented in 0°, 90°, and 0° sequence, each consists of first order of 5 μm thickness, second order of 5–30 μm thickness and 5–60 μm width, and third order of 60–100 nm thickness and 100–380 nm width of aragonite lamellae and is separated by protein layers [52, 53]. The right-angled arrangement of cross-lamellar layers helps in arresting crack leading to high toughness [54].The complex cross-lamellar structure is identical to the cross-lamellar structure with the difference in much more complex interpenetrating fashion [55].

Studies on biomimicking of molluscan shell structures by using different techniques have been explored by Tang et al. [56] who fabricated MMT/PDDA (poly(diallydimethylammonium)) nanocomposites by layer-by-layer technique, and measured the tensile strength and Young's modulus of the nanocomposite, that is, 106 MPa and 11 GPa, respectively, which was close to the naturally occuring nacre. Further, Podsiadlo et al. [57] have experimented this by replacing PDDA (σ = 12 MPA, E = 0.2 GPa) from MMT/PDDA by chitosan (σ = 108, E = 2 GPa) and observed the ultimate strength to be 80 MPa that was lower as compared to chitosan and MMT/PDDA composites. In further advancement in the study, Podsiadlo et al. [58] used DOPA (*L*-3,4-dihydroxyphenylalanine) molecules instead of PDDA, which imparted good adhesion strength to the MTM surface, and found high strength and toughness increased by two and eight times, respectively, as compared to the natural nacre. Podsiadlo et al. [59] used PVA (polyvinyl alcohol) that forms good hydrogen bonding and crosslinking structure with MTM surface, and witnessed the tensile strength and modulus to be 150 MPa and

13 Gpa, respectively. Alternatively, another crosslinking approach, that is, PVA and Na^+ montmorillonite clay nanosheets were studied by Podsiadlo et al. [60] and an increase in tensile strength from 150 to 320 MPa was detected, which was twice higher as compared to natural nacre, and also an increase in Young's modulus was observed from 13 to 60 Gpa that was close to that of natural nacre.

Further, Xu et al. [61] used vacuum filtration technique to synthesize graphene oxide (GO)/PVA composite films and examined it at different wt.% of graphene; the perceived tensile strength and modulus was 110 ± 7 MPa and 4.8 GPa, respectively, at 3 wt.% of graphene, where the tensile modulus was less than that of natural nacre. In advance, Wang et al. [62] manufactured chitosan/reduced graphene oxide sheet with a layered arrangement by vacuum filtration technique and observed that the tensile strength and modulus of chitosan/graphene films enhanced drastically when the reduced graphene sheet was amalgamated up to 6 wt.%. The composite film with 6 wt.% of GO showed 206 MPa tensile strength and 6.3 GPa tensile modulus. Chen et al. [63] contrived organic/inorganic nanocomposites with clay nanoplatelets and polyimide in reduced time frame by a centrifugal deposition process with the sample thickness of 10–200 μm. The tensile strength, stiffness, and hardness extended to 70–80 MPa, 8–9 GPa, and 1–2 GPa, respectively, as compared with the lamellar bones. Further, Walther et al. [64] allied MTM/PVA films that were rapidly formed by papermaking (i.e., vacuum filtration) and doctor blading. The papermaking nacre-inspired structure formed 165 MPa tensile strength and 27 GPa Young's modulus, which slightly exceeded the natural nacre and possessed good properties as compared to doctor blading process. Xia et al. [51] have conducted experiments by using biomineralization technique where they synthesized aragonite-like nanoasperities infused with silica platelets and examined the mechanical properties. The tensile deformation suggested that the incorporation of roughed silica platelets are responsible for toughness, strength, and strain hardening. In advance, Xu et al. [65] have prepared shell-mimicked PLA composites by using injection molding technique where ZnO whiskers were introduced to connect resolute crystalline structure in shear of PLA and observed the nearly double tensile strength and impact toughness of 119.4 MPa and 11.5 KJ/m^2 as compared to normal PLA. Zhang et al. [66] examined poly (TPGDA)/ITO nanocomposite layers on a glass substrate synthesized by self-assembly method and found that the polymerized nanocomposite film has nacre-like laminated construction with a typical spacing of 3 nm. However, operative control over nanostructure and organic content was simultaneously a key issue. To overcome the problem, Lin et al. [67] developed a hybrid assembly method where hydrothermal and electrophoretic techniques were used for the mimicking of the nacre structure. The progression includes dhydrothermally synthesized or electrophoretic-deposited intercalation of polymer into interlying space of montmorillonite and consequent electrophoretic deposition, but the tensile strength and Young's modulus of the film reduced. Wang et al. [68]

fabricated nacre structure synthesized by evaporation-induced self-assembly method based on clay platelet/nanofibrillar cellulose/PVA (polyvinyl alcohol) and obtained two times higher tensile strength of 302 ± 12 MPa and toughness of 3.72 ± 0.63 MJ/m^3 as compared to natural nacre (80–135 MPa and 1.8 MJ/m^3) and the binary MMT/PVA composites. Further, Pai et al. [69] prepared poly(KAMPS)/aragonite-based composites by self-assembly method where negatively charged poly(KAMPS) chains were obtained after the addition of $NaHCO_3$ to an aqueous solution of Ca^{2+}-poly (KAMPS), which resulted in the growth of aragonite nanorods with a width of 120 nm. The tensile modulus and hardness of 44 Gpa and 2.8 GPa of the nanocomposites showed similar orders as compared to the natural nacre and other biocomposites. Tiwary et al. [70] examined a new class of seashell structure, where its model was obtained using simulation software and then fabricated by FDM printer. The results showed that the multifaceted hierarchical geometry can withstand loads that are nearly twice as high as the basic simple shape counterparts. Recently, Yadav et al. [35] have studied the biomimicking of mollusc shell structures (nacre, foliated, crossed lamellae, and complex crossed lamellae) via 3D printing (Figure 6.6), that is, additive manufacturing technique of engineering polymer such as ABS, and observed crossed lamellae validated efficacy as compared to the other structures in terms of high impact characterization and wear resistance (Table 6.1).

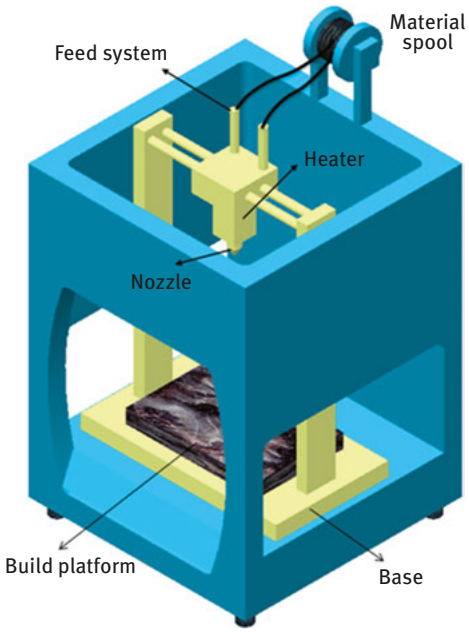

Figure 6.6: 3D printing machine.

Table 6.1: Mollusc shell structures and their flexural strength. From Yadav et al. [35], Mayer and Sarikaya [71].

Type	Flexural strength (MPa)	Elastic modulus (MPa)	Toughness (J/mm^3)
Prismatic	140	15.64 ± 0.35	0.268 ± 0.021
Nacre	220	19.66 ± 0.33	0.248 ± 0.065
Foliated	100	17.76 ± 0.30	0.23 ± 0.028
Crossed lamellar	100	19.42 ± 0.39	0.196 ± 0.022
Complex crossed lamellar	–	7.5 ± 0.41	0.386 ± 0.064

Honeycomb structure

Honeycomb structures are natural or artificial structures, which originate from honey bees lair consist of consistently dispersed double-layered columnar and hexagonal cells [72]. They comprise various mechanical properties such as high stiffness, low density, lightweight, and fatigue resistance due to which they find plentiful engineering applications in the section of mechanical, transportation, aerospace, chemical, biomedical, and so on [73]. Many researchers have proposed the various shapes of honeycomb structures, that is, hierarchical [74], chiral [75], anisotropic hierarchical, auxetic [76], re-entrant auxetic [77], by contouring methodologies like folding, thermoforming, extrusion, and 3D printing (i.e., additive manufacturing technique).

Studies on the biomimicking of honeycomb structures by using different techniques have been explored by Chantarapanich et al. [78] who explored and compared the mechanical properties of 3D honeycomb assembly by using finite element method (FEM) and fabrication technique (i.e., selective laser melting), and observed the elastic modulus of 63.18 MPa and compression strength of 1.1 MPa, respectively. In addition, Alderson et al. [79] accomplished the further study on hexachiral, trichiral, anti-trichiral, tetrachiral, and anti-tetrachiral and found good mechanical properties as compared to the regular hexagonal structures. Further, in advancement in the study, Scrapa et al. [75] studied the compression metier of the chiral honeycomb geometry by using the above-mentioned techniques and observed 3.6 times higher collapse stress as related to the other honeycomb. Hedayati et al. [80] engineered a new geometry, that is, octagonal honeycombs, where they studied the mechanical properties of octagonal honeycomb structure by using analytical (Euler–Bernoulli and Timoshenko), numerical (3D printing), and experimental techniques. The projected octagonal honeycomb edifice was equated with the other honeycomb assemblies (i.e., square, triangular, hexagonal, diamond, and kagome) and found yield stress and elastic modulus values comparable to the consistent hexagonal structure. Similarly, Oftadeh et al. [81]

studied the mechanism of anisotropic honeycombs by using computational and analytical techniques and observed that the anisotropic honeycomb structures with same wall angle was 2–8 times stiffer and two times stronger as compared to the regular honeycomb structure. Further advancement in the study by Ajdari et al. [74] examined the mechanical properties of hierarchical honeycomb geometry by using the above-mentioned techniques and found that first- and second-order structures can be 2 and 3.5 times stiffer as compared to the other structures. Mousanezhad et al. [82] examined a new category of spiderweb honeycomb geometry by experimental, numerical, as well as analytical techniques and elucidates the increase in elastic energy storage by 40% as compared to the triangular honeycomb structure. Ingrole et al. [76] studied compression loading behavior of different honeycomb structures, that is, regular honeycomb, re-entrant auxetic, reinforced auxetic strut, and hybrid structures, by using 3D printing techniques and found that auxetic strut structure exhibited exceptional mechanical property when it showed strength upto 300% more than honeycomb construction and 65% more than auxetic assembly.

Miscellaneous structures

Sommer et al. [83] created silk fibroin hierarchical structures with the help of 3D printing technique (i.e., additive manufacturing technique) of silk-based ink and demonstrated that the 3D printing method offers a flexible podium for the genesis of hierarchical silk fibroin structures imbibed with an excellent degree of organizational control. Further, Schacht et al. [84] performed experimentation by using 3D printing technique where spider silk protein was used as a bio-ink for printing and elucidated that the silk showed less shear thinning behavior as compared to alginate that was frequently used as a bio-ink in the 3D printing.

Cai et al. [85] studied poly (lactic acid)/gelatin composite fibre-rich matrices that were initially synthesized by electrospinning technique and dipped in the replicated body fluid to deposit the flaky materials on the fibre surface. They demonstrated that after proper heating of flaky material it transformed into hexagonal hydroxyapatite crystals, which found similar superficial morphology as of antlers and human tibia. Bian et al. [86] studied biomimetic design of the woodpecker skull where they designed three different models first for impact protection, second and third for protection from vibration isolation by using FEM technique. Based on the analysis they found that the first model protects the inside device by absorbing a strong impact and the second model protects the device from the outside vibrations when frequency is more than 200 Hz. Further, Malik et al. [87] examined the jigsaw-like structure (red-bellied woodpecker) by using computational, optimization, and experimental (3D printing by using ABS materials) techniques and illustrated the pull-out strength and energy absorption of the

structure increases with high interlocking angle structure and higher friction coefficient. Similarly, Luo et al. [88] prepared silk fibre by using the biomimetic microfluidic channel in a chip and found that artificial silk was tougher as compared to the natural silk, where it exhibited 614 MPa breaking strength and 101 KJ/Kg breaking energy. Gan et al. [89] fabricated structures that biomimicked the anatomy of butterfly wings by using dual-beam super-resolution lithography, which serves as a state of the art tool for extracting 3D models from the nature. The result shows that artificial structures have dimensions, controllability, and consistency that display better structural integrity than the natural design that enhanced the Young's modulus of the developed nanowires by 20%. Thiele et al. [90] mimicked the eagle eye by direct 3D printing. Multiple objective lens on a complementary metal oxide semiconductor (CMOS) image sensing device displayed a field understanding of 70° and two cycles per degree angular resolution at the centre of the image can be accomplished four printed doublet lenses that have been manufactured with varied focal lengths. Further, Song et al. [91], with the help of 3D printing technique, mimicked three-spine stickleback that has thick bony plates for protection and peg and socket joints that help in mobility in its natural marine environment. They found that the permeable, sandwiched cross-section was advantageous for enhancing bending stiffness and strength with a least weight. Rudykh et al. [92] prepared hybrid stiff plate and soft matrix materials architecture by using 3D printer that helped to tune the properties of protective covering and flexibility by tweaking the geometrical parameters and proving its efficiency byindentation and bending tests on the prototype materials. The resistance to penetrate the protective shell can be enhanced to a power of 40 while a considerable decrease was observed in flexibility in less than five times. Browning et al. [93] developed fish scale bioinspired by elasmoid fish by utilising FDM technique and which was then cast into silicone rubber that behaved as aelastic base. Three arrangements were examined and observed network of armours reves to distribute predatory attack load over a huge area to alleviate stress foci. Further, Wassenbergh et al. [94] developed a model system for trunkfish and boxfish and then 3D printed in order to check their unique body shapes that enhanced directionability. The CFD (computational fluid dynamics) analysis illustrates that the 3D-printed boxfish produces extreme destabilizing instances, that is, high maneuverability produced by pressure waves (Table 6.2).

6.4.2 Plant-based system

Natural or biological surfaces have been providing a large variety of structures with exceptional capabilities for millions of years as a result of evolution [95]. Mother nature has perfected structures that enhance strength and flexural properties and elevates its functional capability [45]. Plants, like animals, are always making

Table 6.2: Summary of animal based components.

Geometry of structures	Techniques	Results	References
Nacre	Layer-by-layer assembly (LBL) technique	Tensile strength = 106 MPa, Young's modulus = 11 GPa, fracture strain = 8.4, toughness = 0.5	[56]
Nacre	Layer-by-layer assembly (LBL) technique	PDDA (σ = 12 ± 4 MPa, E = 0.16 ± 0.03 GPa, ε = 48 ± 9, toughness = 4.7 ± 2), chitosan (σ = 108 ± 15, E = 1.9 ± 0.3 GPa, ε = 42 ± 9, toughness = 31.6 ± 8.8), and MMT/chitosan (σ = 81 ± 12 MPa, E = 6.1 ± 0.8 MPa, ε = 1.9 ± 0.6, toughness = 0.9 ± 0.4)	[57]
Nacre	Layer–by-layer assembly (LBL) technique	MMT/DOPA(*L*-3,4-dihydroxyphenylalanine) (σ = 200 ± 28 MPa, E = 6.8 ± 0.9 GPa, ε = 3.8±0.7, toughness = 4.2 ± 1.2)	[58]
Nacre	Layer–by-layer assembly (LBL) technique	MMT/PVA polyvinyl alcohol (σ = 150 ± 40 MPa, E = 13±2 GPa, ε = 0.7 ± 0.2)	[59]
Nacre	Layer-by-layer assembly (LBL) technique	PVA and Na^+ tensile strength = 150–320 MPa and tensile modulus = 13–60 GPa	[60]
Nacre	Vacuum filtration	Virgin PVA: Tensile strength 65 ± 5, tensile modulus 2.1 ± 0.2 GPa, at 1% graphene tensile strength = 75 ± 5, tensile modulus = 2.9 ± 0.2, at 3% graphene tensile strength = 110±7 MPa, tensile modulus = 4.8 MPa	[61]
Nacre	Layer-by-layer assembly (LBL) technique	Chitosan (CTS)/reduced graphene oxide (RGO) chitosan: (σ = 88 ± 5 MPa, E = 2.4 ± 0.2 GPa, ε = 19 ± 1), CTS/1 wt.% RGO: (σ = 91 ± 2 MPa, E = 2.9 ± 0.1 GPa, ε = 17 ± 1.0), CTS/3 wt.% RGO: (σ = 130±3 MPa, E = 3.6 ± 0.2 GPa, ε = 10 ± 0.1), CTS/5 wt.% RGO: (σ = 190 ± 4 MPa, E = 4.6 ± 0.3 GPa, ε = 8.9 ± 0.9), CTS/6 wt.% RGO: (σ = 206 ± 6 MPa, E = 6.3 ± 0.2 GPa, ε = 6.5 ± 0.6), CTS/7 wt.% RGO: (σ = 180 ± 5 MPa, E = 6.8 ± 0.5 GPa, ε = 4.6 ± 0.2)	[62]
Nacre	Centrifugal deposition process	Montmorillonite(MMT)/polyamide(PI) sample thickness = 10–200 μm, tensile strength = 70–80 MPa, stiffness = 8–9 GPa and hardness = 1–2 GPa	[63]

Table 6.2 (continued)

Geometry of structures	Techniques	Results	References
Nacre	Vacuum filtration technique	165 MPa tensile strength & 27 GPa Young's modulus	[64]
Shell	Injection moulding technique	Micmicked structure by PLA using zinc oxide whisker: tensile strength 119.4 MPa and impact toughness 11.5 KJ/m^2 double as compared to normal PLA	[65]
Nacre	Evaporation-induced self-assembly method	2 times higher tensile strength and toughness, i.e., 302 ± 12 MPa, Young's modulus 22.8 ± 1 GPa and toughness 3.72 ± 0.63 MJ/m^3 as compared to natural nacre (80–135 MPa and 1.8 MJ/m^3)	[68]
Nacre	Layer-by-layer	Tensile modulus and hardness, i.e., 44 Gpa and 2.8 GPa of the nanocomposites	[69]
Nacre, foliated, crossed lamellae, and complex crossed lamellae	3D printing	Prismatic (Elastic modulus (MPa): 15.64 ± 0.35, toughness: 0.268 ± 0.021), Nacre: (Elastic modulus (MPa): 19.66 ± 0.33, toughness: 0.248 ± 0.065), foliated: (Elastic modulus (MPa): 17.76 ± 0.30, toughness: 0.23 ± 0.028), crossed lamellar: (Elastic modulus (MPa): 19.42 ± 0.39, toughness: 0.196 ± 0.022), complex crossed lamellar: (Elastic modulus (MPa): 7.5 ± 0.41, toughness: 0.386 ± 0.064)	[35]
Honeycomb	Finite element method (FEM) and fabrication technique (i.e., selective laser melting)	Elastic modulus of 63.18 MPa and compression strength of 1.1 MPa	[78]
Honeycomb	3D printing technique	3.6 times higher collapse stress as compared to regular honeycomb structure	[75]
Honeycomb	3D printing technique	Yield stress and elastic modulus values comparable to the hexagonal structure	[80]
Honeycomb	3D printing technique	Anisotropic structures: 2–8 times stiffer, 2 times stronger than hexagonal structure	[81]

(continued)

Table 6.2 (continued)

Geometry of structures	Techniques	Results	References
Honeycomb	Analytical, numerical and experimental (3D printing)	Structures shows 2–3.5 stiffness as compared to regular hexagonal structure with poisons ratio changing from 1 to 0.28	[74]
Honeycomb	3D printing technique	Elastic energy storage increased, i.e., 40% of spider web as compared to the triangular honeycomb structure	[82]
Honeycomb	3D printing technique	Compressive strength, i.e., 65% and 300% higher as compared to auxetic and regular honeycomb structure	[76]
Red bellied woodpecker (jigsaw-like structure)	3D printing technique	Modulus of 1.7 ± 0.2 GPa and a strength of 118 ± 12 MPa	[87]
Artificial Silk	Microfluidic	Artificial silk was tougher as compared to the natural silk, with 614 MPa breaking strength and 101 KJ/Kg breaking energy	
Butterfly wings	Lithography	Artificial structures have superior size, controllability, and uniformity as compared to biological counterparts	[89]
Three-spine stickleback fish	3D printing technique	Porous, sandwich-like cross-section was beneficial for bending stiffness and strength at minimum weight	[91]
Hybrid stiff plate	3D printing technique	High protection and flexibility	[92]
Trunkfish and boxfish	3D printing technique	3D-printed box-shaped fish produces strong destabilizing moments, i.e., high maneuverability	[94]

efforts to achieve a better survival on the earth from its evolution. They come up with various surface structures that agumente its strength and molded to provide adaptability in harsh environmental conditions [46]. Basically, plant is made up of two specialized guiding tissues, that is, xylem and phloem, which transport water, nutrients, and organic compounds from the roots to different parts of the plant structures [96]. Generally, plant-based fibres consist of cellulose, hemicellulose, and lignin, whereas animal-based fibres consist of proteins categorized as natural

fibres, and synthetic fibres were developed by mimicking these natural fibrous entities [97].

Natural fibres such as banana, sisal, jute, and so on have gained much interest in the field of composite industry due to their inexpensive, lightweight, low density, high toughness, renewable, abundant, ecofriendly, biodegradable, and nonabrasive to processing characteristics. Though the property of natural fibres vary with the type of treatment and source, these help in resulting lightweight, high stiffness, and strong composites [97, 98]. Some disadvantages with natural fibres are observed such as easy absorption of water, dimensional irregularity, heat susceptibility, and so on [99]. The common features that influence the mechanical properties of the fibres are under the condition where experiments are being conducted and the length and diameter of the fibres are considered [100].

Plant fibres are divided as primary and secondary fibres. Primary fibres are produced by plants that are grown for producing fibres, and secondary fibres are produced from the wastes of plant products that are not primarily meant for fibre production [100]. The commonly used natural fibres are rice or oat straw, wheat, flax, wood, bamboo, cotton, jute, kenaf, date, date, hemp, and barley [101]. Flax has got applications in automobile interior design parts, door panels, boot and roof linings, parcel shelves, and so on [102]. Application of fibres such as sisal, hemp, jute, kenaf, ramie is highly seen in Asia while in Europe flax fibre is highly used. Generally, fibres with higher cellulose content show higher mechanical performance especially when microfibrils are aligned in the fibre directions, which is a case of bast fibres (hemp, kenaf, flax, jute, ramie, etc.).

It has been observed that if the fibre is harvested 5 days after optimum harvesting duration, then the strength reduces up to around 15% [103], and if the fibre is harvestment harvested manually rather than mechanically, the strength is around 20% higher [104]. With increasing moisture content, the strength of the fibre increases and Young's modulus decreases, however, with an increasing temperature, the strength of the fibre decreases [105]. Various authors reported many properties and few of them have been listed out in Table 6.3 [104, 106–118].

Studies on biomimicking of plant-based components by using different techniques have been investigated by Liu et al. [119] who mimicked lotus leaf-like surface by using soft lithographic imprinting technique and found good superhydrophobic characteristics with the contact angle of more than 150°. Similarly, lotus-like structure was mimicked by Bhushan et al. [120] by using a self-assembly technique and the static and the hysteresis contact angle of the flat surface was observed to be 110° and 60°, respectively. Further, Chang et al. [121] have investigated the lotus leaf-like structure by using nanocasting technique for preparing SEPI coating whose superficial structure was identical to a lotus leaf. The water contact angle of the SEPI coating surface was 87°, which was lower than the natural lotus leaf, that is, 155°. Yang et al. [122] fabricated complex bioinspired eggbeater patterns of the salvinia molesta leaves by using ISA-3D printing technique and observed that the

Table 6.3: Properties of various natural fibres.

Fibre	Density (g/cm^3)	Tensile strength (MPa)	Stiffness/ Young's modulus (GPa)	Specific tensile strength (MPa/g)	Specific Young's modulus (GPa/g)
Ramie	1.5	400–938	44–128	270–620	29–85
Flax	1.5	345–1830	27–80	230–1220	18–53
Hemp	1.5	550–1110	58–70	370–740	39–47
Jute	1.3–1.5	393–800	10–55	300–610	7.1–39
Harakeke	1.3	440–990	14–33	338–761	11–25
Sisal	1.3–1.5	507–855	9.4–28	362–610	6.7–20
Alfa	1.4	188–308	18–25	134–220	13–18
Cotton	1.5–1.6	287–800	5.5–13	190–530	3.7–8.4
Coir	1.2	131–220	4–6	110–180	3.3–5
Silk	1.3	100–1500	5–25	100–1500	4–20
Feather	0.9	100–203	3–10	112–226	3.3–11
Wool	1.3	50–315	2.3–5	38–242	1.8–3.8
E-glass	2.5	2000–3000	70	800–1400	29

artificial structure made with E-glass/MWCNT showed good superhydrophobicity property and petal effect. In addition, Park et al. [123] fabricated an image of a flower by the E-jet 3D printing process with ink, which consists of single-walled carbon nanotubes in water that were surfactant stabilized. The necessary dimension of 1 μm was validated for potential application in the circuit printing.

Further, Li et al. [124] studied biomimetic model of bamboo fibre where they prepared four different types of macro fibre specimens synthesized by using engineering composites like solid, hollow cylinders that are axially aligned, single and double helical hollow cylinders, and determined that the double helical hollow cylinder showed the optimum mechanical properties as compared to the other model. Further, Tong et al. [125] examined the mechanical properties (i.e., abrasive wear, tensile, and impact properties) of bamboo stem by examining its cross-sectional view and elucidated the abrasive wear resistance, tensile strength, and impact strength that the bamboo stem possesses and were amplified as the vascular fibre increased. Markstedt et al. [126] developed a novel ink with biomimetic approach that consisted of cellulose nanofibrils (contain structural properties) and crosslinking hemicellulose matrix for the 3D printing. Nanofibrils mixed with xylan substituted with matrix made up of tyramine participated in the tuning of crosslinking density, the result showed that the amount of tyramine that has been substituted and the ratio of CNF used influenced the printability and crosslinking density (Table 6.4).

Table 6.4: Summary of plant-based components.

Geometry of structures	Techniques	Results	References
Lotus leaf-like structure	Lithographic imprinting techniques	Contact angle more than 150°	[119]
Lotus leaf-like structure	Self-assembly technique	Static contact angle = 110° and contact angle of hysteresis of flat surface = 60°	[120]
Lotus leaf-like structure	Nanocasting technique	SEPI coating surface was 87°, which was lower than the natural lotus leaf, that is, 155°	[121]
Eggbeater patterns of salvinia molesta leaves	3D printing	Good superhydrophobicity property and petal effect	[122]
Bamboo fibre	Model	Flexural strength: Sample A: 251.7, Sample B: 262.2, Sample C: 253, Sample D: 253.9	[124]

6.5 Conclusion

Nature possesses different highly accomplished materials with unique geometry as they offer valuable source of knowledge in the arena of engineering materials. Currently, expeditiously developing industries require different functionalized materials, which exhibit good mechanical properties and are environmental friendly to the ecosystem. Metals and alloys, ceramics, and polymers are the common materials that transform into final finished products, but at the same time they affect the nature authetically. Nowadays researchers are moving towards the natural biocomposites, which exhibits mutually exclusive mechanical properties due to their hierarchical layered microarchitectures. Ever since its inception till date, natural composites are now extensively used in the various applications including defence, biomedical, military, automobile, construction industries and maritime structures etc. due to its lightweight and high strength structures. This present chapter describes the fundamental aspects of the various animal- and plant-based biological materials for engineering applications of biomimicked materials for specific mechanical properties, that is, flexural strength. Owing to an extensive research, the ample researchers have outshined from their original areas of biomimicking of animal- and plant-based biological materials and led to the conclusion that animal and plant structures have good mechanical strength, that is, flexural strength, Young's modulus, and so on, and biodegradable property.

Overall, understanding of animal- and plant-based structures and mimicking them by different mimicking techniques for numerous applications will influence to advance forward in the field of the biomimicking. Biomimicking offers manufacturing challenges to develop novel biomimetic methods for numerous engineering applications and also in constructing next-generation materials and structures in the field of biomimetics. Futuristic study on the bioinspired structures is highly dependent on multifunctional, multiscale, multi-materials, and multidimensional fabrication.

References

[1] Anderson, T.R., Hawkins, E., & Jones, P.D. CO2, the greenhouse effect and global warming: from the pioneering work of Arrhenius and Callendar to today ' s Earth System Models, 2016, Endeavour, Elsevier, 40, 178–187. doi:10.1016/j.endeavour.2016.07.002

[2] Lashof, D.A., & Ahuja, D.R. Relative contributions of greenhouse gas emissions to global warming. Nature, 1990, 344, 529–531. doi:10.1038/344529a0

[3] Mitchell, J.F.B. The "Greenhouse" effect and climate change. Rev. Geophys, 1989, 27, 115. doi:10.1029/RG027i001p00115

[4] Correia, J.R., Almeida, N.M., & Figueira, J.R. Recycling of FRP composites: reusing fi ne GFRP waste in concrete mixtures, J. Clean. Prod., 2011, 19, 1745–1753. doi:10.1016/j.jclepro.2011.05.018

[5] Hall, S. End-of-life recycling options for glass fibre reinforced polymers, plymouth student scientist, 2016, 9, 68–94.

[6] Tirumali, M., Kandasubramanian, B., Kumaraswamy, A., Subramani, N.K., & Fabrication, S. B. Physicochemical Characterizations and Electrical Conductivity Studies of Modified Carbon Nanofiber-Reinforced Epoxy Composites: Effect of 1-Butyl-3-Methylimidazolium Tetrafluoroborate Ionic Liquid, Polym. Plast. Technol. Eng., 2018, 57, 218–228. doi:10.1080/03602559.2017.1320719

[7] Tirumali, M., Balasubramanian, K., & Kumaraswamy, A. Functionally Layered Graphite Reinforced Epoxy Composite Sandwiched Between Epoxy Composites: Their Electrical and Flexural Properties. Mater. Focus, 2017, 6, 691–697. doi:10.1166/mat.2017.1467

[8] Inamdar, A., Cherukattu, J., Anand, A., & Kandasubramanian, B. Thermoplastic-Toughened High-Temperature Cyanate Esters and Their Application in Advanced Composites. Ind. Eng. Chem. Res., 2018, 57, 4479–4504. doi:10.1021/acs.iecr.7b05202

[9] Sanoj, P., & Kandasubramanian, B. Hybrid Carbon-Carbon Ablative Composites for Thermal Protection in Aerospace. J. Compos, 2014, 2014, 1–15. doi:10.1155/2014/825607

[10] Katiyar, N., Balasubramanian, K. Thermal modelling of hybrid composites of nano cenosphere and polycarbonate for a thermal protection system. RSC Adv., 2014, 4, 47529–47535. doi:10.1039/C4RA07973F

[11] Ritchie, R.O. The conflicts between strength and toughness Nat. Publ. Gr., 2011, 10, 817–822. doi:10.1038/nmat3115

[12] Chen, P., Lin, A.Y.M., Lin, Y., Seki, Y., Stokes, A.G., Peyras, J., Olevsky, E.A., Meyers, M.A., & Mckittrick, J. Review article Structure and mechanical properties of selected biological materials, J Mech Behav Biomed Mater., 2008, 1, 208–226. doi:10.1016/j.jmbbm.2008.02.003

[13] Lee, S., & Wang, S. Biodegradable polymers / bamboo fiber biocomposite with bio-based coupling agent, Compos Part A Appl Sci Manuf., 2006, 37, 80–91. doi:10.1016/j.compositesa.2005.04.015

[14] Mohanty, A.K., Misra, M., & Hinrichsen, G. Biofibres. biodegradable polymers and biocomposites: An overview, 2000, 24, 1–24.
[15] Gatenholm, P., Kubát, J., & Mathiasson, A. Biodegradable natural composites. I. Processing and properties. J. Appl. Polym. Sci. 1992, 45, 1667–1677. doi:10.1002/app.1992.070450918
[16] Shibata, M., Oyamada, S., Kobayashi, S., & Yaginuma, D. Mechanical properties and biodegradability of green composites based on biodegradable polyesters and lyocell fabric. J. Appl. Polym. Sci., 2004, 92, 3857–3863. doi:10.1002/app.20405
[17] Gurunathan, T., Mohanty, S., & Nayak, S.K. A review of the recent developments in biocomposites based on natural fibres and their application perspectives. Compos. Part A Appl. Sci. Manuf., 2015, 77, 1–25. doi:10.1016/j.compositesa.2015.06.007
[18] Ohkita, T., & Lee, S.-H. Crystallization behavior of poly(butylene succinate)/corn starch biodegradable composite. J. Appl. Polym. Sci., 2005, 97, 1107–1114. doi:10.1002/app.21741
[19] Wu, C.-S. Performance of an acrylic acid grafted polycaprolactone/starch composite: Characterization and mechanical properties. J. Appl. Polym. Sci., 89, 2888–2895. doi:10.1002/app.12475
[20] Thompson, D. On growth and form, 1968, 2nd Editio, Cambridge: Cambridge University Press.
[21] Huebsch, N., & Mooney, D.J. Inspiration and application in the evolution of biomaterials. Nature. 2009, 462, 426–432. doi:10.1038/nature08601
[22] Swetha, M., Sahithi, K., Moorthi, A., Srinivasan, N., Ramasamy, K., & Selvamurugan, N. Biocomposites containing natural polymers and hydroxyapatite for bone tissue engineering. Int. J. Biol. Macromol., 2010, 47, 1–4. doi:10.1016/j.ijbiomac.2010.03.015
[23] Holbery, J., & Houston, D. Natural-fiber-reinforced polymer composites in automotive applications. JOM. 2006, 58, 80–86. doi:10.1007/s11837-006-0234-2
[24] Chen, P., & Lin, A.Y. Biological materials: Structure and mechanical properties, Prog. Mater. Sci. Elsevier, 2008, 53, 1–206. doi:10.1016/j.pmatsci.2007.05.002
[25] Leiro, V., Moreno, P.M., Sarmento, B., Durão, J., Gales, L., Pêgo, A.P., & Barrias, C.C. Design and preparation of biomimetic and bioinspired materials. in: Bioinspired Mater. Med. Appl., Elsevier, 2017: pp. 1–44. doi:10.1016/B978-0-08-100741-9.00001-2
[26] Gu, G.X., Takaffoli, M., & Buehler, M.J. Hierarchically Enhanced Impact Resistance of Bioinspired Composites. Adv. Mater, 2017, 29, 1700060. doi:10.1002/adma.201700060
[27] Vincent, J. Structural biomaterials, New Jersey, Springer, 1991.
[28] Srinivasan, A., Haritos, G.K., & Hedberg, F.L. Biomlmetlcs: Adwancing man-made materials through guidance from nature, Appl. Mech. Rev, 1991, 44, 463–482, doi: 10.1115/1.3119489.
[29] Ashby, M.F., Gibson, L.J., Wegst, U., & Olive, R. The Mechanical Properties of Natural Materials. I. Material Property Charts. Proc. R. Soc. A Math. Phys. Eng. Sci., 1995, 450, 123–140. doi:10.1098/rspa.1995.0075
[30] Koch, K., Bhushan, B., & Barthlott, W. Multifunctional surface structures of plants: An inspiration for biomimetics. Prog. Mater. Sci., 2009, 54, 137–178. doi:10.1016/j.pmatsci.2008.07.003
[31] Studart, A.R. Towards high-performance bioinspired composites. Adv. Mater., 2012, 24, 5024–5044. doi:10.1002/adma.201201471.
[32] Mishra, N., & Kandasubramanian, B. Biomimetic Design of Artificial Materials Inspired by Iridescent Nacre Structure and Its Growth Mechanism. Polym. Plast. Technol. Eng., 2017, 1–15. doi:10.1080/03602559.2017.1326139
[33] Yadav, R., Naebe, M., Wang, X., & Kandasubramanian, B. Review on 3D Prototyping of Damage Tolerant Interdigitating Brick Arrays of Nacre. Ind. Eng. Chem. Res., 2017, 56, 10516–10525. doi:10.1021/acs.iecr.7b01679

[34] Deoray, N., & Kandasubramanian, B. Review on Three-Dimensionally Emulated Fiber-Embedded Lactic Acid Polymer Composites: Opportunities in Engineering Sector, Polym. Plast. Technol. Eng., 2018, 57, 860–874. doi:10.1080/03602559.2017.1354226
[35] Yadav, R., Goud, R., Dutta, A., Wang, X., Naebe, M., & Kandasubramanian, B. Biomimicking of Hierarchal Molluscan Shell Structure Via Layer by Layer 3D Printing. Ind. Eng. Chem. Res., 2018, 57, 16537–16563. doi:10.1021/acs.iecr.8b01738
[36] Malik, A., & Kandasubramanian, B. Flexible Polymeric Substrates for Electronic Applications. Polym. Rev., 2018, 1–38. doi:10.1080/15583724.2018.1473424
[37] Korde, J.M., Shaikh, M., & Kandasubramanian, B. Bionic Prototyping of Honeycomb Patterned Polymer Composite and Its Engineering Application. Polym. Plast. Technol. Eng., 2018, 1–17. doi:10.1080/03602559.2018.1434667
[38] Klyosov, A.A. Flexural Strength (MOR) ANd Flexural Modulus (MOE) of Composite Material and Profiles, Wood Plast. Compos., 2007, 225–318. doi:10.1002/9780470165935.ch7
[39] ASTM, Standard Test Method for Flexural Strength of Advanced Ceramics at Ambient Temperature. ASTM Int., 2013, 1–19. doi:10.1520/C1161-13
[40] Fu, Q., Saiz, E. Rahaman, M.N., & Tomsia, A.P. Toward strong and tough glass and ceramic scaffolds for bone repair. Adv. Funct. Mater.,2013, 23, 5461–5476. doi:10.1002/adfm.201301121
[41] Shah, V. Handbook of Plastics Testing and Failure Analysis, 2007, John Wiley & Sons, Inc., Hoboken, NJ, USA. doi:10.1002/0470100427
[42] Chen, Q., & Pugno, N.M. Bio-mimetic mechanisms of natural hierarchical materials: A review. J. Mech. Behav. Biomed. Mater., 2013, 19, 3–33. doi:10.1016/j.jmbbm.2012.10.012
[43] Bond, G.M., Richman, R.H., & McNaughton, W.P. Mimicry of natural material designs and processes. J. Mater. Eng. Perform., 1995, 4, 334–345. doi:10.1007/BF02649071
[44] Gore, P. M., Kandasubramanian, B., Functionalized Aramid Fibers and Composites for Protective Applications: A Review, Ind. Eng. Chem. Res., 2018, 57, 16537–16563. doi:10.1021/acs.iecr.8b04903
[45] Sanchez, C., Arribart, H., & Guille, M.M.G. Biomimetism and bioinspiration as tools for the design of innovative materials and systems. Nat. Mater., 2005, 4, 277–288. http://www.ncbi.nlm.nih.gov/pubmed/15875305
[46] Han, Z., Mu, Z., Yin, W., Li, W., Niu, S., Zhang, J., & Ren, L. Biomimetic multifunctional surfaces inspired from animals. Adv. Colloid Interface Sci., 2016, 234, 27–50. doi:10.1016/j.cis.2016.03.004
[47] Morris, J.P., Wang, Y., Backeljau, T., & Chapelle, G. Biomimetic and bio-inspired uses of mollusc shells. Mar. Genomics, (2016), 27, 85–90. doi:10.1016/j.margen.2016.04.001
[48] Zoology, D., Musrirrn, B., & History, N. The mechanical behaviour of some molluscan hard tissues, J. Zool. (Wiley), 1974, 173, 395–406.
[49] Harper, E.M. Are calcitic layers an effective adaptation against shell dissolution in the Bivalvia, 2000.
[50] Wilkerson, R.P., Gludovatz, B., Watts, J., Tomsia, A.P., Hilmas, G.E., & Ritchie, R.O. A Novel Approach to Developing Biomimetic (“ Nacre-Like ”) Metal-Compliant-Phase (Nickel – Alumina) Ceramics through Coextrusion, Adv. Mater., 2016, 28, 1–7. doi:10.1002/adma.20160247
[51] Xia, S., Wang, Z., Chen, H., Fu, W., Wang, J., Li, Z., & Jiang, L. Nanoasperity: Structure Origin of Nacre-Inspired Nanocomposites. ACS Nano., 2015, 9, 2167–2172. doi:10.1021/acsnano.5b00119
[52] Grossman, M., Bouville, F., Erni, F., Masania, K., Libanori, R., & Studart, A.R. Mineral Nano-Interconnectivity Stiffens and Toughens Nacre-like Composite Materials, Adv. Mater., 2017, 29, 1–7. doi:10.1002/adma.201605039.
[53] Zhao, N., Yang, M., Zhao, Q., Gao, W., Xie, T., & Bai, H. Superstretchable Nacre-Mimetic Graphene/ Poly(vinyl alcohol) Composite Film Based on Interfacial Architectural Engineering. 2017. doi:10.1021/acsnano.7b01089

[54] Katti, D.R., & Katti, K.S. Modeling microarchitecture and mechanical behavior of nacre using 3D finite Part I Elastic properties. Kluwer Academic Publishers (Springer) 2001, 6, 1411–1417.
[55] Gu, G.X., Libonati, F., Wettermark, S., & Buehler, M.J. Printing nature: Unraveling the role of nacre's mineral bridges, J. prot. Mech. Behav. Biomed. Mater., 2017, 76, 135–144. doi:10.1016/j.jmbbm.2017.05.007
[56] Tang, Z., Kotov, N.A., Magonov, S., & Ozturk, B. Nanostructured artificial nacre. Nat. Mater.,2003, 2, 413–418. doi:10.1038/nmat906.
[57] Podsiadlo, P., Tang, Z., Shim, B.S., & Kotov, N.A. Counterintuitive Effect of Molecular Strength and Role of Molecular Rigidity on Mechanical Properties of Layer-by-Layer Assembled Nanocomposites. Nano Lett., 2007, 7, 1224–1231. doi:10.1021/nl0700649
[58] Podsiadlo, P., Liu, Z., Paterson, D., Messersmith, P.B., & Kotov, N.A. Fusion of Seashell Nacre and Marine Bioadhesive Analogs: High-Strength Nanocomposite by Layer-by-Layer Assembly of Clay andL-3,4-Dihydroxyphenylalanine Polymer, Adv. Mater., 2007, 19, 949–955. doi:10.1002/adma.200602706
[59] Podsiadlo, P., Kaushik, A.K., Arruda, E.M., Waas, A.M., Shim, B.S., Xu, J., Nandivada, H., Pumplin, B.G., Lahann, J., Ramamoorthy, A., & Kotov, N.A. Ultrastrong and Stiff Layered Polymer Nanocomposites. Science (80-.), 2007, 318, 80–83. doi:10.1126/science.1143176
[60] Podsiadlo, P., Kaushik, A.K., Shim, B.S., Agarwal, A., Tang, Z., Waas, A.M., Arruda, E.M., & Kotov, N.A. Can Nature's Design be Improved Upon? High Strength, Transparent Nacre-Like Nanocomposites with Double Network of Sacrificial Cross Links †. J. Phys. Chem. B., 2008, 112, 14359–14363. doi:10.1021/jp801492n
[61] Xu, Y., Hong, W., Bai, H., Li, C., & Shi, G. Strong and ductile poly(vinyl alcohol)/graphene oxide composite films with a layered structure. Carbon N. Y., 2009, 47, 3538–3543. doi:10.1016/j.carbon.2009.08.022
[62] Wang, X., Bai, H., Yao, Z., Liu, A., & Shi, G. Electrically conductive and mechanically strong biomimetic chitosan/reduced graphene oxide composite films. J. Mater. Chem., 2010, 20, 9032. doi:10.1039/c0jm01852j
[63] Chen, R., Wang, C., Huang, Y., & Le, H. An efficient biomimetic process for fabrication of artificial nacre with ordered-nanostructure. Mater. Sci. Eng. C., 2008, 28, 218–222. doi:10.1016/j.msec.2006.12.008
[64] Walther, A., Bjurhager, I., Malho, J.-M., Pere, J., Ruokolainen, J., Berglund, L.A., & Ikkala, O. prot. Large-Area, Lightweight and Thick Biomimetic Composites with Superior Material Properties via Fast, Economic, and Green Pathways. Nano Lett.,2010, 10, 2742–2748. doi:10.1021/nl1003224
[65] Xu, H., Xie, L., Chen, J.-B., Jiang, X., Hsiao, B.S., Zhong, G.-J., Fu, Q., & Li, Z.-M. Strong and tough micro/nanostructured poly(lactic acid) by mimicking the multifunctional hierarchy of shell. Mater. Horiz., 2014, 1, 546–552. doi:10.1039/C4MH00085D
[66] Zhang, X., Liu, C., Wu, W., & Wang, J. Evaporation-induced self-assembly of organic–inorganic ordered nanocomposite thin films that mimic nacre. Mater. Lett., 2006, 60, 2086–2089. doi:10.1016/j.matlet.2005.12.111
[67] Lin, W., Wang, C., Le, H., Long, B., & Huang, Y. Special assembly of laminated nanocomposite that mimics nacre. Mater. Sci. Eng. C., 2008, 28, 1031–1037. doi:10.1016/j.msec.2007.04.030
[68] Wang, J., Cheng, Q., Lin, L., & Jiang, L. Synergistic Toughening of Bioinspired Poly(vinyl alcohol)–Clay–Nanofibrillar Cellulose Artificial Nacre. ACS Nano., 2014, 8, 2739–2745. doi:10.1021/nn406428n
[69] Pai, R.K., Zhang, L., Nykpanchuk, D., Cotlet, M., & Korach, C.S. Biomimetic Pathways for Nanostructured Poly(KAMPS)/aragonite Composites that Mimic Seashell Nacre. Adv. Eng. Mater., 2011, 13, B415–B422. doi:10.1002/adem.201080136

[70] Tiwary, C.S., Kishore, S., Sarkar, S., Mahapatra, D.R., Ajayan, P.M., & Chattopadhyay, K. Morphogenesis and mechanostabilization of complex natural and 3D printed shapes. Sci. Adv., (2015), 1 e1400052–e1400052. doi:10.1126/sciadv.1400052
[71] Mayer, G., & Sarikaya, M. Rigid Biological Composite Materials: Structural Examples for Biomimetic Design, Exp. Mech. (Springer), 2002, 42, 395–403.
[72] Zhang, Q., Yang, X., Li, P., Huang, G., Feng, S., Shen, C., Han, B., Zhang, X., Jin, F., Xu, F., & Lu, T.J. Bioinspired engineering of honeycomb structure – Using nature to inspire human innovation. Prog. Mater. Sci., 2015, 74, 332–400. doi:10.1016/j.pmatsci.2015.05.001
[73] Bitzer, T. Honeycomb Technology, 1997, Springer Netherlands, Dordrecht. doi:10.1007/978-94-011-5856-5
[74] Ajdari, A., Jahromi, B.H., Papadopoulos, J., Nayeb-Hashemi, H., & Vaziri, A. Hierarchical honeycombs with tailorable properties. Int. J. Solids Struct., 2012, 49, 1413–1419. doi:10.1016/j.ijsolstr.2012.02.029
[75] Scarpa, F., Blain, S., Lew, T., Perrott, D., Ruzzene, M., & Yates, J.R. Elastic buckling of hexagonal chiral cell honeycombs. Compos. Part A Appl. Sci. Manuf., 2007, 38, 280–289. doi:10.1016/j.compositesa.2006.04.007
[76] Ingrole, A., Hao, A., & Liang, R. Design and modeling of auxetic and hybrid honeycomb structures for in-plane property enhancement. Mater. Des., 2017, 117 72–83. doi:10.1016/j.matdes.2016.12.067
[77] Yang, L., Harrysson, O., West, H., & Cormier, D. Mechanical properties of 3D re-entrant honeycomb auxetic structures realized via additive manufacturing. Int. J. Solids Struct., 2015, 69–70 475–490. doi:10.1016/j.ijsolstr.2015.05.005
[78] Chantarapanich, N., Laohaprapanon, A., Wisutmethangoon, S., Jiamwatthanachai, P., Chalermkarnnon, P., Sucharitpwatskul, S., Puttawibul, P., & Sitthiseripratip, K. Fabrication of three-dimensional honeycomb structure for aeronautical applications using selective laser melting: a preliminary investigation. Rapid Prototyp. J., 2014, 20, 551–558. doi:10.1108/RPJ-08-2011-0086
[79] Alderson, A., Alderson, K.L., Attard, D., Evans, K.E., Gatt, R., Grima, J.N., Miller, W., Ravirala, N., Smith, C.W., & Zied, K. Elastic constants of 3-, 4- and 6-connected chiral and anti-chiral honeycombs subject to uniaxial in-plane loading. Compos. Sci. Technol., 2010, 70, 1042–1048. doi:10.1016/j.compscitech.2009.07.009
[80] Hedayati, R., Sadighi, M., Mohammadi-Aghdam, M., & Zadpoor, A.A. Mechanical properties of additively manufactured octagonal honeycombs. Mater. Sci. Eng. C., 2016, 69, 1307–1317. doi:10.1016/j.msec.2016.08.020
[81] Oftadeh, R., Haghpanah, B., Papadopoulos, J. Hamouda, A.M.S., Nayeb-Hashemi, H., & Vaziri, A. Mechanics of anisotropic hierarchical honeycombs. Int. J. Mech. Sci.,2014, 81, 126–136. doi:10.1016/j.ijmecsci.2014.02.011
[82] Mousanezhad, D., Ebrahimi, H., Haghpanah, B., Ghosh, R., Ajdari, A., Hamouda, A.M.S., & Vaziri, A. Spiderweb honeycombs. Int. J. Solids Struct., 2015, 66, 218–227. doi:10.1016/j.ijsolstr.2015.03.036
[83] Sommer, M.R., Schaffner, M., Carnelli, D., & Studart, A.R. 3D Printing of Hierarchical Silk Fibroin Structures. ACS Appl. Mater. Interfaces., 2016, 8, 34677–34685. doi:10.1021/acsami.6b11440.
[84] Schacht, K., Jüngst, T., Schweinlin, M., Ewald, A., Groll, J., & Scheibel, T. Biofabrication of Cell-Loaded 3D Spider Silk Constructs. Angew. Chemie Int. Ed., 2015, 54, 2816–2820. doi:10.1002/anie.201409846
[85] Cai, Q., Feng, Q., Liu, H., & Yang, X. Preparation of biomimetic hydroxyapatite by biomineralization and calcination using poly(l-lactide)/gelatin composite fibrous mat as template. Mater. Lett., 2013, 91, 275–278. doi:10.1016/j.matlet.2012.09.101

[86] Bian, J., & Jing, X. Biomimetic design of woodpecker for shock and vibration protection, in: 2014 IEEE Int. Conf. Robot. Biomimetics (ROBIO 2014), IEEE, 2014: pp. 2238–2243. doi:10.1109/ROBIO.2014.7090670
[87] Malik, I.A., Mirkhalaf, M., & Barthelat, F. Bio-inspired "jigsaw"-like interlocking sutures: Modeling, optimization, 3D printing and testing. J. Mech. Phys. Solids., 2017, 102, 224–238. doi:10.1016/j.jmps.2017.03.003
[88] Luo, J., Zhang, L., Peng, Q., Sun, M., Zhang, Y., Shao, H., & Hu, X. Tough silk fibers prepared in air using a biomimetic microfluidic chip. Int. J. Biol. Macromol.,2014, 66, 319–324. doi:10.1016/j.ijbiomac.2014.02.049
[89] Gan, Z., Turner, M.D., & Gu, M. Biomimetic gyroid nanostructures exceeding their natural origins. Sci. Adv., 2016, 2, e1600084–e1600084. doi:10.1126/sciadv.1600084
[90] Thiele, S., Arzenbacher, K., Gissibl, T., Giessen, H., & Herkommer, A.M. 3D-printed eagle eye: Compound microlens system for foveated imaging. Sci. Adv., 2017, 3, e1602655. doi:10.1126/sciadv.1602655.
[91] Song, J., Reichert, S., Kallai, I., Gazit, D., Wund, M., Boyce, M.C., & Ortiz, C. Quantitative microstructural studies of the armor of the marine threespine stickleback (Gasterosteus aculeatus). J. Struct. Biol., 2010, 171, 318–331. doi:10.1016/j.jsb.2010.04.009
[92] Rudykh, S., Ortiz, C., & Boyce, M.C. Flexibility and protection by design: imbricated hybrid microstructures of bio-inspired armor. Soft Matter., 2015, 11, 2547–2554. doi:10.1039/C4SM02907K.
[93] Browning, A., Ortiz, C., & Boyce, M.C. Mechanics of composite elasmoid fish scale assemblies and their bioinspired analogues. J. Mech. Behav. Biomed. Mater., 2013, 19, 75–86. doi:10.1016/j.jmbbm.2012.11.003
[94] Van Wassenbergh, S., van Manen, K., Marcroft, T.A., Alfaro, M.E., & Stamhuis, E.J. Boxfish swimming paradox resolved: forces by the flow of water around the body promote manoeuvrability. J. R. Soc. Interface., 2014, 12, 20141146–20141146. doi:10.1098/rsif.2014.1146
[95] Koch, K., & Barthlott, W. Superhydrophobic and superhydrophilic plant surfaces: an inspiration for biomimetic materials. Philos. Trans. R. Soc. A Math. Phys. Eng. Sci., 2009, 367 1487–1509. doi:10.1098/rsta.2009.0022
[96] Kramer, P. Physiology of Woody Plants, Londan, Elsevier, 1979.
[97] Noorunnisa Khanam, P., Ramachandra Reddy, G., Raghu, K., & Venkata Naidu, S. Tensile, flexural, and compressive properties of coir/silk fiber-reinforced hybrid composites. J. Reinf. Plast. Compos., 2010, 29, 2124–2127. doi:10.1177/0731684409345413
[98] Hemant Patel, Ashish Parkhe, P.K. Shrama, Mechanical Behaviour of Banana and Sisal Hybrid, Int. J. Res Granthaalayah, 2016, 4, 206–216.
[99] Wayan, S. I, Gusti Agung Kade, S. I, & Arnis, K. Mechanical Properties of Rice Husks Fiber Reinforced Polyester Composites. Int. J. Mater. Mech. Manuf., 2014, 2, 165–168. doi:10.7763/IJMMM.2014.V2.121
[100] Sorieul, M., Dickson, A.,Hill, S., Pearson, H., Plant Fibre: Molecular Structure and Biomechanical Properties, of a Complex Living Material, Influencing Its Deconstruction towards a Biobased Composite, Materials, 2016, 9, 618. doi:10.3390/ma9080618.
[101] Al-Khanbashi, A., Al-Kaabi, K., & Hammami, A. Date palm fibers as polymeric matrix reinforcement: Fiber characterization. Polym. Compos., 2005, 26, 486–497. doi:10.1002/pc.20118
[102] Summerscales, J., Virk, A., & Hall, W. A review of bast fibres and their composites: Part 3 - Modelling. Compos. Part A Appl. Sci. Manuf., 2013, 44, 132–139. doi:10.1016/j.compositesa.2012.08.018

[103] Pickering, K.L., Beckermann, G.W., Alam, S.N., & Foreman, N.J. Optimising industrial hemp fibre for composites. Compos. Part A Appl. Sci. Manuf., 2007, 38, 461–468. doi:10.1016/j.compositesa.2006.02.020.
[104] Bos, H., Van Den Oever, M., & Peters, O. Tensile and compressive properties of flax fibres for natural fibre reinforced composites. J. Mater. Sci., 2002, 37, 1683–1692. doi:10.1023/A:1014925621252.
[105] Charlet, K., Baley, C., Morvan, C., Jernot, J.P., Gomina, M., & Bréard, J. Characteristics of Hermès flax fibres as a function of their location in the stem and properties of the derived unidirectional composites. Compos. Part A Appl. Sci. Manuf., 2007, 38, 1912–1921. doi:10.1016/j.compositesa.2007.03.006
[106] Li, X., Tabil, L.G., & Panigrahi, S. Chemical treatments of natural fiber for use in natural fiber-reinforced composites: A review. J. Polym. Environ., 2007, 15, 25–33. doi:10.1007/s10924-006-0042-3
[107] Shah, D.U., Porter, D., & Vollrath, F. Can silk become an effective reinforcing fibre? A property comparison with flax and glass reinforced composites. Compos. Sci. Technol., (2014), 101 173–183. doi:10.1016/j.compscitech.2014.07.015
[108] Mustafa, A., Bin Abdollah, M.F., Shuhimi, F.F., Ismail, N., Amiruddin, H., & Umehara, N. prot. Selection and verification of kenaf fibres as an alternative friction material using Weighted Decision Matrix method. Mater. Des., 2015, 67, 577–582. doi:10.1016/j.matdes.2014.10.091
[109] De Rosa, I.M., Kenny, J.M., Puglia, D., Santulli, C., & Sarasini, F. Tensile behavior of New Zealand flax (Phormium tenax) fibers. J. Reinf. Plast. Compos., 2010, 29, 3450–3454. doi:10.1177/0731684410372264
[110] Dittenber, D.B., & Gangarao, H.V.S. Critical review of recent publications on use of natural composites in infrastructure. Compos. Part A Appl. Sci. Manuf., 2012, 43, 1419–1429. doi:10.1016/j.compositesa.2011.11.019
[111] Barkoula, N.M., Alcock, B., Cabrera, N.O., & Peijs, T. Fatigue properties of highly oriented polypropylene tapes and all-polypropylene composites. Polym. Polym. Compos., 2008, 16, 101–113. doi:10.1002/pc
[112] Ben Brahim, S., & Ben Cheikh, R. Influence of fibre orientation and volume fraction on the tensile properties of unidirectional Alfa-polyester composite. Compos. Sci. Technol., 2007, 67 140–147. doi:10.1016/j.compscitech.2005.10.006
[113] Carr, D.J., Cruthers, N.M., Laing, R.M., & Niven, B.E. Fibers from Three Cultivars of New Zealand Flax (Phormium tenax). Text. Res. J., 2005, 75, 93–98. doi:10.1177/004051750507500201
[114] Cheng, S., Tak Lau, K., Liu, T., Zhao, Y., Lam, P.M., & Yin, Y. Mechanical and thermal properties of chicken feather fiber/PLA green composites. Compos. Part B Eng., 2009, 40, 650–654. doi:10.1016/j.compositesb.2009.04.011
[115] Huson, M.G., Bedson, J.B., Phair, N.L., & Turner, P.S. Intrinsic Strength of Wool Fibres, Asian-Aus. J. Anim. Sci. 13 Supplement July 2000 C: 267.
[116] Gashti, M.P., & Gashti, M.P. Effect of Colloidal Dispersion of Clay on Some Properties of Wool Fiber. J. Dispers. Sci. Technol., 2013, 34, 853–858. doi:10.1080/01932691.2012.713248
[117] Niu, M., Liu, X., Dai, J., Hou, W., Wei, L., & Xu, B. Molecular structure and properties of wool fiber surface-grafted with nano-antibacterial materials. Spectrochim. Acta - Part A Mol. Biomol. Spectrosc., 2012, 86, 289–293. doi:10.1016/j.saa.2011.10.038
[118] Aruan Efendy, M.G., & Pickering, K.L. Comparison of harakeke with hemp fibre as a potential reinforcement in composites. Compos. Part A Appl. Sci. Manuf., 2014, 67, 259–267. doi:10.1016/j.compositesa.2014.08.023
[119] Liu, B., He, Y., Fan, Y., & Wang, X. Fabricating Super-Hydrophobic Lotus-Leaf-Like Surfaces through Soft-Lithographic Imprinting. Macromol. Rapid Commun., 2006, 27, 1859–1864. doi:10.1002/marc.200600492

[120] Bhushan, B., Jung, Y.C., Niemietz, A., & Koch, K. Lotus-Like Biomimetic Hierarchical Structures Developed by the Self-Assembly of Tubular Plant Waxes. Langmuir., 2009, 25, 1659–1666. doi:10.1021/la802491k

[121] Chang, K.-C., Lu, H.-I., Peng, C.-W., Lai, M.-C., Hsu, S.-C., Hsu, M.-H., Tsai, Y.-K., Chang, C.-H., Hung, W.-I., Wei, Y., & Yeh, J.-M. Nanocasting Technique to Prepare Lotus-leaf-like Superhydrophobic Electroactive Polyimide as Advanced Anticorrosive Coatings. ACS Appl. Mater. Interfaces., (2013), 5, 1460–1467. doi:10.1021/am3029377

[122] Yang, Y., Li, X., Zheng, X., Chen, Z., Zhou, Q., & Chen, Y. 3D-Printed Biomimetic Super-Hydrophobic Structure for Microdroplet Manipulation and Oil/Water Separation. Adv. Mater., 2018, 30, 1704912. doi:10.1002/adma.201704912

[123] Park, J.-U., Hardy, M., Kang, S.J., Barton, K., Adair, K., Kishore Mukhopadhyay, D., Lee, C.Y., Strano, M.S., Alleyne, A.G., Georgiadis, J.G., Ferreira, P.M., & Rogers, J.A. High-resolution electrohydrodynamic jet printing. Nat. Mater., 2007, 6, 782–789. doi:10.1038/nmat1974

[124] Li, S.H., Zeng, Q.Y., Xiao, Y.L., Fu, S.Y., & Zhou, B.L. Biomimicry of bamboo bast fiber with engineering composite materials. Mater. Sci. Eng. C., 1995, 3, 125–130. doi:10.1016/0928-4931(95)00115-8

[125] Tong, J., Ma, Y., Chen, D., Sun, J., & Ren, L. Effects of vascular fiber content on abrasive wear of bamboo. Wear., 2005, 259, 78–83. doi:10.1016/j.wear.2005.03.031

[126] Markstedt, K., Escalante, A., Toriz, G., & Gatenholm, P. Biomimetic Inks Based on Cellulose Nanofibrils and Cross-Linkable Xylans for 3D Printing, ACS Appl. Mater. Interfaces., 2017, 9, 40878–40886. doi:10.1021/acsami.7b13400

Wafa Ouarhim, Mohammed Ouadi Bensalah, Abou el kacem Qaiss, Rachid Bouhfid

7 Hygrothermoelastic behaviour Natural fibers based composites: Mechanisms and formalism

Abstract: Natural fibers have shown their applications grow strongly in recent years, both in construction and in transport and leisure. This chapter discusses the hygrothermoelastic behavior of composites reinforced with natural fibers. Different behaviors have been proved, including hygroscopic, thermal, hygrothermal, hygroelastic, thermoelastic, and hygrothermoelastic behaviors. The mechanisms and formalisms of each behavior are reported concurrently. Finally, the focus is on the application of equations governing the hygrothermoelastic effect in the case of the laminated composite structure.

Keywords: Natural fibers, composite, hygroscopic behavior, thermal behavior, hygrothermal behavior, hygroelastic behavior, thermoelastic behavior, hygrothermoelastic behavior

7.1 Introduction

Nowadays, the use of natural fibers as reinforcement has become an attraction for scientists and researchers as a good alternative for fiber-reinforced composites because of their low cost and are renewable, completely or partially recyclable, and biodegradable [1, 2].Owing to their good environmentally friendly feature, the natural-fiber-containing composites are very popular in engineering markets such as transportation (automobiles, railway coaches, and aerospace), military applications, building and construction industries (ceiling, paneling, and partition boards), packaging, consumer products, and so on. However, one of the main drawbacks of these hydrophilic fibers is the high capacity to absorb moisture.

Wafa Ouarhim, Moroccan Foundation for Advanced Science, Innovation and Research (MAScIR), Laboratory of Polymer Processing, Rabat, Morocco; Mohammed V University, Faculty of Science, Mechanics of Materials Laboratory, Rabat, Morocco
Mohammed Ouadi Bensalah, Mohammed V University, Faculty of Science, Mechanics of Materials Laboratory, Rabat, Morocco
Abou el kacem Qaiss, Rachid Bouhfid, Moroccan Foundation for Advanced Science, Innovation and Research (MAScIR), Laboratory of Polymer Processing, Rabat, Morocco

https://doi.org/10.1515/9783110603699-007

Generally, during both initial fabrication and final use, the composite materials are subjected to changing environmental conditions. The variation of temperature and moisture is considered as the main parameters influencing the composite mechanical behavior [3, 4]. The composite absorbs moisture when subjected to wet conditions. When subjected to increase in the temperature, the heat is conducted into the composite materials. The combined behavior of both temperature and moisture is termed as the hygrothermal effect. This behavior alters some properties of the material and induces necessary dimensional changes,which are referred to as residual stresses [5]. As a result, the stiffness and the strength of the dominated matrix change and the elastic properties of the material degrade, which developed the hygro-thermoelastic behavior. Thus, the expansions and the contractions in the material, which are because of hygroscopic and thermal environments alter the stress and the strain distribution in the composite. In order to make composite materials competitive with other well-controlled materials such as alloys, it is necessary to understand the phenomena related to hygroscopic and thermal behavior and how these two phenomena influence the mechanical properties of the resultant composite. Indeed, the variation of the moisture concentration gradient, which is termed as the diffusion phenomena and the variation of the temperature or pressure gradient termed as permeation are considered as the main mechanisms of moisture absorption. Diffusion is a molecular-scale process, which occurs in the pore network (nanoscale), unlike permeation,which takes place within microcracks or voids of larger dimensions (above ≈30 nm). The processing conditions include compounding process that form microcracks, microspace, or pores because of localized shrinking and swelling during curing facilitated the transport of water [6]. Once the microcracks occurred, more surface area was exposed to moisture. On the other hand, other than the temperature, there are many other parameters influencing the way in which the composite absorbs water, including hygrometric rate, fiber fraction, fiber nature, porosity fraction, reinforcement geometry, and matrix type.

In literatures, S. Brischetto [3] investigated the hygrothermal loading effects in the bending of multilayered composite plates. He showed that the moisture and temperature alter the bending response in the composite structure on increasing the maximum deflection and the discontinuity values of in-plane stresses at the layer interface. Moreover, R. Hu et al. [7] studied the aging behaviors of short jute fiber/polylactide (PLA) composite material under moisture and temperature effect. They have reported that the tensile strength of the studied composite severely decreased after aging and the used matrix underwent a severe degradation. In the same context, D. Scida et al. [4] examined the effect of hygrothermal aging on mechanical properties of the flax–fiber-reinforced epoxy composite. They found that the Young's modulus and tensile strength decrease and the process of degradation is highlighted. However, the effects of the continuous alteration of two conditions, especially concurrently with mechanical loading, remain less explored.

In this chapter, the investigation will be a treat; on one hand, the different behaviors of composites embedded by natural fibers facing moisture, temperature, and elastic loadings, and the combined effect of the previously cited behaviors, and on the other hand, the application of one formalism governing these three combined effects on the case of the laminated composite.

7.2 Different behaviors of natural fiber-based composite facing moisture, temperature, and mechanical loadings: mechanism and formalism

Generally, composite materials reinforced by natural fillers are used in multiple application domains that cause them to experience different environments, including moisture, temperature, and/or mechanical loadings. This section will emphasize on the mechanisms and formalisms of hygroscopic, thermal, and/or elastic behaviors of natural fiber-based biocomposites.

7.2.1 Hygroscopic behavior of natural fiber-based composites

Hydroscopic behavior is the capacity of the composite to absorb moisture by immersion in water. This behavior allows altering some properties of both the matrix and the natural fibers. Indeed, in a wet environment, the natural fibers surrounded by the matrix change their volume because they absorb water molecules through microcracks (Figure 7.1) and then, they are swelled inside the composite that leads to

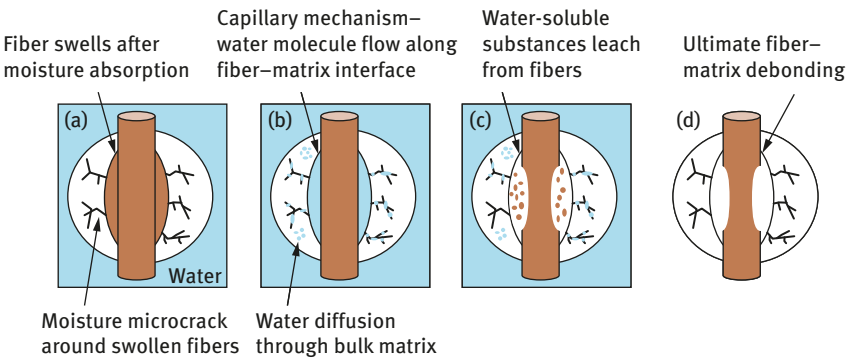

Figure 7.1: Effect of water molecules on fiber–matrix interface.

the development of internal stresses at the fiber–matrix interface and can eventually lead to the damage of the latter (debonding between fiber and matrix) and to a significant degradation of the initial properties of the composite [8, 9].

From a chemical standpoint, the water diffusing into the composite material creates hydrogen bonds with the fibers, which can lead to the reduction in interactions between the fibers and the matrix [8]. Generally, the moisture absorption increases with the volume fraction of natural fibers embedded in the matrix, which is the case of the composite of polyester or hemp immersed in water at 25 °C [10]. The last work showed a decrease in mechanical properties of bending with the amount of water uptake. This result was explained by the swelling of the fibers caused by the moisture absorption that leads to the appearance of microcracks in the matrix. Then, the water seeps through the created microcracks involving the flow of water molecules along the fiber–matrix interface,which results in debonding of the fiber and the matrix.Thus, Bismarck et al. [11] emphasized while the composite immersed in water, the swelling stresses that were created by microcracks increased and led to the composite failure. According to literature, most of the authors highlighted the phenomena of debonding and microcracks investigated in the case of the other biocomposites [7, 12].

Generally, when the natural fiber-based composites are immersed in water, the fibers absorb moisture. Célino et al. [13] demonstrated that water could not only be trapped inside pores, but there is also the specific sites of water absorption in these fibers. Moreover, they showed that these specific polar sites, which are identified by using spectroscopic techniques could be hydroxyl functions of amorphous cellulose and hemicelluloses or carboxylic function of pectins. Thereby, Hatakeyama and Hatakeyama [14] pointed out that the water sorbed by these fibers could be divided into two categories: (1) free and (2) bound water. Free water, also known as mobile water is locked up inside the fiber voids, whereas bound water could relate to specific sites as described previously. Thus, this change in hydrophilic fibers caused by water sorption leads to an altering of several fiber parameters such as their mechanical, chemical, dimensional, and structural properties. In this context, Hatakeyama and Hatakeyama [14] indicate that water can have a plasticization effect on the structure or, on the contrary, forms stable hydrogen bonds leading to an anti-plasticizing effect.

On the other hand, some of the authors focused on the theoretical approaches dedicated to the prediction of the mechanism of moisture uptake in polymeric resins. Among several physical models existing in the literature, Fick's law is the most common model used [15, 16]. However, since not all polymers adapted to the Fickian diffusion, there are other theoretical models that can be used as Langmuir law also named as the two-phase model of Carter and Kibler [17] or a dual-stage Fick's law [18].

According to the *Fick's law*, the fibers have been assumed to be assimilated as a long full cylinder whose length is very large as compared to its radius. Thus, the

diffusion is considered radial, leading to concentration of humidity C as a function of only two parameters: (1) radius r and (2) time t expressed as follows [19]:

$$\frac{\partial C}{\partial t} = D.\left(\frac{1}{r}\frac{\partial C}{\partial r} + \frac{\partial^2 C}{\partial x^2}\right) \tag{7.1}$$

where D is the Fickian diffusion coefficient.

The following expression is found from the analytical solution of the above-mentioned eq. (7.1) after its integration over the cylinder radius $r = a$:

$$\frac{M_t}{M_\infty} = 1 - \sum_{n=1}^{\infty} \frac{4}{a^2\alpha_n^2} \exp\left(-D\alpha_n^2 t\right) \tag{7.2}$$

where M_t is the moisture content at time t, M_∞ is the saturation mass uptake, and α_n are the roots of the first species of Bessel's function at order 0.

To determine the diffusion coefficient (D) and the moisture content at a infinite time (M_∞), the used technique is to minimize the agreement between experimental results and the moisture sorbed predicted owing to eq. (7.2).

Regarding *Langmuir law*, also known as the *Two-Phase Model of Carter and Kibler*, it is often used for polymers that do not present standard Fickian diffusion. Thus, the moisture uptake can be explained quantitatively by assuming that the absorbed moisture consists of both mobile and bound phases. It is worth noting that the molecules of the mobile phase diffuse with the concentration- and stress-independent diffusion coefficient *Dy*, and are absorbed, thereby becoming bound with a probability per unit time y at certain sites such as in voids within the polymer, hydrogen bonding, and heterogeneous morphology. Molecules are emitted from the phase, thus becoming mobile with a probability per unit time β.

For the one-dimensional case, the molecular number densities at time t, in a homogeneous cylinder of radius r, verify the coupled set of eqs. (7.3), (7.4), and (7.5):

$$\frac{\partial n}{\partial t} = D\left(\frac{\partial^2 n}{\partial r^2} + \frac{1}{r}\frac{\partial n}{\partial r}\right) + \frac{\partial N}{\partial t} \tag{7.3}$$

$$\frac{\partial N}{\partial t} = \gamma n - \beta N \tag{7.4}$$

$$\gamma n\infty = \beta N\infty \tag{7.5}$$

where n and N are the number of mobile and bound molecules per unit volume, respectively. The finite difference is the tool that is used for numerically solving these coupled equations. The idea is to test different values of the three parameters: (1) *Dy*, (2) n, and (3) β. The best parameters are when the triplet minimizes the square differences between experimental and theoretical results.

Regarding *dual-stage Fick's law*, it is also used in the case of polymers that represent an anomalous Fickian moisture uptake. It consists of two Fickian diffusion kinetics occurring in parallel [18]. Both the Fickian diffusion models use eq. (7.6) with separate diffusion coefficients (D_1 and D_2) and saturation levels ($M_{\infty 1}$ and $M_{\infty 2}$), respectively. The sum of each saturation level gives the total moisture absorption capacity of the specimen in the steady state of the diffusion process as given in eq.(7.7):

$$M_t = M_{\infty 1}\left(1 - \sum_{n=1}^{\infty} \frac{4}{a^2\alpha_n^2}\exp\left(-D_1\alpha_n^2 t\right)\right) + M_{\infty 2}\left(1 - \sum_{n=1}^{\infty} \frac{4}{a^2\alpha_n^2}\exp\left(-D_2\alpha_n^2 t\right)\right) \tag{7.6}$$

$$M_{\infty 1} + M_{\infty 2} = M_{\infty} \tag{7.7}$$

From these three laws, the results show that a similar diffusive behavior is exhibited by all the fibers in the same environment. A. Célino et al. [20] reported that in immersion, the samples show anomalous absorption kinetics, and Langmuir theory actually well describes diffusion kinetics in such conditions, whereas a Fickian diffusion is followed by the same fibers when they are exposed to vapor during relative humidity aging. To conclude, the hygroscopic behavior of natural fiber-based composites can allow dimensional changes, influence mechanical properties, and structural modification of the composites embedded by natural fibers.

7.2.2 Thermal behavior of composites reinforced with natural fibers

Composite materials reinforced by biofillers experience tremendous improvement in many areas and can now be used in high-temperature situations. Their thermal behavior that often follows the evolution of thermal degradation process and transition temperatures are investigated via thermogravimetric analysis (TGA) and dynamic scanning calorimetry (DSC), respectively [21]. In addition, DSC analysis helps to identify the chemical activity of the fibers as the temperature increases. Moreover, dynamical mechanical thermal analysis (DMTA) is also used to investigate how the fiber adds influence to the thermal properties of the elaborated composites and to know the maximum use temperature of the matrix. Therefore, the nonuniform temperature in composite structure induces thermal deformation and stresses that become important parameters in structural design [22].

The aim of analyzing the thermal behavior of the fiber and composites can be carried out for determining the moisture content and volatile components contained in the composite [23]. From differential thermal analysis curves of different types of treated and untreated natural fibers, they show treated and untreated natural fiber-containing water molecules [23]. Moreover, each natural fiber is characterized by a temperature domain where they are thermally stable. This result is

deducted from the differential thermal curve of the fiber, where this range is characterized by the absence of exothermic or endothermic reactions.

Compared to synthetic fibers (glass fibers, carbon fiber, etc.), the natural fibers featured by lower thermal stability, which caused their limitation in the higher temperature applications [24]. In order to increase the thermal stability of these composites, several ways have been adopted. On one hand, the chemical treatments modify the thermal characteristics of the natural fiber-based composites. Indeed, numerous studies show that the alkali, silane, and acetylated treatments increase the thermal stability of the natural fibers [25, 26]. T. J. Singh et al. [27] highlighted that alkali treatment increases the thermal properties of the bamboo fiber-reinforced composites. This increase in the thermal stability can be interpreted by the fact that the bonding between the cellulose molecules in the fibers increases, which leads to a rise in the crystalline nature of the fibers. On the other hand, R. Jeencham et al. [28] showed that adding flame retardants such as zinc borate (Zb), ammonium polyphosphate (APP), $Mg(OH)_2$, and so on enhance the thermal stability of the sisal fiber-reinforced polypropylene composite. Indeed, the magnesium phosphate glass and MgO are the results of the interaction of APP with $Mg(OH)_2$, which acted as thermal barriers and led to an increase in the thermal stability of the composites. Moreover, the hybridization of the natural fibers with synthetic fibers such as glass fibers leads to an improvement in the thermal properties such as thermal conductivity, diffusivity, and so on because of the presence of Fe^{2+} ions in the glass fibers [29–31].

As mentioned earlier, the thermal behavior, especially thermal degradation of the composites embedded by natural fibers has also been carried out by TGA.The results of TGA show that the thermal degradation of the matrix increased with the addition of fillers [21, 32]. In addition, they show that the degradation temperature of the fillers is high enough to be compatible with the extrusion and injection molding temperatures. When the composite is subjected to thermal stress, premature failure can be present at a weak interface because of differential thermal expansions of fiber and matrix. Indeed, the thermal effects on biocomposite enter the mathematical formulation in the same form as moisture effects.

7.2.3 Hygrothermal behavior of natural fiber-based composites

Hygrothermal behavior is related to the heat and mass transfer in the structure that is subjected to a high temperature and moisture concentration (Figure 7.2).In other words, hygrothermal aging is a method of providing aggressive conditions for the material-accelerated aging test. Composites that are subject to these conditions undergo hygrothermal internal stresses. These stresses generally induce large deformation contributing to the failure of the structure. In hygroscopic and thermal loading, the temperature and moisture content profiles through the shell thickness

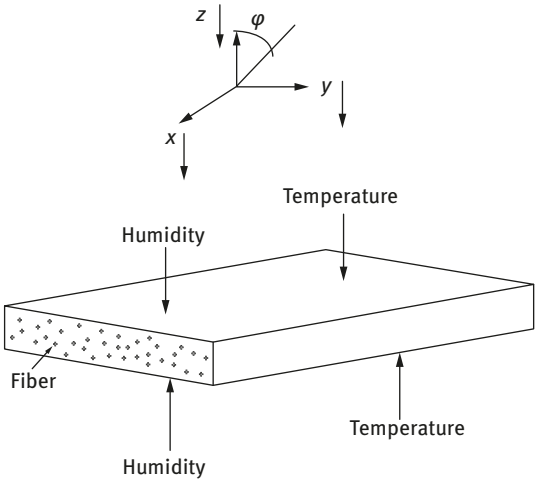

Figure 7.2: Composite plate exposed to hygrothermal environment.

can be assumed or calculated by solving the Fourier heat conduction equation and the Fick's moisture diffusion law, respectively [14]. The water absorption of composites was evaluated by absorbing the moisture uptaking defined by M_t according to the eq. (7.8).

$$M_t = \frac{W_t - W_0}{W_0} \text{x } 100 \ (\%) \tag{7.8}$$

where W_0 is the weight of specimen before its immersion in water and W_t is the weight of specimen at time t after its immersion in water. Generally, there is a strong absorption of water in the first two days and then, there is a slight mass stability. This comes down to the chemical composition of the fibers that contain cellulose that contains the –OH groups capable of bending to water in addition to the fibrous structure containing the capillary pores.

There are several parameters that depend on the way in which the material absorbs water, including the hygrometric rate, temperature, fiber fraction, nature of the fiber, porosity fraction, geometry of the reinforcement, and the type of matrix [4]. The presence of defects within the matrices such as pores, cracks, or microspace that form during the compounding process facilitated the transport of water by its diffusion inside the resin or by capillarity along the interfaces, which present some defects between fibers and matrix. Theoretically, the different categories of diffusion behavior (as Fickian or non-Fickian) can be distinguished by the shape of the sorption curve represented by eq. (7.9):

$$\frac{M_t}{M_m} = k.t^n \tag{7.9}$$

where M_t is the moisture uptake at time t, M_m is its maximum moisture uptake at an equilibrium state, k and n are the kinetic parameters in which n refers to the mode of the diffusion. It obeys the Fick's law when n is equal to 0.5. It obeys the Fick's law when n is equal to 0.5. When the value of n is between 0.5 and 1, the diffusion is submitting to non-Fickian law. When the value of $n > 1$, the diffusion is considered anomalous. For values M_t/M_m lower than 0.6, the initial part of the curve can be correlated by the following eq. (7.10).

$$\frac{M_t}{M_m} = \frac{4}{h}\sqrt{\frac{D.t}{\pi}} \tag{7.10}$$

where h denotes the specimen thickness and D is the diffusion coefficient. In the case where values M_t are less than 60% of the equilibrium value M_m, this diffusion coefficient is determined from the above eq. (7.10) and is given by eq. (7.11):

$$D = \frac{\pi}{(4M_m)^2}\left(\frac{M_t h}{\sqrt{t}}\right)^2 = \pi\left(\frac{k}{4M_m}\right)^2 \tag{7.11}$$

where h is the thickness of the specimen and k is the slope of the linear part of the curve $M_t = f\left(\sqrt{t}/h\right)$.

For the M_t/M_m upper than 0.6, which corresponds to the second half sorption, Shen and Springer [33] proposed the approximation eq. (7.12):

$$\frac{M_t}{M_m} = 1 - \exp\left[-7.3\left(\frac{D.t}{h^2}\right)^{\frac{3}{4}}\right] \tag{7.12}$$

Experimentally, to mount the effect of hygrothermal aging on the material, the specimens are placed into a covered box, which contains some water at its bottom, and then they are together put into an oven. The aging test was terminated until a large amount of defects appeared in the whole structure. In literature, the hygrothermal response has been studied for different types of material that are sensitive to changing hygrothermal environment conditions. Because of the variation in temperature and moisture concentrations that cause a change in material properties, the numerical results, in the case of laminated plates, show that the relationship between their hygrothermal response and the rise of temperature and/or moisture concentrations is no longer linear [34]. Additionally, Rui-Hua Hu et al. [7] found that the moisture absorption and the aging process can be effectively retarded by coating.

The main changes observed on the samples after hygrothermal aging are cited as follows: the color of the sample surface that gradually became white from light

yellow, the microstructure failure including pores and microcracks, which were found on the edge and propagated to the edge of the whole surface with increasing time and delamination of the material that finally took place, the increase in the thickness of the edge compared with the initial thickness, and some studies show that fibers and matrix are completely deboned by the end of aging [7, 35]. At the first stage of aging, the moisture uptake was mainly overpowered by capillary transport of natural fibers, flaws, and gaps between matrix and fibers. It is worth noting that the capillary effect of natural fibers allows moisture to be transported along the fibers.

7.2.4 Hygroelastic behavior of composite reinforced with natural fibers

Unlike metallic materials, composite materials can absorb moisturewhen they are subjected to a hygroscopic environment. Natural fiber swelling caused by moisture induces deformations in the composites. This behavior is called hygro-elastic. In order to foresee a possible damage occurring in the material during its manufacturing or its service life, it is necessary to know these internal stresses. Thus, their investigation seems very important.

As treated before in the hygroscopic behavior section, the swelling of the fibers caused by the moisture absorption leads to the appearance of microcracks in the matrix and therefore a debonding of the fiber and the matrix. Indeed, the large amount of hydroxyl group, which contained natural fibers makes it polar and hydrophilic [36]. On the other hand, the DSC curves also allow showing the presence of water molecules, in the first run, because of wide endotherm between 40 and 150 °C. Sharifah H. Aziz and Martin P. Ansell [23] reported that the presence of water in composite leads to the development of plasticity in the materials and then to poor wetting ability with the resin and weak interfacial bonding between the fiber and matrix, thus lowering their mechanical performances. In the same context, K. S. Meenalochani [9] reported that the flexural strength and the hardness of the composite reinforced with natural fibers decrease in wet conditions. In fact, when the composite reaches the saturation level of water uptake, the free and bound water remains there as a reservoir, which leads to softening of fibers and a weakening of fiber–matrix adhesion, which then resulted in the decrease in mechanical properties. In literature, there are some methods that focused on the calculation of the macroscopic stresses in each ply constituting the composite using finite element analyses or continuum Mechanics-based formalisms and others allow the study of internal stresses in the constituents of the ply using the classical elastic self-consistent scale transition model [37].

The knowledge of interactions between the physical and geometrical properties of fibers helps to determine the resulting material properties. When the fiber is

subjected to a uniform change in the moisture content χ, the stress-free hygro-expensive strain can be quantified as follows:

$$\varepsilon_h = \beta\chi \tag{7.13}$$

where β is the tensor of the effective hygro-expensive coefficients. In case no external load is applied, the average stress is zero, but internal stresses appear in the fiber network [38]. Moreover, if macroscopic mechanical stresses are not neglected in an elastic network, the total strain ε can be expressed as the sum of a hygro-expensive (ε_e) and an elastic part (ε_h) as shown in eq. (7.14):

$$\varepsilon = \varepsilon_h + \varepsilon_e \tag{7.14}$$

And the constitutive relation can be written as follows:

$$\sigma_{ij}(x,t) = a_{ijkl}\,\varepsilon_{kl} - \chi\beta_{ij} = a_{ijkl}\,\varepsilon_{kl} + \chi\theta_{ij} \tag{7.15}$$

where β is the hygrometric compressibility (Pa) expressed as $\beta_{ij} = a_{ijkl}\alpha_{kl}$ and $\theta_{ij} = -\beta_{ij}$.

Knowing that:

$$\overline{\overline{a}} = \begin{pmatrix} \alpha_{11} & \alpha_{12} & 0 \\ \alpha_{21} & \alpha_{22} & 0 \\ 0 & 0 & \alpha_{33} \end{pmatrix} z \tag{7.16}$$

where $\overline{\overline{a}}$ is the hygrometric expansion tensor, it is a dimensionless second-order tensor. $\chi(x,t)$ that denotes the mass fraction (a dimensionless mass ratio).

7.2.5 Thermoelastic behavior of composites embedded by natural fibers

Generally, the elastic properties of a material basically depend on temperature. Indeed, when thermal energy is applied to an elastic material it expands.This attitude of material is denoted by the thermoelastic behavior. Consequently, the nonuniform temperature in the composite structures generates thermal deformations and stresses and becomes important parameters in the structural design.

In literature, numerous study involving the thermomechanical behavior using classical or first-order theories. Indeed, Das and Rath [39] analyzed isotropic, moderately thick rectangular plates for a general temperature variation. They gave closed-form solutions for deflection and thermal stresses using Levy's method and presented results for maximum displacement because of constant thermal moment throughout the plate. On the other hand, Stavsky [40] developed a general thermoelastic theory for homogeneous anisotropic plates. Misra [41] studied the problems of a homogeneous orthotropic plate having two opposite edges that are simply

supported and two others are clamped, and subjected to a linear temperature variation through the thickness. Wu and Tauchert [42, 43] gave closed-form solutions using the double Fourier series for thermal deformations and stresses in rectangular symmetric orthotropic and antisymmetric cross-ply and angle-ply laminates based on Kirchhoff's assumptions. Another point to underline is that C. Campana [44] report that post-curing modifies the mechanical properties of the composite, especially at high temperature (150 °C). Indeed, when the post-curing temperature increases, both tensile strength and elongation at break decrease, whereas the stabilized modulus does not significantly vary.

In the case of the symmetric laminate, which especially consists of orthotropic layers (i.e., layers in which the principal material axes are parallel to the plate axes x, y, and z), equations governing the thermoelastic behavior according to the classical laminated plate theory for the force and moment resultants are expressed by the eqs. (7.17) and (7.18):

$$\begin{bmatrix} N_x \\ N_y \\ N_{xy} \end{bmatrix} = \begin{bmatrix} A_{11} & A_{12} & 0 \\ A_{21} & A_{22} & 0 \\ 0 & 0 & A_{66} \end{bmatrix} \begin{bmatrix} u_x^{'} \\ v_y^{'} \\ u_y^{'} + v_x^{'} \end{bmatrix} - \begin{bmatrix} N_x^T \\ N_y^T \\ 0 \end{bmatrix} \tag{7.17}$$

$$\begin{bmatrix} M_x \\ M_y \\ M_{xy} \end{bmatrix} = \begin{bmatrix} D_{11} & D_{12} & 0 \\ D_{21} & D_{22} & 0 \\ 0 & 0 & D_{66} \end{bmatrix} \begin{bmatrix} -w_{xx}^{'} \\ -w_{yy}^{'} \\ -2w_{xy}^{'} \end{bmatrix} - \begin{bmatrix} M_x^T \\ M_y^T \\ 0 \end{bmatrix} \tag{7.18}$$

where u, v, and w denote the displacement components of the middle surface of the plate in the x, y, and z directions, and a comma stands for differentiation with respect to the subscript. The extensional and bending stiffnesses A_{ij} and D_{ij} for the laminate are related to the reduced stiffness coefficients $(Q_{ij})_k$ for the individual layers $k = 1, 2, \ldots, N$

$$\left(A_{ij},\ D_{ij}\right) = \sum_{k=1}^{N} \int_{z_{k-1}}^{z_k} \left(1, z^2\right) \left(Q_{ij}\right)_k dz \tag{7.19}$$

In addition, eqs. (7.17) and (7.18) are the thermal-force and thermal-moment matrices, given as follows:

$$\begin{bmatrix} N_x^T \\ N_y^T \\ 0 \end{bmatrix} = \sum_{k=1}^{N} \int_{z_{k-1}}^{z_k} \begin{bmatrix} Q_{11} & Q_{12} & 0 \\ Q_{21} & Q_{22} & 0 \\ 0 & 0 & Q_{66} \end{bmatrix}_k \begin{bmatrix} \alpha_x \\ \alpha_y \\ 0 \end{bmatrix}_k T dz \tag{7.20}$$

$$\begin{bmatrix} M_x^T \\ M_y^T \\ 0 \end{bmatrix} = \sum_{k=1}^{N} \int_{z_{k-1}}^{z_k} \begin{bmatrix} Q_{11} & Q_{12} & 0 \\ Q_{21} & Q_{22} & 0 \\ 0 & 0 & Q_{66} \end{bmatrix}_k \begin{bmatrix} \alpha_x \\ \alpha_y \\ 0 \end{bmatrix}_k Tz \; dz \tag{7.21}$$

where T stands for the temperature rise in the laminate, and $(\alpha_x)_k$ and $(\alpha_y)_k$ represent the coefficients of linear thermal expansion for the layer k. The displacement equations of equilibrium, obtained by substituting eqs. (7.17) and (7.18) into the equations for force and moment equilibrium, become:

$$A_{11}u_x' + A_{66}u_y' + (A_{12} + A_{66})v_{xy}' - N_{x,x}^T = 0 \tag{7.22}$$

$$(A_{12} + A_{66})u_{xy}' + A_{66}v_{xx}' + A_{22}v_{yy}' - N_{y,y}^T = 0 \tag{7.23}$$

$$D_{11}w_{xxxx}' + 2(D_{12} + 2D_{66})w_{xxyy}' + D_{22}w_{yyyy}' + M_{x,xx}^T + M_{y,yy}^T = q \tag{7.24}$$

where q denotes the transverse load applied to the plate.

One should notice that contrary to the hygro-elastic model, where the moisture content increment is often substantially different in the fiber and the matrix, the temperature increment delta T is generally considered homogeneous at every scale.

7.2.6 Hygrothermoelastic behavior of composite embedded by natural fibers

The hygrothermoelastic behavior consists of studying the response of the composite material under mechanical loading after exposure to hygroscopic and thermal environment. In literatures, numerous studies showed the effect of moisture and temperature on the response of the composite material. However, the effects of the continuous alteration of the two conditions on the composite reinforced by natural fibers, especially concurrently with mechanical loading, have been less explored.

Generally, some different studies show that the elastic moduli and the strength of composite laminates degrade with an elevation of both temperature and moisture concentrations [34, 45]. Indeed, S. Brischetto [46] proves that the effect of hygroscopic load modifies the bending response of multilayered plate composites by increasing the maximum deflection and the interface discontinuities of in-plane stresses. Moreover, he found that the linear temperature and moisture content profiles are possibly used only for thin plates, while the calculated thermal and hygroscopic profiles could be mandatorily used for thick multilayered structures. In the same perspective, B. F. Boukhoulda et al. [47] show that the hygrometric absorption and temperature variations weaken the mechanical characteristics of the material. To illustrate that behavior, various tests were achieved on dry and saturated samples. They have reported that when the temperature increases, the mechanical properties including longitudinal compressive strength, interlaminar shear

strength, and the tensile strength decrease distinctly in the dry materials. When the temperature and humidity are acting simultaneously, the influence of the ambient humidity is noted. Thus, the degradation of the features of the matrix is because of the distortions in the thermal and hygroscopic expansion. Shen [48] analytically investigated the effects of hygrothermal conditions on the buckling and post-buckling of laminated cylindrical shells based on Reddy's higher-order theory; the results show that the buckling load and post-buckling strength decrease and especially the geometrical imperfection sensitivity becomes slightly weaker with increasing moisture concentration and temperature, so the hygrothermal environment has a significant effect under the combined loading case.

The total strains of an elastic material subjected to the hygrothermoelastic expansions are equivalent to their hygrothermal strains, which are added to their mechanical strains induced by the residual stresses. In other words, strain components ϵ are expressed as a summation of the elastic part ϵ^e, the hygroscopic part ϵ^h and the thermal contribution ϵ^T for each kth lamina. It is assumed that the thermal deformation and moisture deformation are uncoupled. Therefore, the total strains in the kth layer are expressed as follows:

$$\epsilon_k = \epsilon_k^e + \epsilon_k^h + \epsilon_k^T \tag{7.25}$$

$$\{\epsilon\}_k = [S]_k\{\sigma\}_k + \{\alpha\}_k \Delta m + \{\gamma\}_k \Delta T \tag{7.26}$$

$$[A]\{\in\}_k = [A][S]_k\{\sigma\}_k + [A]\{\alpha\}_k \Delta m + [A]\{\gamma\}_k \Delta T \tag{7.27}$$

$$\{\sigma\}_k = [A]\{\epsilon\}_k - [A]\{\alpha\}_k \Delta m - [A]\{\gamma\}_k \Delta T \tag{7.28}$$

Because

$$[A][S] = I \tag{7.29}$$

where $[S]$ is the compliance matrix, $[A]$ is the elasticity matrix, k denotes the layer number, ΔT and Δm are the temperature and moisture concentration rise, respectively, $\{\alpha\}$ and $\{\gamma\}$ are the moisture and thermal expansion coefficient vector, respectively. They are grouped in a vector of (6 × 1) dimension for kth lamina and are verified by eqs. (7.30) and (7.31), respectively:

$$\{\alpha\}_k = \begin{pmatrix} \alpha_{11} \\ \alpha_{22} \\ \alpha_{33} \\ 0 \\ 0 \\ \alpha_{12} \end{pmatrix}_k \tag{7.30}$$

$$\{\gamma\}_k = \begin{pmatrix} \gamma_{11} \\ \gamma_{22} \\ \gamma_{33} \\ 0 \\ 0 \\ \gamma_{12} \end{pmatrix}_k \tag{7.31}$$

Taking $\{\beta\} = [A]\{\alpha\}$ which is the hygroscopic compressibility (expressed in Pascal) and $\{\delta\} = [A]\{\gamma\}$ which is the thermal compressibility (expressed in Pascal/Kelvin), the constitution relation becomes:

$$(\sigma)_k = [A]\{\varepsilon\}_k - \{\beta\}_k \Delta m - \{\delta\}_k \Delta T \tag{7.32}$$

Using the Hooke's law, the resulting stresses are given by eq. (7.33).

$$\{\sigma\}_k = [Q]_k \{\epsilon\}_k \tag{7.33}$$

where $[Q]$ stands for the transformed reduced stiffness of laminate, which is a 6×6 matrix, and it is expressed in the kth layer as follows:

$$[Q]_k = \begin{bmatrix} Q_{11} & Q_{12} & Q_{13} & 0 & 0 & Q_{16} \\ Q_{12} & Q_{22} & Q_{23} & 0 & 0 & Q_{26} \\ Q_{13} & Q_{23} & Q_{33} & 0 & 0 & Q_{36} \\ 0 & 00 & 0 & Q_{44} & Q_{45} & 0 \\ 0 & 0 & 0 & Q_{45} & Q_{55} & 0 \\ Q_{16} & Q_{26} & Q_{36} & 0 & 0 & Q_{66} \end{bmatrix}_k \tag{7.34}$$

On the other hand, the hygrothermal aging had a huge influence on mechanical properties of the composite embedded by natural fibers, especially Young's modulus and tensile strength. Indeed, under temperature effect, the natural fibers undergo a degradation process that allows water to be more absorbed by the fibers leading to a dramatical loss of tensile properties [6]. In addition, the decrease in these composite properties could be explained by a reorientation of fiber microfibrils and the plasticizer effect of water on the matrix [4]. Moreover, the moisture absorption is influenced by the chemical modifications of fiber, which allows a decrease in water uptake that finally leads to an increase in mechanical properties as compared with untreated fiber composites [6].

7.3 Application

In this section, consider a stratified material with a periodic structure according to the third direction (Figure 7.3), and assume that the layers are homogeneous elastic, monoclinic ($\vec{e_3}$), and perfectly adhered together. The mathematical equations used in hygrothermoelastic behavior section are applied and detailed below.

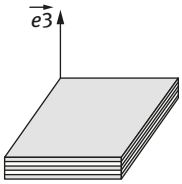

Figure 7.3: Laminated periodic structure.

The elastic matrix of the kth layer of the laminate is expressed as follows:

$$[A]_k = \begin{pmatrix} a_{1111} & a_{1122} & a_{1133} & 0 & 0 & a_{1112} \\ & a_{2222} & a_{2233} & 0 & 0 & a_{2212} \\ & & a_{3333} & 0 & 0 & a_{3312} \\ & & & a_{2323} & a_{2313} & 0 \\ & Sym & & & a_{1313} & 0 \\ & & & & & a_{1212} \end{pmatrix}_k \tag{7.35}$$

The fact that

$$\{\alpha\}_k = \begin{pmatrix} \alpha_{11} \\ \alpha_{22} \\ \alpha_{33} \\ 0 \\ 0 \\ \alpha_{12} \end{pmatrix}_k \tag{7.36}$$

Thus,

$$\{\beta\}_k = \begin{pmatrix} a_{1111}\alpha_{11} + a_{1122}\alpha_{22} + a_{1133}\alpha_{33} + a_{1112}\alpha_{12} \\ a_{1122}\alpha_{11} + a_{2222}\alpha_{22} + a_{2233}\alpha_{33} + a_{2212}\alpha_{12} \\ a_{1133}\alpha_{11} + a_{2233}\alpha_{22} + a_{3333}\alpha_{33} + a_{3312}\alpha_{12} \\ 0 \\ 0 \\ a_{1112}\alpha_{11} + a_{2212}\alpha_{11} + a_{3312}\alpha_{33} + a_{1212}\alpha_{12} \end{pmatrix}_k \tag{7.37}$$

And

$$\{\gamma\}_k = \begin{pmatrix} \gamma_{11} \\ \gamma_{22} \\ \gamma_{33} \\ 0 \\ 0 \\ \gamma_{12} \end{pmatrix}_k \tag{7.38}$$

Given

$$\{\delta\}_k = \begin{pmatrix} a_{1111}\gamma_{11} + a_{1122}\gamma_{22} + a_{1133}\gamma_{33} + a_{1112}\gamma_{12} \\ a_{1122}\gamma_{11} + a_{2222}\gamma_{22} + a_{2233}\gamma_{33} + a_{2212}\gamma_{12} \\ a_{1133}\gamma_{11} + a_{2233}\gamma_{22} + a_{3333}\gamma_{33} + a_{3312}\gamma_{12} \\ 0 \\ 0 \\ a_{1112}\gamma_{11} + a_{2212}\gamma_{11} + a_{3312}\gamma_{33} + a_{1212}\gamma_{12} \end{pmatrix}_k \tag{7.39}$$

The constructive relation could be written as follows:

$$\begin{pmatrix} \sigma_{11} \\ \sigma_{22} \\ \sigma_{33} \\ \sigma_{23} \\ \sigma_{13} \\ \sigma_{12} \end{pmatrix}_k = \begin{pmatrix} \alpha_{1111} & \alpha_{1122} & \alpha_{1133} & 0 & 0 & \alpha_{1112} & -\beta_{11} & -\delta_{11} \\ \alpha_{1122} & \alpha_{2222} & \alpha_{2233} & 0 & 0 & \alpha_{2212} & -\beta_{22} & -\delta_{22} \\ \alpha_{1133} & \alpha_{2233} & \alpha_{3333} & 0 & 0 & \alpha_{3312} & -\beta_{33} & -\delta_{33} \\ 0 & 0 & 0 & \alpha_{2323} & \alpha_{2313} & 0 & 0 & 0 \\ 0 & 0 & 0 & \alpha_{2313} & \alpha_{1313} & 0 & 0 & 0 \\ \alpha_{1112} & \alpha_{2212} & \alpha_{3312} & 0 & 0 & \alpha_{1212} & -\beta_{12} & -\delta_{12} \end{pmatrix} \begin{pmatrix} \varepsilon_{11} \\ \varepsilon_{22} \\ \varepsilon_{33} \\ 2\varepsilon_{23} \\ 2\varepsilon_{13} \\ 2\varepsilon_{12} \\ \Delta m \\ \Delta T \end{pmatrix}_k \tag{7.40}$$

The homogenized constitutive relation is given as follows:

$$\begin{pmatrix} \sigma_{11} \\ \sigma_{22} \\ \sigma_{12} \\ \sigma_{13} \\ \sigma_{23} \\ \sigma_{33} \end{pmatrix}_k = K \begin{pmatrix} \sigma_{13} \\ \sigma_{23} \\ \sigma_{33} \\ \in_{11} \\ \in_{22} \\ \in_{12} \\ \Delta m \\ \Delta T \end{pmatrix}_k \tag{7.41}$$

where K is a tensor to be determined.
Having:

$$\sigma_{11} = a_{1111}\varepsilon_{11} + a_{1122}\varepsilon_{22} + a_{1133}\varepsilon_{33} + 2a_{1112}\varepsilon_{12} - \beta_{11}\Delta m - \delta_{11}\Delta T \tag{7.42}$$

$$\sigma_{22} = a_{1122}\varepsilon_{11} + a_{2222}\varepsilon_{22} + a_{2233}\varepsilon_{33} + 2a_{2212}\varepsilon_{12} - \beta_{22}\Delta m - \delta_{22}\Delta T \tag{7.43}$$

$$\sigma_{12} = a_{1112}\varepsilon_{11} + a_{2212}\varepsilon_{22} + a_{3312}\varepsilon_{33} + 2a_{1212}\varepsilon_{12} - \beta_{12}\Delta m - \delta_{12}\Delta T \tag{7.44}$$

$$\sigma_{33} = a_{1133}\varepsilon_{11} + a_{2233}\varepsilon_{22} + a_{3333}\varepsilon_{33} + 2a_{3312}\varepsilon_{12} - \beta_{33}\Delta m - \delta_{33}\Delta T \tag{7.45}$$

$$\sigma_{23} = 2a_{2323}\varepsilon_{23} + 2a_{2313}\varepsilon_{13} \tag{7.46}$$

$$\sigma_{13} = 2a_{2313}\varepsilon_{23} + 2a_{1313}\varepsilon_{13} \tag{7.47}$$

$$\Delta = 4\left(a_{2323}a_{1313} - a_{2313}^2\right) \tag{7.48}$$

Thus, from eq (7.45), the obtained relation is expressed as follows:

$$\varepsilon_{33} = \frac{1}{a_{3333}}\left(\sigma_{33} - a_{1133}\varepsilon_{11} - a_{2233}\varepsilon_{22} - 2a_{3312}\varepsilon_{12} + \beta_{33}\Delta m + \delta_{33}\Delta T\right) \tag{7.49}$$

And

$$\varepsilon_{23} = 2\frac{a_{1313}}{\Delta}\sigma_{23} - 2\frac{a_{2313}}{\Delta}\sigma_{13} \tag{7.50}$$

$$\varepsilon_{13} = -2\frac{a_{2313}}{\Delta}\sigma_{23} + 2\frac{a_{2323}}{\Delta}\sigma_{13} \tag{7.51}$$

By substituting eq. (7.49) in eqs. (7.42), (7.43), and (7.44), the result is as follows:

$$\sigma_{11} = \left(a_{1111} - \frac{a_{1133}^2}{a_{3333}}\right)\varepsilon_{11} + \left(a_{1122} - \frac{a_{1133}}{a_{3333}}a_{2233}\right)\varepsilon_{22} + \left(\frac{a_{1133}}{a_{3333}}\right)\sigma_{33} + 2\left(a_{1112} - \frac{a_{1133}}{a_{3333}}a_{3312}\right)\varepsilon_{12} + \Delta m\left(\frac{a_{1133}}{a_{3333}}\beta_{33} - \beta_{11}\right) + \Delta T\left(\frac{a_{1133}}{a_{3333}}\delta_{33} - \delta_{11}\right) \tag{7.52}$$

$$\sigma_{22} = \left(a_{1122} - \frac{a_{2233}}{a_{3333}}a_{1133}\right)\varepsilon_{11} + \left(a_{2222} - \frac{a_{2233}^2}{a_{3333}}\right)\varepsilon_{22} + \left(\frac{a_{2233}}{a_{3333}}\right)\sigma_{33} + 2\left(a_{1212} - \frac{a_{3312}^2}{a_{3333}}\right)\varepsilon_{12} + \Delta m\left(\frac{a_{2233}}{a_{3333}}\beta_{33} - \beta_{22}\right) + \Delta T\left(\frac{a_{2233}}{a_{3333}}\beta_{33} - \beta_{22}\right) \tag{7.53}$$

$$\sigma_{12} = \left(a_{1112} - \frac{a_{3312}}{a_{3333}}a_{1133}\right)\varepsilon_{11} + \left(a_{2212} - \frac{a_{3312}}{a_{3333}}a_{2233}\right)\varepsilon_{22} + \left(\frac{a_{3312}}{a_{3333}}\right)\sigma_{33} + 2\left(a_{1212} - \frac{a_{3312}{}^2}{a_{3333}}\right)\varepsilon_{12} + \Delta m\left(\frac{a_{3312}}{a_{3333}}\beta_{33} - \beta_{12}\right) + \Delta T\left(\frac{a_{3312}}{a_{3333}}\delta_{33} - \delta_{12}\right) \tag{7.54}$$

$$\varepsilon_{33} = -\frac{a_{1133}}{a_{3333}}\varepsilon_{11} - \frac{a_{2233}}{a_{3333}}\varepsilon_{22} - 2\frac{a_{3312}}{a_{3333}}\varepsilon_{12} + \frac{1}{a_{3333}}\sigma_{33} + \frac{\beta_{33}}{a_{3333}}\Delta m + \frac{\delta_{33}}{a_{3333}}\Delta T \tag{7.55}$$

Therefore, the *kijkl* are expressed as follows:

$$k_{1133} = \frac{a_{1133}}{a_{3333}};\quad k_{1111} = a_{1111} - \frac{a_{1133}{}^2}{a_{3333}};\quad k_{1122} = a_{1122} - \frac{a_{1133}}{a_{3333}}a_{2233}$$

$$k_{2233} = \frac{a_{2233}}{a_{3333}};\quad k_{1112} = 2\left(a_{1112} - \frac{a_{1133}}{a_{3333}}a_{3312}\right);\quad k_{2211} = a_{1122} - \frac{a_{2233}}{a_{3333}}a_{1133}$$

$$k_{1233} = \frac{a_{3312}}{a_{3333}};\quad k_{2222} = a_{2222} - \frac{a_{2233}{}^2}{a_{3333}};\quad k_{2212} = 2\left(a_{1212} - \frac{a_{3312}{}^2}{a_{3333}}\right)$$

$$k_{1233} = \frac{a_{3312}}{a_{3333}};\quad k_{1211} = a_{1112} - \frac{a_{3312}}{a_{3333}}a_{1133};\quad k_{1222} = a_{2212} - \frac{a_{3312}}{a_{3333}}a_{2233};\quad k_{3333} = \frac{1}{a_{3333}};$$

$$k_{1212} = 2\left(a_{1212} - \frac{a_{3312}{}^2}{a_{3333}}\right);\quad k_{1313} = 2\frac{a_{2323}}{\Delta}$$

$$k_{3311} = -\frac{a_{1133}}{a_{3333}};\quad k_{1323} = -2\frac{a_{2313}}{\Delta};\quad k_{3312} = -\frac{a_{3312}}{a_{3333}}$$

$$k_{2313} = -2\frac{a_{2313}}{\Delta};\quad k_{3322} = -\frac{a_{2233}}{a_{3333}};\quad k_{2323} = 2\frac{a_{1313}}{\Delta}$$

Thus, it is shown that *kijkl* coefficients are expressed according to elasticity coefficients, in which the hygroscopic (*kijm*) and thermal (*kijt*) terms are added to the matrix *K* as follows:

$$\begin{cases} k_{ijm} = \frac{a_{ij33}}{a_{3333}}\beta_{33} - \beta_{ij} \\ k_{33m} = \frac{\beta_{33}}{a_{3333}} \end{cases} (i,j)\epsilon\{1,2\}$$

And

$$\begin{cases} k_{ijt} = \frac{a_{ij33}}{a_{3333}}\delta_{33} - \delta_{ij} \\ k_{ijt} = \frac{\delta_{33}}{a_{3333}} \end{cases} (i,j)\epsilon\{1,2\}$$

Accordingly, the matrix *K* is expressed as follows:

$$[K]_k = \begin{pmatrix} 0 & 0 & k_{1133} & k_{1111} & k_{1122} & k_{1112} & k_{11m} & k_{11t} \\ 0 & 0 & k_{2233} & k_{2211} & k_{2222} & k_{2212} & k_{22m} & k_{22t} \\ 0 & 0 & k_{1233} & k_{1211} & k_{1222} & k_{1212} & k_{12m} & k_{12t} \\ k_{1313} & k_{1323} & 0 & 0 & 0 & 0 & 0 & 0 \\ k_{2313} & k_{2323} & 0 & 0 & 0 & 0 & 0 & 0 \\ 0 & 0 & k_{3333} & k_{3311} & k_{3322} & k_{3312} & k_{33m} & k_{33t} \end{pmatrix}_k$$

The same previously detailed technique is used in the case of homogenized coefficients (*qijkl*) [49] and the results are as follows:

$$q_{1111} = \langle k_{1111} \rangle - \frac{\langle k_{1133} \rangle}{\langle k_{3333} \rangle} \langle k_{3311} \rangle; \quad q_{1233} = \frac{\langle k_{1233} \rangle}{\langle k_{3333} \rangle}; \quad q_{1122} = \langle k_{1122} \rangle - \frac{\langle k_{1133} \rangle}{\langle k_{3333} \rangle} \langle k_{3322} \rangle$$

$$q_{1212} = \langle k_{1212} \rangle - \frac{\langle k_{1233} \rangle}{\langle k_{3333} \rangle} \langle k_{3312} \rangle; \quad q_{1133} = \frac{\langle k_{1133} \rangle}{\langle k_{3333} \rangle}; \quad q_{1112} = \langle k_{1112} \rangle - \frac{\langle k_{1133} \rangle}{\langle k_{3333} \rangle} \langle k_{3312} \rangle$$

$$q_{2211} = \langle k_{2211} \rangle - \frac{\langle k_{2233} \rangle}{\langle k_{3333} \rangle} \langle k_{3311} \rangle; \quad q_{3311} = -\frac{\langle k_{3311} \rangle}{\langle k_{3333} \rangle}; \quad q_{3322} = -\frac{\langle k_{3322} \rangle}{\langle k_{3333} \rangle}$$

$$q_{2222} = \langle k_{2222} \rangle - \frac{\langle k_{2233} \rangle}{\langle k_{3333} \rangle} \langle k_{3322} \rangle; \quad q_{3312} = \frac{\langle k_{3312} \rangle}{\langle k_{3333} \rangle}; \quad q_{3333} = \frac{1}{\langle k_{3333} \rangle}$$

$$q_{2212} = \langle k_{2212} \rangle - \frac{\langle k_{2233} \rangle}{\langle k_{3333} \rangle} \langle k_{3312} \rangle; \quad q_{2233} = \frac{\langle k_{2233} \rangle}{\langle k_{3333} \rangle}; \quad q_{1313} = \frac{\langle k_{2323} \rangle}{D}$$

$$q_{1211} = \langle k_{1211} \rangle - \frac{\langle k_{1233} \rangle}{\langle k_{3333} \rangle} \langle k_{3311} \rangle; \quad q_{1323} = -\frac{\langle k_{1323} \rangle}{D}; \quad q_{2313} = -\frac{\langle k_{2313} \rangle}{D}$$

$$q_{1222} = \langle k_{1222} \rangle - \frac{\langle k_{1233} \rangle}{\langle k_{3333} \rangle} \langle k_{3322} \rangle; \quad q_{2323} = \frac{\langle k_{1313} \rangle}{D}$$

The homogenized coefficients are expressed in the same form as for the elastic behavior, with 7th and 8th columns, which are represented respectively; the hygroscopic and thermal behavior of the material and their terms are determined using the following relationships:

$$\begin{cases} q_{ijm} = \langle k_{ijm} \rangle - \frac{\langle k_{ij33} \rangle}{\langle k_{3333} \rangle} \langle k_{33m} \rangle \\ q_{33m} = -\frac{\langle k_{33m} \rangle}{\langle k_{3333} \rangle} \end{cases} (i,j) \epsilon \{1,2\}$$

$$\begin{cases} q_{ijt} = \langle k_{ijt} \rangle - \frac{\langle k_{ij33} \rangle}{\langle k_{3333} \rangle} \langle k_{33t} \rangle \\ q_{33t} = -\frac{\langle k_{33t} \rangle}{\langle k_{3333} \rangle} \end{cases} (i,j) \epsilon \{1,2\}$$

Finally, the *Q* matrix is expressed as follows:

$$[Q]_k = \begin{pmatrix} q_{1111} & q_{1122} & q_{1133} & 0 & 0 & q_{1112} & q_{11m} & q_{11t} \\ q_{1122} & q_{2222} & q_{2233} & 0 & 0 & q_{2212} & q_{22m} & q_{22t} \\ q_{1133} & q_{2233} & q_{3333} & 0 & 0 & q_{3312} & q_{33m} & q_{33t} \\ 0 & 0 & 0 & q_{2323} & q_{2313} & 0 & 0 & 0 \\ 0 & 0 & 0 & q_{2313} & q_{1313} & 0 & 0 & 0 \\ q_{1112} & q_{2212} & q_{3312} & 0 & 0 & q_{1212} & q_{12m} & q_{12t} \end{pmatrix}_k$$

7.4 Conclusion and perspective

Through this chapter, the hygrothermoelastic behavior of composit-based natural fibers is considered as an important parameter to take into account in the design of the composite. To do so, the protocols to accelerated aging tests representing extremely severe loading conditions will be established. This enables to show and quantify the processes of physical or chemical degradation (plasticization and water absorption) and to evaluate its durability. The use of natural fibers as a reinforcement exacerbated the strong ability to uptake moisture because of their hydrophilic character that allows degrading the mechanical properties of the final composites. In order to reduce the absorption of various natural fibers, several efforts are made for this purpose. Chemical treatments including mercerization, acetylation, etherification, and benzoylation are denoted as the main solution. Regarding the modeling, the effect of temperature compared to concentration gradient of water is usually neglected in the models since the heat diffusion rate is considerably higher than moisture diffusion.

Thus, the approach to overcome the high capacity of natural fibers to absorb moisture will be increasingly highlighted. If this problem is solved, natural fiber-based composites will be a better alternative to composite materials and their scope will be expanded.

Acknowledgments: This work was supported by MAScIR; Moroccan Foundation for Advanced Science, Innovation and Research, MESRSFC; and CNRST, Morocco grant no. 1970/15.

References

[1] Ouarhim, W, Essabir, H, Bensalah, M-O, Rodrigue, D, Bouhfid, R, & Qaiss, AEK. Production and characterization of high density polyethylene reinforced by eucalyptus capsule fibers. J. Bionic Eng., 2018, 15, 558–566.

[2] Essabir, H, Bensalah, MO, Rodrigue, D, Bouhfid, R, & Qaiss, AEK. Biocomposites based on argan nut shell and a polymer matrix: effect of filler content and coupling agent. Carbohydr. Polym., 2016, 143, 70–83.
[3] Brischetto, S. Hygrothermal loading effects in bending analysis of multilayered composite plates. CMES. 2012, 88, 367–417.
[4] Scida, D, Assarar, M, Poilâne, C, & Ayad, R. Influence of hygrothermal ageing on the damage mechanisms of flax-fibre reinforced epoxy composite. Compos. Part B, 2013, 48, 51–58.
[5] Kundu, CK, & Han, J. Nonlinear buckling analysis of hygrothermoelastic composite shell panels using finite element method. Compos. Part B, 2009, 40, 313–328.
[6] Abdul Khalil, HPS, Rozman, HD, Ahmad, MN, & Ismail, H. Acetylated plant-fiber-reinforced polyester composites: a study of mechanical, hygrothermal, and aging characteristics. Polym. Plast. Technol. Eng., 2000, 39, 757–781.
[7] Hu, R, Sun, M, & Lim, J. Moisture absorption, tensile strength and microstructure evolution of short jute fiber/polylactide composite in hygrothermal environment. Mater. Des., 2010, 31, 3167–3173.
[8] Célino, A, Fréour, S, Jacquemin, F, & Casari, P. The hygroscopic behavior of plant fibers: a review. Front Chem., 2014, 1, 1–12.
[9] Meenalochani, KS, & Vrb, G. A review on water absorption behavior and its effect on mechanical properties of natural fibre reinforced composites. Int. J. Innov. Res. Adv. Eng., 2017, 4, 143–147.
[10] Dhakal, HN, Zhang, ZY, & Richardson, MOW. Effect of water absorption on the mechanical properties of hemp fibre reinforced unsaturated polyester composites. Compos. Sci. Technol., 2007, 67, 1674–1683.
[11] Bismarck, A, Aranberri-Askargorta, I, Springer, J, Lampke, T, Wielage, B, Stamboulis, A, et al. Surface characterization of flax, hemp and cellulose fibers; Surface properties and the water uptake behavior. Polym. Compos., 2002, 23, 872–894.
[12] Chow, CPL, Xing, XS, & Li, RKY. Moisture absorption studies of sisal fibre reinforced polypropylene composites. Compos. Sci. Technol., 2007, 67, 306–313.
[13] Célino, A, Gonçalves, O, Jacquemin, F, & Fréour, S. Utilisation de la spectrométrie infrarouge pour une quantification rapide du taux d'humidité dans des fibres végétales. Rev Des Compos Des Matériaux Avancés, 2014, 24, 81–95.
[14] Hatakeyama, H, & Hatakeyama, T. Interaction between water and hydrophilic polymers l. Thermochim Acta., 1998, 308, 3–22.
[15] Jedidi, J, Jacquemin, F, & Vautrin, A. Accelerated hygrothermal cyclical tests for carbon / epoxy laminates. Compos. Part A Appl. Sci. Manuf., 2006, 37, 636–645.
[16] Autran, M, Pauliard, R, Gautier, L, Mortaigne, B, Mazeas, F, & Davies, P. Influence of mechanical stresses on the hydrolytic aging of standard and low styrene unsaturated polyester. Appl. Polym. Sci., 2002, 84, 2185–2195.
[17] Popineau, S, Rondeau-Mouro, C, Sulpice-Gaillet, C, & Shanahan, MER. Free/bound water absorption in an epoxy adhesive. Polymer (Guildf), 2005, 46, 10733–10740.
[18] Loh, WK, Crocombe, AD, Wahab, MMA, & Ashcroft, IA. Modelling anomalous moisture uptake, swelling and thermal characteristics of a rubber toughened epoxy adhesive. Int. J. Adhes. Adhes., 2005, 25, 1–12.
[19] Crank, J. The Mathematics Of Diffusion, Second edi, Clarendon Press, Oxford, 1975.
[20] Célino, A, Fréour, S, Jacquemin, F, & Casari, P. Characterization and modeling of the moisture diffusion behavior of natural fibers. Appl. Polym. Sci., 2013, 130, 297–306.
[21] Avérous, L, & Le Digabel, F. Properties of biocomposites based on lignocellulosic fillers. Carbohydr. Polym., 2006, 66, 480–493.

[22] Khare, RK, Kant, T, & Garg, AK. Closed-form thermo-mechanical solutions of higher-order theories of cross-ply laminated shallow shells. Compos. Struct., 2003, 59, 313–340.
[23] Aziz, SH, & Ansell, MP. The effect of alkalization and fibre alignment on the mechanical and thermal properties of kenaf and hemp bast fibre composites: Part 1 – polyester resin matrix. Compos. Sci. Technol., 2004, 64, 1219–1230.
[24] Monteiro, SN, Calado, V, Rodriguez, RJS, & Margem, FM. Thermogravimetric stability of polymer composites reinforced with less common lignocellulosic fibers – An overview. J. prot. Mater. Res. Technol. 2012, 1, 117–126.
[25] Sreekala, MS, Kumaran, MG, & Thomas, S. Oil palm fibers: morphology, chemical composition, surface modification, and mechanical properties. J. Appl. Polym. Sci., 1997, 66, 821–835.
[26] Li, X, Tabil, LG, & Panigrahi, S. Chemical treatments of natural fiber for use in natural fiber-reinforced composites: A review. J. Polym. Environ., 2007, 15, 25–33.
[27] Singh, TJ, & Samanta, S. Characterization of natural fiber reinforced omposites-bamboo and sisal: a Review. IJRET Int. J. Res. Eng. Technol., 2014, 3, 187–195.
[28] Jeencham, R, Suppakarn, N, & Jarukumjorn, K. Effect of flame retardants on flame retardant, mechanical, and thermal properties of sisal fiber/polypropylene composites. Compos. Part B Eng., 2014, 56, 249–253.
[29] Kalaprasad, G, Pradeep, P, Mathew, G, Pavithran, C, & Thomas, S. Thermal conductivity and thermal diffusivity analyses of low-density polyethylene composites reinforced with sisal, glass and intimately mixed sisal/glass fibres. Compos. Sci. Technol., 2000, 60, 2967–2977.
[30] Ouarhim, W, Essabir, H, Bensalah, M-O, Zari, N, Bouhfid, R, & Qaiss, A el kacem. Structural laminated hybrid composites based on raffia and glass fibers: effect of alkali treatment, mechanical and thermal properties. Compos. Part B Eng., 2018, 154, 128–137.
[31] Essabir, H, Bensalah, MO, Rodrigue, D, Bouhfid, R, & Qaiss, A. Structural, mechanical and thermal properties of bio-based hybrid composites from waste coir residues: fibers and shell particles. Mech. Mater., 2016, 93, 134–144.
[32] Oksman, K, Skrifvars, M, & Selin, JF. Natural fibres as reinforcement in polylactic acid (PLA) composites. Compos. Sci. Technol., 2003, 63, 1317–1324.
[33] Shen, C-H., Springer, GS. Moisture absorption and desorption of composite materials. Compos. Mater., 1976, 10, 2–20.
[34] Lo, SH, Zhen, W, Cheung, YK, & Wanji, C. Hygrothermal effects on multilayered composite plates using a refined higher order theory. Compos. Struct., 2010, 92, 633–646.
[35] Dhakal, H, Zhang, Z, & Richardson, M. Effect of water absorption on the mechanical properties of hemp fibre reinforced unsaturated polyester composites. Compos. Sci. Technol., 2007, 67, 1674–1683.
[36] Yahaya, R, Sapuan, SM, Jawaid, M, Leman, Z, & Zainudin, ES. Water absorption behaviour and impact strength of Kenaf-Kevlar reinforced epoxy hybrid composites. Adv. Compos. Lett., 2016, 25, 98–102.
[37] Jacquemin, F, Fréour, S, Guillén, R, Jacquemin, F, Fréour, S, Guillén, R, et al. A hygro-elastic self-consistent model for fiber-reinforced composites. J. Reinf. Plast. Compos., 2017, 24, 485–502.
[38] Bosco, E, Peerlings, RHJ, & Geers, MGD. Predicting hygro-elastic properties of paper sheets based on an idealized model of the underlying fibrous network. Int. J. Solids Struct., 2015, 56–57, 43–52.
[39] Das, YC, & Rath, BK. Thermal bending of moderately thick rectangular rlates. AIAA J., 1972, 10, 1349–1351.
[40] Stavsky, Y. Thermoelasticity of heterogeneous aeolotropic plates. J. Eng. Mech. Div., 1963, 89, 89–106.

[41] Misra, J. C. On the bending of a heated rectangular anisotropic plate with two opposite edges simply supported and two others built in, due to different temperature distributions on the plane surface. Bull Calcutta Math. Soc., 1971, 63, 183–190.
[42] Wu, CH, & Tauchert, TR. Thermoelastic analysis of laminated plates. I: Symmetric Specially Orthotropic Laminates. J. Therm. Stress, 1980, 3, 247–259.
[43] Wu, CH, & Tauchert, TR. Thermoelastic analysts of laminated plates. 2: antisymmetric cross-ply and angle-ply laminates. J. Therm. Stress, 1980, 3, 365–378.
[44] Campana, C, Leger, R, Sonnier, R, Ferry, L, & Ienny, P. Effect of post curing temperature on mechanical properties of a flax fiber reinforced epoxy composite. Compos. Part A Appl. Sci. Manuf., 2017, 107, 171–179.
[45] H-S, Shen, M.ASCE. Hygrothermal effects on the nonlinear bending of shear deformable laminated plates. J. Eng. Mech., 2002, 128, 493–496.
[46] Brischetto, S. Hygrothermoelastic analysis of multilayered composite and sandwich shells. J. prot. Sandw. Struct. Mater., 2013, 15, 168–202.
[47] Boukhoulda, BF, Adda-Bedia, E, & Madani, K. The effect of fiber orientation angle in composite materials on moisture absorption and material degradation after hygrothermal ageing. Compos. Struct., 2006, 74, 406–418.
[48] Shen, HS. The effects of hygrothermal conditions on the postbuckling of shear deformable laminated cylindrical shells. Int. J. Solids Struct., 2001, 38, 6357–6380.
[49] Nekhlaoui, S, Qaiss, A, Bensalah, MO, & Lekhder, A. A new technique of laminated omposites homogenization. Adv. Theor. Appl. Mech., 2010, 3, 253–261.

Part III: **Machining and Application**

Rahul Kumar, Sumit Bhowmik, Rahul Jayasval

8 Influence of drilling parameters on the thrust force and mechanical properties of biodegradable particleboard composite panels

A review

Abstract: The present work is focused to provide an overview of the influence of drilling parameters on thrust force and mechanical properties of biodegradable particleboard composite panels. The usage of particleboard composite material is augmented substantially in the past few decades and many research works focused on the machining of such materials. Among the numerous conventional machining, drilling is the most commonly used procedure for machining of particleboard, whereas milling and turning are less frequently used in particleboard application. The different machining parameters like feed rate, spindle speed, and drill bit diameter/point angle are found to have major influence on the thrust force during drilling operation. In the present work, a detailed review has been presented considering the effect of machining parameters in the drilling of particleboard. In addition, summarized outlines are presented on the surface characteristics of the hole produced in drilling operation and use of optimization techniques such as Taguchi method, which is a response surface methodology to find the optimized delamination factor. The arrangement of maximum spindle speed with low feed rate was established as an optimum arrangement to produce the minimum thrust force during the drilling operation of particleboard composite panels.

Keywords: Particleboard, drilling, thrust force, delamination, composite panels

8.1 Introduction

Biodegradable particleboard composite panels are widely used for decorative purpose, flooring, and wallboard and in furniture work [1]. Particleboards are made up of two components: first one is the matrix material (also known as “binder” medium) that covers and holds together with other material used as

Rahul Kumar, School of Engineering, Department of Mechanical Engineering, Dayanand Sagar University, Bangalore, India
Sumit Bhowmik, Rahul Jayasval, Department of Mechanical Engineering, National institute of Technology, Silchar, India

https://doi.org/10.1515/9783110603699-008

reinforcement. The desirable properties of particleboards are low density, high machinability, good strength, and good surface characteristics [2]. The particleboards are manufactured using soft powder mixed with resin and pressed together in the form of sheets. Numerous research works have been carried out to investigate the properties of particleboard composite panels produced with natural plant-based fibrous fillers. Among various natural plant-based fibrous fillers, wood filler is the most utilized potential applicant for fabrication of particleboard composite panels. Usually, wood dust is bonded with synthetic adhesive material like thermoset epoxy resin and shaped into sheets using high load press. Generally, the particleboard performance is highly affected by the allocation of density and element size [3]. The utilization of particleboard is varied with production cost, mechanical properties, and weathering resistance. The particleboards are largely employed in wallboards, roof tiles, and furniture works, the application that requires some sort of various industrial-scale machining operations like cutting, shaping, and drilling operations. Drilling is the most frequently used material removal process for machining of particleboard composite panels. Drilling operation performed on particleboard composites can result in surface defects and delamination between layers that appear because of the axial force during machining of particleboards. The delamination between layers can be quantified by calculating the ratio of the highest diameter of drill hole to diameter of the drill bit, also known as delamination factor. The surface characteristics of the hole produced in drilling operation is greatly dependent on the delamination factor and the thrust force generated because of drilling. Therefore, the parametric analysis is required to evaluate the combination of delamination factor and thrust force to produce best possible surface-finished hole. The various input process parameters considered important for parametric analysis in drilling operation are point angle, feed rate, tool material, drill bit diameter, and cutting speed. It is very difficult to find the optimal combination of parameter among different process parameters for drill operation of particleboard. There are several techniques like Taguchi method, grey relational analysis (GRA), response surface methodology, and so forth, which can be used for parametric optimization of input process parameters. Among these techniques, Taguchi method is the most cost- and time-effective parametric optimization process as it reduces the number of experiments, which minimizes the production cost and time consumed. Taguchi's experimental design based on orthogonal array and associated analysis of variance (ANOVA) are applied to determine the optimum value of thrust force and significance of parameters such as feed rate, spindle speed, and point angle in the drilling of particleboards [4–6]. Some researchers applied response surface methodology to examine the surface texture, apart from the utilization of Taguchi's design of experiment to evaluate the combination of optimum process parameters [7–14]. Therefore, there is a need for consolidated overview on the drilling of particleboard composite panels owing to its importance in its industrial-grade applications and also selection of best

possible combination of input process parameters as drilling of particleboard is a challenge in the machining operation.

In view of the above, the present review work demonstrates the overview on the type, manufacturing, and machining of particleboard composite panels. The effect of different parameters such as spindle speed, drill diameter, feed rate on thrust force, delamination factor, and surface characteristic behavior are elaborated in this study. Additionally, the selection of appropriate parameters for optimizing the thrust force and delamination factor are also discussed in detail.

8.2 Materials and machining of particleboard

8.2.1 Selection of materials and fabrication of sample

The cellulosic fiber has been used as reinforcement in composite materials since many centuries ago. Particleboard composite panel is also fabricated by natural fiber-reinforcement composite material. Natural fiber is a very attractive area for engineers, researchers, and scientists alike and recently emerged as the potential alternative to replace conventional petroleum-based reinforcing materials in fiber-reinforced polymer composite. Natural fibers have favorable attributes such as good mechanical properties, low density, excellent economic aspect, and non-abrasive properties. In recent years, it has been observed that combining two or more fibers together like jute, sisal, and coir has resulted in synergetic composite properties. The mechanical properties will improve and the cost will also be reduced. Generally, natural fiber refers to wood fiber leaf, seed, stem fiber, and agro-based bast in composite industry and these natural fibers contribute to the structure performance of plants and if these fibers are used in a plastic composite, then it can provide significant reinforcement for the composite [15]. Natural fibers can also become a cost-effective composite material in the applications of building and construction at locations such as walls, windows, furniture (chair, table, and tools), ceiling, position and door frames, storage device (post boxes, bio gas container, etc.), automobile, railway coach, electronic instruments (outer mobile frame), toys, helmets, and suitcases.

Most of the particleboard (composite material) is made up of two components. One is reinforcement material and another is matrix or binder material that binds with reinforcement. Some of thermosetting and thermoplastic material are used as matrix materials for the development of natural fiber-based particleboards. The various examples of thermosetting matrix is phenolic, epoxy, and polyester resin, whereas same for thermoplastic matrix are poly vinyl chloride (PVC), polypropylene, and polyethylene. Natural fiber composites that are classified are present as commonly used fiber and matrix for polymer composites [16–20].

There are various techniques used for fabrication of particleboard; for instance, pultrusion, hand lay-up, vacuum bag molding, and resin transfer molding. Hand lay-up technique is easier than other fabrication methods. Particleboards are principally manufactured by mixing particles or sawdust with an epoxy resin and the dough mixture is pressed into a sheet form. If required, the particle size is reduced by a disc chipper that has between four and sixteen radial blades or ball mill grinding setup. After this, resin is sprayed in the form of liquid by nozzles onto the wood particles in a prepared glass mold. In other words, particleboard composite is manufactured from lignocelluloses material first in the form of a distinct particle mixed with epoxy-based resin or other binding materials and fixed at certain temperature and pressure. Epoxy and amino formaldehyde are two mainly utilized thermoset resins for particleboard fabrication. As compared to formaldehyde, the epoxy resins are best suitable when keeping in mind the cost and ease of process. Urea melamine resin is used as a water resistance and phenol formaldehyde is normally used in external applications of wood panels, which are owing to the increased water resistance offered by phenolic resins. To intensify the wood-based composite panel properties such as employment of resorcinol resins normally combined with phenolic resins are used. It is generally used with plywood (PLW) for marine applications and also used in composite panel fabrication. Wood-based composite panels that are fabricated involve different chemicals used such as wax, dyes, wetting agents, and releasing agents; after mixing resin with sawdust particles, the mixture of liquid changes to composite panels. The sheets are fabricated and cold compressed to decrease the thickness. Through this way, the size, density, and uniformity of the particleboard composite panel can be conservatively managed.

The wood particleboard composite is classified on the basis of the raw material type, its density, and the manufacturing process used to fabricate it. The different types of particle boards available are medium-density board, fiber board, flake board, and a combination of various woods like hardboard and plyboard. Wood shaving, flakes, wafers, chips sawdust, strands, and wood dust are the types of particle that are used in fabrication of composite board panel.

The properties of thin particleboard panel are mainly affected by the natural fiber particle size. This result has been verified by many researches on thick particleboard panel; however, a difference in direction, amount, and mechanism can make this effect on the properties of the panels built by thin and thick particleboard composite panel. An influence of particle on the modulus of elasticity and modulus of rigidity of the thin panel board is approximately the same as a thick particleboard panel. Particleboard manufactured from lowest particle size exhibits minimum modulus of elasticity and modulus of rigidity and also particle size effect on internal bonding, swelling, thickness, and absorption of water in thin particleboard panels do not regulate all the principles that govern thick particleboard panels. The major issues are increased compression of particles in thin particleboard panels, the ratio of particle size, and thickness of the composite board panels [21].

The density of a conventional wood is less than the particleboard. It is the lightest type of fiberboard used, except the insulation purpose. Minimum-density fiber (MDF) board and hardboard are also known as high-density fiberboard. It is harder than the particleboard composite panel. The drawback of particleboard composite panel tends to be of more extensive and less attractive color because of moisture, when it is not coated with paint or other coating elements. So, it is less applicable outdoors or places having more moisture, with the exception of bathroom and kitchen.

8.2.2 Machining of particle board composite materials

The machining behavior of natural fiber-reinforcing plastic composite as well as particleboard composite panel is a less discussed area as compared to the same for metals and metal matrix composites. The requirement of machining processes like drilling and milling arises to produce the required dimensional requirements for assembly. Particleboard drilling operation is different than metal drilling operation because drill bit has passed through epoxy (matrix) and natural fiber (reinforcement) that are anisotropic in nature. The constituents of physical and chemical properties make understanding of the mechanism of material removal rate fully typical. Machining of composites is having number of fractures because of varied nature and irregular load sharing between matrix and natural fiber (reinforcement) during material removal [22, 23].

Drilling operation of particleboard panels

Drilling is one of the most conventional machining operations used for producing a hole in particleboard composite. The process of drilling on the particleboard composite is considered being a critical operation as there are many issues associated with drilling such as delamination and surface quality of hole that come into play during the process. The most difficulty observed in the drilling of particleboard is that, composite laminated particleboard behaves as a tough machining operation, so as a result of drilling efficiency less and unwanted delamination occurs. Damage-free and accurate hole must be drilled in the elements to secure joint strength and accuracy for rivets and bolted joints. However, machining is difficult in some cases of laminate composite materials such as nonhomogeneous, anisotropic, highly abrasive, and hard reinforcement fiber. Among the above-mentioned problems, delamination is a major problem in the drilling operations [24–32].These issues are overcome by proper selection of cutting parameters and develop a proper technique for minimizing the delamination in drilling operation of fiber-based plastic composite that lies in minimizing the thrust force [33–35] so that damage should

not occur under critical thrust force condition. The machining efficiency and production can be increased by knowing the critical thrust force. The value of critical thrust force is predicated at delaminating drilling on fiber-reinforced plastic composites [36]. The various machining investigations on particleboard carried out by various researchers is listed below.

Ramesh et al. [37] investigated the characteristics of the hybrid composite by varying the spindle speed, feed and tool diameter in the drilling operation. The experimental results showed that the lower feed and maximum or moderate spindle speed are appropriate for drilling of glass–sisal–jute fiber-reinforced hybrid composites in order to reduce the induced damages while drilling.

Drilling of particleboard is also affected by the type of fiber used in composite materials. Therefore, the selection of the machining parameters like cutting speed, feed rate, drill diameter, and cutting tool material should take the consideration of fibre type used as reinforcement. The machining process can be used to produce the desired quality by using the proper selection of process parameter. Many factors affect the machining of glass fiber-reinforcement epoxy composite material. The thrust forces of glass fiber-reinforced epoxy composite with volume fraction of 9.8–2.37% was measured and it was observed that with an increasing spindle speed, the thrust force decreased. It was also found that glass fiber-reinforcement epoxy composite has low feed with low volume fraction [38, 39].

Consequence of torque and thrust force generated during drilling operation

The relationship between drilling parameters such as cutting speed, feed rate, and drill bit diameter affects the quality of the hole during drilling operation on particleboard composite. Thrust force and torque developed during drilling of particleboard mainly depends on parameters such as feed rate, drill diameter, and spindle speed. There were several researches carried out to find the relationship between the thrust force with different drilling parameters.

Jayabal and Natarajan investigated that the value of thrust force is obtained as minimum when smaller drill bit diameter was used and others include low feed rate and highest value of spindle speed in case of drilling of natural fiber-based composite board [40, 41].

Patel et al. [42] studied drilling operation of natural fiber-based composite and observed that the upsurge in feed value and point angle has increased the cutting force. However, with the increase in spindle speed, the cutting force was decreased.

Delamination of particle composite panel is one of the major defect because of push-out and peel-up mechanism. It is attributed to the thrust force during drilling of particleboard. The torque and thrust force are mainly influenced by various drill bit geometry [43, 44].

Jayabal et al. [45] studied hybrid composite materials mixed with polyester and coir/glass fiber. Drilling of composites was done by High speed steel (HSS) drill bit. The feed rate has major effect on the thrust force as compared to spindle speed and drill bit diameter.

There were four different types of point geometry used for fabricated hole in two dissimilar types of composite laminates. The machining parameters for the composite were considered as cutting speed and feed rate; a new artificial neural network was used to estimate the thrust force developed during the drilling operation [46–48].

Balaji et al. [49] investigated the effect of woven and nonwoven coir fiber-reinforcement on delamination coir composite material. It was found that the delamination factor in coir fiber-reinforced composites is lower as compared to glass fiber-reinforced composites.

Chandramohan and Marimuthu [50] investigated that torque was increased with increase in the fiber volume fraction. It was because if increase in the fiber volume fraction that results in the improvement of the resistant of composite materials. Higher value of resistant leads to more thrust force. The results found that the torque was decreased with increase in the spindle speed. Similarly, thrust force was increased with increase in the volume fraction of the natural fiber.

Babu et al. [51] reported that minimum delamination occurs during drilling of hemp natural fiber, whereas jute fibers have more delaminates. The delamination factors were found to be better than glass fiber composite in some cases.

Bandhu et al. [52] studied the thrust force generated during the drilling operation. The thrust force and torque were prime factors for the occurrence of delamination on the composite. There was no machining chart to cover the polymeric composite materials compared to metallic materials. The machining chart directly resolved the issue of selection of suitable conditions while drilling on composite materials.

In order to investigate the drilling-induced damaged on a fiber-reinforced plastic laminated composite, a finite element model was simulated. The drilling parameter (cutting speed and feed rate) were optimized by a finite element model [53, 54].

Gaitonde et al. [55, 56] studied the delamination phenomena in medium-density fiberboard. It was observed that the combination of low feed rate and high cutting speed has effectively minimized the delamination effect.

McKenzie et al. [57] estimated the thrust force and the surface behavior of boards composite by bearing in mind the influencing properties like coefficient of friction and specific gravity. It was observed that the thrust force for each millimeter width of cut was in logarithmic relation with the specific gravity with continuous variation from central plane to the surface. Finally, thrust force was found to be autonomous of the direction of cutting in the plane of the wood-based composite panel.

Zhao and Ehmann [58] experimentally evaluated the thrust force by new-generation spade drill bits on MDF composite. The new type of spade drill bit revealed a low value of thrust force over the entire parametric conditions.

Dippon et al. [59] studied the orthogonal cutting mechanisms of medium-density fiberboard composite as functions of tool material, tool geometry, and uncut chip location. Orthogonal cutting tests had been regulated both perpendicular and parallel to the composite panel. The friction was low on the rake surface and the pressure generated by uncut chip on the rake surface mostly influences the force on the rake surface.

Lin et al. [60] investigated the machining performance of medium-density fiberboard with three different depths of cut of 0.5, 0.75, and 1.0 mm. The board density was observed to have foremost effect on machinability features of fiberboards.

Prakash et al. [61] evaluated the delamination factor in drilling of medium-density fiberboard. In addition, response surface methodology was used for modeling of drilling parameters. It was perceived that the delamination factor was mostly influenced by feed rate followed by drill diameter. Also the upsurge in spindle speed has reduced the delamination factor but increase in drill diameter and feed rate has enhanced the same.

Wang et al. [62] characterized the density effects on fasteners that hold capacities confined to a small area in wood-based panels like oriented strand boards (OSB), medium-density fiberboards, and particle boards. The results showed that the variation of density in wood panels has substantial consequence on the sideways confrontations, screw removal, and head get-through.

Raju et al. [63] deliberated the drilling characteristics of particulate glass fabric-reinforced epoxy-based composite. The thrust force was observed to be affected by the drilling parameters in case of glass fiber-reinforced composite. It was established that the increasing spindle speed and feed has amplified the thrust force. Again, it was evaluated that carbide drill bit tool has performed better than the high-speed steel drill.

Mohan et al. [64] optimized the cutting parameters in the drilling of glass fiber-reinforced composite materials using the Taguchi method. It was observed that the drill size and speed significantly influenced the cutting thrust as compared to the specimen thickness and cutting rate.

Davim et al. [65] analyzed the machining of glass fiber-reinforced plastic (GFRP) by cemented tungsten carbide drill bit with different shapes. The results specified that the increase in input parameters like speed and feed rate has augmented the damage.

Khashaba [66] studied the drilling of glass fiber-reinforced plastic composite produced using many different matrix materials such as epoxy and polyester resins. The thrust force was gradually decreased during the drilling operation on the cross-winding composite. Another conclusion was that matrix has a less influence on the thrust force during the machining of woven composites with distinct influence on

thrust force; however, the torque measured was appreciably higher during the drilling operation on polyester resins composite.

Bosco et al. [67] examined the influence of drilling parameters on delamination behavior of a glass fiber-reinforced sandwich composite. It was observed that the delamination factor has amplified as the feed rate increased from 0.03 mm/rev to 0.12 mm/rev.In addition to this, the thrust force was also increased with feed rate. However, the brad and spur drill bit was found to be efficient in obtaining the lower value of thrust force.

Ogawa et al. [68] elaborated the drilling operation of a glass fiber-reinforced plastics with a drill bit of diameter of 1 mm made of cemented carbide. The thrust force was rapidly decreased if the pre-drilling of hole was done. The required pre-drilling of hole was of 0.4 mm or above.

Wang et al. [69] studied the thrust force in the vibration machining of fiber-reinforced plastic by using carbide and high-speed steel drill bit material. The vibration and conventional drilling operations were performed on carbon fiber-reinforced plastic, glass fiber-reinforced plastic, and printed circuit boards. The final observation was that the thrust force in the case of vibration drilling was lower than the same for conventional drilling.It established the fact that vibration drilling techniques were suitable for fabricating a micro hole in the fiber-reinforcement plastic.

Kavad et al. [70] studied the influence of machining parameters on delamination damage that occurred in glass fiber-reinforced plastics during drilling operation. In traditional machining process, the cutting speed, feed rate, and tool material were found to be the utmost persuasive factor on delamination.Therefore, for lower delamination, higher cutting speed, harder tool material, and lower feed rate were chosen.

Sadek et al. [71] characterized and optimized the vibration-assisted drilling of fiber-reinforced epoxy laminates. It was found that the optimized vibration-assisted drilling conditions have diminished the axial force and cutting temperature, respectively by 40% and 50%. It was also instrumental in producing delamination-free holes without affecting productivity.

Rubio et al. [72] studied the impact of high-speed machining on the performance of drilling operation in glass fiber-reinforced plastics. It was found that the delamination factor decreased with the increase in spindle speed. Also the high-speed machining has ensured less damage during drilling operation of glass fiber-reinforced plastic material.

8.2.3 Optimization of input process parameters

Parametric analysis is necessary to optimize the drilling process parameters such as cutting speed, diameter of drill bit, point angle, feed, drill bit geometry, and

material, as a number of parameters influence the performance as well as the outcomes like surface finish, shape and so on of drilling of particleboard panel. Various optimization techniques, such as Taguchi method, GRA, and other optimization methods were used by various researchers to optimize the different parameters.

Valarmathi et al. [2] studied the optimizing parameters for delamination behavior of particleboard panel. Feed, diameter of drill bit, and cutting speed were found to be the most dominant variables on delamination factor. The optimum values for minimized delamination conditions were maximum cutting speed (4,500 rpm), low feed rate (100 mm/min), and small drill diameter (6 mm) within the range. In other works, Valarmathi et al. [73] investigated the thrust force in machining operation of MDF panel and concluded that at low feed rate, increasing the cutting speed decreased the thrust force.GRA together with Taguchi method has been successfully implemented in drilling with MDF for optimizing the parameters [74–77]. Abilash and Sivapragash [78] studied the combined effect of feed rate and drill diameter for delamination effect. The lower value of drill bit diameter and feed value minimizes the delamination factor and it gives a better surface quality of holes.

8.3 Mechanical properties of particleboard composite panels

The performance of particleboard composites can be characterized by a variety of engineering properties. As particleboards are mainly made up of wood fiber/particle fillers, the density and moisture content of wood filler influence its elasticity, strength, hardness, swelling, and shrinkage.The physical and mechanical properties of wood material are mainly affected by the moisture present in the cell cavities as free water and cell walls as absorbed water. Wood drying and coating can be used to bring the moisture content to the expected value and impede the changes in the moisture content [79]. In addition, uniform distribution of wood particle size and binding materials are major contributing factor in improving the mechanical properties of particleboards.Another factor is reinforcing particle-to-resin ratio, because both physical and mechanical properties mostly depend on this ratio.

Muruganandam et al [80]. evaluated the swelling thickness, bending strength, and internal bonding strength of particleboards fabricated with cotton stalks at different resin percentage and different density ranges. The bending strength was found to be 3.3 N/mm^2 being minimum and 17.9 N/mm^2 being the maximum. In order to maintain particleboard thickness, maximum pressure and temperature were operated in fabricating cotton stalks particleboard. As a result of the enhanced

bonding, strength between particles has been obtained and resulted significant increase in the internal bonding strength of the particleboard composite panels.

The sunflower stalk particle filler and the adhesive materials with urea–formaldehyde were mixed to fabricate the particleboard panels and its modulus of rupture, Young's modulus, internal bonding strength, and screw holding strength were evaluated. It was found that with the increase in quantity of sunflower stalk particles in matrix, the physical and mechanical properties of the particleboard panel was found to be decreasing [81, 82].

The peanut hull and pine wood chips were mixed to fabricate a three-layered particleboard composite with peanut hull ratios of 0, 25, 50, 75, and 100%. Urea formaldehyde has been used as an adhesive material and the particleboard was tested for its physical and mechanical properties (modulus of elasticity, modulus of rupture, and internal bonding). The standard amount of peanut hull for optimum modulus of elasticity and modulus of rupture value was 25% and further increase in peanut hull has reduced the mechanical and physical properties of composite panel.By using the hydrophobic additive, physical property of particleboard can be improved [83, 84].

8.4 Overview and discussion

The machining of particleboard composites is essential for its application in the development and assembly of commercially viable products. Drilling, milling, turning, and other conventional machining operations are applied to MDF board and its effect on tool wear, surface finish, and operating variables are reported by several researchers. Because of the increasing environmental issues and the requirement for lightweight materials, particleboard composites reinforced through natural plant-based filler material, that is, filler obtained from recyclable sources has come up as potential alternative [85, 86]. Natural fiber-based particle boards have shown an increased interest owing to their biodegradability, reusability, and abundant availability of the natural fibrous fillers [87, 88].

Damage occurs on natural fiber-based particleboards during drilling, and it depends on the factors during the cutting (drilling) of the natural fiber-reinforced composites, including machining conditions, machining parameters, drill bit tool material, tool geometry, fiber orientation, and mechanical properties of the natural fiber. It can be reduced by choosing an appropriate combination of input parameters.Feed rate, cutting speed, and drill bit diameter have major impact on the thrust force of fiber-based composite panels during the drilling operation. Drilling parameters like feed value and spindle speed affected the thrust forces and torque on drilling of composite material with different fiber volume fractions.Delamination is the major defect induced during drilling process and its dimension gets increased with

increasing drill bit diameter and feed.It was determined that the increase in feed results in maximum value of thrust force, which in turn increased the delamination area and lowered the bearing property.The peel-up and push-out delamination occurred at the entry and exit of drill bit in a particleboard composite as a result of cutting parameters.

The density of composite panels has shown major effects on its flexural properties and important mechanical properties. On the other hand, the density distribution of particles in different type of fiberboards like MDF, OSB, and PLW board have significantly affected the machinability characteristics and damage occurred during drilling operation. MDF and particleboard composite panels had been uniformly distributed than PLW and OSB composite panels, therefore displaying better finish after machining.

8.5 Conclusions

In this chapter, an overview on the effects of drilling parameters on the thrust force and mechanical properties of particleboard composite panels was demonstrated. The present research work contributes and identifies the various parameters that influence the worth of machining features and provides the direction to choose an input parameter in the particleboard drilling. The following significant facts can be summarized based on the conducted review work:

- There are many fabrication methods based on the type of matrix material that could be used for manufacturing of several types of particleboard.
- The structure integrity of particleboard is highly influenced by drilling operation and helps in evaluating the suitable process parameters that includes drill bit material and its geometry.
- Drilling is most commonly used process for machining of particleboard. Milling and turning are less frequently used in particleboard application.
- As far as reinforcing material is considered, natural and glass fiber-reinforced composites have been similarly investigated. The preferred base material is epoxy-based thermoset resin and twist drill made of high-speed steel is preferred over cemented tungsten carbide drills.
- In the drilling of particleboard composite panels, spindle speed has reverse effect on the resulting thrust force, whereas the feed rate is being increased with the increase in the thrust force.
- The relation between the influencing process parameters like spindle speed, drill bit diameter, and feed rate have affected delamination in the drilling of wood composite panels.

8.6 Future suggestions

The scope of future research works should focus on those measures that can improve surface integrity as well as the mechanical properties of particleboard composite panels to meet the requirements for major commercial-grade applications. The surface-modified wood flake fillers can be used to improve the mechanical properties and capability of particleboard. The potential concern regarding drilling of particleboard is delamination factor; therefore, initial numerical simulation of drilling operation should be run and advance optimization techniques might be used to minimize the observed delamination factor. An approach based on artificial neural computation method might be effective in predicting the thrust force and other required parametric values during drilling operation.

References

[1] Valarmathi, T. N., Palanikuma, K., & Latha, B. Measurement, 2013, 46, 1220–1230.
[2] Valarmathi, T. N., Palanikumar, K., & Sekar, S. Indian J Sci Technol., 2013, 6, 4347–4356.
[3] Rowell, R. M. Handbook of wood chemistry and wood composites, CRC Press, 2005, 2nd ed. Chapter 13, 365–378.
[4] Navanth, A., & Sharma, T. K. Inter. J. Engg. Sci. Emerg. Technol., 2013, 6, 65–75.
[5] Tsao, C. C., & Hocheng, H. Int. J. Mach. Tool. Manuf, 2004, 44, 1085–1090.
[6] Kumar, J. P., & Packiaraj, P. Int. J. Adv. Eng. Res. Stud, 2012, 1, 150–154.
[7] Haq, A. N., Marimuthu, P., & Jeyapaul, R. Int. J. Adv. Manuf. Technol, 2008, 37, 250–255.
[8] Kumar, P., Barua, P. B., & Gaindhar, J. L. Qual. Reliab. Eng. Int., 2000, 16, 475–485.
[9] Elajrami, M., Miloud, R., & Boukhoulda., F. B. Int. J. Manuf. Mater. Mecha. Engg., 2013, 1, 250–253.
[10] Palanikumar, K., Prakash, S., & Manoharan., N. Mater. Manufact. Process., 2009, 24, 1341–1348.
[11] Laemlaksakul, V. Int. J. Chem. Mole. Nucl. Mater. Metall. Eng, 2010, 4, 507–511.
[12] Gaitonde, V. N., Karnik, S. R., & Davim, J. P. Mater. Manuf. Processes, 2008, 23, 377–384.
[13] Gaitonde, V. N., Karnik, S. R., & Davim, J. P. J. Mater. Process. Technol., 2008, 196, 73–78.
[14] Davim, J. P., Clemente, V., & Silva., S P. I. Mech. Eng. B J. Eng. Manuf., 2007, 221, 655–658.
[15] Kumar, R., Kumar, K., Sahoo, P., & Bhowmik, S. Proc. Mater. Sci.,2014, 6, 551–556.
[16] Facca, A. G., Kortschot, M. T., & Yan, N. Composite Part A: Appl. Sci. Manuf., 2006, 37, 1660–1671.
[17] Shrivastava, R., Christy, A., Telang, A., & Rana., R. S. Int. J. Eng. Res. Appl., 2015, 5, 70–75.
[18] Nassar, M. M. A., Arunachalam, R., & Alzebdeh., K. I. Int. J. Adv. Manuf. Tech., 2016, 88, 2985–3004.
[19] Sanjay, M. R., Arpitha, G. R., & Yogesha., B. Mater. Today: Proc., 2015, 2, 2959–2967.
[20] Shivakumar, S., & Guggari, G. S. Int. J. Adv. Eng. Technol., 1963, 1, 218–226.
[21] Rakesh, P. K., Sharma, V., Singh, I., & Kumar, D. Sci. Res., 2011, 3, 549–554.
[22] Bhattacharyya, D., & Horrigan, D. P. W. Compos. Sci. Technol., 1998, 58, 267–283.
[23] Bandhu, D., Sangwan, S. S., & Verma, M. Int. J. Curr. Eng. Technol., 2014, 4, 1749–1752.
[24] Azuan, S. A. S., Juraidi, J. M., & Muhammad, W. M. W. Appl. Mech. Mater., 2012, 232, 106–110.
[25] Hocheng, H., & Tsao., C. C. J. Mater. Process. Technol., 2003, 140, 335–339.

[26] Zitoune, R., & Collombet, F. Compos. Part A: Appl. Sci. Manuf., 2007, 38, 858–866.
[27] Wong, T. L., Wu, S. M., & Croy, G. M. 14th Nati. Samp. Tech. Conf. 1982, 1–483.
[28] Vankanti, V. K., & Ganta, V. J. Mater. Res. Technol., 2014, 3, 35–41.
[29] Liu, D., Tang, Y., & Cong, W. L. Compos. Struct., 2012, 94, 1265–1279.
[30] Hocheng, H., & Tsao, C. C. Int. J. Mach. Tool. Manuf., 2006, 46, 1403–1416.
[31] Capello, E. J. Mater. Process. Technol., 2004, 148, 186–195.
[32] Abrao, A. M., Faria, P. E., Rubio, J. C., Reis, P., & Davim, J. P. J. Mater. Process. Technol., 2007, 186, 1–7.
[33] Hough, C. L., Lednicky, T. E., & Griswold, N. J. Test. Eval., 1988, 16, 139–145.
[34] Davim, J. P., & Reis:, P. Compos. Struct., 2003, 59, 481–487.
[35] Davim, J. P., & Reis, P. Mater. Des., 2003, 24, 315–324.
[36] Zhang, L. B., Wang, L. J., & Liu, X. Y. P. I. Mech. Eng. Part B: J. Eng. Manuf., 2001, 215, 135–146.
[37] Ramesh, M., Gopinath, A., & Deepa, C. Indian J. Sci. Technol., 2016, 9, 1–7.
[38] Krishnaraj, V., Vijayarangan, S., & Kumar, A. R. Int. J. Comp. Ass. Tomo. Res., 2007, 28, 87–93.
[39] Guler, C., Bektas, I., & Kalaycioglu, H. For. Prod. J. 56, 2006, 56(4), 56–60.
[40] Jayabal, S., & Natarajan, U. Bull Mater Sci., 2011, 34 1563–1567.
[41] Jayabal, S., & Natarajan, U. Int. J. Adv. Manuf. Technol., 2010, 51, 371–381.
[42] Patel, K., Gohil, P. P., Chaudhary, V., & Patel, K. Int. Confer. On Civil, Mater. Environ. Sci., 2015, 1 201–205.
[43] Bajpai, P. K., Debnath, K., & Singh, I. J Thermoplast. Compos. Mater., 2017, 30, 30–46.
[44] Yallew, T. B., Kumar, P., & Singh, I. Proc. Inst. Mech. Eng. L: J Mater: Des. Appl., 2016, 230, 288–298.
[45] Jayabal, S., Natarajan, U., & Sekar, U. Int. J. Adv. Manuf. Technol., 2011, 55, 263–273.
[46] Tsao, C. C., & Hocheng, H. J. Mater. Process. Technol., 2007, 192, 37–40.
[47] Dhawan, V., Debnath, K., Singh, I., & Singh, S. FME Transactions, 2016, 44, 36–42.
[48] Ramkumar, J., Aravindan, S., Malhotra, S. K., & Krishnamurthy, R. Int. J. Adv. Manuf. Technol., 2004, 23, 240–244.
[49] Balaji, N. S., Jayabal, S., Kalyana, S. S., Rajamuneeswaran, S., & Suresh, P. Adv. Mater. Res., 2014, 984, 185–193.
[50] Chandramohan, D., & Marimuthu, K. Int. J. Adv. Eng. Res. Stud., 2011, 1, 134–145.
[51] Babu, D., Babu, K. S., & Gowd, B. U. M. Am. J. Mater. Sci. Technol., 2012, 1, 1–10.
[52] Bandhu, D., Sangwan, S. S., & Verma, M. Int. J. Curr. Eng. Technol., 2014, 4, 1749–1752.
[53] Farrokhpayam, S. R., Valadbeygi, T., & Sanei, E. J. Ind. Acad. Wood Sci., 2016, 13, 1–6.
[54] Khan, M. A., & Kumar, A. S. J. Manuf. Processes, 2011, 13, 67–73.
[55] Gaitonde, V. N., Karnik, S. R., & Davim, J. P. Mater. Manuf. Processes, 2008, 23, 377–384.
[56] Gaitonde, V. N., Karnik, S. R., & Davim, J. P. J. Mater. Process. Technol., 2008, 196, 73–78.
[57] McKenzie, W. M., Ko, P., Cvitkovic, R., & Ringler, M. Wood Sci. Technol., 2001, 35, 563–569.
[58] Zhao, H., & Ehmann, K. F. Int. J. Machine Tools Manuf., 2002, 42 1403–1414.
[59] Dippon, J., Ren, H., Amara, F. B., & Altintas, Y. Forest Prod. J., 2000, 50, 25–30.
[60] Lin, R. J. T., Houts, J. V., & Bhattacharyya, D. Holzforschung, 2006, 60, 71–77.
[61] Prakash, S., Palanikumar, K., & Manoharan, N. Int. J. Adv. Manufact. Technol., 2009, 45, 370–381.
[62] Wang, X., Salenikovich, A., & Mohammad, M.. Forest Prod. J., 2007, 57, 103–109.
[63] Raju, B. R., Suresha, B., Swamy, R. P., & Kanthraju, B. S. G.. J. Miner. Mater. Charact. Eng., 2013, 1, 101–109.
[64] Mohan, N. S., Ramachandra, A., & Kulkarni, S. M.. Compos. Struct., 2005, 71, 407–413.
[65] Davim, J. P., Reis, P., & Antonio, C. C. Compos. Sci. Technol., 2004, 64, 289–297.
[66] Khashaba, U. A. Compos. Struct., 2004, 63, 313–327.

[67] Bosco, M. A. J., Palanikumar, K., Prasad, B. D., & Velayudham, A. Procedia Eng., 2013, 51, 758–763.
[68] Ogawa, K., Aoyama, E., Inoue, H., Hirogaki, T., Nobe, H., Kitahara, Y., Katayama, T., & Gunjima, M. Compos. Struct., 1997, 38, 343–350.
[69] Wang, X., Wang, L. J., & Tao, J. P. J. Mater. Process. Technol., 2004, 148, 239–244.
[70] Kavad, B. V., Pandey, A. B., Tadavi, M. V., & Jakharia, H. C. Procedia Technol., 2014, 14, 457–464.
[71] Sadek, A., Attia, M. H., Meshreki, M., & Shi, B. CIRP Ann. Manuf. Technol., 2013, 62, 91–94.
[72] Rubio, J. C., Abrao, A. M., Faria, P. E., Correia, A. E., & Davim, J. P. Int. J. Mach. Tool. Manufact., 2008, 48, 715–720.
[73] Valarmathi, T. N., Palanikumar, K., & Sekar, S. Procedia Eng., 2012, 38, 1828–1835.
[74] Prakash, S., Mercy, J. L., Salugu, M. K., & Vineeth, K. S. M. Materials Today: Proceedings, 2015, 2, 1541–1551.
[75] Sridharan, V., & Muthukrishnan, N. Proc. Eng., 2013, 64, 1003–1012.
[76] Patel, M. T. Int. J. Adv. Res. Eng., 2015, 4, 1–15.
[77] Sahoo, A. K., Baral, A. N., Rout, A. K., & Routra, B. C. Proce. Engg., 2012, 38, 1606–1627.
[78] Abilash, N., & Sivapragash, M. J. K. S. U. Eng. Sci., 2016, 28, 92–102.
[79] Palanikumar, K., Prakash, S., & Manoharan, N. Mater. Manuf. Processes, 2009, 24, 1341–1348.
[80] Muruganandam, L., Ranjitha, J., & Harshavardhan, A. Int. J. Chem. Tech. Res., 2016, 9, 64–72.
[81] Guler, C., Copur, Y., & Tascioglu, C. Bioresour. Technol., 2008, 99, 2893–2897.
[82] Santhanam, V., & Chandrasekaran, M. Ind. J. Appl. Res., 2014, 4, 194–199.
[83] Bektas, I., Guler, C., Kalaycioglu, H., Mengeloglu, F., & Nacar, M. J. Compos. Mater., 2005, 39, 467–473.
[84] Bridges, R. R. Forest Prod. J. 1971.
[85] Kumar, R., Bhowmik, S., & Kumar, K. Intern. Polymer Processing, 2017, 32, 308–315.
[86] Kumar, R., Kumar, K., & Bhowmik, S. J Polym Environ, 2018, 26, 2522–2535.
[87] Kumar, R., Kumar, K., & Bhowmik, S. Wood Sci. Technol., 2018, 52, 677–699.
[88] Kumar, R., Kumar, K., & Bhowmik, S. Procedia Materials Science, 2014, 5, 688–696.

Vivek Kumar Gaba, Anil Kumar Tiwari, Shubhankar Bhowmick

9 A numerical study of rotating functionally graded annular fin

Abstract: Performance analysis of rotating annular fins made of functionally graded material is reported in this study. The governing differential equation for such fins of rectangular and triangular profiles has been derived to evaluate the temperature distribution and efficiency of the fins with insulated tip boundary condition. Nonlinearity in the governing equation material heterogeneity and rotation at various speed is imposed and analyzed to compare the performance for both rectangular and triangular cross section. The results are presented in graphical form. The formulation is validated with benchmark results and good agreement is observed.

Keywords: Triangular and rectangular annular fin, functionally graded material (FGM), rotating shaft

9.1 Introduction

The thermal analysis of annular fins has been, throughout, of greatest interest to many researchers across the world due to its widespread applications in industry. The study has become much more feasible in the past few decades due to the intensified application of numerical methods in new generation computational machines. Thermal analysis of annular fin provides many fronts in which research is carried out unidirectionally.

The efficient design of a annular fins to dissipate maximum amount of heat depends on their shape, weight, and the material used. The main purpose of an extended surface or a fin is to increase the rate of heat transfer from a heated surface to a cold fluid. Of these, annular fins find numerous applications in compact heat exchangers, specialized installations of single- and double-pipe heat exchangers, electrical apparatus with efficient heat dissipation, cylinders of air-cooled internal-combustion engines, and fuel cans in nuclear reactors to name a few. The design of a fin is considered to be optimum when the fins require minimum cost of manufacturing, offer the minimum resistance to the fluid flow, are light in weight and are easy to manufacture. On the basis of a set of idealized assumptions, the efficiency of rectangular and hyperbolic annular fins is reported [1]. Brown [2] derived an equation to obtain optimum dimensions of uniform annular fin, that is, the

Vivek Kumar Gaba, Anil Kumar Tiwari, Shubhankar Bhowmick, Department of Mechanical Engineering, National Institute of Technology, Raipur, India

https://doi.org/10.1515/9783110603699-009

width, length, and volume, in terms of the total heat to be dissipated by the fin. Duffin and McLain [3] worked to maximize the heat dissipation of cooling fin of given constant weight when it is attached to a cylinder with convex cross section by properly tapering the fin wherein the differential equation for heat flow is converted into a saddle point variational problem. Ullmann and Kalman [4] worked for increasing the heat dissipation of annular fins at specified mass and performed the analysis for four different cross-section shapes like constant thickness, constant area for heat flow, triangular, and parabolic fin shapes. The optimal dimensions of convective-radiating circular fins with variable profile, heat-transfer coefficient, and thermal conductivity, as well as internal heat generation, were obtained [5]. It was found that a (quadratic) hyperbolic circular fin with $n = 2$ gives an optimum performance. Performance of annular fins of different profiles subject to locally variable heat transfer coefficient was investigated by Mokheimer [6], wherein the fin performance in terms of fin efficiency as a function of the ambient and fin geometry parameters in the form of curves known as the fin-efficiency curves for different types of fins is reported. Bahadur and Bar-cohen [7] proposed an optimization methodology for a thermally conductive polyphenylene sulfide polymer staggered pin fin heat sink, for an advanced natural convection cooled microprocessor application. The coefficient of thermal performance defining the cooling ability to the energy invested in the formation of the heat sink has been reported for such heat sinks and compared with conventional/aluminum heat sinks. In another work [8], composite annular fin with hyperbolic thickness variation has been analytically modeled using an infinite series of orthogonal eigen functions. Heat transfer and temperature distribution equations for longitudinal convective–radiative porous fins were presented by Hatami and Ganji [9] using Al, SiC, and Si_3N_4 being the ceramic porous materials. Thermal performance of functionally graded rectangular annular fin has been reported by Aziz and Rahman [10].

Literature review indicates that two-dimensional analysis of annular fins is scarce. The temperature distribution and heat transfer rate for orthotropic two-dimensional, annular fins subject to convective-tip boundary condition and the contact resistance at the fin base have been studied in [11, 12]. Dimensionless heat transfer rates are presented and fin efficiency ratio is plotted as a function of Biot numbers and fixed values of geometric parameters.

In a recent study, analytical solution to the thermal performance of a radial longitudinal fin of rectangular and various convex parabolic profiles mounted on a rotating shaft and losing heat by convection to its surroundings [13] is presented based on convection heat transfer coefficient, assumed to be a function of both the radial coordinate and the angular speed of the shaft. Aziz and Lopez [14] studied the heat transfer process in a continuously moving sheet or rod of variable thermal conductivity that loses heat by convection and radiation simultaneously. The effects of five dimensionless parameters, namely, Peclet number (Pe), thermal conductivity parameter

(a), convection–conduction parameter (N_c), radiation–conduction parameter (N_r), and sink-to-base temperature ratio (q_a), on the temperature distribution, base heat conduction rate, and surface heat loss were reported.

Aziz and Khani [15] developed an analytical solution for heat transfer in a moving fin of variable thermal conductivity, thus losing heat by both convection and radiation. It was compared with the direct numerical solution to validate the accuracy of the analytical results. The differential transformation method was used to study heat transfer in a moving fin with variable thermal conductivity losing heat by convection and radiation [16]. The results demonstrate that the differential transformation method is very effective in generating analytical solutions for even highly nonlinear problems. In a recent work [17], the performance of functionally graded parabolic annular fin having constant weight is reported, wherein the effect of grading and geometry parameter has been investigated and dependence of fin performance on profile and grading is described.

In this work, the temperature distribution along the fin radius is investigated for functionally graded annular fin subject to rotation. The fin parameter, hence, has two components to be studied. One being the nonrotating, m_f, is the usual fin parameter while other, m_{fr} is applicable only due to rotation of the fin. The effect of these on the fin performance has been investigated and reported for rectangular and triangular fin profile in this work.

9.2 Mathematical Formulation

Rotation of fin is assumed to effect the convective heat transfer coefficient assuming a linear function of angular velocity ($\boldsymbol{\omega}$) in the following form [13]:

$$h = p + qr\omega \tag{9.1}$$

The second-order differential equation for the heat transfer through the fins has to be developed to determine the temperature profile. For calculating the heat balance, the details for a control volume of length "dr" of a fin is shown in Figure 9.1. The correlation equation (second-order differential equation) has been derived using thermal energy balance:

$$Q_r = Q_{r+dr} + Q_c \tag{9.2}$$

Using eq. (9.2), the fin geometry and physical parameters are normalized using the following expressions:

$$\phi = \frac{\theta}{\theta_0} \quad \xi = \frac{r - R_0}{R_1 - R_0} = \frac{r - R_0}{L}, \quad R_f = \frac{R_1}{R_0}$$

The functional grading of the fin material is assumed to follow the power law:

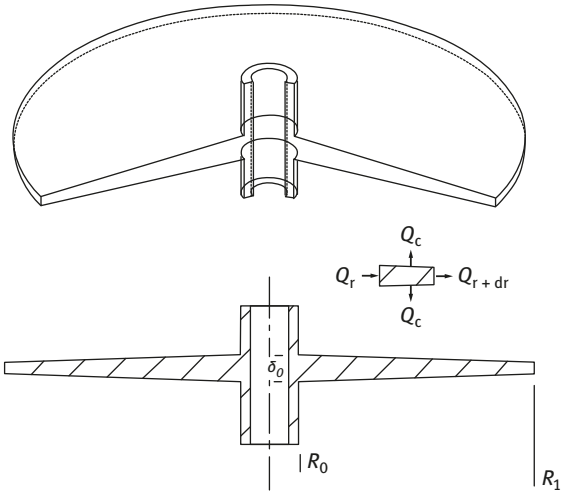

Figure 9.1: Sectional isometric view of annular fin.

$$k_r = ar^b \tag{9.3}$$

so $k_0 = aR_0{}^b$

$$\delta = \delta_0(1 - n\xi^m) \tag{9.4}$$

Upon introducing the normalized variables, the governing equation becomes

$$\frac{d^2\phi}{d\xi^2} + A_1\frac{d\phi}{d\xi} + A_2\phi = 0 \tag{9.5}$$

Here,

$$A_1 = \frac{1}{\delta}\frac{d\delta}{d\xi} + \frac{L}{L\xi + R_0} + \frac{1}{k_r}\frac{dk_r}{d\xi}$$

$$A_1 = \frac{-nm\xi^{m-1}}{1 - n\xi^m} + \frac{L}{L\xi + R_0} + \frac{Lb}{L\xi + R_0} \tag{9.6}$$

$$A_2 = -\frac{\left(m_f + m_{fr}\left(\xi + \frac{R_0}{L}\right)\right)\left[\sqrt{\frac{\delta_0^2}{4L^2}.\left(m.n.\xi^{m-1}\right)^2 + 1}\right]}{(1 - n\xi^m)}\left(\frac{R_0}{L\xi + R_0}\right)^b \tag{9.7}$$

where

$$m_f = \frac{2L^2p}{k_0\delta_0} \tag{9.8}$$

$$m_{fr} = \frac{2L^3 \omega q}{k_0 \delta_0} \tag{9.9}$$

Equation (9.5) can be generalized for varying thermal conductivity for rectangular profile (by keeping $n = 0$) and triangular profile (by keeping $m = 1$). Equation (9.5) is solved using the following boundary conditions:

$$\phi|_{x=0} = 1, \phi'|_{x=1} = 0$$

Efficiency of the fin is obtained from the general eq. (9.5),

$$\eta = \frac{-(\phi')_{\xi=0}}{\left(m_{\mathrm{f}} + \frac{m_{\mathrm{fr}}}{2L}(R_0 + R_1)\right) \int_0^1 [((R_f - 1)\xi + 1)\sqrt{\left(\frac{\delta_0 mn}{2L}\right)^2 \xi^{2m-2} + 1}]d\xi} \tag{9.10}$$

9.3 Result and Discussion

The temperature distribution and heat transfer of the fin is calculated by evaluating the first derivative of temperature at the fin base by solving second-order differential equation in MATLAB using subroutine ***bvp4c*** [18]. Subroutine ***bvp4c*** is an established technique to solve boundary value problems by choosing a continuous piecewise polynomial that adjusts to the boundary conditions. The remaining unknown coefficients are determined by collocating the algebraic equations at several points. It is an adaptive finite difference code that employs three-stage Lobatto III-a collocation formula by computing a cubic spline on each subinterval $[x_i, x_{i+1}]$ of a mesh. The approximate continuous solution is obtained by controlling the residual over each subinterval $[x_i, x_{i+1}]$ approximated using a five-point Lobatto quadrature formula.

Literature survey points toward the nonexistence of studies addressing the problem of functionally graded rotating annular fins. As a consequence, the validation of the proposed formulation is carried out for a homogeneous annular fin of rectangular profile [13]. The temperature distribution along the fin radius for given fin variables is validated with the benchmark results (Figure 9.2) and a good agreement is observed. The validation is presented for fin variables defined by C_1 and C_2, where

$$C_1 = \frac{0.5 m_f}{\left(1 - R_f^{-1}\right)^2}$$

$$C_2 = \frac{0.5 m_{fr}}{\left(1 - R_f^{-1}\right)^2}$$

A parametric investigation of rotating annular fins of rectangular and triangular profile for different grading parameters is reported next. The results obtained at

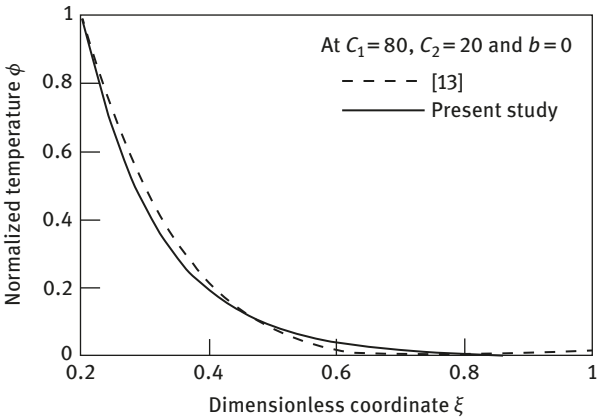

Figure 9.2: Temperature Distribution along the radial direction.

different grading parameter and rotational speeds are presented in the following graphs. For triangular profile, the effect of aspect ratio on the temperature distribution over the surface of the fin is shown in Figure 9.3. It is observed that tip temperature decreases with an increase in the aspect ratio for grading parameter $b = -1$. This is due to the fact that for shorter fin length, temperature distribution over the surface is higher, thus causing a higher performance of the fin.

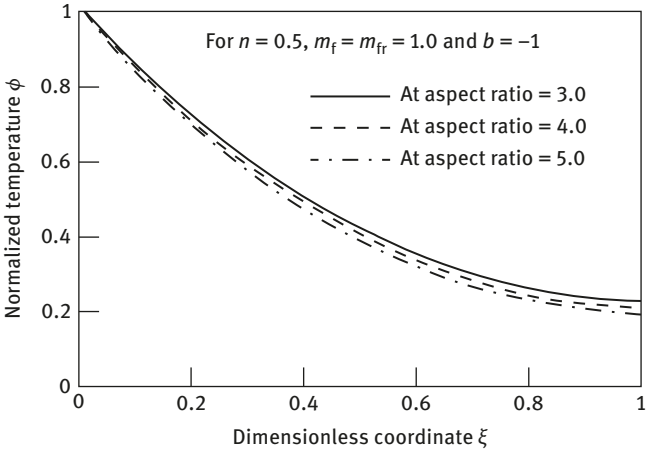

Figure 9.3: Normalized Temperature distribution along with the fin radius for different aspect ratio.

The performance of fin is also analyzed by varying grading parameter b and are depicted in Figure 9.4. It is evident from the figure that a decrease in grading

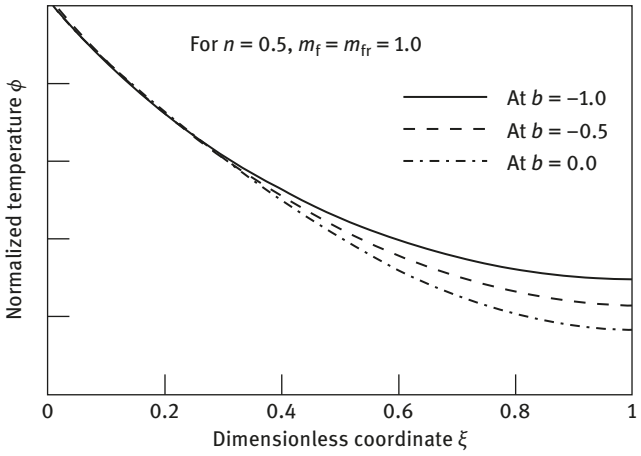

Figure 9.4: Normalized Temperature distribution along with the fin radius at different grading parameter *b*.

parameter improves the fin performance. This may be attributed to the fact that lower the value of *b*, higher is the temperature at fin periphery. Hence, the temperature distribution obtained results in higher heat transfer rate for lower values of *b*. The larger the heat transfer, better is the efficiency as maximum efficiency is theoretically obtained when the fin is completely maintained at the base temperature.

The fin performance is measured by evaluating the fin efficiency for rectangular and triangular annular fins at different fin and grading parameters and is reported next. In Figure 9.5, the effect of fin parameters m_f and m_{fr} on fin efficiency for rectangular and triangular profiles is plotted. It is evident from Figure 9.5 that the lower value of m_{fr} yields higher fin efficiency. This is due to an increase in convective heat transfer coefficient with an increase in m_{fr}, which results in lower temperature profile over the surface of the fin.

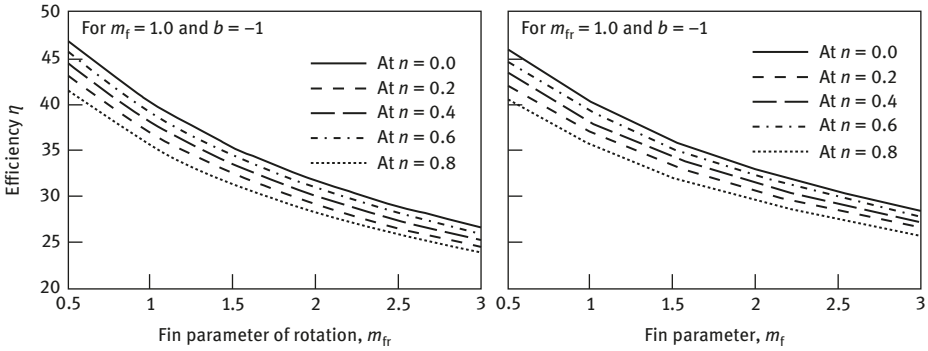

Figure 9.5: Effect of fin parameters on fin efficiency for different geometry parameter *n*.

In addition, for rectangular profile (i.e., n = 0), higher efficiency is obtained in comparison to triangular profile, because of larger surface area available at the base for triangular fins. However, an interesting insight into the problem is yet to be addressed in form of constant mass constraint [17], wherein the efficacy of using varying geometry may score over the rectangular one of same mass. In Figure 9.6, the effect of fin parameters m_f and m_{fr} over the fin efficiency is plotted for different geometry parameters. Using eq. (9.6), different triangular fin profile (at m = 1) can be analyzed by varying parameter n. As n increases, the convective area of the fin decreases, which results in lowering the performance of the fin as shown in Figure 9.6. Furthermore at n = 1, the thickness at the periphery of the fin becomes zero. Value of n less than one is practically not plausible.

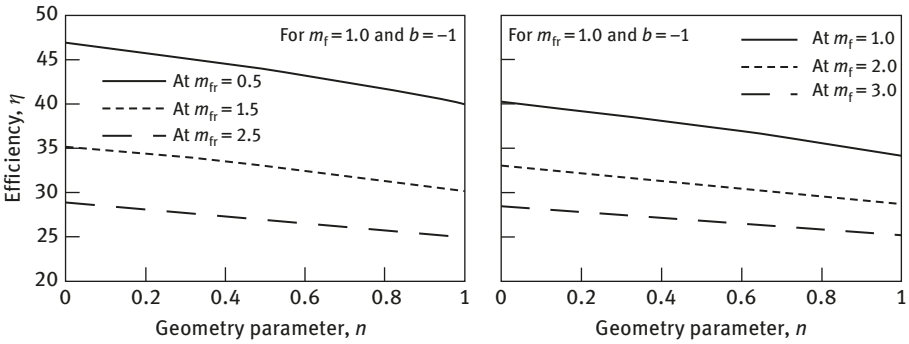

Figure 9.6: Effect of geometry parameter *n*on fin efficiency.

9.4 Conclusions

A detailed parametric study of functionally graded *rotating* annular fins having rectangular and triangular fin profile is reported. The study is carried out for different value of fin parameter m_f, rotating fin parameter m_{fr}, geometry parameter n and grading parameter b. It is observed that lower values of fin parameter m_f and rotational speed parameter m_{fr} yield better fin performance. The study of effect of grading parameter on fin performance indicates that both temperature distribution and performance of fin are enhanced for negative grading parameter b.

Nomenclature

a, b	Grading parameter for thermal conductivity
m_f, C_1	Fin parameter [–]

m_{fr}, C_2	Parameter for rotation of fin [–]
H	Convection heat transfer coefficient [W/m^2°K]
k_0	Thermal conductivity of the fin material at base [W/m°K]
k_r	Thermal conductivity of the fin material at any radius [W/m°K]
L	Fin length [m]
n, m	Geometry parameter [–]
p	Coefficient for convective heat transfer coefficient [W/m^{2}K]
q	Coefficient for convective heat transfer coefficient[(Ws)/(rad m^{3}K)]
Q_r, Q_{r+dr}	Rate of heat flow by conduction into and out of element at r [W]
Q_c	Rate of heat flow by convection from surface between r and $r+dr$ [W]
R_f	Aspect Ratio, constant for fin shape relations (R_1/R_0) [–]
r	Fin radius at the start of element [m]
R	Radius [m]
T	Temperature [°C]
ξ	Dimensionless radial coordinate [–]
δ	Fin thickness [m]
δ_0	Fin thickness at the axis [m]
Φ	Dimensionless temperature (ϑ/ϑ_0) [–]
Φ'	Nondimensionless temperature gradient [–]
ω	Angular velocity of shaft [rad/s]

References

[1] Gardner, K.A. Efficiency of extended surfaces. Trans. ASME, 1965, 67, 621–631.

[2] Brown, A. Optimum dimensions of uniform annular fins. Int. J. Heat Mass Transfer, 1965, 8, 655–662.

[3] Duffin, R.J., & McLain, D.T. Optimum shape of a cooling fin on a convex cylinder. J. Math. Mech., 1968, 17, 769–784.

[4] Ullmann, A., & Kalman, H. Efficiency and optimized dimensions of annular fins of different cross-section shapes. Int. J. Heat Mass Transfer, 1989, 32, 1105 –1105.

[5] Khan, J., & Zubair, S. M. The optimal dimensions of convective-radiating circular fins. Heat and Mass Transfer, 1999, 35, 469–478.

[6] Mokheimer, E. M. A. Performance of annular fins with different profiles subject to variable heat transfer coefficient. Int. J. Heat Mass Transfer, 2002, 45(17), 3631–3642.

[7] Bahadur, R., & Bar-Cohen, A. Thermal design and optimization of natural convection polymer pin fin heat sinks. IEEE Trans. Compon. Packag. Technol., 2005, 28(2), 238–246.

[8] Campo, A., & Cui, J. Temperature/heat analysis of annular fins of hyperbolic profile relying on the simple theory for straight fins of uniform profile. J. Heat Transfer, 2008, 130(5), 0545011–4.

[9] Hatami, M., & Ganji, D. D. Thermal behavior of longitudinal convective – radiative porous fins with different section shapes and ceramic materials (SiC and Si3N4). Ceram. Int., 2014, 40(5), 6765–6775.

[10] Aziz, A., & Rahman, M. M. Thermal performance of a functionally graded radial fin. Int. J. Thermophys., 2009, 30, 1637–1648.

[11] Yovanivich, M. M., Culham, J. R., & Lemczyk, T.F., 1987, Simplified solutions to circular annular fins with contact resistance and end cooling, J. Thermophys., 1987, 2(2), 152–157.
[12] Mustafa, M.T., Zubair, Syed, M, & Arif,, A. F. M. Thermal analysis of orthotropic annular fins with contact resistance: a closed form analytical solution. Appl. Therm. Eng., 2011, 31(5), 937–945.
[13] Aziz, A., & Khani, F. Analytic solution for a rotating radial fin of rectangular and various convex parabolic profiles. Commun. Nonlinear Sci. Numer. Simul., 2010, 15, 1565–1574.
[14] Aziz, A., & Lopez, R. J., Convection-radiation from a continuously moving variable thermal conductivity sheet or rod undergoing thermal processing. Int. J. Therm. Sci., 2011, 50(8), 1523–1531.
[15] Aziz, A., & Khani, F. Convection-radiation from a continuously moving fin of variable thermal conductivity. J. Franklin Inst., 2011, 348, 640–651.
[16] Torabi, M., & Yaghoobi, H. Analytical solution for convective – radiative continuously moving fin with temperature-dependent thermal conductivity. Int. J. Thermophys., 2012, 33, 924–941.
[17] Gaba, V. K., et al. Thermal performance of functionally graded parabolic annular fins having constant weight. J. Mech. Sci. Technol., 2014, 28(10), 4309–4318.
[18] Shampine, L.F., et. al. Solving Boundary Value Problems for Ordinary Differential Equations in Matlab with bvp4c, 2010, www.mathworks.com/bvp_tutorial.

Index

https://doi.org/10.1515/9783110603699-010